UNIVERSITY OF SOUTHAMPTON

Simulating Temperature and Chlorophyll Variability in the Western English Channel: An Integrated Observational/Numerical Approach

William Hugo Spooner

Doctor of Philosophy

Faculty of Science
School of Ocean and Earth Science

January 2002

UNIVERSITY OF SOUTHAMPTON

ABSTRACT

FACULTY OF SCIENCE
SCHOOL OF OCEAN AND EARTH SCIENCE

Doctor of Philosophy

Simulating Temperature and Chlorophyll Variability in the Western English Channel: An Integrated Observational Numerical Approach

William Hugo Spooner

Physical/biological shelf-sea systems are controlled, to a great extent, by meteorologically and tidally forced vertical processes of heating and mixing. These processes form the basis of many simple water column models that have proven capable of realistically simulating shelf-sea temperature and chlorophyll distributions. The continued development of such models is hampered, however, by the lack of observational databases available for their validation.

This thesis compares the ability of an established water-column model (Prestidge & Taylor, 1995) to accurately simulate the observed temperature and chlorophyll distributions of a 60km by 60 km study region off Plymouth, UK, over a variety of temporal and spatial scales. An integrated observational database that resolved multiple scales of variability was compiled, consisting of data collected from a variety of platforms including boat, satellite and remote buoy.

The comparison of model simulations with the observational database suggested that model performance differed strongly between scales of variability. Frequency analysis was used to reveal two scales in particular between which model performance differed; the annual waveform of temperature was significantly more accurately simulated than the diurnal waveform of temperature, for which the amplitude response to meteorological forcing was overestimated by three-fold.

Due to the dependence on short time-scale mixing of the annual chlorophyll distribution, it was concluded that, even though the model provided a quantitatively accurate description of annual temperature distribution, its chlorophyll simulations over all scales resolved by the model were of questionable validity. The possibility that this finding extends to water-column models other than that of Prestidge & Taylor (1995) cannot be discounted.

Whilst the validity of using the Prestidge-Taylor model for diagnostic shelf-sea applications is questioned, the identification of its limitations over short time-scales does, however, provide a targeted focus for model development.

List of Contents

List of Figures

4. REULTS PART 2 – IN-SITU OBSERVATIONS

5. MODEL SIMULATIONS

6. SPECTRAL ANALYSIS AND CONCLUSIONS

List of Tables

Acknowledgements

I would like to acknowledge the following for assisting me during this work;

- P.M. Holligan and J. Aiken for supervising the project.
- S. Groom and staff at NERC Remote Sensing and Data Analysis Service (RSDAS) for supplying remote sensed images and development of custom processing packages.
- A.H. Taylor for supplying the numerical physical/biological model.
- B. Sinha and C. Griffiths for supplying tidal data.
- M. Pinkerton for supplying PlyMBODy data.
- G. Gibson for supplying water depth data.
- I. Bellan and C. Barrett for supporting the UOR instrument.
- The crew of the R.V. Squilla for support and encouragement whilst at sea

The project was funded by the Environmental Optics Programme of the Office of Naval Research. Award number N000149610009.

1. Introduction

1.1 Background

Shelf seas are important regions both industrially and environmentally. They support tourism and leisure, fisheries, transport, waste disposal and mineral extraction industries. They are also often areas of strategic military importance. As temperature and chlorophyll concentration are fundamental properties of shelf sea waters, an understanding of the processes controlling their distribution has important implications for many shelf-based activities.

Biological processes perform pivotal roles within global biogeochemical cycles. These cycles contribute to the systems that regulate global environmental conditions. It is the maintenance of these conditions that enables life to be sustained on earth. Within these cycles, shelf sea ecosystems are highly significant. Not only are they regions of high biological productivity, but, due to their proximity to land, they are highly susceptible to anthropogenic disturbance.

In view of the role of shelf seas in supporting industry, and in contributing to earth systems, it is important to understand and monitor the processes that control shelf sea temperature and chlorophyll distributions. Significant advances in this field have come through the development of coupled physical/biological models. These use mathematical representations of environmental processes, and are run on modern computers. They are needed to explain the processes causing observed variability (heuristic models) and to forecast conditions in the future (predictive models). Example applications of such models are wide-ranging and topical:

- To determine the response of shelf-sea physical/biological processes to climate change.
- To determine the biological response to, and fate of, anthropogenic inputs to shelf seas.
- To provide tools to aid the industrial (e.g. fisheries, mineral extraction) exploitation of shelf seas.
- To provide information on physical processes from observations of physical and biological variability, via inverse modelling.
- To aid in the design/implementation of interdisciplinary shelf-sea studies.
- To provide a tool for the quality control of observational data.

Surprisingly few shelf sea models have been applied to the above applications. Two recent reviewers, Franks (1995), and Smith (1993), blame the dearth of such models on the lack of availability of observational data that is appropriate for model verification. There is a requirement, therefore for closer integration between modelling and observational programmes.

Shelf sea temperature and chlorophyll concentrations vary over well-defined scales, both temporal and spatial. Their distributions result from the characteristic variability of the external physical forcing mechanisms (e.g. solar irradiation, air/sea heat flux, wind and tidal mixing). It is the premise of this thesis that an objective test of a marine system model is to analyse the accuracy of its simulations over a range of scales of variability. Some measures of each of these scales of variability must therefore be obtained, against which the model can be verified. This can only be achieved by using data collected from variety of sampling platforms (e.g. boat, buoy and satellite).

The waters off Plymouth in the Western English Channel provides a convenient location for studies of shelf sea systems. Due to their proximity of the UK's oldest marine laboratory (the Marine Biological Association of the UK's Plymouth Marine Laboratory, or PML), these waters have been extensively studied for over 100 years (see Southward, 1995). The sampling sites of E1, (50°02'N, 4°22'W) and L4 (50°15'N, 4°12'W), for example, have been the focus of numerous previous studies, and were sampled during this project. A map of the study region is shown in Figure 1.1.

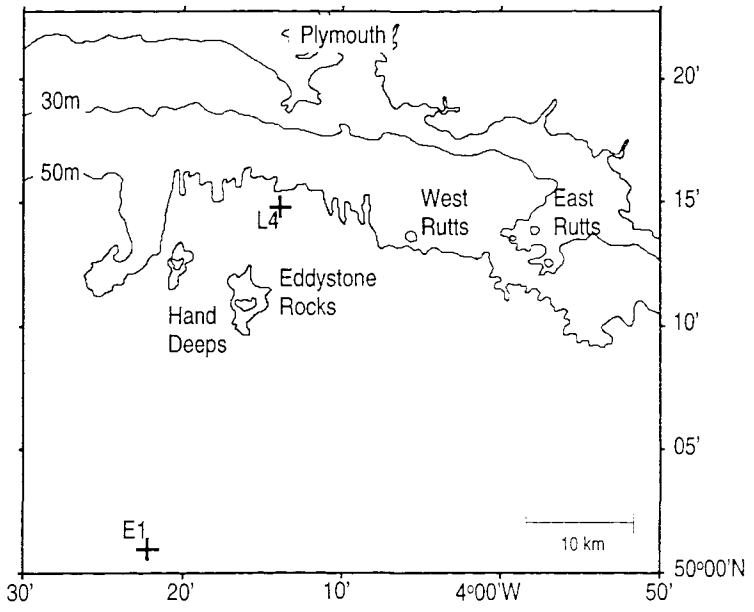

***Figure 1.1** – The Study Region: Plymouth Coastal Waters. E1 and L4 are established sampling sites.*

The physical/biological model used during this project is that of Prestidge & Taylor (1995) (termed the Prestidge/Taylor model). This model was designed as an operational model of the Irish Sea, to be used for fisheries research. Whilst more advanced models have been developed, this model has the significant advantage of simplicity. Simpler models facilitate tracing of events, have fewer free parameters and are less computationally expensive. This project focuses on comparison of the model simulations with in situ data, rather than on optimising the performance of the model itself.

1.2 Scales of Temperature Distributions in Shelf Seas

Vertical Processes Controlling Water Temperature

The vertical temperature profile of the water column results from the balance between heating and mixing. It is also modified by lateral advection. In the simplest case, temperature is vertically homogenous, and the water column is described as well mixed. If the surface heats, then its density is reduced, and energy, from wind, tide and convective cooling, is required to mix it down through the water column. If insufficient energy is available, then a layer of warm water will persist above cooler water below, and the water column becomes thermally stratified. A thermocline temperature gradient will be present between the surface mixed layer (SML) and the bottom mixed layer (BML).

The energy balance between heating and mixing forms the basis of simple 1 dimensional numerical models of ocean temperature structure. Examples of such models include; Kraus & Turner (1967), Garwood (1977), and Price *et al* (1986). These models generally simulate SML temperature and thermocline depth and extent. They are described as 'bulk' models, because the temperature of the surface mixed layer is assumed homogenous. Similar models have been developed for shelf seas which additionally simulate temperature of waters below the thermocline as a pseudo-homogenous BML (e.g. James, 1977, Van Aken, 1984)

Bulk models are driven by estimates of the heat flux across the air/sea interface. Edinger *et al* (1968) and Stigebrandt (1985), for example, have modelled the air/sea heat flux (Q_T), as follows;

$$
\begin{aligned}
Q_T &= Q_S - Q_B - Q_E - Q_C \\
Q_s &= f\left(E_d{}^0\right) \\
Q_B &= f\left(T_s, n_c\right) \\
Q_C &= f\left(w, (T_s - T_a)\right) \\
Q_E &= f\left(w, P_r, h_m\right)
\end{aligned}
\qquad \text{(1.1a to e)}
$$

Where: Q_S is absorbed solar radiation; Q_B is net back radiation from the sea to the atmosphere; Q_C is heat lost by turbulent transfer (sensible heat exchange); Q_E is heat lost by evaporation; $E_d{}^0$ is the downwelling irradiance at the sea surface, T_s is the sea surface temperature, n_c is the cloud cover; T_a is the air temperature; P_r is the mean sea level pressure, and h_m is the relative humidity.

The above equation introduces a range of meteorological variables that affect air/sea heat flux. The variables with the greatest effect, however, are the downwelling irradiance at the sea surface (also termed 'global radiance'), and the air/sea temperature difference (Edinger *et al*, 1968).

The change in potential energy (PE) of the water column due to this heat flux, assuming that a thin surface layer is initially heated, is as follows (Simpson & Hunter 1974):

$$PE_{heat} = Q_T \alpha g h \Big/ 2C_p \qquad (1.2)$$

Where: α is the thermal expansion coefficient of water, g is the gravitational acceleration, h is the water depth, and C_p is the specific heat capacity.

Changes in PE due to heating flux are distributed through the water column by tidal mixing from the sea bed, wind mixing from the sea surface, and convective overturn. The wind and tide therefore reduce the surface PE as follows (Simpson & Bowers 1984);

$$
\begin{aligned}
PE_{tide} &= -\varepsilon k_b \rho_w \overline{u^3} \\
PE_{wind} &= -\delta k_s \rho_s \overline{w^3}
\end{aligned}
\qquad \text{(1.3a, b)}
$$

Where: ε and δ are the mixing efficiencies of the tide and wind, k_b and k_s are sea bed and sea surface drag coefficients; ρ_w and ρ_s are densities of sea water and air; u and w are tidal and wind speeds.

The change in PE of the water column is the sum of the PE due to heating, tidal mixing and winds mixing. Simpson & Bowers (1981) suggest that the efficiency of wind and tidal mixing should be modified by the existing stratification of the water column, therefore introduce a variable efficiency term as follows;

$$\frac{dPE}{dt} = PE_{heat} - f\left(PE_{tide} + PE_{wind}\right)$$
$$\text{while } f < T_0, f = \sqrt{\frac{V_0}{V_0 + PE}}, \text{ else } f = T_0 \qquad (1.4)$$

Where: V_0 and T_0 are empirical constants.

The temperature of the SML due to the heat flux is determined, as follows;

$$\Delta T_{SML} = Q_T \Big/ \rho_w C_p h_{SML} \qquad (1.5)$$

Where: h_{SML} is the depth of the surface mixed layer.

The volume of water mixing between each layer will further modify their temperatures.

Temporal Scales of Temperature Variability; the Importance of Meteorological Forcing.

Station E1 in the western English Channel displays the typical seasonal cycle of temperature variability observed in mid-latitude shelf seas. During the winter, low irradiance and air temperatures create conditions of negative heat flux into the water column. This results in convective overturn that maintains a well mixed water column. As the heat budget becomes positive (generally in mid-March, Pingree & Pennycuick, 1975), the water column has the potential to become stratified. Stratification will become established at a later date, once the mean buoyancy flux due to heating exceeds mean mixing energies due to wind and tide. In mid-October, the heat budget returns to negative values, causing the stratification to break down soon after. Using an average of 70 years of temperature observations at E1, Maddock & Swann (1977) identified the presence of water column stratification between mid-March and late-October.

Following the onset of stratification, SML temperatures at E1 increase rapidly to a maximum in August. SML temperatures fall after August due to the reduction of solar heating and increase in mixing that occurs during the autumn. BML temperatures are controlled by mixing down of heat from the SML, which is inversely related to the strength of stratification. As a result, BML temperatures increase in a fairly linear manner between April and October (Maddock & Swann, 1977).

Using the same data base as Maddock & Swann (1977), Pingree *et al* (1977a) presented contours of the average monthly temperature distribution. The plot can be used as an indication of the depth envelope in which the thermocline is generally located. The

range was from the surface to 40 m, with the maximum gradient being located nearer the surface during the summer months, consistent with lower wind mixing energies.

In addition to temperature, salinity distribution can have a significant effect on the stability structure of shelf seas. Salinity affects are the strongest in regions influenced by riverine discharge (e.g. the Norwegian coast of the North Sea, Elliot & Li, 1995). For the western English Channel, however, Pingree *et al* (1977a): calculated that the salinity contribution to the stability structure at station E1 was generally < 10%.

Spatial Variability in Shelf Seas, the Importance of Tidal Mixing and Water Depth.

In addition to atmospheric forcing, tidal currents and water depths have a strong influence on the hydrography of shelf seas (see equation 1.4). Tides and depths vary over shorter spatial scales than meteorological fields, and therefore control the in-water variability over these scales.

As tidal mixing increases, the tendency for the water column to stratify is reduced. At a certain threshold, sufficient mixing will occur to prevent stratification occurring at any stage in the seasonal cycle. If tidal flows increase along a horizontal transect, at some point along its length the water column will become well mixed. Such a boundary between thermally stratified and tidally mixed water masses is termed a 'tidal front'. Tidal fronts are often characterised by horizontal gradients in measured variables such as sea surface temperature (SST). Simpson & Hunter (1974), used an energy balance argument to predict the position of such a front in the Irish Sea. The front occurred at a critical value of the parameter h/U^3, where h was the water depth and U the observed surface current speed at spring tides.

The front will occur when the following equality is met;

$$\frac{h}{D_t} = \frac{2c\varepsilon_t}{\alpha g \Delta Q} \quad (1.6)$$

Where; h is the water depth; c is the specific heat capacity of water; ε_t is the efficiency of tidal mixing; α is the thermal expansion coefficient of water; g is the acceleration due to gravity and ΔQ is the heat input to the water.

The general applicability of the h/U^3 parameter for predicting the position of tidal fronts has been demonstrated by its application to shelf seas from North America (Garrett *et al*, 1978, Bowman & Esais, 1981) to New Zealand (Bowman *et al*, 1981). Pingree & Griffiths (1978) used a similar model (shown in equation 1.7), to predict the position of

tidal fronts for the whole of the North West European Continental Shelf, using tidal data calculated from a numerical model. Their stratification parameter, S, is used later in the thesis. Pingree & Griffiths (1978) noted that fronts form over a range of values of S (1 to 2, assuming C_D of 0.0025, tides in cm s^{-1}, and water depth in m). Holligan (1981) estimated that this range covers approx. 12% of the area of the North West European continental shelf.

$$S = \log_{10}\left[\frac{h}{C_D(|u^3|)}\right] \qquad (1.7)$$

Where: S is the stratification parameter; h is the height of the water column; C_D is the bottom drag coefficient; |u| is the semi-diurnal depth mean tidal stream velocity along the semi-major axis of the tidal ellipse.

The complexity of the basic h/U^3 model was increased with the addition, by Simpson *et al* (1978) and Loder & Greenberg, (1986), of wind-induced turbulence at the sea surface. Bowers & Simpson (1987) concluded that the including wind mixing increased model accuracy in shallow water, but its significance diminished with water depth. That stratification itself inhibits vertical mixing was considered by Simpson & Bowers (1981), whose model incorporated variable mixing efficiencies.

Several studies have questioned the validity of the h/U^3 parameter. Simpson & Hunter (1974) assumed that a fraction of the tidal kinetic energy loss is available for vertical mixing, spread evenly throughout the water column. Loder & Greenberg (1986), however, suggest that mixing efficiency decreases relative to the fourth power of distance from the sea bed, resulting in a revised criterion of h^4/U^3. Other criteria are also suggested. Simpson & Sharples (1994) and Sharples & Simpson (1996) used a turbulence closure model to assess the validity of the different criteria. The h/U criteria was shown to be significant for fronts in waters greater than 100 m deep, or where there was a significant cyclonic component to the tidal currents. Final resolution of the correct h/U^n criteria has yet to be resolved either empirically or theoretically.

1.3 Physical Water Column Models

Simulations of Water Column Variability over Seasonal Scales

The ability of a 1-D bulk physical model to simulate the seasonal temperature distribution in shelf seas was demonstrated by James (1977). The model was run for various positions in the Celtic Sea. The meteorological data required for model forcing were calculated by fitting sinusoidal curves to mean monthly meteorological fields

collected at the nearby meteorological stations. The simulations of SML and BML temperatures were qualitatively similar to the features described above, and quantitatively similar (+/- 1°C) to average monthly temperatures calculated from in-situ measurements over a number of years. Simpson & Bowers (1984) subsequently used a 1-D bulk model forced with sinusoidal varying meteorology to successfully simulate the Celtic Sea heat budget over the seasonal cycle.

When comparing model simulations with integrated measures from observations (e.g. temperature climatologies), it is assumed that the observational errors are negligible. This assumption, however, is not always justified. For example, in a modelling study of ocean currents, Walstad & Robinson (1990) blamed differences between simulations and integrated observational measures on limitations in the analysis of the observations. It is desirable, therefore, to compare simulations with discrete observations wherever possible.

To simulate discrete in-situ observations, it is necessary to force the model using discrete meteorological observations. Meteorological measurements of 3-hour resolution were used by Agoumi *et al* (1985) to successfully simulate the shelf sea temperature cycle for a specific year. The model simulation agreed well (to +/- 1°C) with eight discrete measurements of SML and BML temperature, evenly distributed through the period of the year during which the water column was stratified.

Observations from moored buoys provide measurements with far greater temporal resolution than those collected by boat surveys, and therefore provide a more thorough analysis of the accuracy of 1-D model simulations. In a recent study, Ruardij *et al* (1997) examined simulations of temperature distribution against buoy observations from the North Sea. The accuracy of the SML and BML simulations were +/- 1°C throughout the year. Their analysis was confined to distributions over the seasonal cycle. Whilst shorter scale variability was apparent on their simulation plots, it was not discussed.

The influence of small-scale variability in meteorological forcing on seasonal trends was highlighted by Ridderinkhof (1992), again using a 1-D bulk model. The averaging interval of wind mixing data was varied between model runs, and it was shown that the seasonal heat content of the water column altered in response. The greatest summertime heat content was achieved with the highest resolution (hourly) wind data. The differences in heat content affect both SML and BML temperatures and depths.

In view of the effect that different wind regimes have on seasonal water column structure, it is desirable to use realistically varying wind speeds to force physical

models, even if model simulations are only to be compared against average seasonal distributions of temperature. Elliott & Li (1995), for example, used a 1-D turbulent diffusion model forced with simulated stochastic (i.e. varying over multiple time scales) wind speeds. Their temperature simulation for the Western English Channel agreed with the average seasonal cycle to within +/- 1°C. The numerical increases in model accuracy gained by using stochastic wind forcing were not, however, described. The turbulent diffusion model used in this study represents an alternative approach to bulk models for simulating water column structure. Here, the water column is considered as a number (~50) of fixed layers. An estimate of the turbulent diffusion coefficient is then used to control the exchange of heat and energy between the layers.

It is interesting to note that the highly complex model of Elliott & Li (1995) performed no more accurately than the simple bulk model of James (1977). Whilst it is accepted that turbulent diffusion models provide a more realistic description of the physical processes acting within the water column, they still suffer from many of the same limitations of bulk models, e.g. the inability to resolve advective effects. Studies have been carried out that directly compare the performance of different models in simulating oceanic mixed layer temperatures. In a study by Large *et al* (1994), turbulent diffusion models were shown to provide slightly more accurate simulations when compared with observed data than bulk models.

Simulations of Water Column Variability over Sub Seasonal Scales

The studies described above were each focused on simulating the seasonal cycle of temperature distribution. The works of Ridderinkhof (1992) and Elliott & Li (1995) recognised the influence of small scale meteorological forcing on the characteristics of the seasonal cycle, but fewer studies have analysed the ability of models to reproduce the in-situ temperature variability in shelf seas over sub seasonal scales. A major limitation of such studies is that these small-scale differences are masked by the underlying seasonal variability. Efforts have been made to separate seasonal and mesoscale variability in modelling studies of open oceans (e.g. Stramska & Dickey, 1993), but these procedures are not applicable to shelf sea systems where mesoscale variability results from changes in stratification rather than horizontal advection.

Atmospheric forcing over sub-seasonal time scales has an immediate impact on the temperature structure of the water column. Increased wind speeds decrease the PE of the water column at the surface, resulting in increased vertical exchange between the SML and thermocline. Observations of increased vertical mixing and increased

pycnocline depth in response to wind events have been observed (e.g. Kiorboe & Nielsen, 1990, Klein & Coste, 1994)

The accuracy of simulations over a 13 day period presented by Marra & Ho (1993) suggest that 1-D bulk models can provide a reasonable qualitative simulation of water column temperature distribution over shorter than seasonal scales in the open ocean. The study covered the period of the onset of seasonal stratification, where seasonal variations are large and obvious. It follows, therefore, that the simulation reproduced an aspect of the seasonal cycle, rather than variability over sub seasonal time scales. In addition, the presented analysis of model performance was of a qualitative nature. There is a requirement for studies that quantitatively analyse simulations of sub seasonal variability at various stages of the seasonal temperature cycle in shelf seas.

Heat flux varies greatly over the diurnal cycle. During the day, increased buoyancy due to solar heating inhibits mixing. During the night, however, convection due to surface cooling is an additional source of vertical mixing. The daytime SML is therefore characterised by higher temperatures and shallower depths than at night (Woods, 1980). Woods & Barkmann (1986) showed that diurnal variations in the depth of the mixed layer have their largest amplitudes shortly after the onset of seasonal stratification. Taylor & Stephens (1993) used a 1-D bulk model to provide a realistic simulation of the diurnal variation of mixing rates observed during April in the north east Atlantic.

Horizontal Advection and Simulations of Spatial Variability

Several of the 1-D water column models described earlier have been used to simulate spatial variability of shelf sea temperature. This is achieved by running the model at a number of positions. The simplest examples are where the model is run at two points, and the spatial variability is determined by interpolation (James 1977). More complicated schemes, such as that of Elliott & Li (1995) and the Prestidge/Taylor model, involve running the model at each point on a grid, producing simulated maps.

Horizontal movement of water (horizontal advection) can have significant effects on water column temperatures (e.g. Taylor & Stephens, 1980). 1-D models, however, are not designed to resolve advective effects. Concerning tidal advection, which is significant in shelf seas, one must assume that the modelled water column is not fixed in space, but moves bodily with the tide (James, 1977). For detailed analysis of small scale variability, several studies have attempted to remove the tidal advective signal from the observations before comparison with simulations (e.g. Simpson & Bowers, 1981).

Often, the ability of a 1-D model to accurately simulate the observations is taken as evidence that vertical rather than horizontal processes control the variability over the scale in question, and vice versa. The success of both the James (1977) and Agoumi *et al* (1985) 1-D modelling exercises suggested that vertical processes dominate the seasonal temperature cycle of the Western English Channel and Celtic Sea. This conclusion is similar to that arrived at by other methods, such as the analysis of trends in surface salinity (Colebrook & Taylor, 1979), the analysis of vertical salinity structure (Pingree & Pennycuick, 1975), and the analysis of heat budgets (Taylor & Stephens, 1983, Pingree & Pennycuick, 1975). Similarly, the success of the h/U^3 parameter suggested that vertical processes dominate the spatial temperature distribution over large areas of shelf seas. Residual advection can, however, significantly alter temperature distribution in some shelf sea regions. Several studies have identified these regions by analysing the accuracy of 1-D model simulations run over spatial grids (e.g. Prestidge & Taylor, 1995).

Residual advection is variable in strength and direction, dependant on wind direction and speed (Carruthers, 1935). A theoretical modelling study for the North West European continental shelf was presented by Pingree & Griffiths (1980), who demonstrated marked differences in current speed and direction depending on the direction of the prevailing wind. Advection also responds to the seasonal cycle of atmospheric forcing. Whilst they concluded that advection was insignificant in the summer, Pingree & Pennycuick (1975) explained the differences between simulated and observed heat budgets at station E1 by suggesting that advection from the Atlantic was significant during the winter.

Various observational and theoretical studies have estimated that the rate of residual advection in the Western English Channel is ~1 to 2 km day^{-1} (Harvey, 1925, Taylor & Stephens, 1988). However, mean residual circulation patterns in this region are poorly defined, and considerable variability occurs over short time scales (Pingree *et al*, 1976). In addition to wind driven residual currents, baroclinic flows can also be significant in shelf seas. Stigebrandt (1981), for instance, used a 2-dimensional model to show that cross thermocline flow will significantly affect water column density structure. More recently, Franks (1992), showed that the measured length scales of a variety of fronts was greater than that predicted by geostrophic balance, and they must, therefore, have undergone relaxation due to cross frontal transfer.

The recent development of coupled mixed-layer/primitive-equation models has allowed the assumption of zero advection to be tested. These models work by calculating the 1-dimensional vertical structure for several positions (in a line if the model is to be 2-

dimensional). These profiles are then used to solve the equations of motion between the grid points, thereby estimating advection (e.g. Franks & Chen, 1996).

Single value h/U^3 type model predict average position of a tidal fronts by using representative parameters for heat flux, wind and tidal mixing. These parameters, however, vary significantly over spatial and temporal scales. Pingree *et al* (1977b), for instance, suggested that the large changes in mixing rate over the spring-neap tidal cycle cause changes in frontal position. Simpson & Bowers (1981) observed that the position of a front in the Celtic Sea varied by 2 to 4 km in response to the spring-neap cycle, with a time lag of 2 days. Recent studies of the Georges Bank have reported frontal adjustments of up to 8 km (Mavor & Bisagni, unpublished), with time lags of 3 days (Bisagni & Sano, 1993). Simpson & Bowers (1981) used a 1-D bulk model to confirm that the observed frontal adjustment could indeed result from variation in vertical mixing over the spring-neap tidal cycle. More recently, however, Sharples & Simpson (1996) suggested that their 1-D turbulent diffusion model tended to overestimate frontal adjustment by a few km, although their model was not compared directly with observations.

1.4 Scales of Chlorophyll Distributions in Shelf Seas

Vertical Processes Controlling Chlorophyll Distribution in Shelf Seas

Biomass concentration at a point is a result of its integrated gains and losses through time. Biomass gains result from gross primary productivity, whilst losses result from respiration, mortality and grazing by zooplankton. Chlorophyll-a concentration is often used as a measure of biomass, whereas primary productivity is generally measured in carbon units, and biomass itself is defined as cellular dry-weight per volume. Chlorophyll can vary widely in terms of cellular quota due to species composition, photoadaptation, nutrient availability, temperature and other factors. In temperate, shelf-sea waters, where the environmental conditions are heterogeneous over short spatial and temporal scales, the chlorophyll per cellular dry weight, and the ratio of chlorophyll to carbon, can vary widely (e.g. by a factor of 4, Newton & Morello, 1998). Even considering this limitation, the measurement of chlorophyll remains the most widely used method for estimating phytoplankton biomass distributions.

Gross primary productivity is defined as the rate of photosynthesis. Photosynthesis is the mechanism by which phytoplankton harvest light energy to produce organic

compounds. In addition to light, photosynthesis also requires the presence of inorganic nutrients. A lack of light or some essential nutrient will limit photosynthesis, and hence primary productivity. The most significant growth limiting nutrients in shelf seas are aqueous compounds of nitrogen, phosphorus and silicon.

Vertical processes alter both the light and nutrient regimes to which phytoplankton are subjected. The link between vertical turbulence and phytoplankton growth is demonstrated in Svedrup's (1953) critical-depth theory. Monochromatic light of constant angular distribution is attenuated exponentially with depth as shown in equation 1.8, and gross productivity decreases correspondingly, but respiration remains constant. The compensation depth, is that at which time-integrated respiration and photosynthesis are equal over 24 hrs. If the mixed layer exceeds the critical depth, cells spend an appreciable time below the compensation depth, and depth integrated respiration will exceed gross photosynthesis, therefore net productivity will be less than zero. Thermal stratification, however, reduces mixed layer depth, impedes vertical mixing, allowing the biomass accumulation which results in phytoplankton blooms. Once stratified, however, phytoplankton utilise nutrients in the SML. The thermocline presents a barrier to vertical mixing, thereby reducing the vertical flux of nutrients from the nutrient replete BML. Surface nutrients therefore become depleted and productivity slows due to nutrient limitation.

$$I_{(z,\lambda)} = I_{(0,\lambda)} e^{-k_{(\lambda)} z} \qquad (1.8)$$

Where; $I(z,\lambda)$ is the irradiance at depth z and wavelength λ; $I(0,\lambda)$ is the irradiance just below the sea surface; $k(\lambda)$ is the diffuse attenuation coefficient.

Seasonal Patterns of Chlorophyll Distribution

Using the arguments outlined above, vertical processes can be used to explain the classical seasonal distribution of chlorophyll concentration in mid-latitude shelf seas: During winter, low light levels lead to low productivity, hence low chlorophyll concentrations, throughout the water column. Once the seasonal water column stratification commences in spring, productivity increases hugely, leading to the spring bloom. During the summer months, under stratified conditions, SML chlorophyll concentrations decline. Finally, in the Autumn, sporadic mixing events followed by re-stratification mix nutrients back into the surface layer, resulting in the Autumn phytoplankton bloom. This seasonal pattern of spring and autumn blooms has been observed for station E1 in the English Channel (Holligan & Harbour, 1977).

Another feature of shelf sea chlorophyll distribution is the presence of a sub-surface chlorophyll maxima, located in the region of the thermocline during the summer. This feature can again be explained by considering vertical processes: Under conditions of stratification, the thermocline layer presents a region that is located above the compensation depth, affords vertical stability, and is adjacent to the nutrient rich bottom waters. These conditions are exploited by the phytoplankton, resulting in the formation of a sub-surface chlorophyll bloom. Such a feature is characteristic of station E1 (Holligan & Harbour, 1977) and of thermally stratified shelf seas of the Western English Channel (Aiken & Taylor, 1984).

Variations in physical forcing lead to regimes of contrasting physical conditions. Different groups of phytoplankton are each adapted to exploit differing levels of light and nutrient availability. As light and nutrients availability are controlled by physical forcing, different physical regimes tend to be dominated by different groups of phytoplankton. The seasonal changes of stratification and mixing therefore lead to a seasonal succession of phytoplankton species. Such a succession was observed for station E1 by Holligan & Harbour (1977): The spring and autumn blooms, characterised by high nutrient and low light levels, were dominated by diatoms, species that best exploit these conditions. Between these periods were early and late summer mixed populations of dinoflagellates and diatoms, separated by a mid summer population of dinoflagellates in the thermocline, with small flagellates in the surface mixed layer.

Spatial Patterns of Chlorophyll Distribution

Using arguments based on light availability and nutrient supply, spatial patterns of shelf sea chlorophyll distribution can also be explained by considering vertical processes. The timing of the onset of the spring bloom, for example, is controlled by the timing of the onset of stratification: In the English Channel, the spring bloom first becomes established in the regions with lowest tidal currents, to the west (Pingree *et al* 1976). As heating increases through the spring, the bloom extends eastward as progressively more tidally energetic waters become stratified Pingree (1980).

During the summer, tidal fronts are often characterised by intense blooms of phytoplankton, with low chlorophyll concentrations found to both the mixed and stratified sides. The low concentrations to the stratified side can be explained by nutrient limitation, whilst those to the well mixed side are explained by light limitation. In the frontal region itself, however, the combined effects of vertical mixing and surface stabilisation maintain favourable nutrient and light conditions for phytoplankton growth (Pingree *et al*, 1975).

As the light and nutrient regimes change with transects across a tidal front, so do the phytoplankton species: diatoms are found to the well mixed side, dinoflagellates at the frontal boundary, and flagellates in the mixed layer above the thermocline (Holligan, 1981, Holligan *et al* 1984a).

Various observations have been made of enhanced biomass extending to the stratified sides of frontal boundaries (e.g. Pingree *et al*, 1977b). Such observations have been used as indications of an enhanced nutrient supply to these regions. Pingree *et al*, 1975, suggested that the nutrient supply occurred as a result of the frontal adjustment due to the spring-neap cycle described earlier. As the tidal mixing energy reduces, the front moves into progressively more nutrient enriched waters. Other mechanisms have been suggested for the transfer of nutrients across frontal boundaries. These include; shedding of baroclinic eddies from the front into the stratified area (Pingree *et al* 1978); enhanced cross-pycnocline vertical transfer (Loder & Platt, 1985); and mixing caused by internal friction due to opposing baroclinic flows on either side of the front (Garrett & Loder, 1981). Loder & Platt (1985) estimate the relative contributions to be 12:8:20:1 for spring-neap, eddy, vertical and frictional nutrient transfer respectively, for the Ushant front.

The slope of the sea bed is a significant factor in determining rate of cross-frontal nutrient supply. For a sea bed with a shallow gradient, the front will move over a larger area for the same change in mixing than for a steep sea bed. This factor will tend to increase cross-frontal mixing as the front moves in response to the spring-neap tidal cycle. For a steep sea bed, however, the frontal boundary will also be steep, therefore leading to enhanced baroclinic flows therefore greater cross frontal nutrient transfer (Loder & Platt, 1985).

In addition to the slope of the sea bed, the water depth in which the front is located will also affect chlorophyll distributions. Blooms at deep water fronts, such as those in the English Channel and Celtic seas, are located to the stratified side (Holligan, 1981). Those in shallow water, however, show a biomass maxima to the mixed side, which may not be light limited (e.g. Cohen *et al*, 1982).

It has also been suggested that wind direction may alter the stability structure, hence chlorophyll concentrations, at fronts: (Franks & Walstad, 1997). Their suggestion was that steep fronts enhanced the surface chlorophyll maxima, whilst shallow ones enhanced sub-surface maxima.

In addition to *in-situ* phytoplankton growth, passive accumulation mechanisms have also been suggested to explain the observations of enhanced phytoplankton

concentrations at shelf-sea frontal boundaries (e.g. LeFevre 1986 and references therein), due, for example, to advective convergence at frontal boundaries.

1.5 Physical/Biological Models

The Biological Component – Models of Primary Productivity

Physical/biological models generally couple a physical water column model to a model of primary productivity. Primary productivity models use mathematical representations of photosynthetic rate and biological losses (e.g. respiration, cell mortality and zooplankton grazing). To maintain consistency with observed databases, biomass distributions are often simulated as chlorophyll concentrations. Simple models, such as the Prestidge/Taylor model, assume a constant ratio between algal productivity and chlorophyll concentration, but, as discussed earlier, this simplification is not valid under all circumstances due to the variation in the cellular quota of chlorophyll over time and space.

The chlorophyll concentration is calculated as the integration through time of the chlorophyll gains and losses as shown in equation 1.9. A correction is made for biomass advection, assuming that chlorophyll is a passive contaminant. Transport is therefore calculated along with the physical exchanges of water that are explicit in 1 or 2-D models. There are a variety of numerical models based on such arguments, and often used examples include those of Fasham *et al* (1990), Fasham *et al* (1984), Taylor *et al* (1986), Tett & Edwards (1984) and Franks *et al* (1986)

$$\frac{\mathrm{d}(chlorophyll)}{\mathrm{d}(time)} = photosynthesis - (respiration + mortality + grazing) \pm advection \qquad (1.9)$$

Photosynthetic rate depends on the availability of light and nutrients. The response of phytoplankton to irradiance has been measured in numerous field and laboratory experiments (see Jassby & Platt, 1976, Walsh, 1988 and references therein). These have lead to various photosynthesis-irradiance (PI) relationships being proposed, either empirical (e.g. Platt *et al*, 1980), or based on physiological models of photosynthetic reactions (e.g. Fasham & Platt, 1983). Mathematical modelling of the PI relationship generally produces curves of the shape shown in figure 1.2A. Parameters used to describe them include; the initial slope of the curve α, the maximum productivity μ_M, the saturation light intensity I_S, the half saturation light intensity I_k, and some formulation of photo-inhibition.

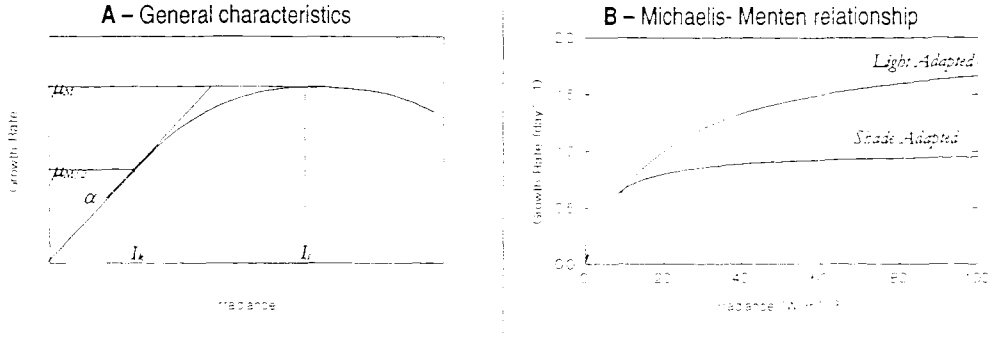

***Figure 1.2** – The photosynthesis - irradiance relationships.*
***A:** Schematic diagram of the general characteristics*
***B:** The numerical Michaelis-Menten relationship proposed by Taylor et al (1991) with parameterisation for light adapted (μ_M = 2 day^{-1}, I_k = 20 W m^{-2}) and shade adapted (μ_M = 1 day^{-1}, I_k = 5 W m^{-2}) phytoplankton*

Taylor *et al*, (1986), and the Prestidge/Taylor model, used a simple rectangular hyperbolic PI relationship, as shown in equation 1.10, which depends on only two parameters, μ_M and I_k. This simple formulation does not predict the light saturation or photo-inhibition effects that are commonly observed in the experimental analyses of PI relationships. Experimentally, the PI relationship depends on phytoplankton species (e.g. Richardson *et al*, 1983). This is reflected in the mathematical representations by changing the parameterisation. The two curves presented in figure 1.2B are for light adapted and shade adapted respectively. In addition to differences between species, variations within individual species occur as they adapt to prevailing light conditions (Marra *et al*, 1990). Simple ecological models, however, tend to assume a single, representative, phytoplankton species (e.g. Taylor, 1986), with fixed photosynthesis-irradiance parameter values. This scenario is avoided by explicitly modelling a number of phytoplankton species with differing parameter values (e.g. Varela *et al*, 1995).

$$\mu_R = \frac{\alpha_M I}{I + I_k} \qquad (1.10)$$

Where; μ_R is the growth rate in nutrient replete systems, I is the irradiance.

The relationship between photosynthetic rate and nutrient concentration is often modelled by the cell quota model (Droop, 1983), which is dependent on internal nutrient concentration. Nutrient uptake is then modelled using a Michaelis-Menten relationship (Dugdale, 1967). Several models (e.g. Tett *et al*, 1986) have used the cell quota approach for modelling phytoplankton. Irradiance and nutrient control of productivity are combined alternatively, following Blackman's (1905) modification of Leibig's 'Law of the Minimum'. A simpler approach, used by Taylor *et al* (1986) and the Prestidge/Taylor model, represents nutrient control of productivity as a direct

Michaelis-Menten relationship, combined simultaneously with the PI relationship (equation 1.10), as shown in equation 1.11.

$$\mu_G = \frac{\mu_R N}{N + N_h} \qquad (1.11)$$

Where; μ_G is the growth rate, N is the nutrient concentration, N_h is the nutrient half saturation coefficient.

Nutrient concentration is modelled in a similar way to chlorophyll: Gains result from regeneration, and losses due to uptake, as shown in equation 1.12. The net changes due to advection are modelled as for chlorophyll.

$$\frac{\mathrm{d}(nutrients)}{\mathrm{d}(time)} = biological\ regeneration - uptake \pm advection \qquad (1.12)$$

Biological losses include respiration, cell mortality and zooplankton grazing. In simple phytoplankton models such as Taylor *et al* (1986) and the Prestidge/Taylor model, all the losses are considered together as a fraction of total biomass for each time step. This is an obvious oversimplification. Respiration rate varies between species (Falkowski *et al*, 1985), and is therefore better represented by multiple phytoplankton models (e.g. Varela *et al*, 1995). The relationship between primary production and grazing is complex (Kiorbe, 1992 and references therein), and the use of simple formulations in physical/biological models is widespread. An alternative to the fixed ratio of grazing per unit biomass is provided by an Ivlev functional response (e.g. Franks *et al*, 1986), where grazing increases exponentially with biomass up to a maximum value.

There are also various approaches to the modelling of the biological regeneration of nutrients. The simplest of these is to consider that a fixed proportion of mortality is regenerated (e.g. Taylor *et al*, 1986 and the Prestidge/Taylor model). Those models that separate zooplankton from other mortality terms can separate regeneration likewise (e.g. Franks *et al*, 1986). Those models that contain multiple phytoplankton species can assign a separate regeneration rate to each. Most of the more complex models consider some combination of number of nutrients, e.g. nitrate, nitrite, ammonia, phosphorus and silica, allowing the nutrient preferences of different algal species to be represented (e.g. Varela *et al*, 1995). Others incorporate bacteria and dissolved organic nitrogen to explicitly model the microbial loop (Taylor & Joint, 1990).

Complexity is increased upon the inclusion of a greater number of species and nutrients, and on the mathematics used to link them. The major drawbacks of such complex models is that they rely on a large number of imprecisely known parameter values, are computationally expensive to run, and do not allow events to be traced easily. The

model of Varela *et al* (1995), for instance, requires 42 parameters to calculate primary productivity, whilst that of the Prestidge/Taylor modle uses just 7.

Modelling the Temporal Distribution of Chlorophyll

Various studies have used 1-D physical/biological models to simulate the seasonal variability of chlorophyll distribution. Agoumi *et al* (1985), coupled a simple biological model to their physical model described earlier, but whilst the simulation correctly predicted the timing of the spring phytoplankton bloom, concentrations over the rest of the year were overestimated. As the model did not include a thermocline layer, the SML and BML were adjacent, and it is likely that vertical nutrient fluxes were overestimated, which is a characteristic of 2-layer representations (Ridderinkhof, 1992). More recently, 3 layer bulk physical/biological models have been developed which provide fairly accurate simulations of the seasonal variation in SML chlorophyll concentrations (e.g. Ruardij *et al*, 1997). Although three layers are included, such models have little success in realistically simulating the sub-surface thermocline bloom (e.g. Tett *et al*, 1993)

The most simple physical/biological models use fixed representations of seasonal temperature structure, and simulate nutrient flux through the relationship between wind speed and eddy diffusivity. Such models have successfully simulated the sub-surface chlorophyll maximum (e.g. Parker, 1986). At the other end of the spectrum, Sharples & Tett (1994) reported that their complex, turbulent diffusion model could also simulate the sub-surface chlorophyll maximum. This could only be achieved, however, when daily meteorological data rather than seasonal averages were used. This suggests that the changing stratification of the water column over short temporal scales is a crucial aspect in determining vertical chlorophyll distributions.

That the small scale changes in water column stratification is an important aspect in the control of biological variability was also identified by Ruardij *et al* (1997). Here, realistic simulations of seasonal chlorophyll distribution were only achieved when thermocline thickness was allowed to vary.

As described earlier, mesoscale atmospheric forcing alters mixing within the water column. Wind events increase the mixing of nutrients into the SML, resulting in elevated chlorophyll concentrations. Observations of this response have been described by Kiorboe & Nielsen (1990), for example, who observed a 3-fold increase in SML chlorophyll with a time lag of 5 days following the wind event. The bloom lasted for a further 4 days. Simulation studies of the phytoplankton response to wind events have also predicted elevated concentrations (e.g. Lenhart *et al*, 1995).

Variability over diurnal time-scales are also biologically important. Over the diurnal cycle, variations in nutrient supply due to convective mixing and irradiance lead to cycles of chlorophyll concentration. Such a relationship was modelled by Taylor & Stephens (1993), who predicted a diurnal chlorophyll variability of +/- 0.5 mg m^{-3}, which fitted well with the observed distribution. It was estimated that the inclusion of diurnal variability shifted the predicted onset of the spring bloom by about 1 week, and could account for the depth penetration of some spring blooms. In addition to supplying nutrients, physical forcing de-coupled trophic interactions, thereby reducing zooplankton grazing (Holligan *et al* 1984b).

An assumption made by simple biological models, including the Prestidge/Taylor model, is that the system is dominated by a single phytoplankton species. Seasonal succession of phytoplankton species, however, is significant in shelf seas. Biological models which include multiple phytoplankton species are capable of simulating such a succession (e.g. Ruardij *et al*, 1997).

Another assumption made by simple biological models, including the Prestidge/Taylor model, is that a single nutrient is limiting. This assumption may be invalid for some regions, but it appears reasonable at station E1 in the English Channel. Pingree *et al* (1977a) demonstrated that the nitrate to phosphorus ratio at E1 reduced during the summer months, indicating that nitrate was limiting. This conclusion is typical of shelf seas, and results from the slower regeneration rate of nitrogen compared to phosphorus (Ryther & Dunstan, 1971)

The Prestidge/Taylor model assumes that diffusion from the sediment is the single source of nutrients from outside the system. The flux is proportional to the difference between the variable BML concentration, and a fixed sediment concentration. A separate seasonal flux at E1, however, is likely to be associated with eastwards advection of nutrient rich Atlantic water during the winter. Furthermore, Davies *et al* (1992) concluded that sub seasonal scale atmospheric forcing also alters the external nutrient supply to E1, and Jordan & Joint (1998) observed unexplained nitrate pulses at E1 during the summer. Other modelling approaches consider nutrient sources in more detail. Benthic processes may be modelled explicitly (e.g. Blackford & Radford, 1995), and 2 or 3-D physical models provide estimates of nutrient sources due to advection (e.g. Chen & Beardsley, 1995).

Modelling the Spatial Distribution of Phytoplankton

Spatial distributions of phytoplankton in mid-latitude shelf seas are dominated by the presence of chlorophyll blooms at tidal fronts. The potential for vertical processes to cause such blooms was shown quantitatively by the 1-D modelling exercise of Tett (1981). This approach used a simple model of primary productivity and coupled with estimates of eddy diffusion.

As outlined earlier, the spring-neap cycle increases cross-frontal nutrient supply, causing elevated chlorophyll blooms at tidal fronts. Sharples (in press) used a 1-D turbulent diffusion model to assess the significance of this process. He concluded that frontal adjustment could result in an extra 6 mg m^{-3} chlorophyll in the bloom.

The spring-neap adjustment of the position of the tidal front is effectively a vertical process. It is therefore easily simulated using 1-D physical models. Within the context of 1-D physical/biological models, it is therefore convenient to assume that all cross-frontal nutrient supply to frontal chlorophyll blooms results from this process. As outlined earlier, however, advective mechanisms that are not included in 1-D models are also likely to be significant. To assess this problem, Sharples & Simpson (1996) used a 1-D turbulent diffusion model to show that earlier estimates of nutrient transfer due to the spring-neap cycle were ~50 % too low. Their new estimate led to simulations of chlorophyll enhancements due to vertical processes that were consistent with observations, implying that the other mechanisms are not as significant as previously thought. Furthermore, nutrient pulses associated with the spring-neap cycle have been observed directly (Morin *et al,* 1985, Morin *et al,* 1993).

Resolution of the relative significance of the various methods of cross-frontal nutrient transfer can only be gained by using biological models coupled to analytical 2 or 3-D physical models, including both heat flux and horizontal and vertical advection components. Such models (e.g. Franks & Chen, 1996) represent the current state of the art in the physical/biological modelling of shelf seas.

1.6 Summary and Scientific Trends

A number of physical/biological models of shelf seas have been developed, of varying complexity. Each has been capable of simulating some aspect of the observed temperature and chlorophyll distribution. In heuristic terms, the general agreement between 1-D model simulations and in-situ observations has indicated that vertical

processes dominate temperature and chlorophyll variability over the majority of shelf sea regions.

To verify and improve physical/biological models, there is an increasing need for consistent measurements of the in-water variability covering a number of scales. This requirement has been expressed by a large number of authors in recent years (e.g. Baretta *et al*, 1998, Franks & Chen, 1996, Blackford & Radford, 1995, Oreskes *et al*, 1994, Franks, 1995, Large *et al*, 1994). The current dearth of appropriate data sets for model verification is a major limitation in the development of operational marine system models (Lynch *et al*, 1995, and Smith, 1993). A separate but related requirement is the need for analytical techniques to measure model performance (Baretta, *et al*, 1998, Lynch *et al*, 1995). Standard methods would allow the performance of different parameter sets or different models to simulate a data base to be objectively determined.

Physical processes operating over mesoscale and diurnal scales are highly significant in controlling physical and biological variability. The measurement of in-water distributions over such scales is problematic. Modern oceanographic techniques, however, are providing observations with increasing resolutions. Remote buoys, such as the Plymouth Marine Bio-Optical Data Buoy (PlyMBODy, Pinkerton & Aiken, 1997), measure oceanographic variables over long time periods with a temporal resolutions of less than 10 seconds. The Undulating Oceanographic Recorder (UOR, Aiken & Bellan, 1990) measure depth profiles with a horizontal resolution of less than 1 km.

Satellite observations provide the ideal basis for comparisons of model simulations over large spatial scales. Sea surface temperature (SST) images have been used since the 1970's for this task (Le Fevre, 1986 and references therein). Simpson & Bowers, 1981, for instance, measured the frontal position from a time series of Advanced Very High Resolution Radiometer (AVHRR) SST images to estimate spring-neap frontal adjustment. The time series of measurements from the AVHRR is now reaching 20 years, and numerical techniques such as automated front detection (Cayula & Cornillon, 1992, 1995) have been developed. This data is now being used to track patterns of movement of tidal fronts (Mavor & Bisagni, unpublished). A further use of satellite SST data within primary productivity modelling has been to determine some empirical relationship between nitrate and SST concentrations. The retrieved nitrate concentration from SST images can then be used for input into productivity models (Dugdale *et al*, 1989, Morin *et al*, 1993)

Ocean colour remote sensing provides a synoptic measurement of biomass, usually empirically normalised to chlorophyll-a concentration. Coastal Zone Colour Scanner (CZCS) images were used by Holligan *et al* (1983) to monitor chlorophyll

concentrations at tidal fronts in the English Channel. Information on the spatial distribution of attenuation coefficients, which control the underwater light field, can also be retrieved from ocean colour images (Austin & Petzold (1981). CZCS failed in 1985, and its replacement, SeaWiFS, was not launched until September 1997. Due to the lack of ocean colour data between 1985 and 1997, there has been little effort to use ocean colour data to validate physical-biological models (e.g. Ishizaka, 1990). Recent work, however, has focused on the use of assimilation techniques to integrate SeaWiFS data with the output of physical/biological models (Fasham & Evans, 1995).

1.7 Objectives

It is well established that shelf-sea temperature and chlorophyll distributions are characterised by their response to the variability of external physical forcing (e.g. meteorology, tides), and that such responses can be explained using theoretical models.

Recent models have used theoretical concepts to provide diagnostic tools for shelf-sea research, and the Prestidge-Taylor physical/biological model represents one published example of this type. Before use in diagnostic or predictive applications, models must be thoroughly validated through comparison with observational data sets, and their limitations understood. Comparisons of model performance between different periods in the time domain and locations in the space domain are often used as model verification procedures. The aim of this thesis, however, is to analyse the performance of a given model at different scales of temporal and spatial variability, introducing an additional procedure for use during the verification of shelf-sea physical-biological models.

Due to sampling limitations of traditional oceanographic methods, the scope of many oceanographic data sets is restricted in terms of the scales of temporal and spatial variability that they represent. The use of such data for model verification, however, can easily lead to the following assumption: the ability of a given model to provide an adequate representation of the observed variability for a single data set is evidence that it provides a good representation of the system in general. This assumption is extended to formulate the null hypothesis used for this work:

"The ability of a given shelf-sea physical-biological model to simulate temperature and chlorophyll distributions at one scale of variability will be the same as its ability over all of the scales of variability defined by the scope of the model."

The above hypothesis requires qualification in two respects:

1. How is the scope of a model defined?

2. How can the performance of a model at a given scale of variability be measured?

For this thesis, the scope of the model is defined in terms of the environment and processes that the model was designed to simulate. In the case of the Prestidge-Taylor model, the scope covers shelf-sea waters in temperate latitudes (e.g. the shelf-sea region off the UK), for simulations of temperature, nutrient (nitrite + nitrate concentrations), and chlorophyll variability. Scope is additionally confined to the scales of variability that can be resolved by the model. The maximum temporal resolution of the Prestidge-Taylor model is 1 hour, and, whilst the model is 1-dimensional (i.e. spatial scales are not resolved), variability in 2-dimensions can be simulated by combining multiple model runs, each corresponding to a location along a transect, with a spacing of the order of 1 km.

The analysis of model performance for a given scale of variability requires comparison between model simulations, and some independent estimate of the 'real' variability over the same scale, as derived from observational data. In order to consider multiple scales of variability, a combination of multiple observational data sets, collected from different observational platforms, must be used. Furthermore, the observational data must be coincident in both time and space with available model simulations.

The final determination of model accuracy for a given scale of variability requires the statistical comparison of modelled and observational data. Simple statistical measures such as correlation coefficients can be calculated. However, for periodic signals, frequency spectra (determined by Fourier transforms of the original signal) can simplify complex observed/simulated signals into a small number of coefficients representing the phases, amplitudes and shapes of the dominant periodic waveforms contained in the signal. A comparison of spectral coefficients between modelled and observed data represents an additional measure of model performance to with direct relevance to the 'scales of variability' approach.

2. Methodology

The study region and its bathymetry are shown in figure 2.1. Within the study region three stations (E1, L4 and S2), linked by two transects, were identified as the focus for a more intensive investigation of variability. Station E1 has been sampled by many previous studies (as described in the introduction) and L4 is the site of an ongoing study (Laabir et. al., 1998). Station S2 was chosen to provide a contrast to E1 and L4 due to the presence of stronger tidal mixing at this site. The three stations were sufficiently close together to allow the sampling of all three within a day's boat trip.

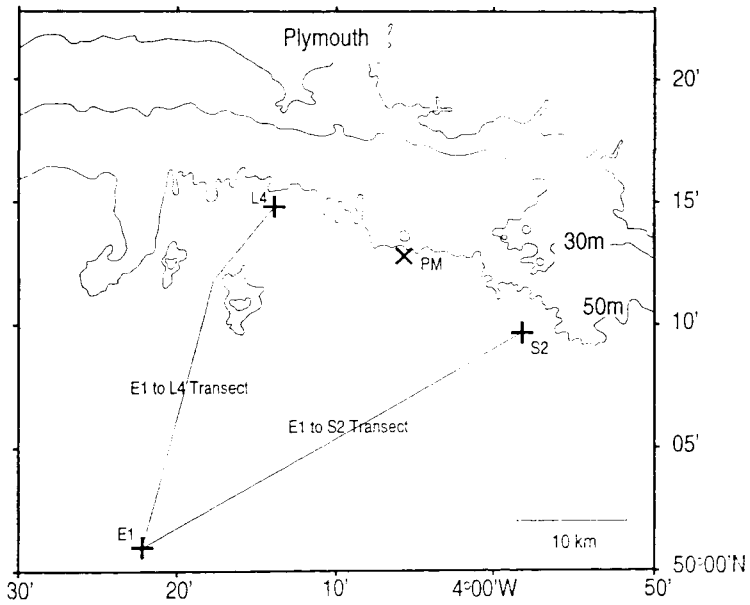

***Figure 2.1** – The study region. E1, S2 and L4 are study sites. PM is the site of PlyMBODy. Two transects, E1 to L4 and E1 to S2 are also marked.*

A field survey was designed such that the hydrographic and biological variability over the relevant scales could be resolved within a 1-year period. The observational techniques used are listed in table 2.1.

	UOR	PlyMBODy	Satellite
1 year	N	Y	Y
1 month	N	Y	Y
1 day	N	Y	N
20 km horizontal	Y	N	Y
40 m vertical	Y	N	N

***Table 2.1** – Analysis of the variability resolved by each observational platform used during the study. 'Y' indicates that the scale could be resolved, 'N' indicates that the scale could not be resolved. UOR is the Undulating Oceanographic Recorder; PlyMBODy is the Plymouth Marine Bio-Optical Data buoy.*

The Figure 2.2 shows the relationship between the main components of the project;

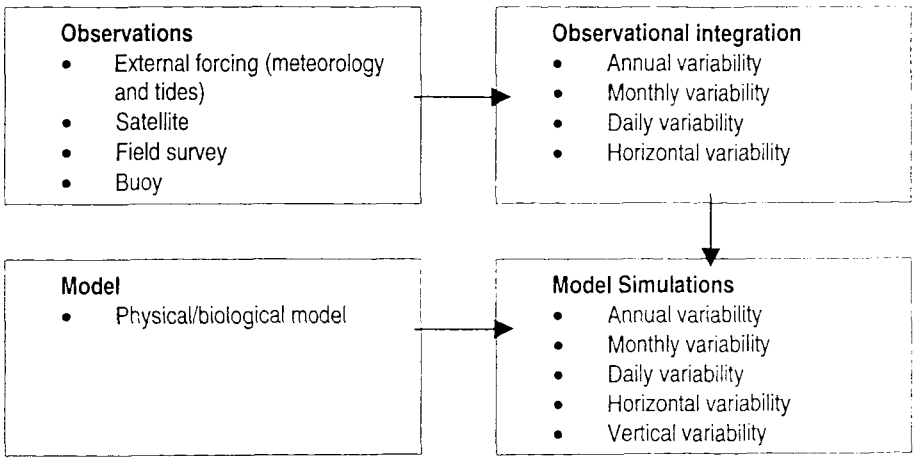

***Figure 2.2** – Flow diagram of the major project components.*

2.1 External Forcing

Meteorological Data

The meteorological fields that were of interest during this project are listed in table 2.2, listed in terms of atmospheric forcing variables. Measurements of the meteorological variables at hourly intervals for the years 1982 to 1997 were obtained from the UK Meteorological Office. Relative humidity was exceptionally supplied at 3 hour intervals. Hourly humidity was estimated by linear interpolation. In addition, any data that was missing due to sensor malfunction was also estimated by interpolation.

Data from two meteorological stations was used, Plymouth and Camborne (see table 2.2). The Plymouth station is sited at 50.35°N, 4.12°W at an altitude of 50 m. Camborne is sited at 50.22°N, 5.32°W at an altitude of 87 m, and is ~100 km WNW of Plymouth.

As there were no meteorological fields in common between the Plymouth and Camborne datasets, a direct comparison of the meteorological conditions at the two stations has not been possible. However, given the relative proximity of the two stations, their similar situations (each on high ground within a few hundred metres of the coastline), and the characteristic spatial scales of atmospheric variability in temperate regions (typically of the order of 100 km, Lenhart et al, 1995), it is assumed that the meteorological variability was of similar magnitude and phase for each station.

Meteorological conditions in the coastal zone are highly variable over short scales, where differential land-sea heating and coastal topography are highly significant. The common presence of an atmospheric front in the locality of the land/sea interface identifies a difference in prevailing meteorological conditions between the two regimes (Rotunno, 1994). Given this limitation, the atmospheric conditions at Plymouth and Camborne are assumed to be representative of the study region as a whole, simply due to the fact that no appropriate offshore meteorological data were available. As both meteorological stations were in near-coastal locations, no scaling factor was used to adjust wind speed measurements to their presumably higher offshore values (see, for example, Lavin-Perigrina, 1984, who used a factor of 1.3 for the Irish Sea).

Hourly meteorological data for each field (as supplied by the meteorological office) were then used to calculate mean daily and monthly values. Inter-annual monthly averages and standard deviations for each field were then calculated from the monthly averages for each year. Data processing was carried out using the Microsoft Excel spreadsheet package

Atmospheric Forcing Variable	Fields Required	Source
Air/sea heat exchange	Downwelling irradiance at the sea surface	Camborne MS
	Wind speed	Plymouth MS
	Relative humidity	Plymouth MS
	Cloud cover	Plymouth MS
	Mean sea level pressure	Plymouth MS
	Air temperature (dry bulb)	Plymouth MS
Wind mixing	Wind speed	Plymouth MS
Residual advection	Wind speed	Plymouth MS
	Wind direction	Plymouth MS
Photosynthetically active radiance (PAR)	Downwelling irradiance at the sea surface	Camborne MS

***Table 2.2** – Atmospheric forcing variables, the meteorological fields required for their estimation, and their source (MS refers to meteorological stations of the Meteorological Office).*

Tidal Data

Tidal data were supplied by B. Sinha and C. Griffiths (Plymouth Marine Laboratory) in the form of tidal ellipse properties, calculated from the model of Sinha & Pingree (1997), based on the European shelf sea model of Pingree & Griffiths (1978, 1981). Simulations of the semi-diurnal (M_2) cycles were used. The accuracy of these M_2 simulation (RMS error) is typically within ~2% of observations for both amplitude and phase (Sinha & Pingree, 1997).Simulations of the spring-neap (S_2) cycle were not available in time to be included in the thesis. The limitations of this omission are discussed in chapter 3.

The model was run over a 2.5' latitude 5' longitude grid (~5 km by 5 km) for the North West European continental shelf. This resulted in 64 individual grid points within the study region (8 in the x-axis, 8 in the y-axis). The method used to convert the ellipse properties into tidal currents is shown in equations 2.1a to 2.1i. The tidal ellipse characteristics for the study region are presented in Appendix 1. This includes values for the length of the major axis, ratio of the major to minor axes, phase, direction, tidal stream amplitude and mean cube tidal stream amplitude.

The tidal currents were calculated with a time step of 0.2 hr. These currents were integrated over a tidal cycle to calculate the mean current speed, and mean cubed current speed.

Where tidal currents at a point or along a line were required, these were calculated from the regular grid values using spatial interpolation.

$$a_u = \tfrac{1}{2}(a-b)\cos(\phi - g) + \tfrac{1}{2}(a+b)\cos(\phi + g) \quad (2.1a)$$

$$b_u = \tfrac{1}{2}(a-b)\sin(\phi - g) - \tfrac{1}{2}(a+b)\sin(\phi + g) \quad (2.1b)$$

$$a_v = \tfrac{1}{2}(a-b)\sin(\phi - g) + \tfrac{1}{2}(a+b)\sin(\phi + g) \quad (2.1c)$$

$$b_v = \tfrac{1}{2}(a+b)\cos(\phi + g) - \tfrac{1}{2}(a-b)\cos(\phi - g) \quad (2.1d)$$

$$u = a_u \cos\sigma t + b_u \sin\sigma t \quad (2.1e)$$

$$v = a_v \cos\sigma t + b_v \sin\sigma t \quad (2.1f)$$

$$U = \sqrt{u^2 + v^2} \quad (2.1g)$$

$$\overline{U} = \int_0^{12.4\,\mathrm{hr}} \left(u^2 + v^2\right)^{1/2} dt \quad (2.1h)$$

$$\overline{U} = \int_0^{12.4\,\mathrm{hr}} \left(u^2 + v^2\right)^{3/2} dt \quad (2.1i)$$

- Given tidal ellipse properties; a is major axis (cm s^{-1}); b is minor axis (cm s^{-1}); g is phase; θ is direction (10 times degrees north).
- a, b, g & ϕ are used to calculate u (east-west tidal velocity) and v (north-south tidal velocity) (equations 1.1a to 1.1f).
- u & v are used to calculate tidal speed ($|U|$) (equation 1.1g), which is integrated with respect to time over an M2 tidal cycle (12.4 hr) to give mean tidal stream amplitude ($\overline{U}$) (equation 1.1h), and the mean cubed tidal stream amplitude ($\overline{U^3}$) (equation 1.1i).

Depth Data

Fully processed bathymetric data were provided by Mr S. Gibson, Plymouth Marine Laboratory. The data coverage was 50 to 50.3°N, -4.6 to -3.7°E over a 1 by 1 km grid. The original data sources were from Admiralty charts, and various other 3rd party hydrographic surveys.

2.2 Archived Data for Station E1

Data held on the computer archive of the Marine Biological Association of the UK were recently updated and archived with the British Oceanographic Data Centre, at the Proudman Oceanographic Laboratory, Bidston, Mersyside. Information on the methods used for data collection are detailed in Jordan & Joint (1998) and Southward (1995).

Whilst oceanographic data has been collected at E1 since 1902, for this project, only data from the years 1974 to 1987 were considered. This is the period was chosen as it is the period over which monthly nitrate measurements were made at E1. In addition to nitrate measurements (made using the procedure of Wood *et al*, 1967), temperature

measurements (unreported methods) and chlorophyll concentration measurements (made using the procedure of Yentsch & Menzel, 1963) over the same period were also used. The data were averaged to produce inter-annual monthly means and standard deviations.

2.3 Satellite Remote Sensed Data

The preliminary processing of all satellite remote sensed data used during this project had been carried out by the Natural Environmental Research Council's Remote Sensing Data Analysis Service (RSDAS). Thermal images were obtained as maps of sea surface temperature distribution, and ocean colour images as maps of chlorophyll distribution.

Advanced Very High Resolution Radiometer (AVHRR)

The AVHRR produces images of sea surface temperature (SST) with a sensitivity of 0.05°C to 0.12°C, and an uncertainty of 0.2°C to 0.5°C (Robinson, 1985). For a description of the AVHRR series of sensors, see Robinson (1985).

The automatic data processing and archiving scheme used at RSDAS is described in Miller *et al* (1997). Of the various levels of processing available, the one used was level-2 local area coverage (LAC) data. The images had been geolocated, cloud screened and annotated. Sea surface temperature (SST) had been calculated from radiometer response using a 3-band algorithm (see Miller et al, 1997).

The study region for this project fell within a larger region, extending from 6° to 2°W, 48° to 51° N, and termed the "PACE" region for historical reasons. AVHRR images covering the PACE region have been routinely archived at RSDAS since mid 1996. During 1997, the four operational AVHRR equipped satellites; NOAA 14, 12, 11 and 9 collected a total of either 5 or 6 overpasses of the PACE region per day, a total of ~2000 per year.

Processing of the AVHRR data was required in addition to that performed by RSDAS. The extra procedures, used for screening each supplied image, are listed below:

- Images were collected between 23:00 to 09:00 GMT (unless indicated otherwise). Daytime images, which may have been contaminated by localised heating of the surface skin (Robinson 1985), were therefore discarded.
- The study region was greater than 40% cloud clear.

- No cloud was present within a 20-km radius of an individual pixel.
- If data deviated significantly from the underlying trend, then the image was visually inspected for evidence of cloud contamination that had not been picked up by the cloud screening algorithms, and rejected if cloud effects were detected.
- ~150 images were identified as reliable, and these are detailed in Appendix 2.

Temporal data from four discrete positions within the PACE region were available (E1, L4, S2 and the PlyMBODy site, see figure 2.1). SST data from the image pixels corresponding to the discrete positions were extracted from each image. These measurements represent the average SST over the pixel's footprint (~1 km^2). The accuracy of the RSDAS geolocation is typically to +/- 1 pixel, (1 km). The spatial uncertainty of the pixel with respect to the discrete position was therefore +/- 2 km.

Spatial data from 2 transects were also extracted (E1 to L4 and E1 to S2, see figure 2.1). To achieve this, the latitude and longitude at 0.1 km intervals along each transect was calculated. Each location fell within an AVHRR pixel. The temperature value assigned to this pixel was extracted and associated with the location. A single pixel could therefore provide a number of SST values along each transect (up to 15). The latitude and longitude values were then converted into a measure of distance along each transect (see equation 2.2). The procedure was designed by the Author, and the computer program written by the RSDAS group using IDL software.

$$D = \sqrt{((y_{E1} - y)A)^2 + ((x_{E1} - x)B)^2} \qquad (2.2)$$

Where: D is distance from E1 (km): y_{E1} is decimal latitude of E1: y is decimal latitude of point on transect: A is distance in km per degree latitude at E1 (111.1 km/°Lat): x_{E1} is longitude of E1; x is decimal longitude of point on transect; B is distance in km per degree longitude at E1 (71.4 km/°Lon).

Satellite images are generally presented as bitmaps, where the area corresponding to an individual pixel is assigned a colour from a pre-determined palette, depending on its temperature value. For areas with a small number of pixels, however, the blocks of colour make the temperature distribution appear angular and such images are difficult to interpret. To avoid this problem, SST data for the study region was extracted from the 8-bit array in tabulated ASCII format, identified using the pixel centre positions. SST data could then be presented as contours of temperature against longitude vs. latitude.

Sea-viewing Wide Field of view Sensor (SeaWiFS)

SeaWiFS provides images of ocean chlorophyll concentration and diffuse attenuation coefficients, over the upper optical depth of the water column. For a description of the SeaWiFS sensor, see Hooker et al (1992).

RSDAS are currently developing their operational processing of SeaWiFS images (Lavender, pers. com.). At present, the 2 band ratio algorithm of O'Reilly et al (1998) is being used. This type of algorithm has proved successful at estimating chlorophyll concentrations where phytoplankton and associated products are the dominant optically active material in the water column (Clark, 1981), which are termed 'case 1' waters (Morel & Prieur, 1977). Estimates are less accurate at higher chlorophyll concentrations (>1.5 mg m^{-3}, Gordon et al, 1983), or where materials that have not been formed in-situ are optically significant (Gordon & Morel, 1983, termed 'case 2' waters). Whilst empirical algorithms for case 2 waters have been determined (e.g. Voillier & Sturm, 1984), the calibrations are site specific. For the study region, no site-specific calibrations were available. The reliability of chlorophyll estimates are therefore questionable when case 2 waters are prevalent in the study region. These conditions will tend to occur when water columns are well mixed, or when surface phytoplankton blooms are present.

The SeaWiFS sensor collects an average of 1.5 overpasses day^{-1} at 50° latitude. Data have been acquired since September 1997. Data from several overpasses of the study region collected throughout 1998 are presented in this thesis. These are maps of the distribution of chlorophyll concentration within the Western English Channel, as calculated using the O'Reilly et al (1998) algorithm..

2.4 Field Survey Programme

A sampling strategy was developed, consisting of the deployment of appropriate sampling equipment along the route of a standard boat track (figure 2.1). The major logistical characteristics of the standard track are listed in Appendix 3. The PML vessel, R.V. Squilla was used for all sampling events, and ship's data are listed in Appendix 4. Eight individual days of sampling were carried out by the Author between June and September 1997. The cruise track followed for each of these events are presented in Appendix 5.

The measurement techniques used during the project are summarised in table 2.3. *In situ* data were collected by deployment of the Plymouth Marine Laboratory's

Undulating Oceanographic Recorder (UOR). Surface water samples were collected from the R.V. Squilla's pumped sea water supply, and subsurface samples using NIO water bottles. Data collected from the Plymouth Marine Bio-Optical Data buoy (PlyMBODy) were also used during this project, and its position is marked on figure 2.1. The scientific logs for each of the sampling events are presented in Appendix 6, and the water sampling logs in Appendix 7.

Sampling Platform	Measurement Type	Measurement Technique	Measurement Variables
UOR	Physical	Thermistor	Temperature
	Optical	Transmissometer	Beam attenuation, c(670)
	Biological	*In-vivo* fluorescence	Chlorophyll concentration
Water Samples	Biological	*In-vitro* fluorescence	Chlorophyll concentration
PlyMBODy	Physical	Thermistor	Temperature
		Conductivity meter	Salinity
	Biological	*In-vivo* fluorometer	Chlorophyll concentration

***Table 2.3** – Measurement Techniques Used During the Field Programme. UOR is the Undulating Oceanographic Recorder; PlyMBODy is the Plymouth Marine Bio-Optical Data buoy; Detailed descriptions of the various sensors are as described later this chapter.*

2.5 Undulating Oceanographic Recorder (UOR)

The Undulating Oceanographic Recorder (Aiken & Bellan, 1990), is a towed sampling platform which undulates through the surface layer of the water column. The UOR was equipped with a suite of instruments, measuring depth, temperature, salinity, *in-vivo* chlorophyll fluorescence, beam attenuation, upwelling radiance and downwelling irradiance. The UOR is the focus of an ongoing development programme. The exact configuration used during the project is therefore described here. A schematic diagram of the UOR layout as used is shown in figure 2.3.

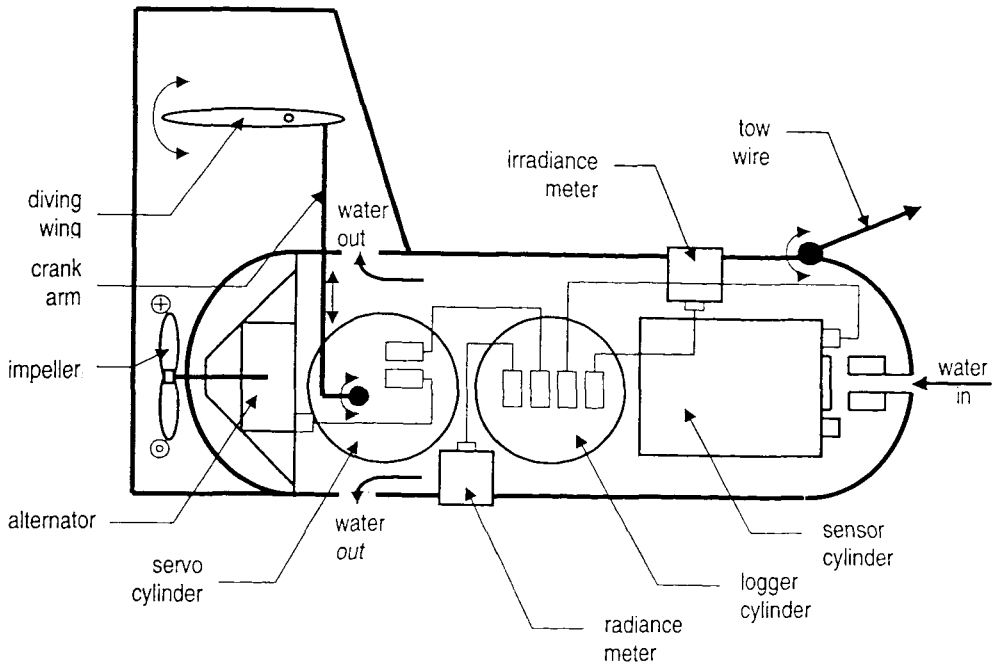

***Figure 2.3** – Schematic diagram of the Undulating Oceanographic Recorder (UOR) showing mechanical and sensor configuration used during the project..*

Depth Control

Changes in UOR depth are controlled by the attitude of a diving wing, which is pre-programmed with respect to time. The wing is attached to the servo via a crank arm. As the arm moves vertically, the wing pivots and its attitude changes. The vertical movement of the arm is produced through rotation of an electric motor within the servo cylinder.

Once deployed, the wing is rotated to maximum dive, and held until the UOR reaches a pre-set start depth, detected by an integral pressure sensor. The wing angle 'dive' programme is then initiated, and run until maximum depth is reached, whereupon control is transferred to the climb programme.

Figure 2.4 is a typical example of dive wing attitude and depth against time for a UOR undulation, with the depth range set from 5 to 40 m. The UOR generally overshoots its pre-set depths by up to 10 m.

Over the course of the project, minimum depths were varied from 0 to 5 m, and the maximum depth held at 40 m. The wing angle programme used resulted in typical undulation frequencies of 1 each 2 min, giving an undulation pitch length of 0.6 km at a towing speed of 10 kts. The relative changes in wing angle attitude with time are user-

adjustable before UOR deployment. The settings used for the UOR as used during this project are shown in Appendix 8.

In addition to the pre-programmed wing angle programme, undulation characteristics are strongly influenced by the speed of the boat through the water, (determined by water currents and prevailing meteorology) and speed of the UOR body through the water (determined by boat speed and cable length). Towing speeds were typically 8 to 10 kts, and cable lengths 100 to 200 m (8 mm unfaired steel cable)

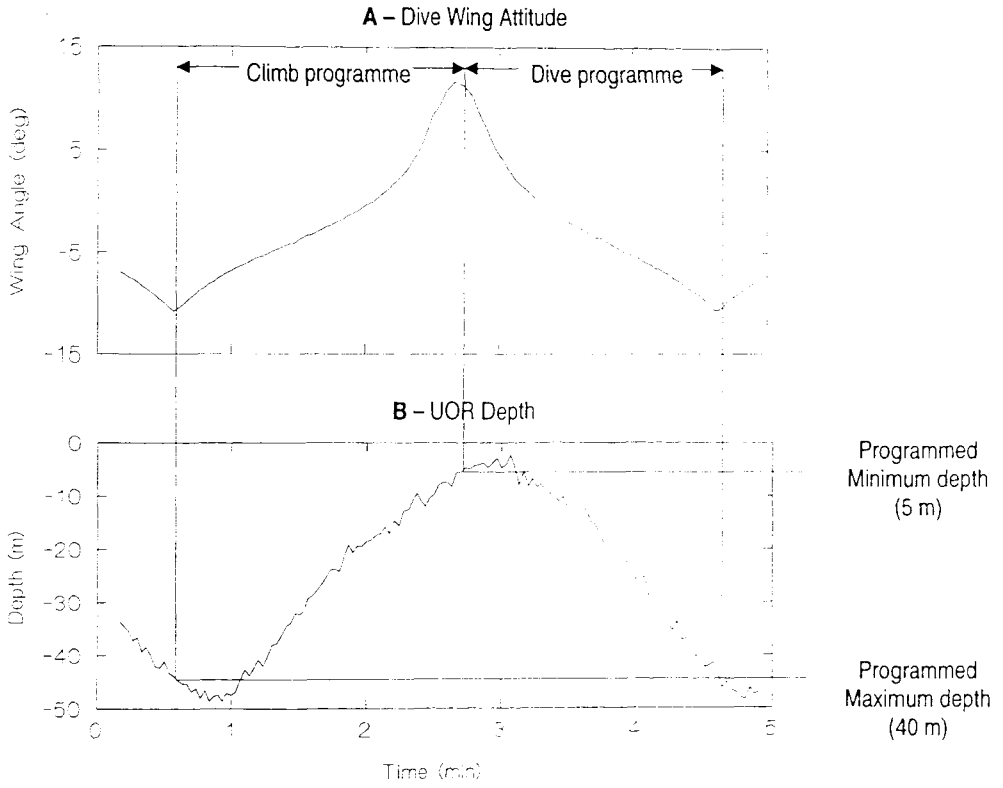

***Figure 2.4** – An example of the UOR depth control, the data was collected on 28th August 1996: **A:** dive wing attitude, **B:** UOR depth.*

Instrumentation

Temperature, salinity, depth and chlorophyll fluorescence were measured by a linear response platinum resistance thermometer, inductive coil resistance meter, pressure sensor and fluorometer (Lorenzen, 1966), respectively. These sensors (manufacturers unknown) were housed in a single sensor cylinder developed and built at Plymouth Marine Laboratory. The fluorometer excitation flash peaked at 425 nm (200 nm bandwidth) and was detected at 685 nm (30 nm bandwidth).

Beam attenuation coefficient (defined in equation 2.3), was measured by a beam transmissometer, mounted in the UOR nose.

$$I(z,\lambda) = I(0,\lambda)e^{-zc(\lambda)}$$
$$\Rightarrow c(\lambda) = \frac{\ln I(0) - \ln I(z,\lambda)}{z} \qquad (2.3)$$

Where; $I(0,\lambda)$ is the intensity of the emitted light source at wavelength λ; $I(z,\lambda)$ is the light intensity at distance z from the source; and $c(\lambda)$ is the beam attenuation coefficient at wavelength λ. After Austin & Petzold, 1977

Two transmissometer systems were used, a Chelsea Instruments Alpha Tracka II, and a SeaTech 25 cm Transmissometer. Both instruments had 25 cm path lengths and 670 nm light sources.

Downwelling irradiance was measured by a Satlantic OCI-200 light meter. This measured the radiant energy falling on a flat collector, 86 mm in diameter. The instrument response was calibrated with respect to the average cosine of the hemispherical radiance field. As the sensor was mounted in the UOR pointing vertically up, its measurement can be mathematically described as downwelling spectral irradiance, $E_d(\lambda)$, as shown in equation 2.4;

$$E_d(\lambda) = \int_{2\pi}^{0} L(z,\lambda,\theta,\phi)\cos\theta d\omega$$
$$d\omega = \int_{\theta=0}^{\pi/2}\int_{\phi=0}^{2\pi} d\theta d\phi \qquad (2.4)$$

Where; λ is the wavelength; θ is the zenith angle; ϕ is the azimuth angle.

OCI-200 measured light in 7 discrete wavebands (10 or 20 nm spectral bandwidth), isolated using interference filters. 6 of these bands corresponded to the wavelengths used by the SeaWiFS ocean colour satellite sensor.

Vertical attenuation coefficients are calculated from a regression of the measured light and depth data as shown in equation 2.5.

$$K_d(z,\lambda) = -\frac{\Delta \ln E_d}{\Delta z} \qquad (2.5)$$

Where: K_d is the diffuse attenuation coefficient of downwelling irradiance; z is the water depth.

Of the 6 measured wavelengths, most attention was placed on the 490 nm channel. This wavelength was chosen as it is strongly modified by the presence of suspended phytoplankton in the watercolumn due to its proximity to the chlorophyll-a absorption maximum at 443 nm (Sathyendranath & Morel, 1983), but is relatively unmodified by

pure water (Smith & Baker, 1978). The 490 nm wavelength has also been the focus of other studies (e.g. Austin & Petzold, 1981)

Due to the non asymptotic nature of the underwater light field, a radiometer's attitude with respect to the vertical is an important consideration. An arbitrary limit of 10° from the vertical (Mueller & Austin, 1995) was used to screen the light data. Values of irradiance for which the tilt exceeded 10° were rejected. The attitude of the UOR was measured by pitch (angular deviation from horizontal of the UOR body parallel to the direction of tow) and roll (deviation perpendicular to the line of tow) sensors mounted in the UOR servo cylinder. The tilt was calculated as shown in equation 2.6.

$$Tilt = \mathrm{a}\cos\left[\frac{1}{\sqrt{(\tan p)^2 + (\tan r)^2 + 1}}\right] \qquad (2.6)$$

Where; p is pitch; r is roll.

A single on-board data logger was used to record measurements made by all of the UOR instruments. Up to 21 analogue input channels are digitised and then stored in solid state memory. The frequency of sampling the analogue signal is user specified and was 0.5 Hz during this project.

Two levels of digitisation are available; 10 bit (scale from 0 to 1024 counts), and 12 bit (0 to 4096 counts). The analogue input range is 0 to 5 V, which is digitised with resolution equivalent to 4.8 mV for 10 bit and 1.2 mV for 12 bit. To reduce electrical noise, the input is over sampled by ×32 for 10 bit and ×8 for 12 bit to give a maximum total of 32768 counts. 16 input channels are 12 bit, and 5 to 10 bit as shown in table 2.4;

Each sample record contains 21 data values (one for each signal), each requiring 2 bytes solid state memory. The 1 Mbytes logger memory can therefore store 2.50×10^4 records. At a sampling frequency of 0.5 Hz, the memory will last for approx. 14 hr.

Cha-nnel	Signal	Dig'n (Bit)	Cha-nnel	Signal	Dig'n (Bit)	Cha-nnel	Signal	Dig'n (Bit)
01	Depth	10	08	$E_d(490)$	12	15	$L_u(490)$	12
02	Temperature	12	09	$E_d(510)$	12	16	$L_u(510)$	12
03	Conductivity	12	10	$E_d(555)$	12	17	$L_u(555)$	12
04	Fluorescence	10	11	$E_d(665)$	12	18	$L_u(665)$	12
05	Transmission	10	12	$E_d(683)$	12	19	$L_u(683)$	12
06	$E_d(412)$	12	13	$L_u(412)$	12	20	Pitch	10
07	$E_d(443)$	12	14	$L_u(443)$	12	21	Roll	10

***Table 2.4** – UOR logger input channels showing signal input and digitisation level (Dig'n).*

2.6 UOR Data Calibration

Throughout the project, extensive data comparison was required, both within and between measurement techniques. The Author was therefore required to design and implement a careful calibration procedure for the UOR measurements. This procedure is described in detail below.

Calibration coefficients were required to convert digital data values into standard measurement units. These coefficients were expressed as linear regressions.

Numerical standard uncertainties were calculated from the calibration data following the protocol of Taylor & Kuyatt (1994). It was assumed that the values of the error ("real" value minus the measurand) were approximately normally distributed about the mean error, and that the unknown "real" value was believed to lie in the interval defined by twice the standard deviation of the standard uncertainty with a level of confidence of approximately 95 percent.

The details of individual regressions carried out during this project are included in Appendix 9. This appendix also lists the coefficients used during the data processing of each UOR deployment.

Analogue to Digital Conversion

Logger cylinder response was calibrated against analogue signals in the range of 0 to 5 V, measured by a digital voltmeter (Black Star 4503). Each channel was calibrated independently, and results merged to calculate coefficients for each digitiser (10 and 12 bit). If certain channels exhibited statistically different responses to the mean, separate coefficients were calculated. Standard uncertainty of logger cylinder response was calculated as 0.002 V (12 bit) and 0.004 V (10 bit)., with sensitivities of 0.001 and 0.004 V respectively.

Depth

Sensor and servo cylinder pressure gauges were calibrated using compressed air over the range of 0 to 200 psi. Pressure measurements were made using a pressure gauge (Standard Tech. Gauge, Brandenberg Gauge Co.). Sensor cylinder voltage outputs were measured by a digital voltmeter (Black Star 4503). The standard uncertainty of depth measurements was 0.7 m (sensor cylinder), and 0.5 m (servo cylinder), with a sensitivity of 0.1 m

Temperature

The sensor cylinder thermistor was calibrated in a stirred water bath over a temperature range of 0 to 35°C. Temperature measurements were made using a digital thermometer (Cormack Microprocessor Thermometer) optimised using standard mercury thermometers (ZEAL BS1900 0-10° and 10-20°). Voltage outputs were measured by a digital voltmeter (Black Star 4503). Standard uncertainty of temperature measurement was calculated as 0.075°C, with a sensitivity of 0.01°C.

In-Vivo Fluorescence

Fluorometer response was calibrated by regressing *in-situ* fluorescence measurements against contemporaneously collected discrete chlorophyll concentrations (measured by the *in-vitro* fluorescence method detailed later). Most of the discrete water samples (10 to 30 per sampling event) were taken from 2-m depth, and a smaller number (8 per event) from 5 and 40 m, following the procedure also described later.

The closest *in-vivo* measurements to each water sample were identified, and averaged over a 1 m depth interval. The horizontal uncertainty of each match up was +/-1 km, and the vertical accuracy was between +/-1 m and +/- 8 m depending on the sampling event. In regions of high chlorophyll gradient, the spatial deviation between the water sample and the *in-vivo* measurement caused a high degree of scatter in the calibration. For instance, those events where the vertical uncertainty was >5 m (e.g. 10th and 11th July 1997) were not included in the calibration. Reliable data from all sampling events for a specific UOR sensor cylinder were pooled, and a single set of calibration coefficients determined. Regressions for the two cylinders (JA4 and ARE1) used during the 1997 sampling events are shown in figure 2.5. The scatter evident in the regressions is due, to some extent, to the differences in fluorescence response per unit chlorophyll with respect to phytoplankton speciation (Pingree et al, 1982) and ambient light levels (Prezlin & Ley, 1980). No corrections were made to take into account either of these factors. The fluorescence response is therefore expected to change both within and between sampling events.

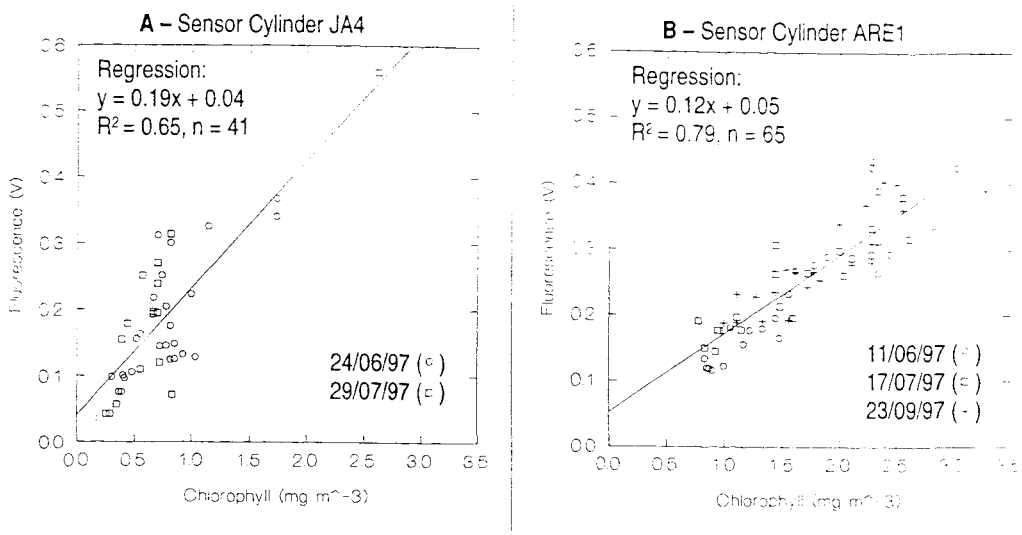

***Figure 2.5** – Example calibrations of the UOR's in-vivo fluorometers against discrete chlorophyll measurements (determined by in-vitro fluorescence) for two separate UOR sensor cylinders: **A:** Sensor cylinder JA4. **B:** Sensor cylinder ARE1.*

Radiance and Irradiance

Light meters were calibrated following the protocols of Muller & Austin (1995). Response to light intensity from a standard light source (FEL 1000 W) was measured by a digital voltmeter (HP 34401A multimeter) for each spectral band. The spectral response of each band was determined using a monochromator (Monospek 600). The sensor acceptance angles were also measured.

Beam Attenuation

The transmissometer response to air calibration and dark voltage (detector obscured) were carried out as follows: The optical windows adjacent to the source and detector were cleaned (isopropyl alcohol) and the output measured (using a digital volt meter, Black Star 4503). This represented 100% transmission in air (V_{air}). The path of the light beam was blocked, and the voltage measured, representing 0% transmission (V_{blank}). The equation for converting from output of a 25 cm path length transmissometer (V_{water}) to in-water values of c(670) is shown in equation 2.7.

$$e^{-c(670)z} = \frac{0.913V_{air} - V_{blank}}{V_{water} - V_{blank}} \qquad (2.7)$$

$$\Rightarrow c(670) = 4[\ln(0.913V_{air} - V_{blank}) - \ln(V_{water} - V_{blank})]$$

In pure water, $c(670)$ is 0.364 m^{-1} (Chelsea Instruments, 1990), hence an immersion correction factor of 0.913 is applied to V_{air}.

JGOFS measurement protocols (1995, pp.15), report significant temperature bias in c(670) measurements of SeaTech 25 cm transmissometers. This bias was not apparent in either the calibration or the deployment data, and was therefore considered insignificant during this project.

Tilt

Servo cylinder pitch and roll sensors were calibrated against known angles in the range of -25° to 25°, measured using a vernier protractor. The standard uncertainty of pitch and roll measurements was 1°.

2.7 UOR Data Processing

Data processing was a major consideration with respect to the UOR data. A significant advantage of using a central logger to store raw data is that all variables share a common time stamp, and data can therefore processed simultaneously. Due to the developmental nature of the instrument, processing procedures have been neither formalised nor documented previously. During the course of the project, an entirely new data processing procedure was developed. A novel aspect of the procedure was the introduction of a standard navigation identifier based on the standard boat track. This identifier allowed direct spatial comparison between repeats of the boat track, remote sensed imagery, and spatially resolving models. A further novel aspect was the calculation of water column summary data for each vertical profile, based on a 3-layer estimation of water column structure. Data of this type can be directly compared with output from the Prestidge/Taylor 3-layer model described later.

The personal computer package "Systat" was used for all data processing. The computer code written for the task by the Author (in Systat Basic) is shown in Appendix 10. The processing scheme is presented using example data, which was collected on 11th September 1997 between 10 and 11 GMT.

Stage 1 - Calibration

Data was downloaded from the logger into a personal computer, and saved as an ASCII text file. The typical file for a repeat of the standard track contained 10 000 records for each of the 21 measured variables. The text file was converted into Systat data format (conversion program supplied by Mr G. Moore, PML). The raw data (in digital counts) was converted into standard units for each signal variable. This was achieved using the linear calibration coefficients listed in Appendix 9.

Each record at this stage of the processing was identified by date, time of day (GMT), and depth fields. Example plots of depth and temperature against time of day are presented in figures 2.6A and B. The UOR undulated to a depth of 40 m with a cycle duration of 5.5 min. The apparent minimum depth (2.5 m), however, requires some qualification: The UOR logger cylinder operated over a voltage range of 0 to 5 V. The output of the depth sensor used intercepts 0 V at 2.5 m depth (see the calibration coefficients, Appendix 9). Sensor output at depths less than 2.5 m were therefore logged as 2.5 m. This problem did not affect depths greater than 2.5 m or any of the other depth sensors listed in Appendix 9.

Stage 3 – Identification of Vertical Profiles

The UOR depth data was smoothed using a 40 point running mean. Turning points were then identified by numerical differentiation. Vertical profiles within the continuous data stream were separated using the turning points. The average time stamp of each profile was calculated, and assigned to each record within a profile.

Quality control procedures were then carried out. External consistency checks involved comparing data with expected values. Automatic internal consistency checks, e.g. screening light data against tilt, were also carried out. Final quality control involved the detailed visual inspection of the data set.

Figures 2.6C and D show examples of depth and temperature data at this stage in processing. The spatial resolution of the vertical profiles was ~0.8 km. The deviation between profile position and the standard transect did not exceed 0.1 km in this case.

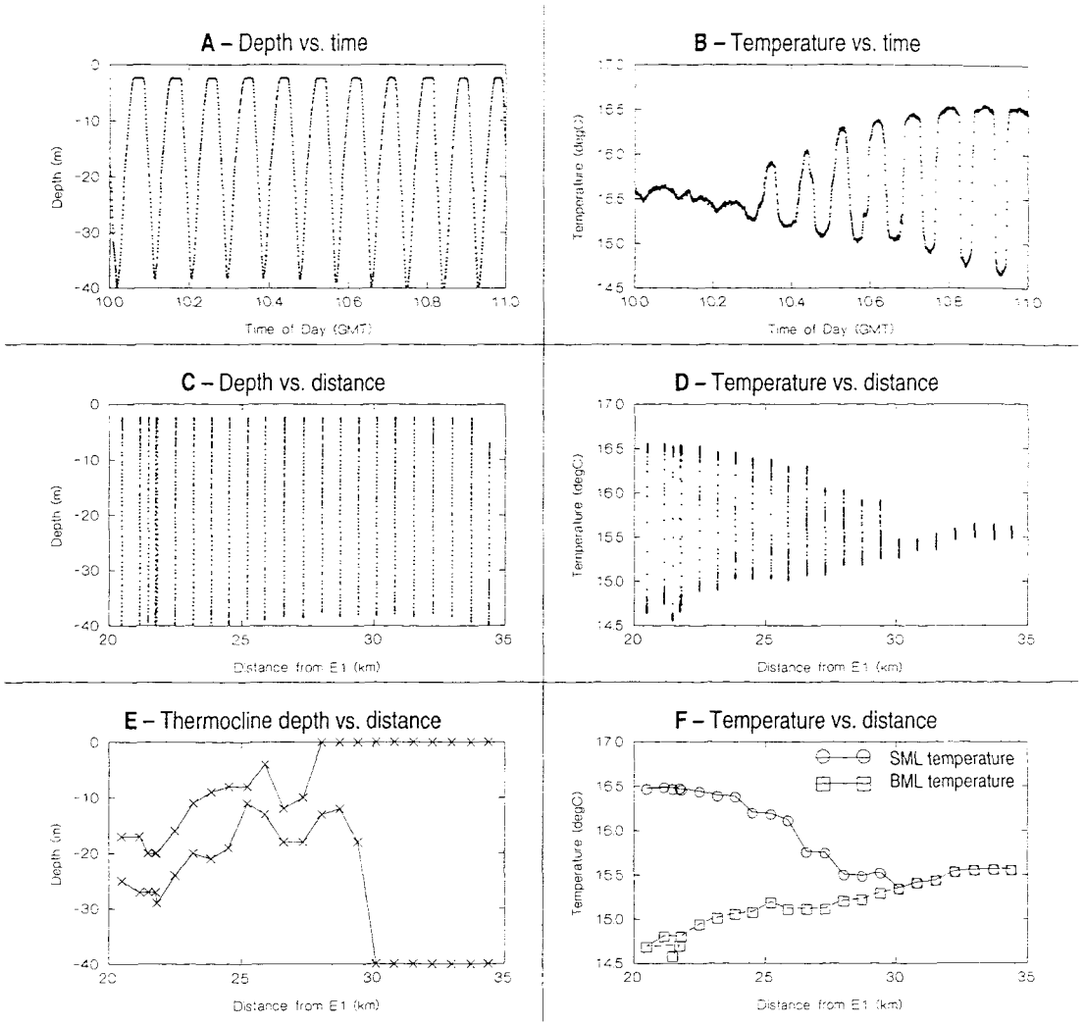

***Figure 2.6** – An example of the UOR processing scheme. Data is from 11th Sept '97, 10:00 to 11:00 GMT:*

***A:** depth vs. time, **B:** temperature vs. time **C:** depth vs. distance from E1 (E1 to S2 transect), **D:** temperature vs. distance from E1 (E1 to S2) **E:** thermocline depth vs distance from E1, **F:** temperature vs. distance from E1.*

Stage 4 – Calculation of Water Column Summary Data

The water column can be visualised as three discrete layers, the surface mixed layer (SML), thermocline and bottom mixed layer (BML). Each temperature profile was used to determine the vertical extent of each layer. Automated procedures for extracting layer depths (e.g. with a change in temperature of 0.2°C from surface values, Marra & Ho, 1993) can be inaccurate due to noise in the data. As a result, the layer depths here were estimated by inspection. Such a procedure obviously introduces a degree of subjective error to the analysis, mitigated in part by the fact that all of the profiles were analysed by the same person, and therefore assessed in a consistent way. Example profiles are presented in figure 2.7.

Once determined, the layer depths were digitised, and merged with the UOR data. The average temperature, chlorophyll and beam attenuation was then calculated for each layer of each profile. In an effort to reduce the bias caused by uneven depth distribution of UOR measurements, the data had previously been merged onto a regular depth grid, with a vertical resolution of 1 m.. Examples of thermocline depths and temperature data in this final form are presented in figures 2.6E and F.

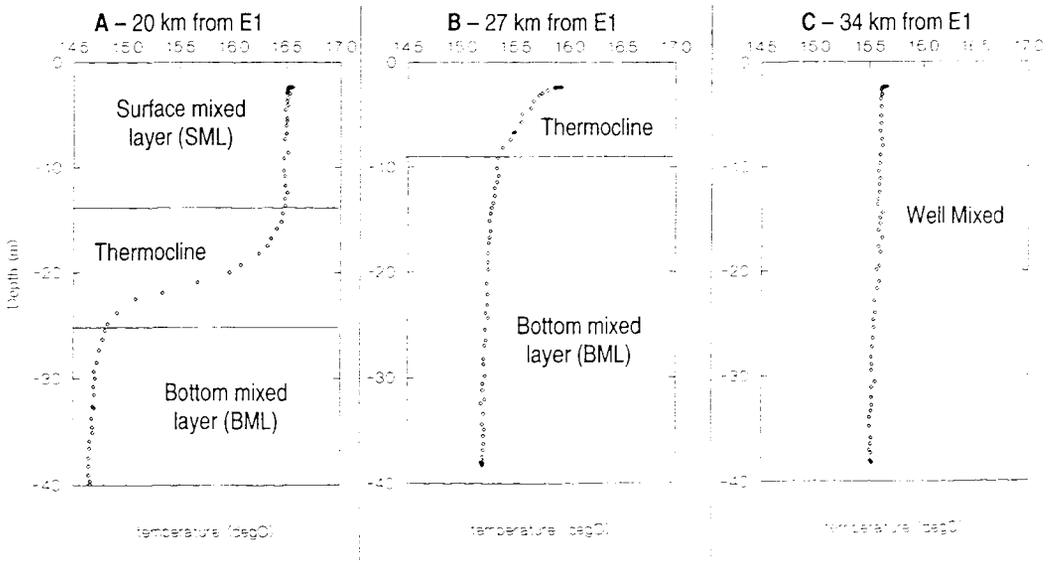

***Figure 2.7** – Examples of vertical temperature profiles collected by the UOR, and their separation using the 3-layers simplification of water column structure. Data is from 11th Sept 1997:*
***A:** 20 km from E1.* ***B:** 27 km from E1.* ***C:** 34 km from E1.*

2.8 WATER SAMPLING

Two different water sampling strategies were used during the field programme:

- Underway sampling of the surface water from the R.V. Squilla's pumped sea water supply, whilst the boat was steaming. The intake depth was at 2 m:
- Samples from two water column depths (5 and 40 m), using National Institute of Oceanography (NIO) 10 l water bottles.

For both pumped and water bottle collection, water samples (1 l) were taken and filtered (4.5 mm GF/F filters, nominal pore size 0.7 μm, pressure < 150 mbar). Glass fibre GF/F filters have been shown to retain the vast majority of chlorophyll containing particles in natural sea water (Chavez et al, 1995). The pressure filtration apparatus is shown schematically in figure 2.8. The filtration frame held six bottles, which were used simultaneously driven by an oil free pump (GAST model DOA-702). The filters were stored at -4°C in a freezer (where the chlorophyll concentration will not change significantly for several days, Gieskes & Kraay, 1983). Each sample was stored within 5 minutes of filtration.

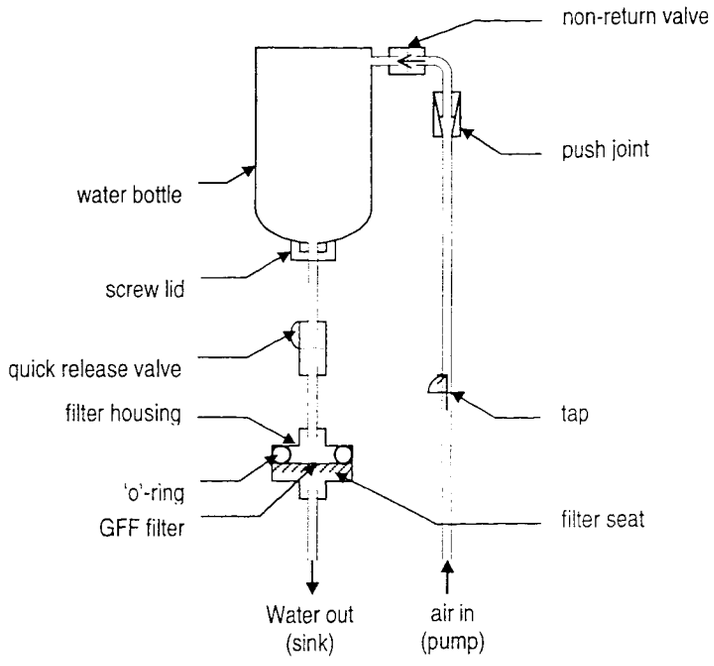

***Figure 2.8** – A schematic diagram of the pressure filtration apparatus used for the separation of suspended matter from water samples.*

In-vitro fluorescence

Chlorophyll concentrations were determined using the *in-vitro* fluorescence procedure of Yentsch & Menzel, (1963). The analysis was carried out within 48 hours of collection. Pigments were extracted from the filter by immersing in 90 % acetone (10 ml) for 24 hrs at -4°C, whereupon the extraction liquid was decanted. The fluorescence of the extract (~5 ml) was measured (Turner Designs Model 10 Series fluorometer) before and after the addition of 2 drops of 10 % HCl. The equation used for converting fluorescence measurements into chlorophyll concentration is shown in equation 2.8:

$$[Chl] = f_D\left(R_A - R_B\right)\left(\frac{V_{ext}}{V_{filt}}\right) \quad (2.8)$$

Where; $[Chl]$ is the chlorophyll-a concentration (mg m^{-3}), f_D is a constant calculated from fluorescence responses to chl-a + pheophytin-a standard (mg m^{-3}, as maintained by Dr R. Head, PML); R_B is the fluorescence before acidification; R_A is the fluorescence after acidification; V_{filt} is the volume of sea water filtered (ml); V_{ext} is the volume into which the pigment is extracted (ml).

2.9 Plymouth Marine Bio-Optical Data Buoy (PlyMBODy)

PlyMBODy is a moored, autonomous, optical buoy, primarily designed for vicarious calibration of the SeaWiFS ocean colour satellite. The instrument was designed and constructed by Mr M. Pinkerton (PML). A full description is contained in Pinkerton & Aiken (1997). The system configuration during the study is shown schematically in figure 2.9. It was positioned at 50° 13' N, 4° 05' W (marked on figure 2.1).

Dates of PlyMBODy deployment, recovery and maintenance during 1997 are detailed in Chapter 4. The only PlyMBODy data used in this thesis were those collected by the Chelsea Instruments Aquapack instrument. This is an *in-situ* conductivity-depth-temperature-fluorescence probe similar to that deployed on the UOR (as described earlier). The Aquapack was mounted at a distance of 2.5 m below the buoy's water line. Data was supplied by M. Pinkerton in fully calibrated form. Calibration of the Aquapack's temperature and depth was similar to that described for the UOR temperature and depth described earlier. Calibration of conductivity was based on the sensor response to varying resistance. Calibration of fluorescence was based on sensor response to varying concentration of chlorophyll-a standard.

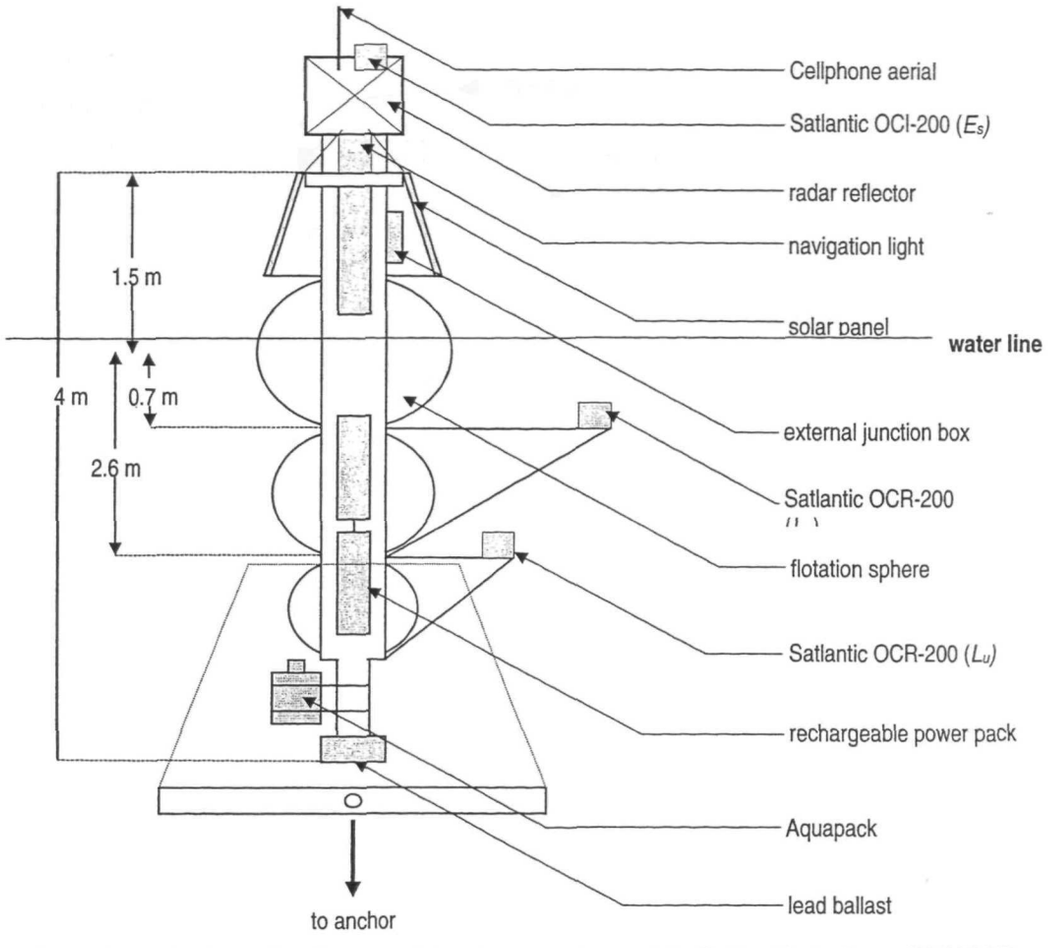

***Figure 2.9** – A schematic diagram of the Plymouth Marine Bio-Optical Data Buoy (PlyMBODy, Pinkerton & Aiken, 1997)*

2.10 The Physical/Biological Model

Temperature and chlorophyll distributions were simulated using the established physical/biological model described by Prestidge & Taylor (1995). A schematic diagram of the model is shown in figure 2.10. The table of parameters is shown in Appendix 11.

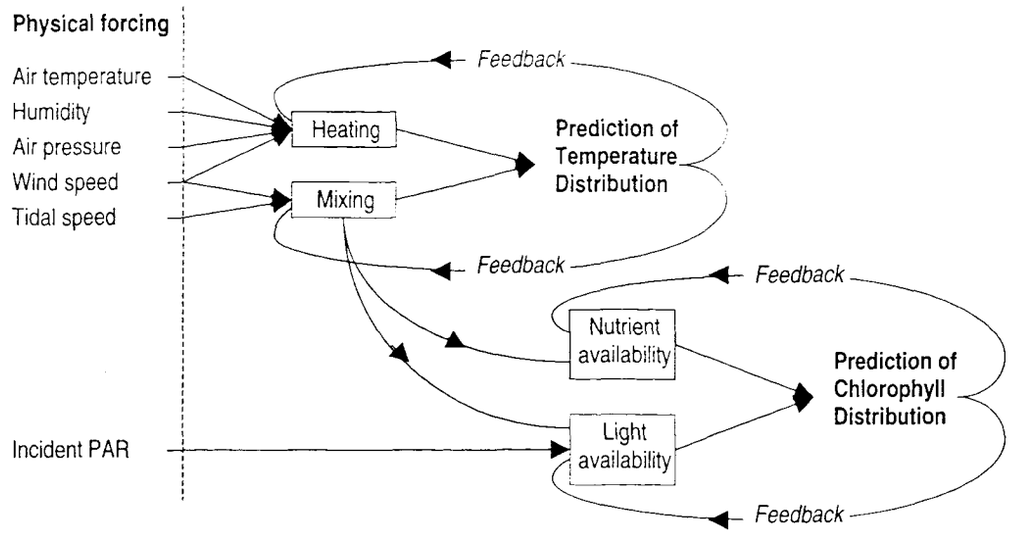

***Figure 2.10** – A schematic diagram of the Prestidge-Taylor physical/biological model*

Physical Component

The physical structure of the water column is calculated as a three-layer potential energy model, where the layers are: surface mixed layer (SML), thermocline, and bottom mixed layer (BML). Potential energy inputs due to atmospheric heat flux, wind mixing and tidal mixing are conserved (where possible) by modification of water-column thermal structure. The potential energy of the water column is defined as the integrated gravitational potential energy over the depth. The expression for water-column potential energy used by the model, relative to its well-mixed state, is presented as equation 2.9:

$$\Phi = g\left[\int_d^0 \rho_z z\,\mathrm{d}z - d\int_d^0 \rho_z\,\mathrm{d}z\right] \qquad (2.9)$$
$$\rho_z = (bS_z - aT_z)\rho_w$$

Where: Φ id the potential energy of the water column, g is the acceleration due to gravity, ρ_z is the density at depth z, d is the depth of the water column, b is the dependence of density on salinity S_z is the salinity at depth z, T_z is the temperature at depth z, p_w is the density of water

The model procedure for the calculation of water column density structure at each time step is summarised as follows, and shown diagrammatically in figure 2.11:

1. A temporary surface layer (of initial depth 1 m) is created, with a density of the SML layer from the previous time step.

2. The heat flux across the air/sea interface is calculated by the algorithms of Stigebrandt (1985), as summarised in the introduction (equation 1.1). The energy input due to atmospheric heat flux is accounted for as follows:

    a. The heat flux is conserved by changing the temperature, and therefore density, of the temporary surface layer (equation 2.10).

$$\partial T_{[1]} = q/\rho_w c h_{[1]} \qquad (2.10)$$

Where: $\delta T_{[1]}$ is the change in temperature of the surface layer due to heat flux over the time step, q is the heat flux, c is the specific heat capacity of water, $h_{[1]}$ is the depth of the surface layer (initially set to 1 m).

    b. If the potential energy input due to heating (equation 2.11) is greater than zero, a density inversion will have occurred, which is balanced by entrainment of water (and resultant adjustment of layer depths) into the surface layer from the underlying layer(s), which can be either the SML, thermocline, or BML, depending on the depth of each layer, and the volume of the required entrainment.

$$\partial \Phi_{[heat]} = -\frac{q(d-1)ga}{2c} \qquad (2.11)$$

Where: $\delta\Phi_{[heat]}$ is input of potential energy over the time step due to heating, q is the heat input to the water surface, g is acceleration due to gravity, a is the thermal expansion coefficient of sea water.

For entrainment from the surface layer, the entrainment volume can be calculated directly, as shown in equation 2.12. For the thermocline, however, which is a gradient layer, the volume is determined iteratively, using recursive solutions of equation 2.13 for differing values of thermocline width until a correct value is obtained.

$$\partial h_{[1]} = \frac{2\partial \Phi_{[input]}}{g h_{[1]} \partial \rho_{[1]}} \qquad (2.12)$$

where: $\rho_{[1]}$ is the density of the surface layer, $\Phi_{[input]}$ is the potential energy of the input variable (heat, fraction of heat, wind, or tide)

$$\Phi_{[thermocline]} = \frac{g\rho_w a h^3_{[thermocline]}}{12} \cdot \frac{dT}{dz}$$

$$\partial \Phi_{[thermocline]} = \frac{g\rho_w a}{4} \cdot \frac{dT}{dz} \cdot \left[\frac{\partial h^3}{3} + h_{[1]} \partial h^2 - h_{[1]} h_{[thermocline]} \partial h \right] + \frac{g h_{[1]} \left| \rho_{[1]} - \rho_{[thermocline]} \right|}{2} \qquad (2.13)$$

Where: $\Phi_{[thermocline]}$ is the potential energy of the thermocline, $h_{[thermocline]}$ is the width of the thermocline, dT/dz is the thermocline temperature gradient.

c. A fraction (K_c) of any positive potential energy released in removing a temperature inversion results in further entrainment from the underlying layer, with the assumption that the rest is dissipated through turbulence. The energy calculations are those described for equations 2.12 and 2.13.

The water column will now contain from 1 to 4 layers, one of which being the newly formed temporary surface layer.

3. Potential energy input into the surface layer due to wind speed (equation 2.14) is accounted for. The potential energy input is balanced by entrainment of water into the surface layer from the underlying layer(s), with resultant adjustment in layer depths. An exponential delay is applied to wind forcing to account for the delay in the conversion of mixing energy to potential energy. The energy-balance algorithm uses equations similar to 2.12 and 2.13.

$$\partial\Phi_{[wind]} = KW^3\rho_a f_0 k_0$$
$$K = \Phi_0/(\Phi_0 - \Phi) \text{ when } \Phi < -3\Phi_0 \quad (2.14)$$
$$K = 0.25 \text{ otherwise}$$

Where: W is wind speed, ρ_a is air density, f_0 is wind mixing efficiency, k_0 is wind drag coefficient, $\Phi_{[wind]}$ is potential energy due to wind, Φ_0 is the constant for variable mixing efficiency

4. Potential energy input into the BML due to tidal speed (equation 2.15) is accounted for. The potential energy input is balanced by entrainment of water into the BML from the overlying layer(s), with resultant adjustment in layer depths. No delay is required, as tidal mixing speed is a constant parameter of the model. The energy-balance algorithm uses equations similar to 2.12 and 2.13.

$$\partial\Phi_{[tide]} = KU^3\rho_w f_3 k_3 \frac{4}{3\Pi} \quad (2.15)$$

Where: U is tide speed, ρ_w is water density, f_3 is tide mixing efficiency, k_3 is tide drag coefficient.

5. The model may now have from 1 to 4 layers. The SML is assigned the top layer (generally the temporary surface layer), the BML is assigned the bottom layer, and the thermocline is assigned any remaining middle layers. The temperature gradient of the thermocline is re-calculated to balance potential energy.

6. Finally, a diffusion term is applied that exchanges a volume of water between adjacent layers, related to the inverse density difference between the layers, and the thermocline temperature gradient re-calculated. The diffusion calculation is made using equation 2.16:

$$V = \frac{e_1}{(\rho_j - \rho_i)/\rho_w + e_2} \qquad (2.16)$$

Where: V is the volume of water exchanged, ρ_j is the density of the deeper layer, ρ_i is the density of the deeper layer, e_1 and e_2 are constants

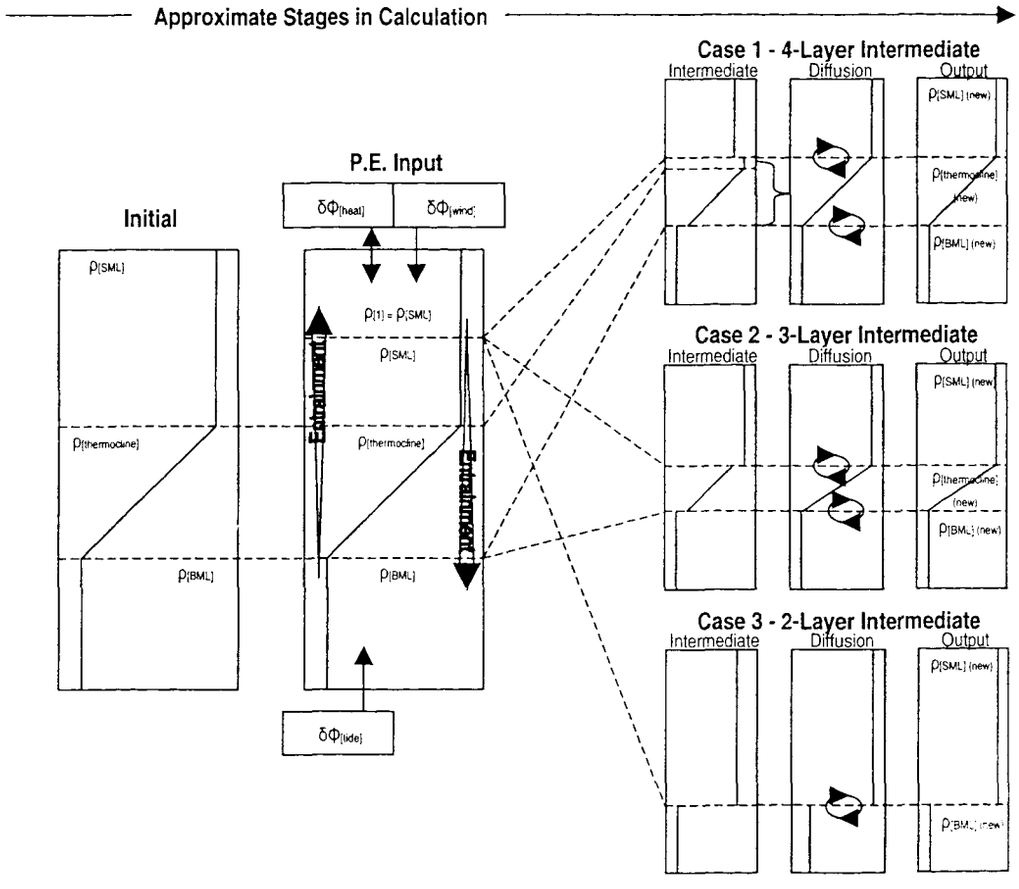

***Figure 2.11** – Schematic Diagram of the Calculation of water column structure by the Prestidge-Taylor model.*

Of the downwelling irradiance at the sea surface, 50 % is assumed to penetrate as photosynthetically active irradiance (PAR). Total PAR at depth 0 (just below the sea surface) is divided equally into two wave bands, 'red' (rapidly attenuated) and 'green' (attenuated more slowly). Attenuation at a given water column depth is calculated as the sum of the clear-water absorption, the chlorophyll specific absorption, and a sediment absorption term related to salinity and tidal speed, as shown in equation 2.17:

$$k_{z[r]} = k_{w[r]} + k_{chl[r]}.P_z + \left(\frac{k_{s1}U^3}{d} + k_{s2}(S_0 - S_m) \right) \qquad (2.17)$$

Where: $k_{z[r]}$ is the attenuation coefficient of red light at depth z, $k_{w[r]}$ is the attenuation coefficient of red light by pure water, $k_{chl[r]}$ is the chlorophyll-specific attenuation coefficient for red light, P_z is the chlorophyll concentration at depth z, k_{s1} is the tidal component of sediment attenuation, k_{s2} is the salinity component of sediment attenuation, S_0 is the bottom salinity, S_m is the mean salinity of the water column.

Biological component

The biological component of the model is very simple, and based on the single nutrient, single phytoplankton scheme of Taylor et al (1991). The model is run for each layer of the water column in turn. The control of productivity by both light and nutrient are calculated simultaneously using Michaelis-Menten functions, as shown in equation 2.18. A proportion of the phytoplankton is lost at each time step due to respiration, mortality and grazing. This proportion varies sinusoidally with the time of year. Further loss results from sinking. The phytoplankton balance is modified by volume exchange between the layers due to the mixing estimated by the physical component of the model. Concentrations cannot fall below a minimum level.

$$\frac{dN_i}{dt} = -\gamma\left(\frac{\alpha N_i}{N_i + N_h} - \eta m \right) P_i + transports \qquad (2.18a)$$

$$\frac{dP_i}{dt} = \left(\frac{\alpha N_i}{N_i + N_h} - m - \frac{v}{h_i} \right) P_i + \frac{v.P_{i-1}}{h_i} + transports \qquad (2.18b)$$

$$\text{where } \alpha = \alpha_{max}.2^{(T_i - T_{max})/10}.\int \frac{I_{(z)}.dz}{I_{(z)} + I_h} \qquad (2.18c)$$

Where: N_I is the nitrogenous nutrient (nitrate + nitrite) concentration in layer i; t is time; γ is the carbon to chlorophyll ratio; N_h is the nutrient half saturation coefficient; η is the nutrient recycling efficiency; m is the mortality rate; P_I is the chlorophyll concentration in layer i; v is the phytoplankton sinking rate; h_I is the vertical extent of layer I; T_i is the temperature of layer I; T_{max} is temperature coefficient for growth rate.

A fraction of the phytoplankton loss is recycled as nutrient. The vertical nutrient balance is also modified by volume exchange. An additional nutrient flux into the bottom mixed layer is attributed to diffusion from the sea bed. The value of this flux is calculated by assuming a constant nutrient concentration of the sediment, and a diffusive rate proportional to the concentration difference at the sea bed, as shown in equation 2.25.

$$N_{diff} = e_{sed}(N_0 - N_3) \qquad (2.25)$$

Where: N_{diff} is the sediment/water nutrient flux (dN_{BML}/dt), e_{sed} is the coefficient for sediment/water nutrient flux, N_0 is the sediment nutrient concentration, N_3 is the bottom water layer nutrient concentration.

Model parameterisation

The full set of model parameters, as used during this study, is included in appendix 11. The majority of these were taken directly from Prestidge & Taylor (1995), except for those discussed below.

Initially, the model was parameterised using the values presented by Prestidge & Taylor (1995). However, of concern was the fact that value of the wind drag coefficient presented by Prestidge & Taylor (1995) was 1.3×10^{-3}, which differed considerably from the accepted value of 6.4×10^{-5} (e.g. Simpson & Bowers, 1981). As no explanation could be found for the change to the Prestidge-Taylor value from the experimentally determined value, the accepted value for the wind drag coefficient was re-instated. However, on making this change, the model simulated surface temperatures that were unrealistically high (>30°C during summer). The original calculation of wind mixing efficiency by Simpson & Bowers was empirical, based on fitting with simulations of a 2-layer physical water column model. It was therefore assumed valid to alter this parameter to achieve a realistic temperature simulation for the Prestidge-Taylor model. The wind mixing efficiency was therefore increased from 4×10^{-2} (simpson & Bowers, 1981) to 8×10^{-2}. As the ratio of wind to tidal mixing efficiency were estimated using an assumption of a constant ratio (Simpson & Bowers, 1981), the tidal mixing efficiency was increased accordingly (from 4×10^{-3} to 8×10^{-3}).

Temperature simulations were further improved by altering the parameters controlling thermocline diffusion (e_1 from 5.8×10^{-10} to 4.5×10^{-9}, and e_2 from 5×10^{-5} to 1×10^{-4}). Although not mentioned in the Prestidge-Taylor paper, these parameters had been determined empirically, and alteration to the new values was suggested (A. Taylor, pers. com.)

That 1-D bulk models using parameter values found in the literature can underestimate the degree of mixing has been shown in other studies (e.g. Large et al, 1994). It is uncertain whether the need to change parameter values between similar models to achieve a realistic simulation is due to differences in the model calculations, uncertainties in the parameter values, or changes in physical processes with location. Work is currently underway to resolve the contradictions between the parameter values used by the Prestidge & Taylor and Simpson & Bowers models (A. Taylor, pers. com.).

Model Inputs and Outputs

The algorithms used to simulate physical conditions were repeatedly solved using a computer program written in FORTRAN. Numerical integration of the biological model was carried out by the same program, using a forward finite difference method with a time step of 1 hr. Numerical checks were used to ensure that phytoplankton concentration did not fall below a minimum threshold (see Appendix 11).

Hourly meteorological variables were used to calculate wind mixing (wind speed), heat exchange across the air/sea interface, and photosynthetically active radiance. Of the model parameters listed in Appendix 11, it was assumed that only mean tidal currents and water depth were site specific.

The model outputs width (m), temperature (°C), nutrient (mmol N m^{-3}) and chlorophyll (mg Chl m^{-3}) for each of three layers (SML, thermocline, BML).

Each model run was a year in length, from 1st January to 31st December. The meteorological database, however, consisted of continuous data from 1st January 1982 to 31st December 1997. For all simulations presented in this thesis, 16 individual model runs were performed (one for each year from 1982 to 1997), and the data concatenated into a single time series. Model temperature and nutrients were initialised to the inter-annual average temperature and nutrient concentrations from the E1 archive data set prior to each run (i.e. On 1st January for each year of the simulation) to ensure that errors due to advection during the winter did not accumulate over the 16 year period (see chapters 3 and 5 for further justification). The chlorophyll concentrations for the 1st January of each year used the simulated concentrations from 31st December of the previous year. The chlorophyll concentration was, however, invariably at the minimum level permitted by the model on 31st December.

Heat Flux Model

Modifications to the Prestidge–Taylor model were made to provide the capability for estimating heat flux across the air/sea interface based on SST and meteorological observations. The inputs were hourly meteorological values (described above) and hourly SST, calculated from discrete AVHRR SST measurements using linear interpolation. Within the model, observed SST substituted the simulated SML temperature, and the heat flux calculated correspondingly. This new heat flux was the single output from the modified model. The heat flux simulations are presented independently of the simulations made using the Prestidge–Taylor model.

3. Results Part 1 – Physical Forcing and Remote Sensed Observations

The following two chapters describe the data required to test the model simulations of temperature and chlorophyll variability for the study region. The key characteristics of the data relevant to physical forcing are described, and empirical links between these and other observations are proposed. These empirical links are used to test the hypotheses stated in the introduction.

3.1 Data Selection Criteria

Physical Forcing Data

The first part of this chapter presents data that show the typical scales of physical forcing for the study region. It is assumed that the physical forcing is dominated by vertical processes caused by meteorology and tides. Meteorology and tides vary over several characteristic scales. Several of these scales are summarised in table 3.1.

Time plots of the complete (1982 to 1997) meteorological data set for downwelling irradiance, wind speed and air temperature are presented To highlight the scales of variability, the results of the spectral analysis of the above fields are also presented. The Fast Fourier Transform (FFT) and filtering techniques used are described in Chapter 2.

In addition to the spectral analysis, the observational or modelled data was filtered using a simple averaging process. This simple filtering was used for comparison with data for which the full spectral analysis was not appropriate due to the length of available continuous data. The averaging interval used to isolate each scale is also presented in table 3.1.

Meteorology			Tides		
Scale length	Terminology	Data averaging	Scale length	Terminology	Data averaging
12 months	Seasonal (climatology)	Monthly means averaged over several years.	–	–	–
12 months	Seasonal (single year)	Monthly means for a single year	–	–	–
4 to 20 days	Meteorological event	Daily means	14 days	Spring-neap (S_2).	Daily means.
24 hours	Diurnal	Hourly means	12.4 hours	Semi-diurnal (M_2)	Hourly means
–	–	–	Several km	Mesoscale	1 km^2 (grid)

***Table 3.1** – Characteristic scales of meteorological and tidal variability within the study region, and the data averaging used to isolate them.*

Of the nine meteorological fields listed in the Methods section, four are of particular importance; downwelling irradiance at the sea surface, air temperature, wind speed, and wind direction. Global radiance and air/sea temperature difference are the variables that dominate net heat flux into the water column (Edinger et al, 1968). Wind speed and heat flux control water column mixing at the surface (Simpson & Bowers, 1981). Wind direction and speed strongly influence the residual advection of the water column (Carruthers, 1935).

The selection criterion for the presented meteorological data was twofold. Firstly, the data had to display some aspect of the characteristic scales of meteorological variability. Secondly, the data had to be contemporaneous with available temperature and chlorophyll observations. Due to the patchy nature of the observations provided by the techniques used, this second criteria was the major determining factor in most cases. The selected meteorological data, the scale which it represents, and the contemporaneous observational technique are presented in Table 3.2.

Selected Meteorological Data	Scale	Contemporaneous Data
1982 to 1997	Seasonal (Climatology)	E1 archive: 1974 to 1987. (Chapter 4)
Jan. 1997 to Dec. 1997	Seasonal (Single Year)	AVHRR (Chapter 3)
4th Jul 97 to 3rd Aug 97 27th Sep 97 to 27th Oct 97	Meteorological events (summer) Meteorological events (Autumn)	AVHRR (Chapter 3)
8th Aug 97 to 11th Aug 97 25th Sep 97 to 28th Sep 97	Diurnal (summer) Diurnal (Autumn)	PlyMBODy (Chapter 4)
10th Jun 00:00 to 24:00 11th Jun 00:00 to 24:00	Diurnal (single day)	UOR (Chapter 4)

***Table 3.2** – Selection of meteorological data, the characteristic scale of variability that is represented, and the type of contemporaneous observational data.*

A complete set of M_2 tidal currents for the study region, calculated from the model of Sinha & Pingree (1997), was available. Data for the S_2 tide, however, were not available in time to be included in the thesis. This omission was likely to be significant due to the ratio of S_2 to M_2 tidal amplitude at station E1 (~0.3), and the importance of the spring-neap cycle in modifying the temperature and chlorophyll distribution in shelf seas in general (as discussed in the introduction). The selection criteria of the presented M_2 tidal data were also controlled by the availability of observational data. The selected tidal data, the scale which it represents, and the contemporaneous observational technique are presented in Table 3.3.

Selected Tidal Data	Scale	Contemporaneous Data
Station E1 (50°02'N 4°22'W)	Semi-Diurnal (Offshore)	E1 Archive, UOR Track
Station L4 (50°15'N 4°13'W) Station S2 (50°10'N 3°58'W)	Semi-Diurnal (Onshore, low tide) Semi-Diurnal (Onshore, High tide)	UOR Track
E1 to L4 Transect E1 to S2 Transect	Mesoscale	UOR Track
Study Region 2-D Grid (50°00'-50°20'N, 4°30'-3°50'W)	Mesoscale	AVHRR Image

***Table 3.3** – Selection of tidal data, the characteristic scale of variability that is represented, and the type of contemporaneous observational data.*

Remote Sensed Data

The second part of this chapter presents AVHRR Sea Surface Temperature (SST) data that show the typical distribution of SST for the study region over characteristic scales. SST values from single points are used to demonstrate the seasonal variability, values along transects are used to demonstrate the evolution of mesoscale variability through the year, and images are used to demonstrate 2-D patterns of SST variability.

The selection criteria for the presented SST data were; availability, and information content concerning some aspect of the characteristic scales of variability. The selected data, the characteristic scale of variability that is represented, the number of images used, and the averaging intervals are shown in Table 3.4. A list of all the images used is included in appendix 2.

Selected Data	Scale of Variability	Number of images	Averaging Interval
All 1997 data, Station E1	Seasonal + meteorological	150	None
Jan 97 to Dec 97, E1, L4, S2	Seasonal (single year)	150	30-day
4th Jul 97 to 3rd Aug 97, E1, L4, S2	Meteorological events (summer)	~20	None
27th Sep 97 to 27th Oct 97, E1, L4, S2	Meteorological events (autumn)	~8	
Study Region 2-D Grid	Mesoscale (typical patterns)	4	None
E1 to L4 Transect E1 to S2 Transect	Mesoscale (seasonal evolution)	6	None

***Table 3.4** – Selection of SST data, the characteristic scale of variability that is represented, the number of images used, and the averaging intervals.*

In addition, 4 SeaWiFS images from 1998 are also presented to demonstrate typical spatial patterns of chlorophyll variability for the Western English Channel. The analysis of SeaWiFS data was limited by its availability, i.e. from September 1997 onwards.

Climatological Variability over Seasonal Time Scales (1982 to 1997)

A seasonal climatology of meteorological variability was compiled by taking the average value of the monthly mean for each year of the hourly meteorological data set from 1982 to 1997.

The 15-year (1982 to 1997) seasonal climatologies of downwelling irradiance (Camborne), and wind speed, wind direction and air temperature (Plymouth) are shown in figure 3.1 (open squares). Mean downwelling irradiance increased from a minimum in December (25 W m^{-2}), corresponding to midwinter, to a maximum in June (225 W m^{-2}), which is midsummer. Mean wind speeds were higher during the autumn and winter months (maximum 12.5 m s^{-1}) than the spring and summer months (minimum 8.5 m s^{-1}). Air temperature rose from a minimum in February (7°C), to a maximum in July (17°C). The variability for each field was approximately sinusoidal. Sinusoidal variability of the seasonal climatology for the adjacent Celtic Sea region has been modelled by James (1977). Such variability is characteristic of the average monthly atmospheric forcing for the South West of England.

Each value for the climatological monthly mean on Figure 3.1 is associated with an inter-annual standard deviation (error bars are equal to 1 standard deviation). The error bars represent the variability in the average meteorological conditions for that month from year to year. 67% of all monthly averages from individual years are likely to fall within the limits of the error bar for the appropriate month, assuming that the monthly mean data for each year are normally distributed about the mean. This equates to ~3

months outside the SD in an "average" year. During 1997, 6 months were outside the SD for irradiance, 5 for wind speed, and 4 for air temperature. 1997 was therefore an unusual year in terms of meteorological conditions.

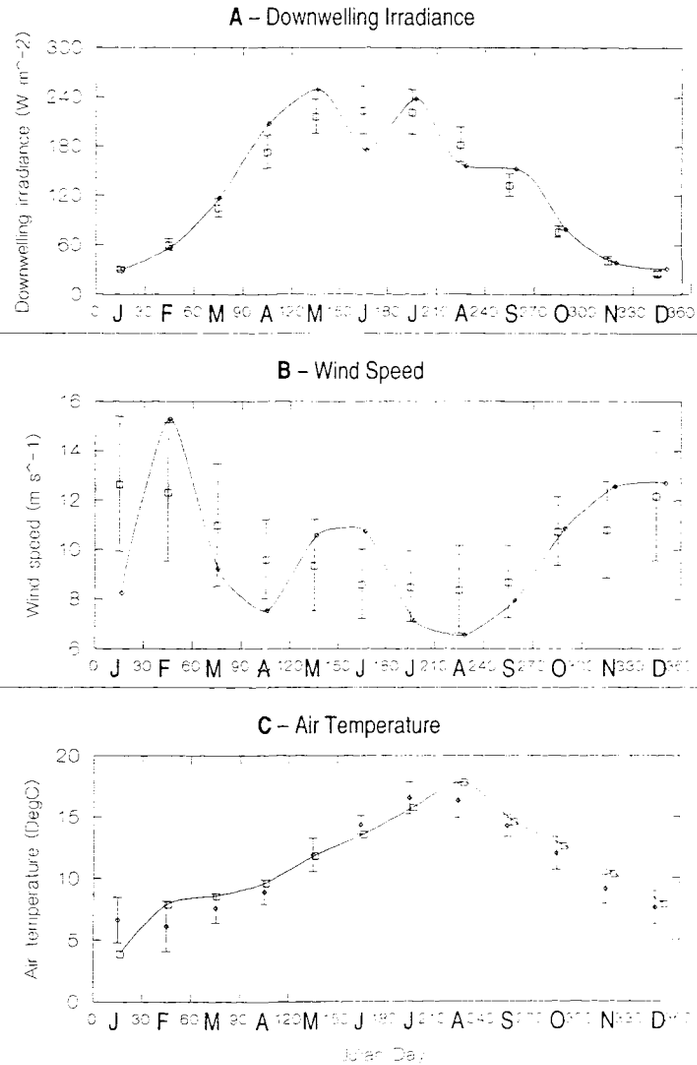

***Figure 3.1** – Monthly meteorology. Open squares are mean values from 1982 to 1997. Error bars represent 1 standard deviation of the mean. Small circles connected by continuous lines are 1997 values.*

***A:** downwelling irradiance (Camborne). **B:** wind speed (Plymouth). **C:** air temperature (Plymouth).*

Meteorological Variability over Seasonal Time Scales (1997)

The monthly mean meteorological data for 1997 are plotted in figure 3.1, overlaid on the seasonal climatology. Several months during 1997 varied significantly from the

climatological mean. June, for example, was dull and windy, compared to average. July, in contrast, was bright and still, whilst January was calm and cold. A statistical comparison of the climatological and 1997 seasonal variability is shown in table 3.5. (Note that neither the climatological or 1997 data were averaged prior to the statistical calculations, hourly data were used throughout, and that the quoted standard deviations are those for all data within the time period). The seasonal meteorological variability during 1997 had both greater range and standard deviation than the climatological values for each of the irradiance, wind speed and air temperature fields.

	Irradiance (W m^{-2})		Wind speed (m s^{-1})		Air Temperature (°C)	
	Climatology	1997	Climatology	1997	Climatology	1997
Minimum	26	31	8	7	6	4
Mean	120	130	10	10	11	11
Maximum	220	250	13	15	17	18
S.D.	77	80	1.6	2.7	3.7	3.9

***Table 3.5** – A statistical comparison of the climatological and 1997 monthly average downwelling irradiance (at Camborne), and wind speed and air temperature (at Plymouth).*

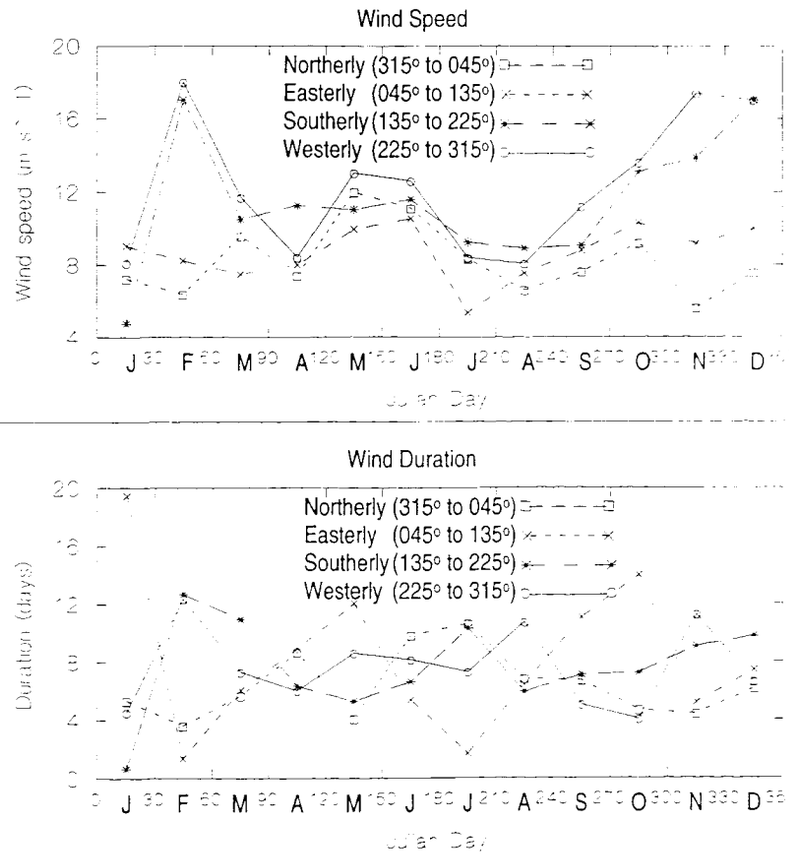

***Figure 3.2** – Average monthly winds at Plymouth during 1997.*
***A:** Wind speed, sub-divided by quadrant.* ***B:** Wind duration, from each quadrant.*

The monthly average wind speeds for 1997 are presented in more detail in figure 3.2. The strongest winds were from the West and South, reflecting the prevailing wind direction for the region. This increased wind speed was especially apparent during February, November and December, when average westerly wind speeds were greater than 16 m s^{-2}. In terms of the duration for each month (figure 3.2B), the greatest variability was apparent in the easterly winds. Easterly winds accounted for >12 days during January, May and October, but less than 4 days during February and July. Northerly, westerly and southerly winds each accounted for between 4 and 12 days of each month.

Meteorological Variability over Sub-Monthly Time Scales (Summer and Autumn 1997)

Daily average meteorological data from two, 1 month long periods; 4th July to 3rd August 1997, and 27th September to 27th October 1997, are presented in Figure 3.3. These periods represent summer and autumn conditions respectively. Summer conditions were brighter, calmer and warmer than autumn conditions. During the summer, calm, still, warm periods (meteorological events 1, 3 and 5 on figure 3.3, table 3.6) were interspersed with dull, windy (mainly westerly), cool periods (meteorological events 2, 4 and 6). The data presented in figure 3.3 was used to separate the continuous data into discrete meteorological events. Each event was defined as having either higher or lower than average irradiance and/or wind speed. Each of the identified events lasted for 3 to 8 days, consistent with the typical time scales of meteorological events prevalent in temperate regions. During the autumn, variability in each field was apparent over similar scales (meteorological events 7 to 11), but correlations between them were not as clear as for summer conditions. High wind speeds, for example, were not associated with either higher or lower air temperatures.

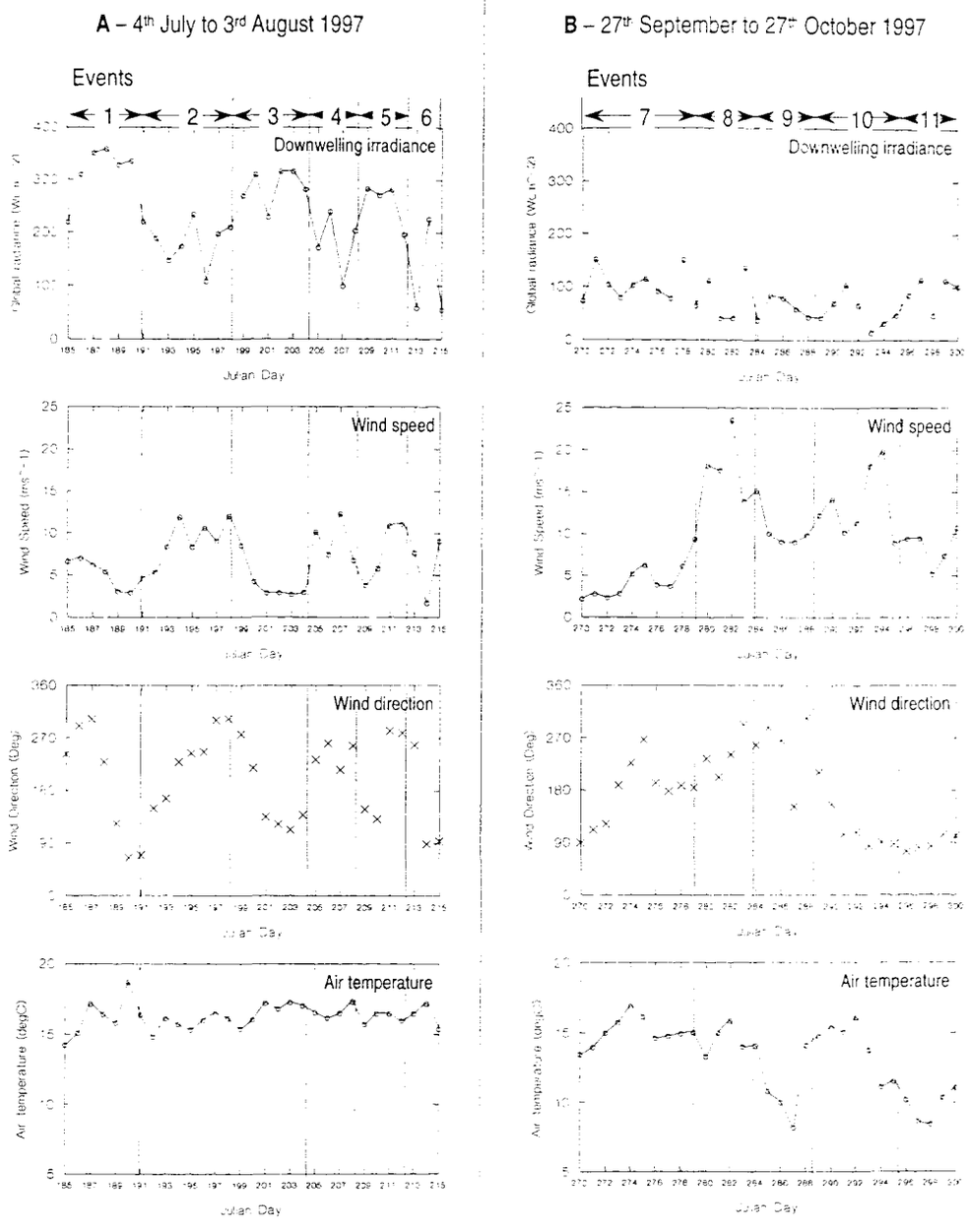

Figure 3.3 *– Daily average downwelling irradiance (at Camborne), wind speed, wind direction and air temperature (at Plymouth) over month long periods during 1997 (11 meteorological events were identified, and overlaid on the graphs).*
A: *4th July to 3rd August.* ***B:*** *27th September to 27th October.*

Event	Duration (days)	Typical Downwelling irradiance (W m^{-2})	Typical wind speed (m s^{-1})	Typical wind direction (°)	Typical air temperature (°C)
1	6	350	5	290 falling	17
2	7	200	10	90 rising	16
3	6	300	4	270 falling	17
4	4	200	8	250	17
5	4	300	Variable	Variable	17
6	3	variable	Variable	Variable	15
7	9	100	5	Variable	15
8	5	80	18	180 rising	15
9	5	70	10	Variable	10
10	6	60	15	180 falling	15 falling
11	5	70	8	90	10

***Table 3.6** – Identification of meteorological events from daily average meteorological data. Events correspond to those marked on Figure 3.3*

Meteorological Variability over Diurnal Time Scales (Summer and Autumn 1997)

Hourly meteorological data from two, 3-day long periods during 1997 are presented in Figure 3.4. The first of the periods was during early August, and the other during late September. The periods represent late summer and early autumn conditions respectively. The plots show various characteristics associated with meteorological variability over diurnal time scales both from day to day, and between one month and the next.

Diurnal variability in the downwelling irradiance field was apparent, both during August and September. During August, the patterns of irradiance variability were similar for each of the 3 days: the irradiance varied from 0 W m^{-2} during the night to 800 W m^{-2} during the day, and the curves were irregular in shape. During September, different patterns of variability were apparent for each day: during day 269 (26th September), the irradiance varied from 0 W m^{-2} during the night to 600 W m^{-2} during the day, and the curve was smooth. By contrast, during the following day (27th September), the irradiance only reached 250 W m^{-2} during the day, and the curve was irregular.

During both August and September, significant variability in the wind speed field was apparent over hourly scales, but with no specific periodicity. Winds varied from dead calm to 12 m s^{-1}, with the largest ranges occurring on days 222 (10th August) and 269 (26th September). Wind direction was less variable than wind speed. During August, winds changed from southerly to northerly, back to southerly, and then to easterly, with

the changes from one direction to the next occurring rapidly (<3 hrs.). During September, the winds were predominantly easterly.

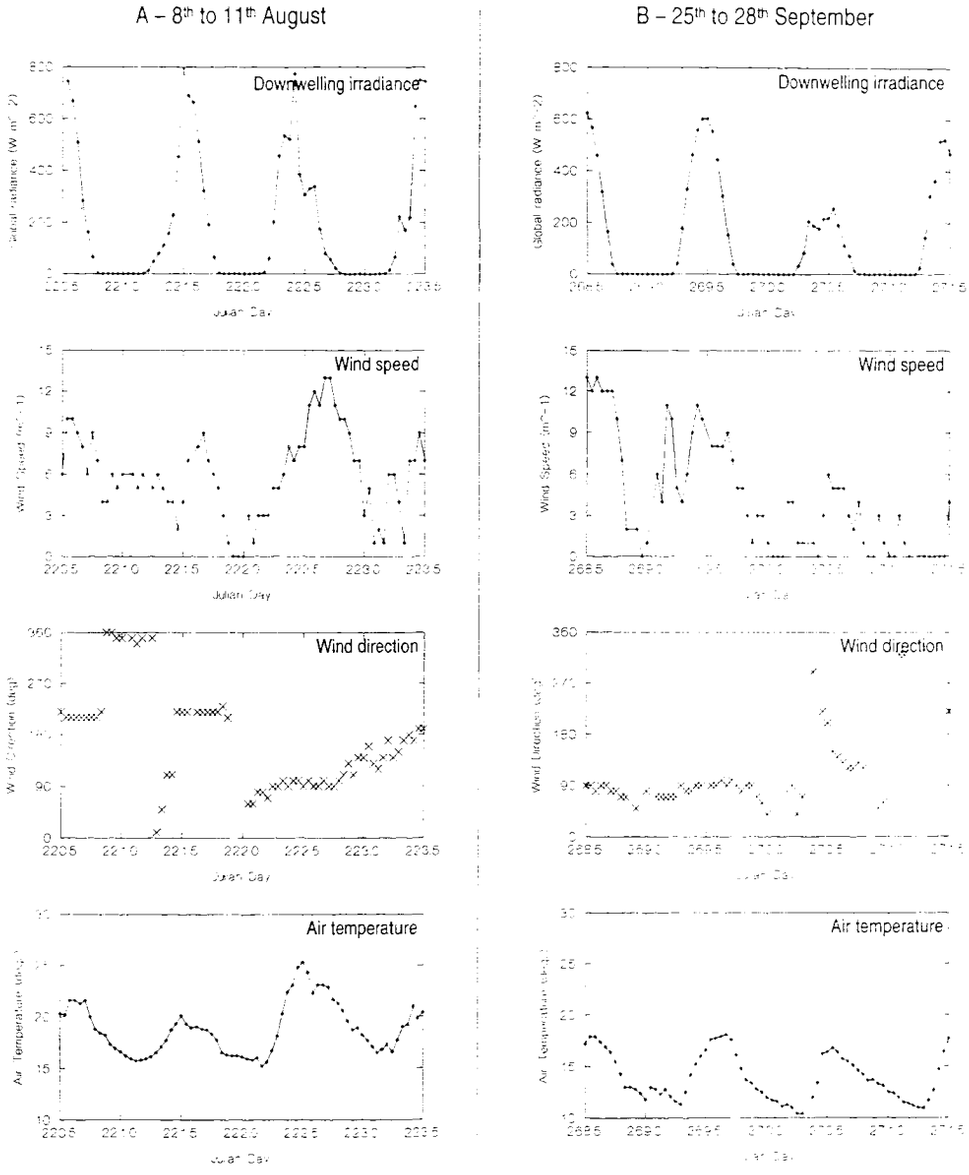

Figure 3.4 *– Hourly downwelling irradiance (at Camborne), wind speed, wind direction and air temperature (at Plymouth) over 3-day periods during 1997.*
A: *8th to 11th August.* ***B:*** *25th to 28th September.*

Air temperature for both September and August showed clear patterns of diurnal variability, increasing during the day, and decreasing at night. The amplitude of the variability changed significantly from day to day; 5°C on 9th August (15°C to 20°C), 12°C on 10th August (15°C to 27°C), 7°C on 26th September (10°C to 17°C), and 5°C on 27th September (11°C to 16°C).

Diurnal variation of solar irradiance at the top of the atmosphere is predictable, increasing from zero at dawn, to a maximum at local noon, and can be modelled as a truncated sine curve (Ikushima, 1967). Under clear skies, the irradiance at the sea surface can also be modelled as a sine curve. The sea surface irradiance distribution is, however, strongly modified by atmospheric interference (e.g. clouds). Cloud effects were therefore responsible for each of the irregular irradiance curves observed presented in figure 3.4, whereas the smooth curve on 26th September resulted from clear skies. Clouds also affect air temperature; under clear skies, air temperature increases rapidly during the day (solar heating), and decreases rapidly at night (radiant cooling). Both the heating and cooling are reduced when clouds are present. This can be used to explain the decreased daytime temperature, increased night time temperature and decreased diurnal temperature range from 26th September (when skies were clear) to 27th September (when clouds were present). Wind direction also significantly affects air temperature; the movement of a cool air mass from the north on 9th August resulted is lower maximum temperatures than those observed on 10th August, when the winds were easterly.

3.2 Tidal Advection and Mixing

Tidal Ellipses at E1, L4 and S2

The extent of tidal advection at each of the sampling stations is presented in terms of their tidal ellipses (Figure 3.6). The longest (~10 km) and most rectilinear tide is found at S2. It is orientated along a ENE - WSW axis. The tide maintains its orientation with distance eastwards along the coast, but diminishes in strength (to ~5 km by L4). The orientation at E1 is offset from the coastal stations by ~45°, and runs ESE to WNW. The major axis at E1 is almost parallel to the E1 to S2 standard transect (see figure 2.1).

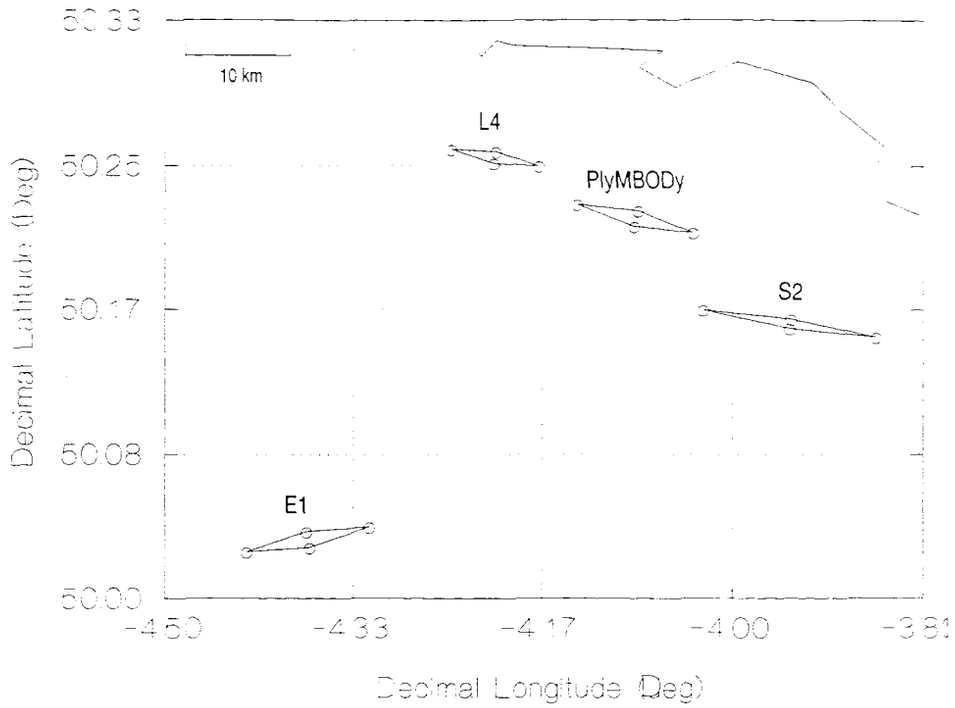

***Figure 3.6** – Semi-diurnal (M2) tidal ellipses at sampling stations E1, L4, S2 and at PlyMBODy, taken from the tidal model of Sinha & Pingree (1997).*

Tidal Currents at E1, L4 and S2

Semi-diurnal (M2) tidal curves for the sampling stations E1, L4 and S2 are presented in figure 3.7. The frequency of the tide is 12.2 hrs, regardless of position. For each of the stations, the largest component of the current was east-west, as suggested by the tidal ellipses presented above. Scalar tidal currents were greatest at S2 (average speed of 37 cm m^{-1}), followed by E1 (28 cm s^{-1}) and L4 (20 cm s^{-1}). High tide was reached first at E1, then at L4 (33 min after high water at E1), followed by S2 (43 min after high water at E1).

Both the tidal ellipses and tidal currents at E1, L4 and S2, as presented above, are consistent with the characteristic tides of the Western English Channel. These can be visualised as a wave propagating eastwards down the Channel from the Atlantic to the North Sea (Pingree, 1980). Although the M_2 (semi-diurnal) tide, is the dominant tide of the Channel, the spring-neap tide, (frequency of 14 days), is also significant. The S_2 tide has an amplitude of approx. 33% that of the M_2 tide (Pingree, 1980).

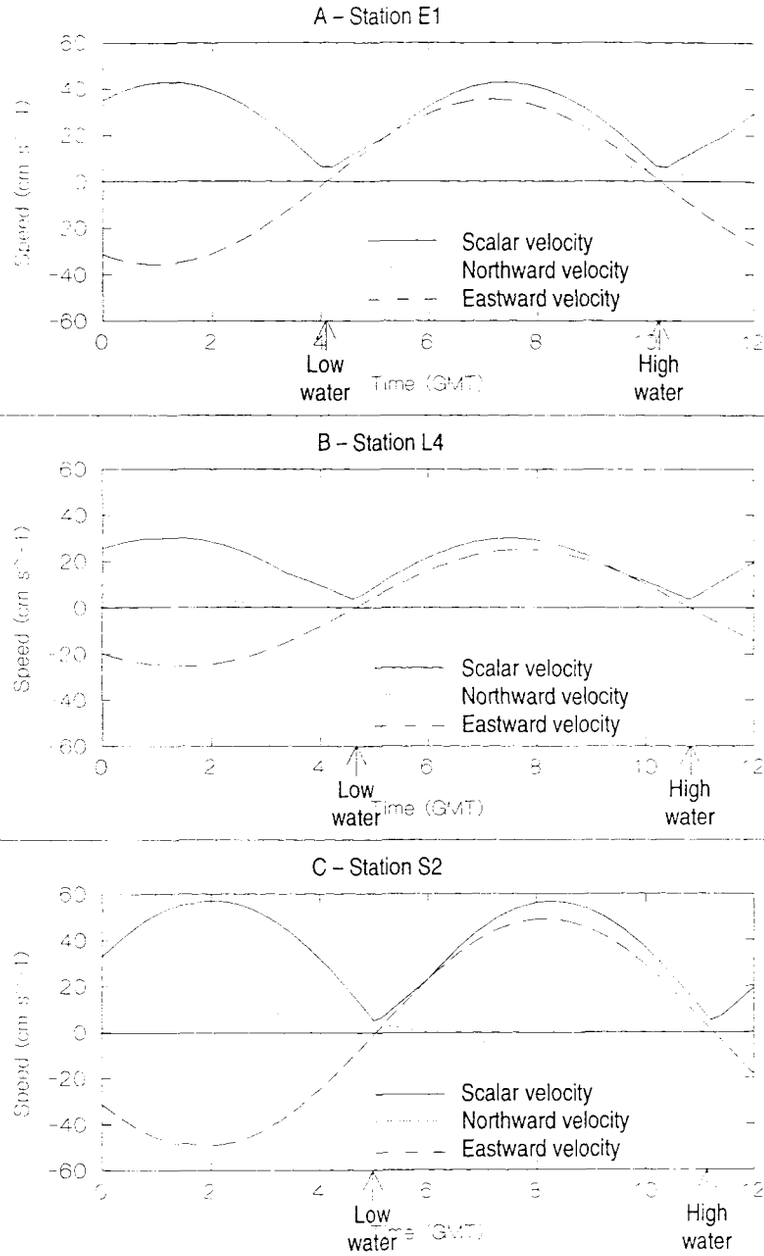

Figure 3.7 – *Semi-diurnal (M2) tidal curves at the sampling stations, taken from the tidal model of Sinha & Pingree (1997).* ***A:*** *Station E1.* ***B:*** *Station L4.* ***C:*** *Station S2.*

Tidal Mixing within the Study Region

Tides act to mix the watercolumn with energy that is proportional to the cube of the current speed. The water depth constrains the vertical extent over which this energy is distributed. The stratification parameter, S, (=h/($C_D U^3$), units=CGI (after Pingree & Griffiths, 1978) if h=m, U=cm s^{-1}, Pingree & Griffiths, 1978) can therefore be used as a

measure that is inversely related to tidal mixing. Tidal data from the model, and bathymetric data, have been used to construct Figure 3.8, which presents S contours over the study region.

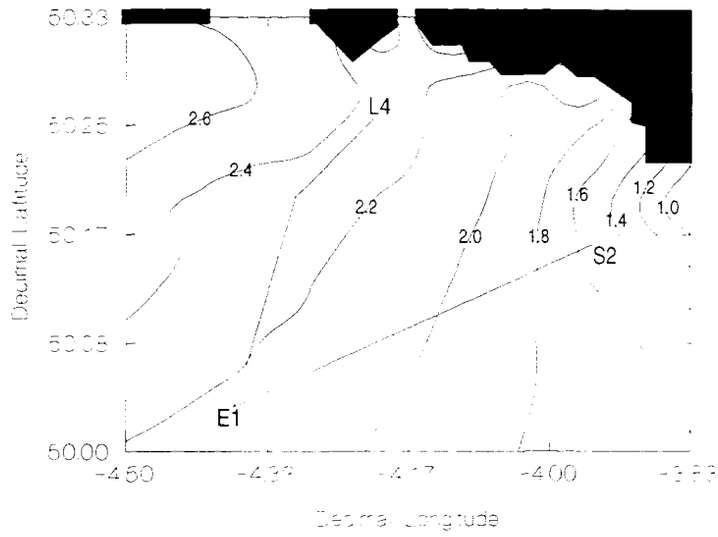

***Figure 3.8** – Stratification parameter (S) over the study region. S<2 represents the zone in which tidal fronts may be located during summer months. Also marked are the standard transects, E1 to L4 and E1 to S2.*

Tidal fronts are likely to occur at a critical value of S, empirically determined to be between 1 and 2 (CGI units) (Pingree & Griffiths, 1978). Stratified waters have higher values, and well-mixed waters have lower values. For the majority of the region, S is greater than 2, indicating that the watercolumn will be thermally stratified during the summer months. However, to the East, the values decrease, (to a minimum of 1) indicating that a tidal front is likely to occur during the summer, especially when vertical mixing is increased by periods of high winds or convective overturn.

The expected variations in tidal mixing along the standard transects are shown in figure 3.9. Along the E1 to L4 transect, S increases, suggesting that the water column will become progressively more stratified with distance from E1 during the summer months. Along the E1 to S2 transect, S decreases, indicating a reduction in stratification. The S = 2 threshold is crossed at a distance of 17 km from E1, suggesting that a tidal front may be located along the transect, close to S2, during the summer months.

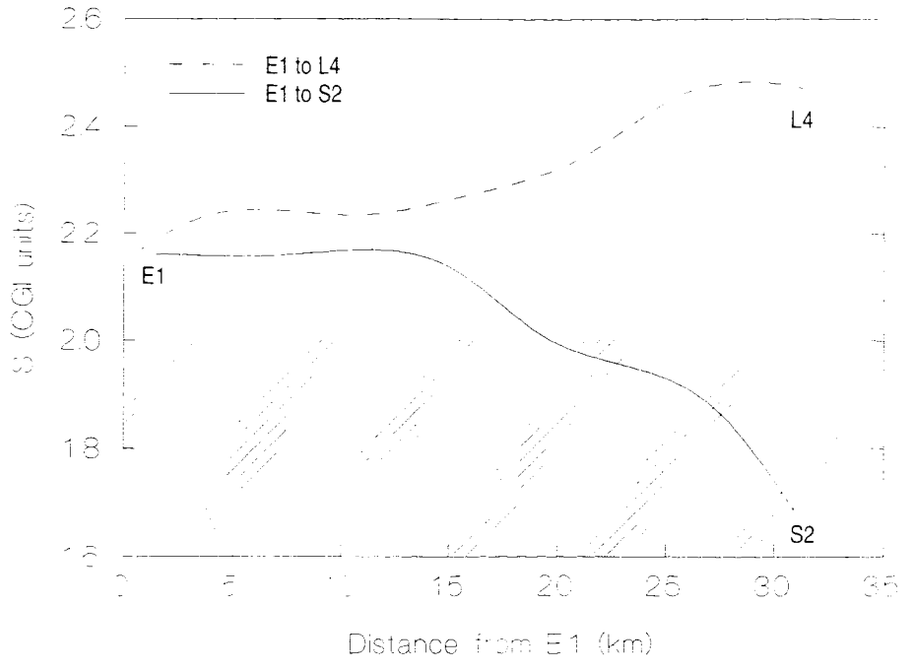

***Figure 3.9** – Stratification parameter (S) along two transects. The shaded area represents the zone in which tidal fronts may be located during summer months.*

3.3 Heat Flux at Station E1 During 1997

The heat flux model (described in the Methods chapter) was used to estimate the hourly air-sea heat flux throughout 1997 for station E1. The model required hourly 1997 SST data from E1, and hourly 1997 meteorological data. Daytime SST measurements are discarded from most analyses as the daytime heating of the sea surface 'skin' (top few mm) can lead to elevated temperatures that obscure the underlying temperature distribution (Robinson, 1985). These elevated temperatures do, however, contribute to heat flux. For the heat flux calculation, therefore, daytime AVHRR images were included.

The results for both monthly and daily heat fluxes for station E1 during 1997 are presented in figure 3.10. During January, February, October, November and December, the monthly average heat budget was negative, indicating that heat was being lost from the sea surface into the atmosphere. During the rest of the year (spring and summer), heat was being gained by the sea surface. The daily heat fluxes, however, indicate that even in mid summer, heat was lost on certain days, notably for a period during late June. In addition, frequent, rapid changes between positive and negative heat flux into the water column occurred during the months of March and September.

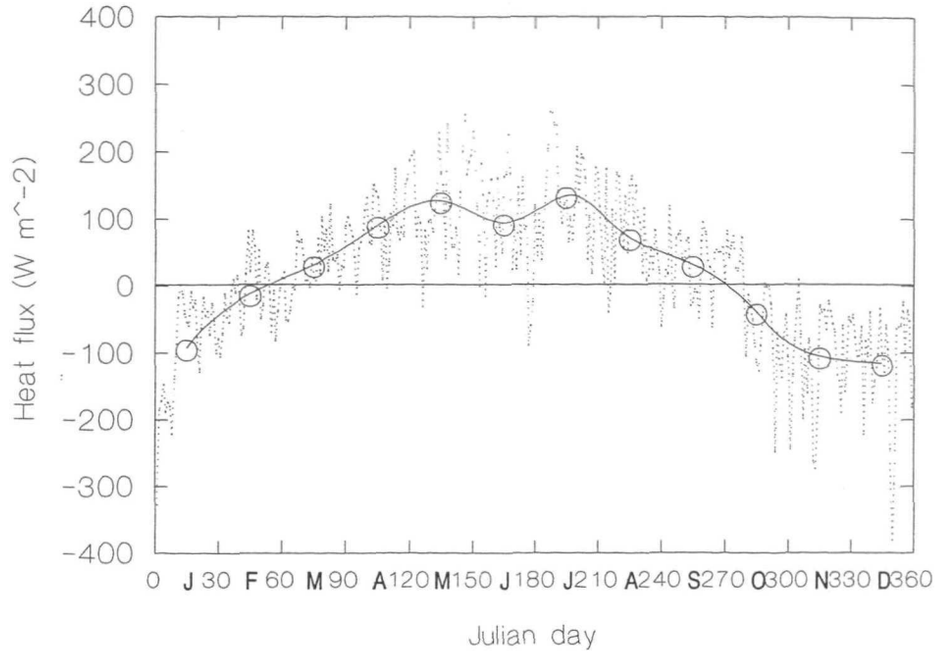

***Figure 3.10** – Heat flux across the air-sea interface at E1 during 1997. Dotted line is daily values. Open circles and solid line are monthly values.*

Positive heat flux will increase the average temperature of the watercolumn. For example, a sustained flux of 100 W m^{-2} will heat the watercolumn at E1 by 0.03°C day^{-1}. When vertical mixing can no longer redistribute the thermal potential energy, stratification occurs. Stratification reduces the depth over which the heat is distributed, leading to an increased heating of the SML per unit heat flux. Conversely, when heat flux becomes negative, convective mixing results, tending to erode the thermocline, mixing cool water from the BML, leading to a decreased cooling of the SML per unit heat flux.

Over the whole of 1997, the heat flux model calculated an average heat flux into the watercolumn was 18 W m^{-3}. Three explanations are suggested to account for this imbalance: That the specific meteorological conditions during 1997 lead to enhanced the air/sea heat transfer, and the system was therefore not in steady-state over the year. That the average horizontal advection of the water column transported cooler water past E1, thereby enhancing the "real" air/sea heat flux. That the method used to calculate heat flux, or the estimates of the measured input variables overestimated the "real" heat flux, therefore leading to biased heat flux estimates.

3.4 Variability of SST over Seasonal Time Scales

AVHRR SST Observations at E1 During 1997

A time series of AVHRR SST pixel measurements for 1997 corresponding to sampling station E1. is shown in figure 3.11. All night time images, screened as described in the methods chapter, have been included in the plot. Six distinct intervals were identified, separated by the general rate of change of SST with time. The seasonal trend of SST can be described by the rate of change of SST for the intervals, which are listed in table 3.7. A similar procedure was carried out for the L4 and S2 sampling stations. During interval 1 (January to March), SST increased slowly with time, from a minimum of 8.4°C. For interval 2 (April to June), SST increased more rapidly. The fastest SST increase occurred during interval 3 (July and early August), to a maximum of 20.4°C. The temperature maximum was followed by an extremely rapid decrease in SST, falling by 4.3°C over 16 days (interval 4). After a period of stable SST (interval 5, covering September and October), SST fell sharply again until the end of the year (interval 6).

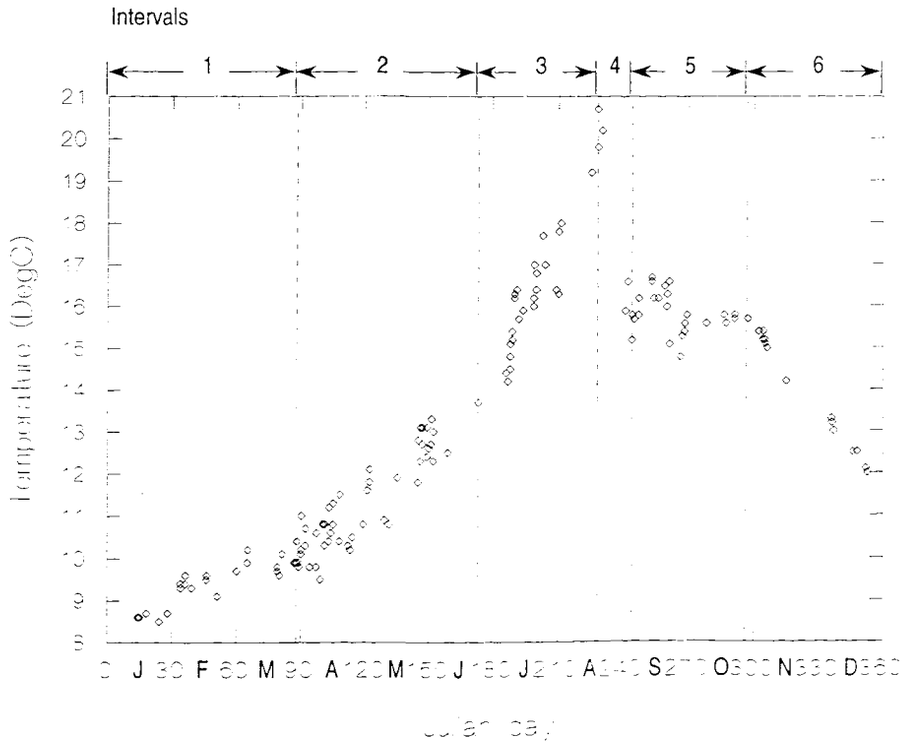

***Figure 3.11** – Night time AVHRR SST measurements at station E1 during 1997.*

Interval #	Start (Julian day)	Start temperature (°C)	Heating rate (°C day^{-1})	Pearson correlation of Date and Temperature
1	0	8.4	0.02	0.72
2	88	10.0	0.04	0.81
3	173	13.7	0.11	0.79
4	228	20.4	-0.30	0.94
5	244	16.1	-0.01	0.06
6	297	15.6	-0.06	0.99

***Table 3.7** – Characteristics of the intervals identified from the seasonal cycle of SST at E1 during 1997.*

The difference in the heating rate between intervals 1 and 2 can be explained by the onset of stratification. Heat flux into the water column becomes positive during March (figure 3.10). The balance between the increasing heat flux and vertical mixing determined the point at which the thermocline becomes stratified. At E1, this event can occur as early as late March (Maddock & Swann, 1977). Following the onset of stratification, heating rate increases, as shown by interval 2.

During July and August, wind speeds declined (see figure 3.1), promoting stratification, and leading to an increase in the rate of surface heating (interval 3, figure 3.11), with SST reaching a maximum in mid August. The SST collapse represented by interval 4 corresponds to a trough in the heat flux shown in figure 3.11. It is likely, therefore, that the temperature decrease was caused in part by a degree of convective overturn leading to increased mixing between surface and bottom layers of the watercolumn. During interval 5 (September/October), temperatures were fairly stable, and followed by winter cooling during interval 6 (November/December).

Variability of SST over Seasonal Time Scales; Comparison Between 1997 Observations and the Climatology at E1

A comparison between monthly mean SST during 1997 and the monthly means from the E1 archive data set (see Methods chapter) are presented in figure 3.12. The 1997 temperature range (11°C) was significantly larger than for the archived data (7°C), or for the long term (1903-1961) average (8°C) presented by Pingree & Pennycuick (1975). In addition to the increased amplitude, 1997 conditions differed significantly from the climatology in other respects; March, April, May, August October and November conditions were warmer than normal, whilst January and June conditions were cooler.

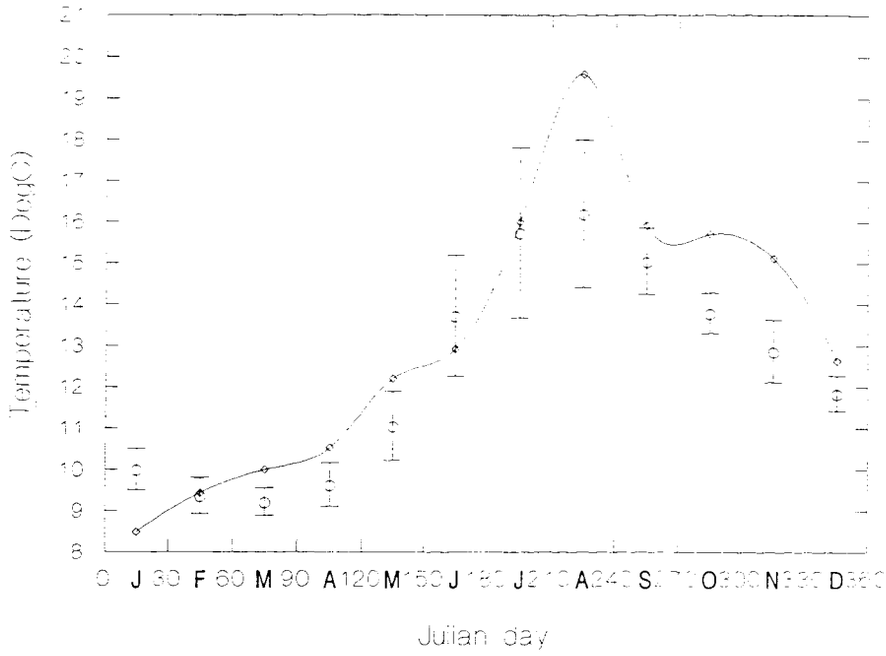

***Figure 3.12** – Monthly average SST at E1 during 1997 (AVHRR, continuous line) and monthly average surface temperature at E1 from the 1970 to 1984 (E1 data archive, open circles). Error bars represent 1 standard deviation of the climatological monthly means.*

That vertical processes of heat flux and wind mixing dominate the seasonal cycle of surface temperature at E1 was suggested by Pingree & Pennycuick (1975). It is possible, therefore, to explain the anomalies in the 1997 SST conditions with reference to anomalies in the 1997 meteorological conditions (as presented in figure 3.1). The elevated August SST, for example, can be accounted for by the lower than average wind speeds resulting in a shallower than normal thermocline. Similarly, the depressed June SST resulted from low global radiance (resulting in low heat flux) and high wind speeds (resulting in a deeper thermocline).

Comparison of Seasonal Variability of SST between E1, L4 and S2

Monthly SST at stations E1, L4 and S2 during 1997 are compared in figure 3.13. The SST distribution during 1997 was similar for each of the three stations, with correlation coefficients of ~0.98. Significant differences were, however, apparent: E1 was generally warmer than L4, which was warmer than S2. The differences between the stations were greatest during January (E1 = (L4 + 0.5°C) = (S2 + 1.2°C)), and August (E1 = (L4 + 0.3°C) = (S2 + 0.8°C)). Conversely, the differences between the stations was minimal during May, September and October.

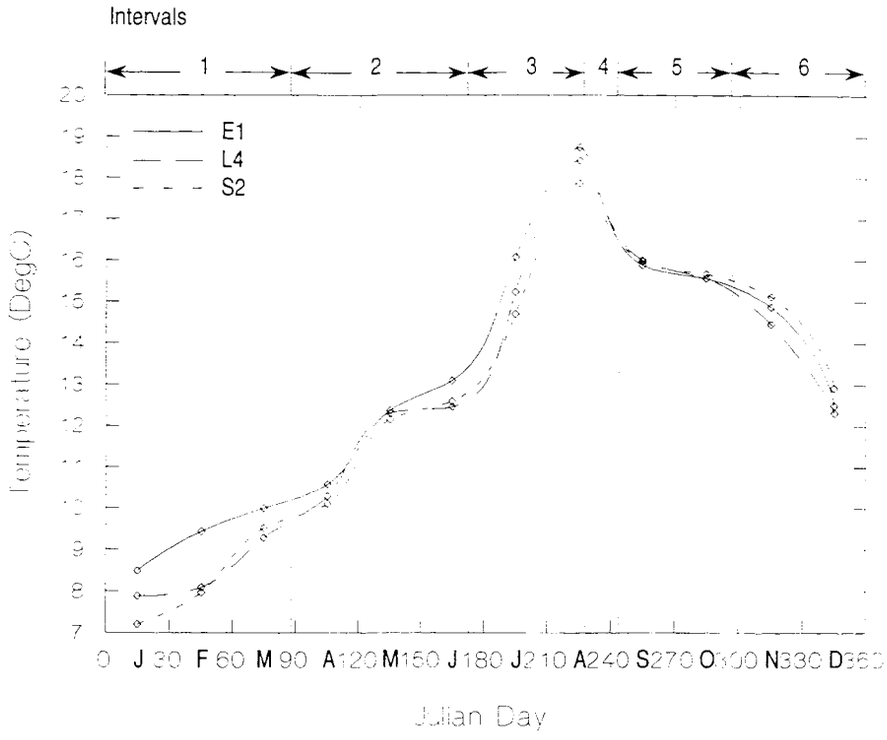

***Figure 3.13** – Comparison of monthly average SST at stations E1 (solid line), L4 (long dashed line) and S2 (short dashed line) during 1997.*

Given that the study region is small in comparison with the characteristic spatial scales of atmospheric variability, (typically of the order of 100 km, Lenhart et al, 1995), atmospheric forcing can be assumed to be constant across the region. It follows, therefore, that SST differences between two points within the region will be a result of differences in water depth, tidal stream, or horizontal advection (see Pingree, 1980). E1 is an offshore station, whilst S2 and L4 are onshore stations, S2 with a much greater tide than L4. Physical characteristics of the stations are listed in table 3.8.

Station Name	Distance offshore (km)	Water depth (m)	Mean M2 tidal speed (cm s^{-1})	Stratification Parameter (cgs units)
E1	35	72	28	2.2
L4	8	50	20	2.5
S2	12	60	37	1.7

***Table 3.8** – Some Characteristics of the Sampling Stations*

The differences in physical characteristics between the stations can be used to explain some aspects of the differences in SST. During the winter, the extra depth at E1 with respect to S2 affords it extra heat capacity, thereby reducing heat flux, leading to higher water temperature. During the summer, the higher value of S at E1 with respect to S2

reduces the cross-thermocline mixing of cool water from the BML into the SML, leading again to increased temperature.

The summertime differences in temperature between E1 and L4 cannot, however, be explained using the differences between physical characteristics shown in Table 3.8. The value of S at E1, for instance, is lower than that of L4. One would therefore predict a lower level of stratification at E1 than L4, and lower summer time SML temperatures. The observations, however, indicate that E1 was warmer than L4. This feature is investigated in more detail later in the thesis.

3.5 Variability of SST over Sub-Monthly Time Scales

Comparison of the Sub-Monthly SST Variability Between E1, L4 and S2

The analysis of distributions over different scales of variability is an important component of this thesis. It is useful, therefore, to develop methods by which the variability within each of the scales can be isolated. The seasonal temperature signal, for instance, will disguise, to some extent, temperature variability over scales of less than 1 month. A simple approach, used by Maddock & Swann (1977), defined sub-monthly variability as the standard deviation for each individual month. This approach, however, incorporates the seasonal trend of SST. In this thesis, a modified procedure for de-coupling seasonal and sub-monthly variability is proposed: The seasonal variability at E1 was described earlier as 6 intervals, identified by their rate of change of SST (see table 3.7). Correspondingly, 6 linear equations were determined and the deviation from them calculated using the least squares approximation. The sub-monthly SST variability was then defined as the deviation from the seasonal trend, averaged over each month.

The comparison of monthly deviation from the seasonal trend for stations E1, L4 and S2 is presented in figure 3.14. For E1, the distribution was dominated by 3 peaks to >0.4°C; during April, June and September. For L4, the first peak was diminished, and the September peak was not present, but the June peak was intensified (to ~0.6°C). For S2, only 1 peak was identified (at ~0.3°C, during July). The minimum values for each of the stations occurred during November and December at <0.2°C.

There are several processes that cause SST to vary over periods shorter than 1 month. These include; variations in heating rates, wind mixing (Ridderinkhof, 1992), tidal mixing (Simpson & Bowers, 1984), residual advection (Walstad *et al*, 1991), and the effect of each of these on cross thermocline mixing. Maddock & Swann's (1977) analysis of sub-monthly variability of surface temperature at E1 indicated a range from ~0.7°C for well-mixed mid-winter conditions during winter, to ~1.3°C for the stratified mid-summer conditions. That the distribution shown in figure 3.14 has both lower range and absolute values than this is an indication of the effects of removing the variability due to the seasonal cycle. Furthermore, the sub-monthly variability during 1997 showed features not present in the climatological analysis of Maddock & Swann. The features include peaks during April and September. One explanation for them is that the weak thermocline prevailing during these periods would have increased sensitivity to variations in physical forcing, which would be reflected by increased SST variability.

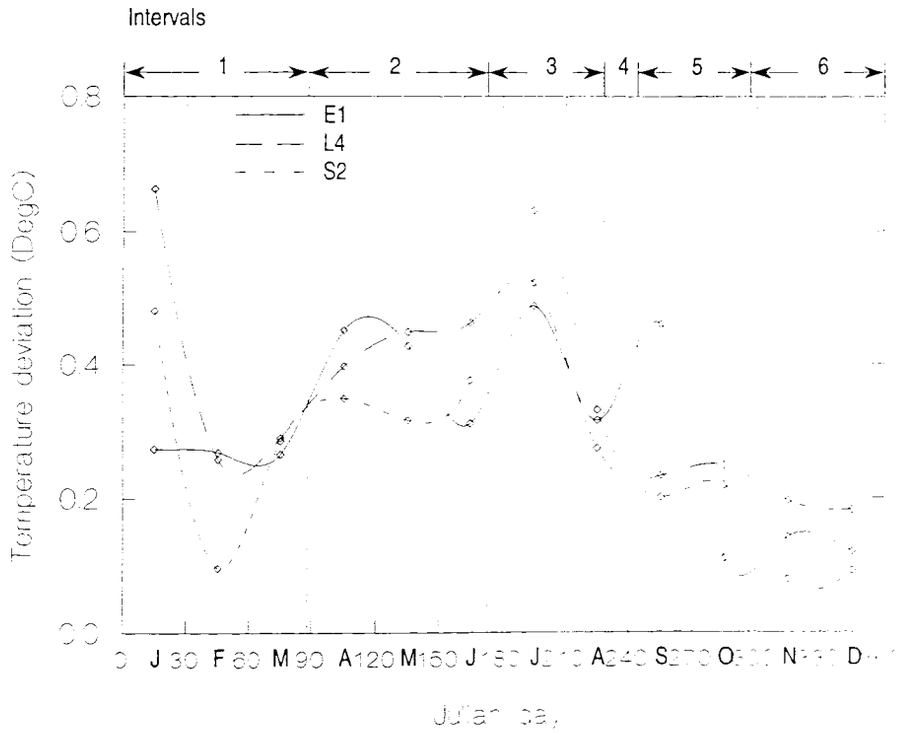

***Figure 3.14** – Comparison of monthly deviation of SST from the underlying trend at stations during 1997.*

The theory that the strength of the thermocline will affect temperature variability can be extended to explain the differences between patterns observed at E1, L4 and S2. As SST at L4 was more varied than E1 during May and June, it follows that the thermocline was less well established, indicating that L4 stratified later than E1. Furthermore, during

July, there was more variation at S2 than L4, suggesting that S2 stratified later still. The September maximum was only observed at E1, suggesting that, following the SST collapse (interval 4), the thermocline was only significantly re-established at E1, with L4 and S2 remaining well-mixed for most of the period. The order of tendency to stratify is therefore E1>L4>S2, a trend that was suggested earlier to explain the differences in monthly SST. It must be recognised, however, that the SST data set contains certain limitations, such as irregular coverage and sensor uncertainties (Miller *et al*, 1997) that may have affected the analysis.

Comparison Between Two Months of SST Variability During 1997

The SST distributions over two, 30 day periods, representing summer conditions (4th Jul to 3rd Aug 1997) and autumn conditions (27th Sep to 27th Oct 1997) at E1 are presented in figures 3.15A & B respectively. During the summer period, SST at each of the three stations varied in phase, with a quasi-regular frequency of ~10 days, and an amplitude of ~2°C. Also evident during the summer was an underlying heating trend, increasing by ~4°C over the 30 day period at each station. During the autumn period, SST variability had diminished in amplitude, and no regular frequency was identified. In addition, no underlying temperature trend could be identified.

The periods covered by figure 3.15 correspond to that of the meteorological data presented in figure 3.3. The meteorological events identified in figure 3.3 and described in table 3.6 could therefore be overlaid on the SST plots. One would expect meteorological variability over sub-seasonal time scales such as those presented in figure 3.3 to affect SST. Enhanced global radiance will lead to increased heat flux into the surface waters, increasing stratification, thereby reducing the entrainment of cooler deep water, and resulting in elevated SST. Conversely, enhanced wind mixing will lead to increased entrainment of deep water, reducing surface temperatures. The response of surface temperature to individual meteorological events has been observed previously (e.g. Large *et al* 1994).

The SST distributions apparent in figure 3.15 can be explained with reference to the meteorological distributions shown in figure 3.3. During the summer month, periods of high radiance and low wind speeds were associated with periods of elevated SST (events 1, 3 &5), and vice versa (events 2 & 4). This observation is consistent across all three sampling stations (E1, L4 and S2). Due to the irregular coverage of the AVHRR data, the magnitude of the SST response to the meteorological events is not well defined, but was of the order of 2°C over ~3 days. During the autumn month, however,

SST variation was low, and no correlation can be made with the meteorological events. This suggests that the water columns were well-mixed and therefore insensitive to short time scale meteorological variability.

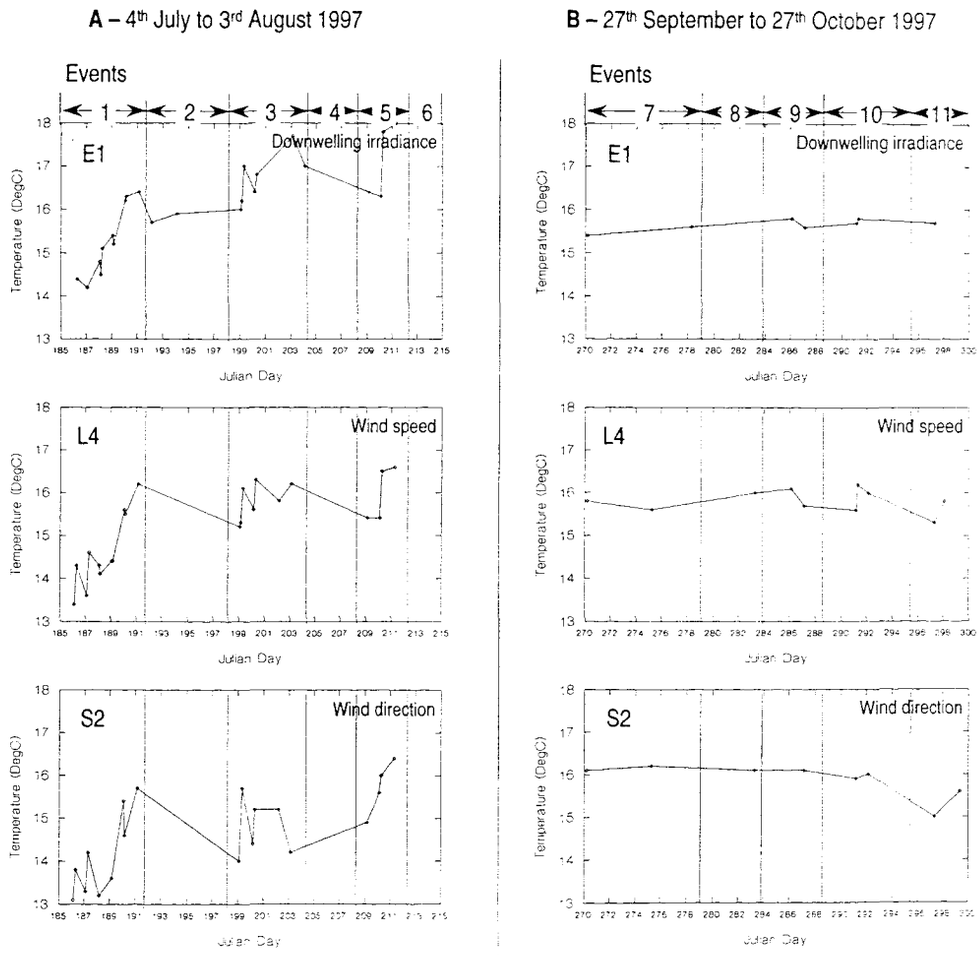

Figure 3.15 *– SST at stations E1, L4 and S2 over month long periods during 1997;* ***A:*** *4th July to 3rd August 1997,* ***B:*** *27th September to 27th October 1997.*

3.6 Satellite images; Spatial Variability Within the Study Region

Example Data From AVHRR Overpasses of the Study Region During 1997

Over the seasonal cycle, the sampling stations E1, L4 and S2 showed small but consistent differences with respect to SST variability. These differences between the stations suggest the existence of frontal regions in the study area. To characterise these fronts, 6 AVHRR overpasses of the study region during 1997 were selected. The overpasses were spaced at intervals of ~2 months, i.e. 15th Feb, 15th Apr, 10th Jul, 16th Aug, 24th Sep, and 3rd Dec.

To assess the overall context of each overpass, standard SST images of the western English Channel from 48 to 51°N and 2° to 6°W, are presented in the following sections. As the temperature differences between the images were greater than the horizontal temperature differences across each image, it was not possible to use an identical colour palette for each image. To obtain good resolution for an individual image, the minimum temperature for the colour palette was allowed to vary. To maintain consistency between the images, the temperature range of each colour palette was set to 3°C.

To enhance the horizontal SST distribution within the study region itself, data from the 6 overpasses were extracted over a smaller range; 50 to 50.3°N, and 3.8 to 4.5°W. With a smaller number of pixels, standard presentational techniques tend to result in "blocky" figures. In addition, smaller horizontal ranges also result in smaller temperature ranges, providing a degree of visual subjectivity in the image analysis. To avoid these limitations, SST data for the study region are presented as smoothed contour plots. To ensure consistency between the plots for each image, the contouring interval was maintained at the same level (0.2°C) throughout.

Two transects within the study region were identified as the focus for a more intensive study of horizontal variability. These run from stations E1 to L4, and stations E1 to S2. The data along these transects are identified by their distance in km from station E1. SST data along each transect from each of the six 1997 AVHRR overpasses was extracted. These data are presented as plots of SST against distance from E1 for each transect. These plots allow the features displayed in the SST images of the Western

English Channel, and the contour plots of the Study Region to be examined in more detail.

AVHRR Overpass, 15th February 1997

SST distributions for the 15th February 1997 from the AVHRR overpass at 03:26 GMT are presented in figure 3.17. This figure consists of four plots; the SST image for the western Channel, the SST contour plot for the study region, and SST against distance for each of the two transects, E1 to L4 and E1 to S2. The "masked" feature at –4.0°W, 50.0°N is a gridline indicator carried over from the original RSDAS image annotation, and is present on each of the presented AVHRR images.

For the western English Channel (figure 3.17A), the waters of the Atlantic (to the left of the image) were warmer than those on the Channel (to the right of the image). A band of warm water extended from the Atlantic, down the centre of the Channel. For the study region itself (figure 3.17B), the SST isotherms within the study region generally ran parallel to the isobaths (see figure 1.1), from east to west. Temperatures increased with distance towards shore, from 9.5°C at E1, to ~7.6°C at the coastline. The thermal gradient that was observed within the study region was part of the Atlantic/Channel front which dominated the SST distribution of the western English Channel. The same feature was also apparent along the two transects, E1 to L4 (figure 3.17Ci), and E1 to S2 (figure 3.17Cii). Along the E1 to L4 transect, the steepest thermal gradient occurred between 20km from E1 and station L4 (at 27 km from E1). Along the E1 to S2 transect, the steepest gradient occurred between 12 and 20 km from E1.

The data presented in the transects (figure 3.18Ci & Cii) can be used to calculate horizontal temperature gradients; along the E1 to L4 transect, the strongest gradient was ~0.1°C km^{-1}, whilst that along the E1 to S2 transect was ~0.2°C km^{-1}. For these gradients to be true representations of frontal gradients, the transect must have crossed the front perpendicular to the isotherms. This assumption can be tested by analysing the contour plot (figure 3.17B), on which both the isotherms and transects are plotted. Both of the transects do indeed run perpendicular with the isotherms, to within an angle of ~45°. An offset of 45°, for instance, would result in an underestimate of the temperature gradient by 30%.

During winter, net heat flux into the watercolumn tends to be negative, i.e. from the sea surface into the atmosphere, causing cooling of the sea surface. Furthermore, negative heat flux causes

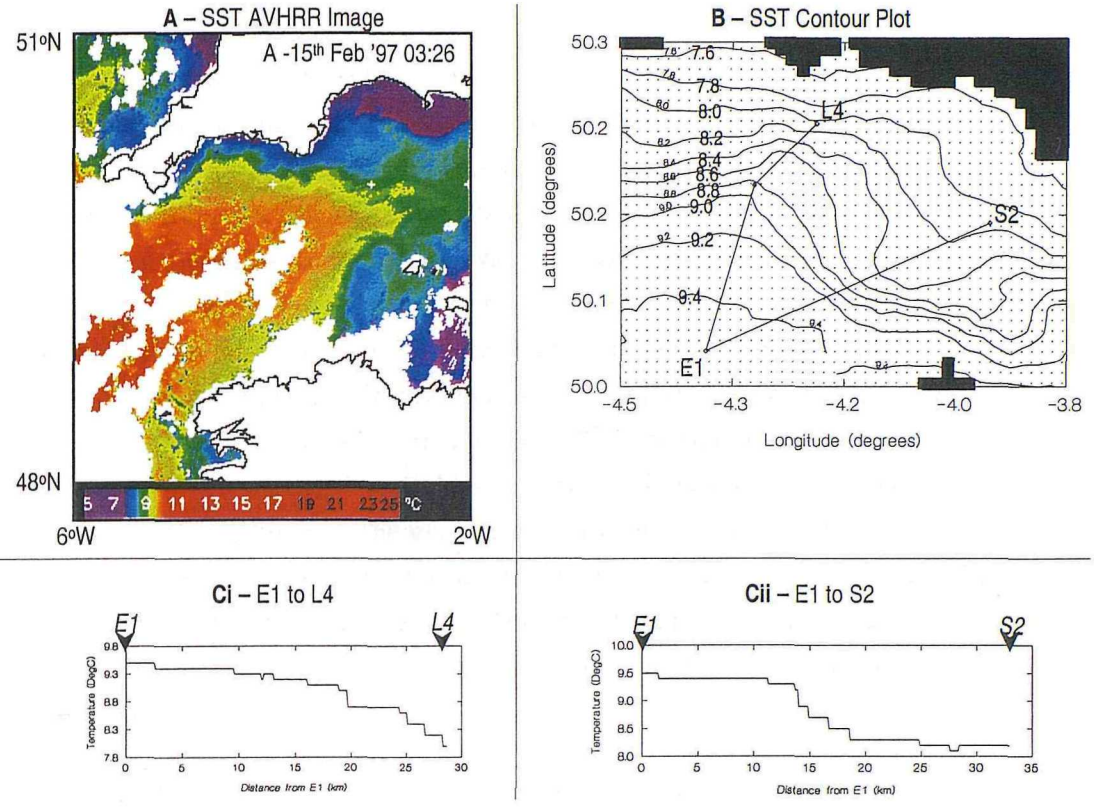

***Figure 3.17** – AVHRR SST for 15th February 1997, 03:26GMT.*
***A:** AVHRR SST image of the western English Channel. Temperature scale range = 3°C.*
***B:** SST contour plot of the study region. Contour interval = 0.2°C.*
***Ci:** SST transect from E1 to L4. **Cii:** SST transect from E1 to S2*

convective mixing. This mixing ensures that the water columns of shelf seas remain well mixed. During winter, therefore, heat lost from the sea surface is related to water depth. I.e. deeper water columns contain more stored thermal energy, and therefore cool more slowly. Areas where the water is deep will therefore tend to be warmer during late winter than those areas where the water is shallow. This process can be used as a qualitative hypothesis to explain the observation that the deeper Atlantic waters were warmer than the shallower Channel waters during February 1997. This theory is supported by the observation that the SST distribution within the study region was correlated in a positive manner with water depth.

As an alternative to vertical heat flux, the horizontal advection of warm water from the Atlantic into the western Channel could also have resulted in the horizontal SST variability observed on 15th February. This theory is supported by observation that strong, westerly winds prevailed February (see figure 3.2), which would tend to drive water from the Atlantic into the Channel.

If vertical heat flux rather than advection was responsible for the observed SST distribution, then a simple heat flux model will be able to account for the temperature differences between stations E1, L4 and S2. An appropriate heat flux model, driven by hourly meteorological and SST data, was described in Chapter 2, and was used for the following analysis. The water column was assumed vertically homogenous, with differences between stations controlled by water depth. Model simulations and AVHRR SST observations at E1, L4 and S2 were compared over the first 100 days of 1997. At E1, the observed temperature increased at a faster rate than simulated temperature, obtaining a maximum divergence of 1.4°C on 10th February. The predictions and observations for L4 and S2 diverged less rapidly, with maximum differences of less than 0.5°C by 10th February. The unexplained heat flux at E1 was calculated as 0.02°C day^{-1} (equivalent to 70 W m^{-2}). This inconsistency between observed and calculated winter temperatures at E1 has been noted previously (Pingree & Pennycuick, 1975). Vertical heat flux cannot, therefore explain the horizontal SST distribution observed on 15th February.

In addition to vertical processes, horizontal processes can also strongly affect temperature distribution (as discussed in Chapter 1). This is shown numerically in equations 3.1 and 3.2.

$$\frac{\partial T}{\partial t} = \frac{-\partial(vT)}{\partial x} + (\text{local heating/cooling}) \qquad (3.1)$$

Where: T is surface temperature,. t is time, v is surface horizontal advective velocity, and x is horizontal direction.

$$\frac{\partial(vT)}{\partial x} = \left(v\frac{\partial T}{\partial x} + T\frac{\partial v}{\partial x} \right) \qquad (3.2)$$

Assuming that horizontal velocity gradients were approximately constant in the region of E1 during early 1997, then the heat flux divergence due to horizontal advection can be estimated as the product of velocity and temperature gradient at E1 along an east-west axis (equation 3.2).

Estimates for advective velocity in the region of E1 have been made previously, and a value of ~1.5 km day^{-1} in an easterly direction is reasonable, calculated from data provided by Taylor & Stephens, (1983). The average local temperature gradient over the first 41 days of 1997, in a line running for 7 km West of E1, was calculated from AVHRR images, and equalled 0.010°C km^{-1}. Using these figures, an estimate of the heat flux divergence due to advection over the first 41 days of 1997 is -0.015°C day^{-1}.

The estimated heat flux divergence due to advection (-0.015°C day^{-1}) was of the same order of magnitude as the total observed heat flux divergence discussed earlier (-0.02°C day^{-1}). It is likely, therefore, that horizontal advection was an important factor in controlling SST distributions at E1 during early 1997.

AVHRR Overpass, 15th April 1997

SST distributions for the 15th February 1997 from the AVHRR overpass at 03:26 GMT are presented in figure 3.18. Atlantic waters were still warmer than those of the Channel (figure 3.18A), but the temperature gradients had reduced with respect to the 15th February situation. The strongest feature on the image was a front extending from the tip of Cornwall, running in a straight line south-easterly to the north coast of France. Along this front, an excursion into the Channel occurred, characterised by a diffuse boundary to the eastern edge, with a stronger boundary to the northern edge.

The northern edge of the excursion observed on the SST image extended into the study region, and is presented in more detail on the study region contour plot (figure 3.18B). Within the study region, temperatures offshore were lower than those onshore (10.6°C at E1 cf ~10.2°C at the coastline). Isotherms ran in a similar direction to those observed in February, from north-east to south-west. The transects (figure 3.18Ci & ii) also indicate that temperature gradients were low in the study region on 15th April. The maximum gradient along the E1 to L4 and E1 to S2 transects were 0.02 and 0.04°C km^{-1} respectively. These gradients are an order of magnitude lower than those observed during February.

Two processes are proposed for the reduced thermal gradients observed across the western Channel on 15th April. Firstly, during spring, advection will be less significant than during winter due to the reduced strength of westerly winds (see figure 3.2). This theory has been confirmed by Pingree & Pennycuick (1975), due to the agreement between the calculated and predicted heat and salinity budgets during these seasons. Secondly, during spring, heat flux into the water column is, on average, positive. Here, shallow waters will heat more quickly than deeper waters as they have less depth through which to distribute the additional heat. During spring, and before the onset of stratification, wintertime temperature gradients between deep and shallow water will therefore tend to diminish.

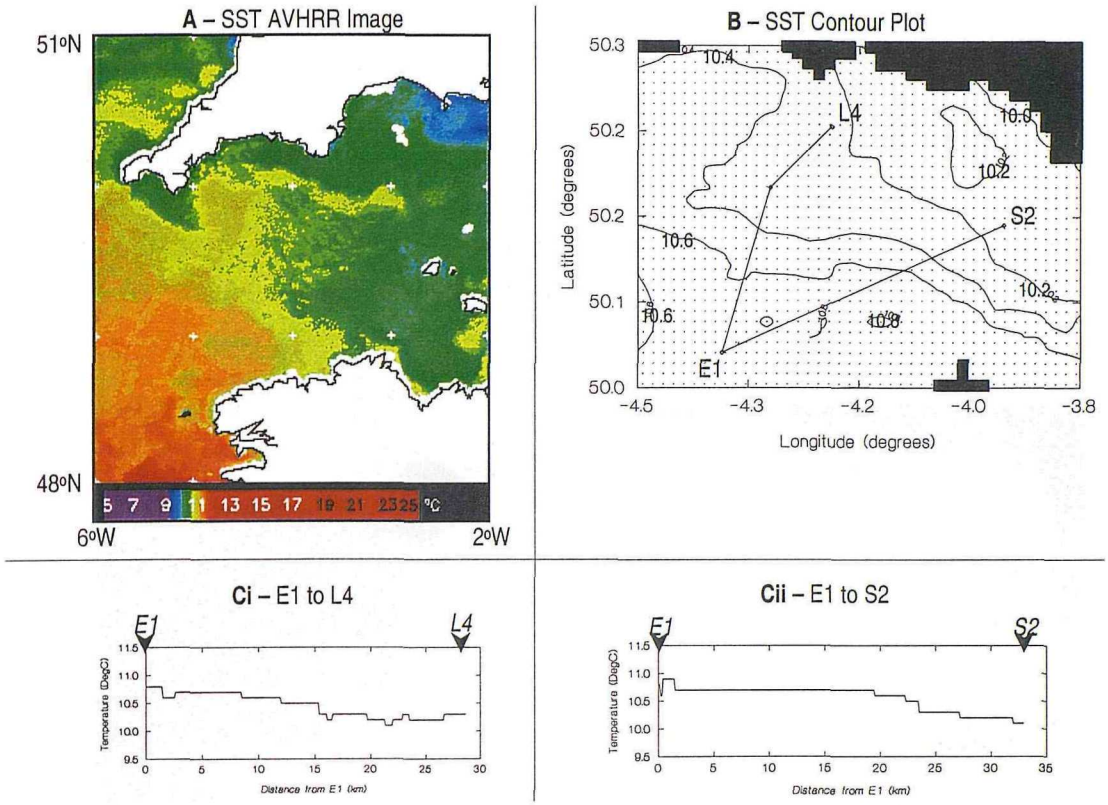

***Figure 3.18** – AVHRR SST for 15th April 1997, 02:44GMT.*
***A:** AVHRR SST image of the western English Channel. Temperature scale range = 3°C.*
***B:** SST contour plot of the study region. Contour interval = 0.2°C.*
***Ci:** SST transect from E1 to L4. **Cii:** SST transect from E1 to S2*

By mid-April, stratification has generally become established at station E1 (Maddock & Swann, 1977), and for the western Channel in general. The western Channel temperature distribution for this period is generally dominated by tidal front to the south of Plymouth (Pingree, 1980). Differences in the timing and degree of stratification were therefore produced horizontal temperature gradients on 15th April 1997 (Figure 3.18). It is suggested that the shallow, tidally vigorous Channel waters remained well mixed, whilst the deep, tidally slack Atlantic waters became stratified. In support of this hypothesis is the observation that the temperature distribution along the E1 to S2 transect (figure 3.18Cii) correlated positively with the distribution of the stratification parameter (see figure 3.9). When stratification has developed, SSTs in the well mixed, tidally energetic waters to the north of France are generally lower than for the stratified central Channel. On 15th April, however, these waters were warmer than for the central Channel. It appears, therefore, that the horizontal temperature distribution on 15th April was complex, and resulted in a combination of heat flux, advective and stratification processes.

AVHRR Overpass, 10th July 1997

By 10th July a strong thermal front had become established that ran from the north-west coast of France (the Ushant Peninsula), across the western Channel, and up to the south coast of England (figure 3.19A). The front reached the English coast within the study region, for which the temperature distribution is presented in more detail (figure 3.19B).

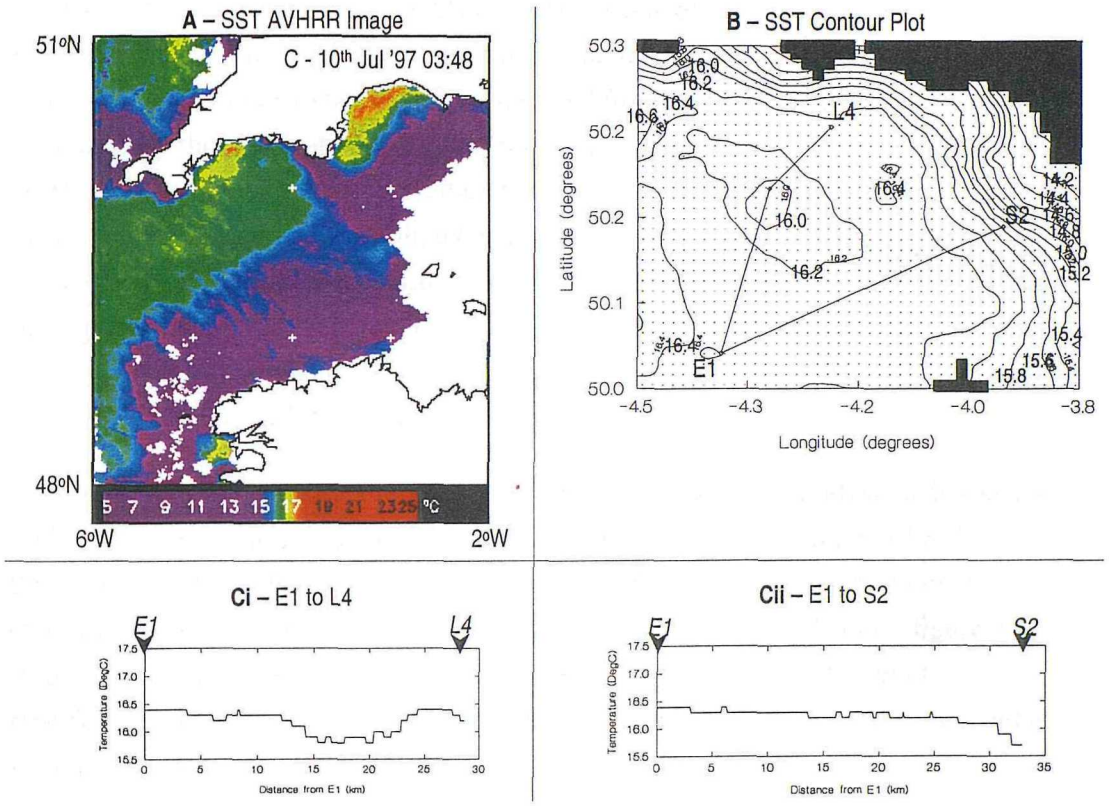

***Figure 3.19** – AVHRR SST for 10th July 1997, 02:44GMT.*
***A:** AVHRR SST image of the western English Channel. Temperature scale range = 3°C.*
***B:** SST contour plot of the study region. Contour interval = 0.2°C.*
***Ci:** SST transect from E1 to L4. **Cii:** SST transect from E1 to S2*

Temperatures were fairly constant (16.2 to 16.4°C) for most of the study region (figure 3.19B). Temperatures declined rapidly, however, near to the coastline at the north of the region, and at the right hand edge of the figure, at the east of the region. The isotherms at the gradient to the north were aligned parallel to the coast, whilst those to the east ran parallel to the contours of stratification coefficient (S, see figure 3.8). A temperature depression (to <16°C) was observed in the location of the Eddystone Rocks (see figure 1.1).

The transects for 10th July (figure 3.19Ci & ii) were mainly located within the isothermal area of the study region, outside of the major temperature gradients to the north and east. The E1 to L4 transect did, however, intersect the temperature depression in the vicinity of the Eddystone Rocks, which extended for ~15 km (12 to 27 km from E1), and caused temperatures to fall by ~0.5°C.

The front observed on the satellite image on 10th July is typical of the tidal front observed in the western English Channel during summer months (Pingree, 1980). This front marks the boundary between stratified Atlantic waters to the West and tidally mixed Channel waters to the East. That the tidal front extended into the study region is supported by the observation that the temperature distribution to the east of the region correlated closely with the stratification parameter. In addition, the location of the maximum thermal gradient within the region occurred at a for S of ~1.5 cgi units. This is the typical value for the location of tidal fronts over the shelf seas of the UK during the summer months (Pingree & Griffiths, 1978). Neither of the transects intersected major temperature gradient, suggesting that the water column was thermally stratified along the length of each transect.

The location of the isolated SST depression in the vicinity of the Eddystone Rocks on 10th July is consistent its creation due to the island stirring effect, as described by Simpson & Tett (1986). Further evidence to support this theory is its orientation, elongated along a NWW–SEE axis, the same as the tidal ellipse at L4 (see figure 3.6). It is likely that a fall in temperature of 0.5°C resulted from a decreased level of stratification due to additional mixing that the entire breakdown of stratification and a well mixed water column.

AVHRR Overpass, 16th August 1997

A strong thermal front was also present in the western English Channel on 16th August 1997 (figure 3.20A). By this date, the front had expanded further south and north than on 10th June. Within the study region (figure 3.20B) strong temperature gradients were present throughout, with the isotherms orientated from NEE to SWW. Temperatures fell from 20.6°C at E1 to a minimum of 16.8°C at the coastline to the east of the region. Compared to 10th July, temperature gradients from east to west at the eastern edge of the study region were reduced. The maximum horizontal temperature gradients along the E1 to L4 and E1 to S2 transects were 0.2 and 0.1°C km^{-1} respectively. The lower gradients along the E1 to S2 transect is an underestimate as the transect did not cross parallel to the isotherms.

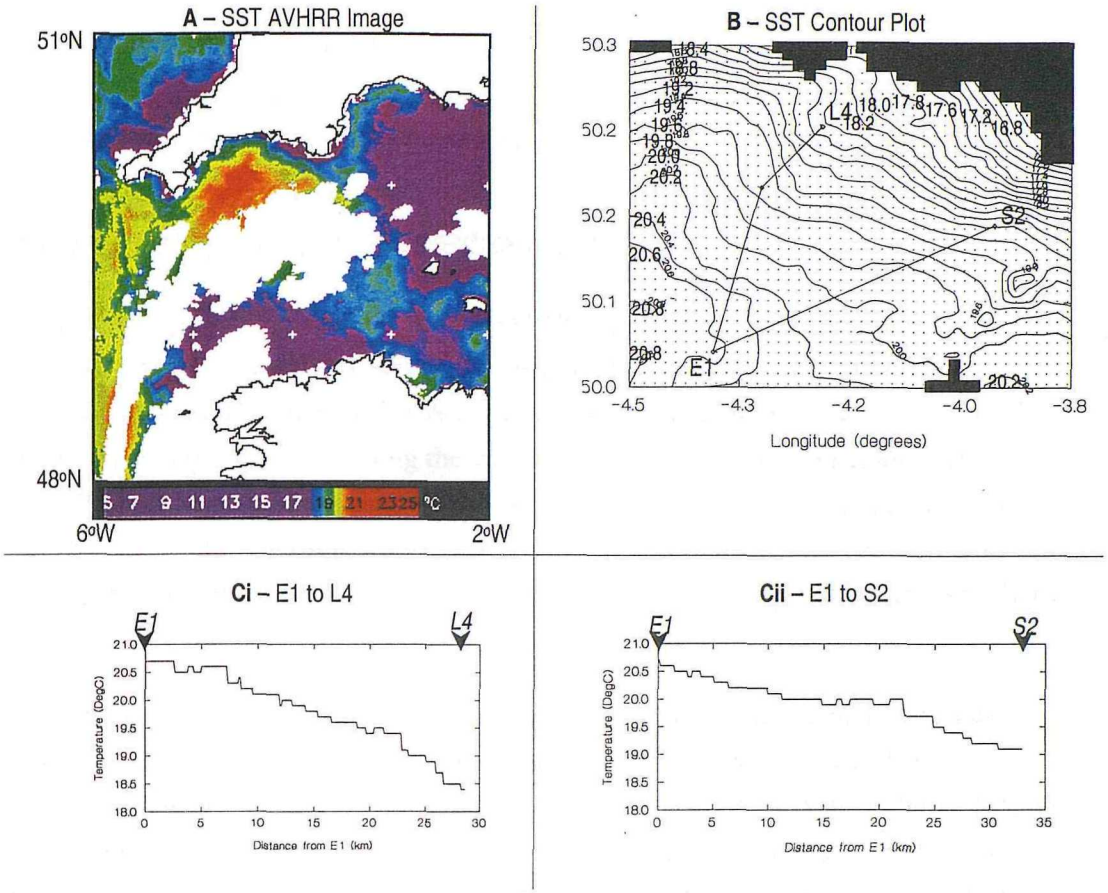

Figure 3.20 *– AVHRR SST for 16th August 1997, 03:45GMT.*
A: *AVHRR SST image of the western English Channel. Temperature scale range = 3°C.*
B: *SST contour plot of the study region. Contour interval = 0.2°C.*
Ci: *SST transect from E1 to L4.* ***Cii:*** *SST transect from E1 to S2*

The front observed on the satellite image on 16th August was a similar tidal front to that observed on 10th July. With extra heating and reduced wing mixing, the area covered by stratification had expanded, as tidally energetic waters became progressively more stratified.

The 16th August represents the highest SST recorded at each of the three sampling stations during 1997 (20.7°C at E1, 18.4°C at L4 and 19.1°C at S2). 16th August also represents the highest temperature difference observed during 1997 between stations E1 and L4 (2.4°C). The low wind speeds during August (see figure 1.1) resulted in the formation of a very thin (<8 m) surface mixed layer, which heated rapidly. As the volume of this mixed layer was low, small variations in vertical fluxes led to large variations in the temperature of the layer. The SST transects for the 16th August are therefore characterised by considerable temperature gradients, even though the watercolumn was highly stratified throughout. This type of argument is not well

documented in the literature. Bisagni (1990), however, proposed that during spring tides the surface mixed layer would be thin and therefore susceptible to wind mixing, but presented no observations in support of this theory.

AVHRR Overpass, 24th September 1997

On 24th September (figure 3.22), the temperature gradients within the western English Channel had reversed from the July and August situation, with the warmest waters to the East, and cooler waters to the West. The temperature gradients had also reversed within the study region and along the transects, with the coolest temperatures at E1 (15.4°C), with warming towards L4 and S2 (reaching 16°C). The onshore temperature distribution within the study region was characterised by small scale variability, and reflected, to a certain extent, the patchy nature of the underlying bathymetry (see figure 2.1).

By 24th September, convective overturn and increased wind mixing had caused the seasonal stratification over the western English Channel to break down. The temperature distribution reflected the average heat content of the water column. During the summer, under stratified conditions the air-sea temperature difference was lower than for mixed conditions, resulting in lower heat flux into the water column. Once stratification had broken down, those areas that had been stratified during the summer became cooler than those that had been well mixed. This pattern was repeated within the study region and along the transects.

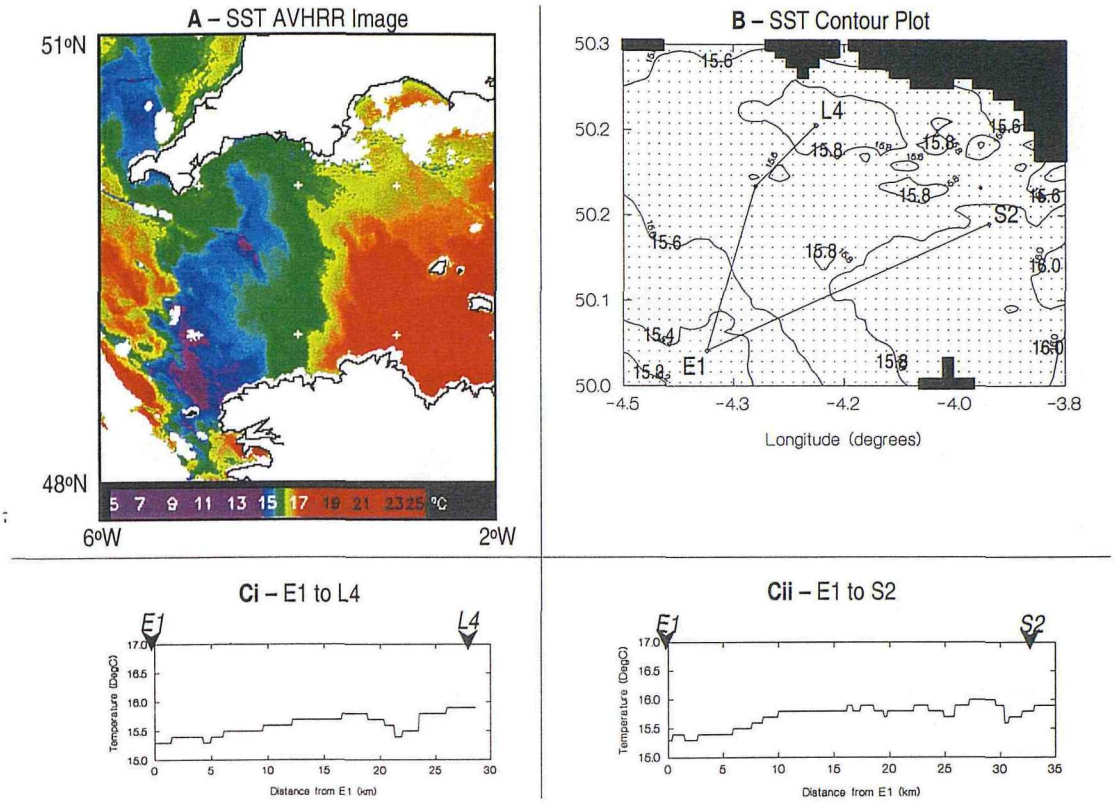

***Figure 3.21** – AVHRR SST for 24th September 1997, 03:20 GMT.*
***A:** AVHRR SST image of the western English Channel. Temperature scale range = 3°C.*
***B:** SST contour plot of the study region. Contour interval = 0.2°C.*
***Ci:** SST transect from E1 to L4. **Cii:** SST transect from E1 to S2*

AVHRR Overpass, 3rd December 1997

By 3rd December (figure 3.22A), the thermal gradients over the whole of the cloud free area of the AVHRR image had diminished. SST gradients were also low throughout the study region. In general, isotherms ran from south-west to north-east. with the warmest temperatures found to the south-east. These low-gradient conditions reflected well-mixed winter conditions. The lack of an advective signal on this date (in comparison to February) was due to the lack of temperature gradients over a wider area.

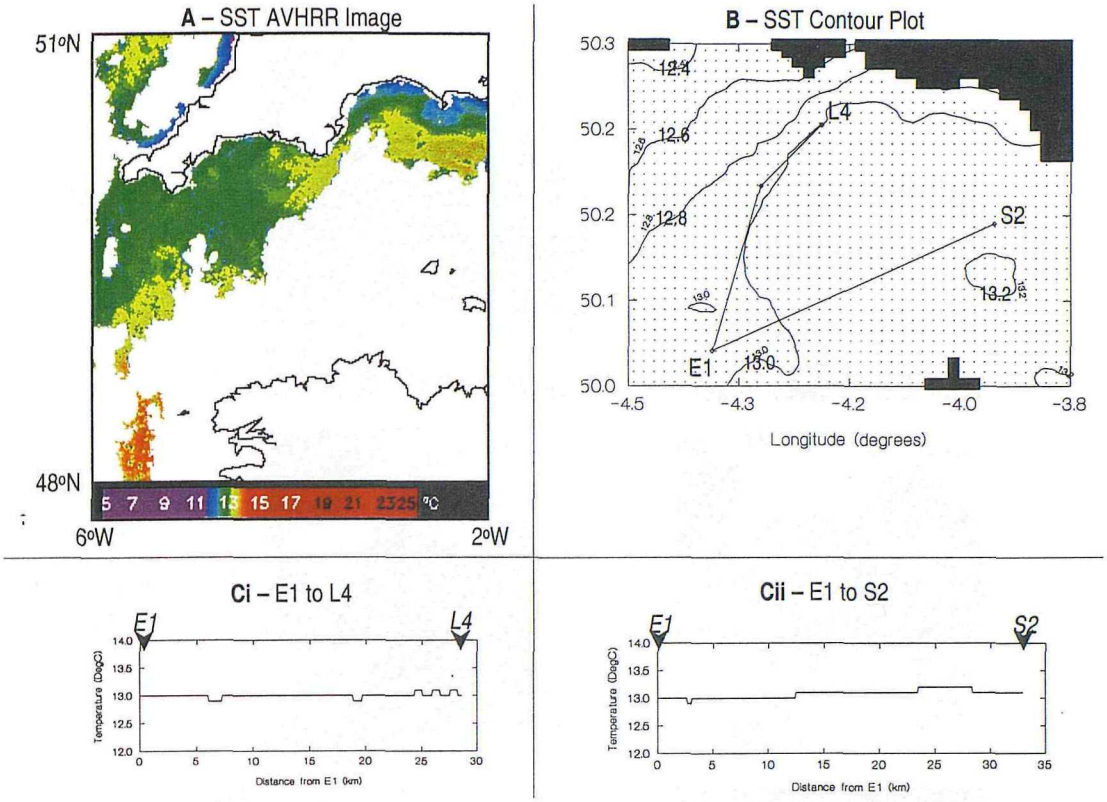

***Figure 3.22** – AVHRR SST for 3rd December 1997, 03:55GMT.*
***A:** AVHRR SST image of the western English Channel. Temperature scale range = 3°C.*
***B:** SST contour plot of the study region. Contour interval = 0.2°C.*
***Ci:** SST transect from E1 to L4. **Cii:** SST transect from E1 to S2*

SeaWiFS Images for 1998

SeaWiFS data was not available for 1997, and was therefore not contemporaneous with other data presented in this thesis. It is useful, however, to present SeaWiFS images collected during 1998, with appropriate AVHRR SST images. Comparisons between synoptic physical and biological variability provide qualitative links between physical and biological processes. Four SeaWiFS images of the western English Channel for 1998 are presented in figure 3.23. These represent winter conditions (20th January), summer conditions (15th June and 5th August), and Autumn conditions (19th September). Night time AVHRR images from the same dates are also presented.

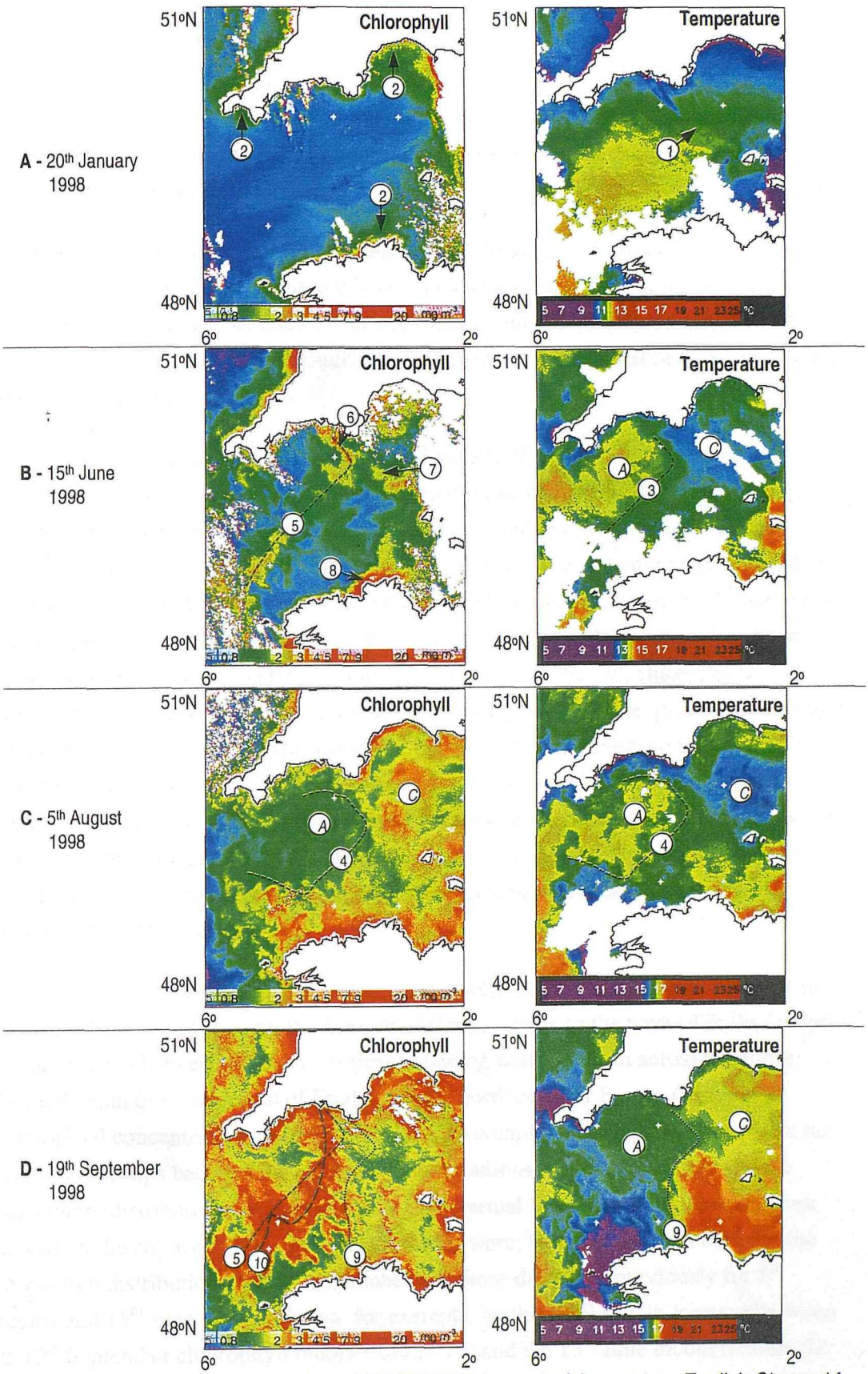

***Figure 3.23** – SeaWiFS Chlorophyll and AVHRR SST, images of the western English Channel for '98'*

The temperature distribution on 20th January 1998 (figure 3.23A) shows a band of warm water extending from the Atlantic in the west and up the Channel to the east (marked on the image as feature 1). The chlorophyll distribution for 20th January shows low concentrations throughout the area, with slight elevations towards the English and French coasts (marked as feature 2).

The temperature distributions on 15th June and 5th August 1998 (figure 3.23B & C) were similar. These identify the location of front (features 3 and 4) between warm Atlantic water (*A* on the image) and cooler Channel water (*C* on the image). The fronts each extended from the edge of the clouded areas to the north-west coast of France, up to the south coast of England.

Whilst the temperature distributions on 15th June and 5th August were similar, the corresponding chlorophyll distributions differed significantly: On 15th June, elevated chlorophyll concentrations were located in a band running along the thermal front (feature 5). The chlorophyll bloom was strongest (3 to 4 mg m^{-3}) and narrowest (a few km across) in an area to the East of the study region, in the vicinity of S2 (feature 6). A discrete patch of elevated chlorophyll was also present extending eastwards from the frontal bloom into cooler waters (feature 7). Away from the front, chlorophyll concentrations were elevated in a narrow band edging the coastline, particularly evident off the north coast of France (feature 8). In contrast, on 5th August the frontal bloom was absent, and high chlorophyll concentrations were found in the cooler channel waters to the east and south, with low concentrations in the warmer Atlantic waters. The covariance between chlorophyll and temperature was high and negative on 5th August. This point is highlighted by the similarity in location between the thermal and chlorophyll fronts (feature 4).

On 19th September (figure 3.23D), temperatures were higher in the Channel waters to the east (*C* on the image), and lower on the Atlantic waters to the west (*A* in the image). A front existed between these two regimes, running north to south across the entire Channel, from the south coast of England to the north coast of France (feature 9). Chlorophyll concentrations on this date showed a complex distribution. There were no clear relationships between the chlorophyll distributions on 19th September and the temperature distributions on the same date (the thermal front, feature 9, has also been marked on the chlorophyll image). Relationships were, however, evident between the chlorophyll distributions on 19th September and those discussed previously for 5th August and 15th June. This is shown, for example, by the similarity in location between the 19th September chlorophyll bloom (feature 10) and the 15th June bloom (feature 5).

In general, on 19th September, chlorophyll concentrations were higher to the West, and lower to the East.

The chlorophyll distributions described above can be explained qualitatively using the theory of light and nutrient regulation of phytoplankton growth: During the winter months, low light levels (see, for example, the downwelling irradiance values during winter presented in figure 3.1), limit phytoplankton productivity. On 20th January, for instance, chlorophyll values were uniformly low throughout the channel. The apparent chlorophyll elevation at the land-sea margins on this date (feature 1 on figure 3.23A) may have resulted from increased suspended sediment load in shallow waters. Such chlorophyll elevation along the land-sea margin was also observed on 15th June (feature 8 on figure 3.23B).

The temperature front observed on the images for both 15th June and 5th August 1998 were typical of a tidal front. Tidal fronts are often associated with changes in chlorophyll distribution (e.g. Pingree *et al*, 1975). Classically, tidal fronts are areas of enhanced phytoplankton productivity, hence elevated surface chlorophyll. It is reasonable to suggest, therefore that the elevated chlorophyll concentrations observed at the tidal front on 15th June 1998 (feature 5 on figure 3.23B) resulted from enhanced productivity. Summer chlorophyll enhancement along the tidal front in the English Channel has been described previously, using colour satellite images (Holligan *et al*, 1983, Hochman et al, 1995). On 15th June, there was a discrete area of elevated chlorophyll in the mid-Channel which was not associated with frontal temperature distributions on the same date (feature 6 on figure 3.23B). However, such a frontal distribution was observed in this area on 10th July 1997 (see figure 3.19). It is likely, therefore, that this area was stratified immediately before or after 15th June 1998, and this may have been responsible for the observed chlorophyll bloom.

On the 5th August, there was no clear chlorophyll elevation along the tidal front (feature 4 on figure 3.23C). Elevated chlorophyll concentrations on this date extended eastwards and southwards from the front, into the well-mixed Channel waters. Blooms in normally well-mixed waters can occur if there is either; short periods of stratification, or sufficient light to bring the whole water column above the compensation depth.

On 19th September 1998, the temperature distribution was similar to that described previously for 24th September 1997. This distribution is characteristic of the area immediately following the breakdown of seasonal stratification. This period is characterised by the formation of the autumn phytoplankton bloom. Convective overturn mixes nutrients into previously stratified surface layers, thereby promoting

productivity. Such a bloom will not occur over areas that were previously well mixed, or where the nutrients had been depleted throughout the water column. This an explanation for the observation that, on 19th September 1998, high chlorophyll concentrations were observed in the region that had been stratified during the summer, and low concentrations were observed in the region adjacent to the frontal zone on the well mixed side.

3.7 Conclusions

The study region is characterised by strong temporal and spatial gradients in SST. These gradients are typical of those previously documented for this region, and shelf seas in general.

Atmospheric forcing was shown to significantly effect the seasonal distribution of SST at E1. The differences between the 1997 and climatological average monthly SST distribution were clearly correlated with the differences between the 1997 and climatological meteorology.

Atmospheric forcing was related empirically to the distribution of SST over synoptic time scales. During the summer, dull, windy, cool periods were associated with falls in SST, whilst bright, still, warm periods were associated with elevated SST. After stratification had broken down, however, SST distribution was less sensitive to synoptic meteorological events. That SST variability is related to the strength of stratification was shown using a novel analysis of monthly average variability of mesoscale SST.

It was shown that horizontal advection of the water column significantly effected SST distribution at E1 during the early part of 1997. The advective effect was less significant for L4 and S2, and had diminished at E1 by late March.

The seasonal and mesoscale variability of SST indicates that the tendency for the water column to stratify at the stations is E1>L4>S2. This is different to the tendency predicted using stratification parameter arguments (L4>E1>S2). Similarly, horizontal SST gradients between E1 and S2 can be related empirically to horizontal variation in water depth and tidal mixing, whilst the observed gradients between E1 and L4 cannot. It is argued that the E1 to L4 transect is more complex due to the effect of the Eddystone Rocks on local mixing. This theory is supported by observations of island mixing effects on SST images that intercept the E1 to L4 transect.

The features described for the study region are part of larger scale structures, which dominate the physical characteristics of the Western English Channel.

The chlorophyll distribution during 1998 could be linked qualitatively with temperature distributions, although the relationships between the two were not always clear. Chlorophyll distributions often resulted from previous physical regimes, and therefore related most closely to previous temperature distributions.

The analysis of water column structure from SST observations relies on assumptions of sub-surface processes, and the likely degree of stratification. These assumptions are supported by descriptions in the literature, and on archived data. It is desirable, however, to test these assumptions against sub-surface temperature observations. Observations of this type are presented in the next chapter.

4. Results Part 2 – In-Situ Observations

4.1 Data Selection

The first part of this chapter presents data from the E1 archive. This consists of monthly averages of all temperature, nitrate + nitrite and chlorophyll data routinely collected at E1 between 1974 and 1987. These data provide a depth-resolved, summary of the average seasonal distribution of temperature, nutrients and chlorophyll concentrations at E1. The contouring procedure for the data was as follows: Each measurement was assigned a depth bin (bins were at 5 m intervals from 0 to 80 m depth), and a month bin (bins represented calendar months). The data for each month/depth combination were averaged, and field contours plotted against depth vs. month. The "Systat" computer package was used for producing the contour plots.

The second part of the chapter presents data collected during 8 field sampling events carried out during 1997, between June and September. This covers the period of the study for which the most comprehensive set of reliable in-situ data was collected. This period is characterised firstly by the build up of stratification through the summer, followed by its break-down in autumn. The data for these events consisted mainly of depth resolved temperature, chlorophyll and beam attenuation, collected using the UOR.

The 8 sampling events, with the total number of UOR profiles and chlorophyll samples, are listed in table 4.1. Additional information concerning these events is included in Appendix 6 The data from each sampling event was separated into the corresponding transect of the boat-track, i.e. E1 to L4 and E1 to S2. The data collected over each transect is also listed in table 4.1. In order to provide spatial consistency over each sampling event, data collected from a perpendicular distance of greater than 2 km from the "standard" boat track were removed from the analysis. The sum of the number of data for each transect is therefore lower than the total for each event.

UOR measurements, with a horizontal resolution of ~1 km, were used to generate the contour plots (produced using the Systat package) presented in the following sections.

The measurements are plotted against distance from E1 along the E1 to L4 and E1 to S2 transects. Surface chlorophyll measurements are also presented, as scatter plots.

Sampling Event	Number of UOR Profiles			Number of Surface Chlorophyll Samples		
	Total	E1 to L4	E1 to S2	Total	E1 to L4	E1 to S2
10th Jun 97	114	31	34	20	9	7
24th Jun 97	162	47	75	30	13	15
10th Jul 97	170	44	69	29	11	12
11th Jul 97	143	43	48	25	9	9
29th Jul 97	185	52	75	35	15	14
11th Sep 97	123	35	51	24	7	11
17th Sep 97	129	36	47	25	12	9
23rd Sep 97	138	44	58	25	9	9

***Table 4.1** – Amounts of data collected during the sampling events carried out between June and September '97. E1 to L4 and E1 to S2 refer to the repeated transects of the standard boat track.*

The third part of this chapter presents data collected by PlyMBODy. Reliable data were retrieved for two periods during 1997, 8th August to 21st August and 5th September to 29th November. The system was cleaned periodically, as shown in table 4.2. From the total, two 3-day long periods are presented, 8th to 11th August 1997 and 25th to 28th September 1997. These are used as examples of the characteristic variability of temperature and chlorophyll concentrations over short temporal scales.

Julian Day	Date	Time (GMT)	Activity
167	16-Jun-97	10:30	System deployed
220	08-Aug-97	13:30	System fully operational
233	21-Aug-97	10:00	Data failure start
248	05-Sep-97	09:00	Data failure end
260	17-Sep-97	09:00	Cleaned
272	29-Sep-97	13:00	Cleaned
287	14-Oct-97	11:30	Cleaned
304	31-Oct-97	09:30	Cleaned
339	05-Dec-97	11:30	System recovered

***Table 4.2** – Deployment and Maintenance of PlyMBODy During 1997.*

The final part of this chapter presents bio-optical data collected during the 8 sampling events of 1997. These data are relevant as they provide information pertinent to the analysis of ocean colour images as measured from satellite. Although no ocean colour images were contemporaneous with other data presented in this thesis, they are likely to be an important source of chlorophyll observations in the future as shown, for example, by the SeaWiFS images presented in chapter 3.

4.2 E1 Archive – Mean Monthly Distribution of Temperature, Chlorophyll and Nitrate

In the previous chapter, various reasonable assumptions about sub-surface temperature were used to explain the observed distribution of sea surface temperature during 1997. The validity of these assumptions can be tested through direct observations. The average monthly temperature distribution for the watercolumn at E1, produced from a large data archive (see Jordan & Joint, 1998) is presented in figure 4.1A. As figure 4.1 is the average of a number of years of data, the average vertical extent of the thermocline is larger than would normally be observed from an individual vertical profile. It provides a estimate of the envelope in which the thermocline is usually located; e.g. between 40 m and 10 m depth during the summer.

Figure 4.1A shows the development of the thermocline in April (temperature change of <0.5°C) and its increase in strength until August (temperature change of >3°C). Between April and August, the depth of the surface mixed layer (SML) and the horizontal extent of the thermocline decrease. In September, the cross-thermocline temperature difference decreases, with the thermocline becoming entirely eroded by October. These observations are similar to those presented previously for the average seasonal temperature distribution at Station E1 (e.g. Pingree *et al*, 197).

Figure 4.1B shows the decrease in nutrient concentrations from >6 mg m^{-3} in February to <1 mg m^{-3} in the SML during July, with the most rapid decrease occurring during April and May. Concentrations increase again following July, re-gaining values of >6 mg m^{-3} by November. During the summer months, nutrient concentrations in the SML are lower than those in the bottom mixed layer (BML) (<1 cf. >1 mg m^{-3} respectively). Chlorophyll concentrations (figure 4.1C) increase from <0.5 mg m^{-3} during February to >2 mg m^{-3} in the SML during May, representing the spring bloom. Concentrations fall during the summer (e.g. <0.5 mg m^{-3} in the SML during July), whilst meanwhile showing evidence of a sub-surface chlorophyll maximum (of >1 mg m^{-3}). The autumn bloom occurs during September (concentrations of >1.5 mg m^{-3} in the SML), and wintertime concentrations are re-established during mid-November.

The distribution of average monthly temperature (figure 4.1A) can be related to both average monthly wind speeds (see figure 3.1), and average monthly heat flux (see figure 3.10). During the spring, stratification is initiated by positive heat flux and moderate winds. During the summer, additional heat flux increases the surface buoyancy, and

reduced wind speeds reduce the depth over which it is mixed. Therefore, the degree of stratification increases, and the depth of the thermocline decreases, over this period. In the autumn, heat flux decreases (often becoming negative and causing convective overturn) and wind speeds increase. This causes mixing which increases the SML depth, and decreases the thermocline temperature difference, eventually destroying the thermocline.

The mean monthly distribution of chlorophyll at E1 has been discussed previously by Holligan & Harbour, 1977. Their fig.3 is an idealised diagram of the distribution based on 2 years of data (1975 and 1976). This schematic and the contour plot drawn from real values (figure 4.1C) share many similarities. During April, the onset of stratification causes the spring bloom. This bloom depletes nutrients throughout the water column (figure 4.1B), leading to the surface chlorophyll minimum during July. Regeneration of nutrients in the BML, their mixing into the thermocline, and the presence of the thermocline within a well-illuminated region leads to the development of the thermocline chlorophyll maxima during July and August. Finally, the mixing of nutrients into the surface layer during September leads to the development of the autumn bloom.

There are various reasons for the differences between Holligan & Harbour's (1977) schematic description of chlorophyll distribution and the monthly mean situation in figure 4.1(C). Holligan & Harbour's description was based on the analysis of discrete profiles, whereas the monthly averages were calculated from a number profiles which vary over time. The averaging process leads to the blurring of sharp features such as the spring bloom and the thermocline chlorophyll maximum that are present on individual profiles.

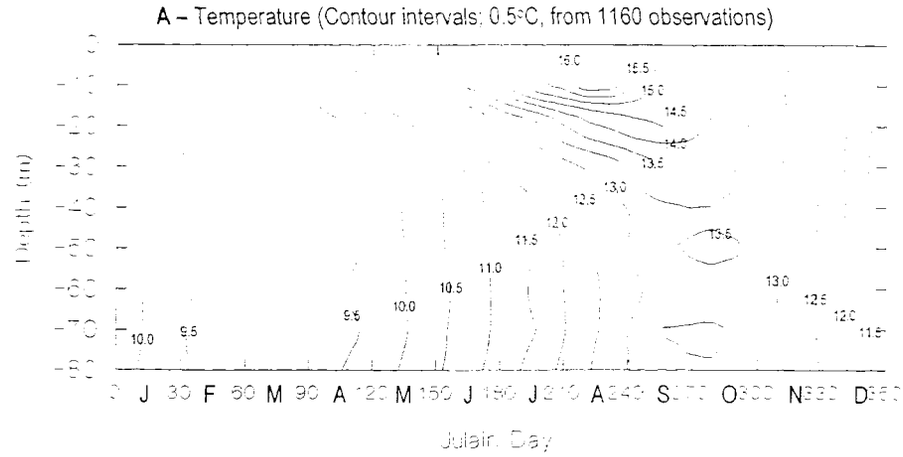

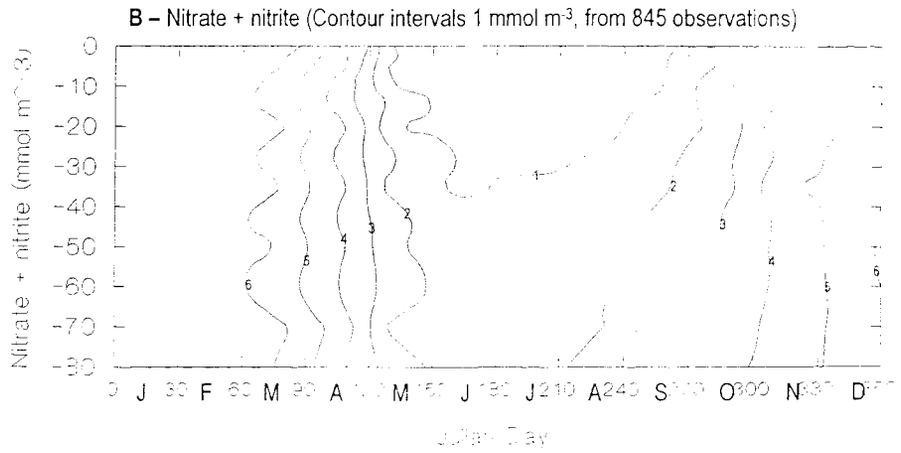

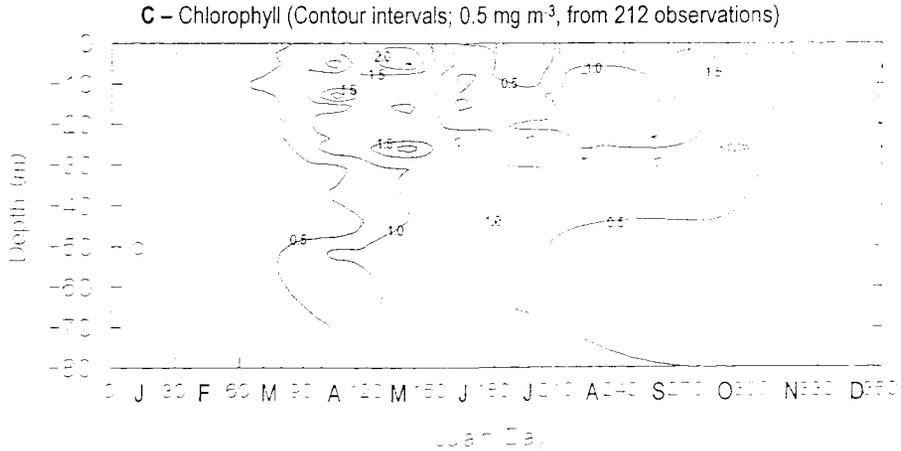

Figure 4.1 – *Mean annual distributions at E1 From the E1 archive database (1970 to 1984):*

***A** – Temperature,*

***B** – Nitrate + Nitrite,*

***C** – Chlorophyll.*

4.3 UOR Observations From June to September 1997

10th and 24th June 1997 – Early Summer Conditions.

Contour plots of temperature and chlorophyll concentrations along the E1 to L4 and E1 to S2 transects measured on 10th June 1997 are presented in figure 4.2. No beam attenuation data are available for this date.

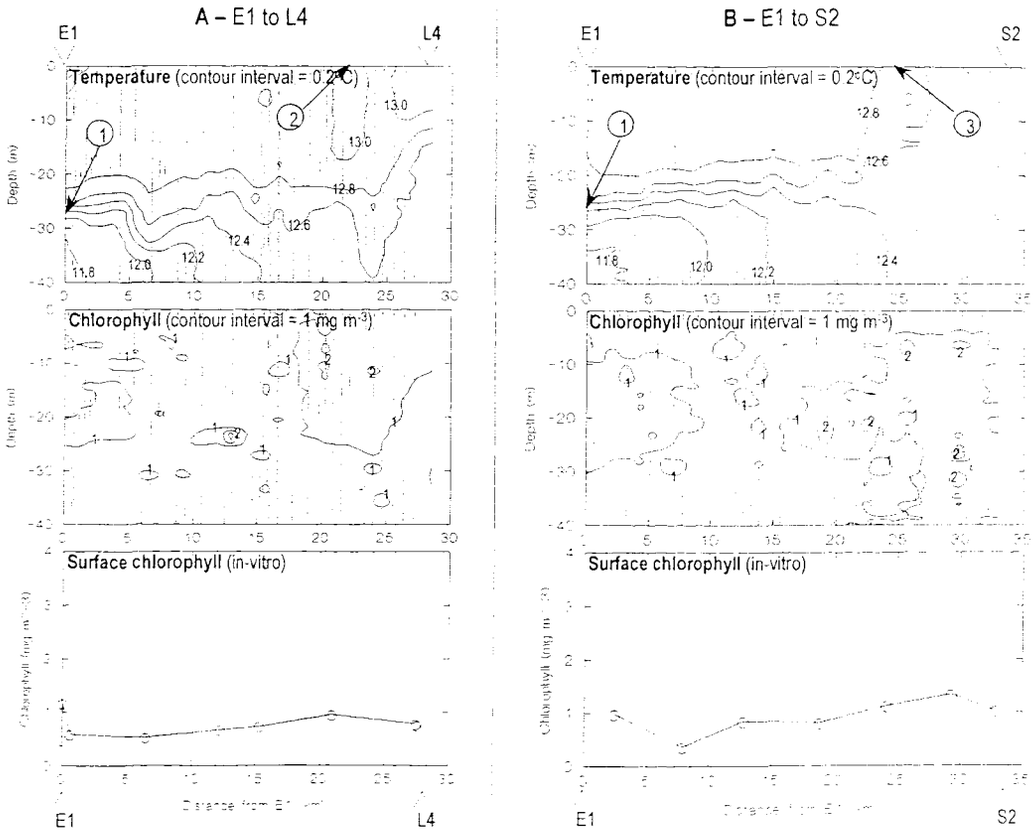

Figure 4.2 – *Temperature and chlorophyll along two transects on 10th June '97:*
***A** – E1 to L4,*
***B** – E1 to S2.*

At E1, the water column was stratified (figures 4.2A, B), with a cross-thermocline temperature difference of ~1°C. The thermocline (indicated as feature 1 on figures 4.2A & B) extended from ~20 to ~30 m depth. The cross-thermocline temperature difference decreased with distance towards both L4 and S2. Along the E1 to L4 transect (figure 4.2A), the thermocline persisted throughout, reaching a minimum of ~1°C at a distance of 23 km from E1 (feature 2 on figure 4.2A). The water column did, however, become

well mixed along the E1 to S2 transect (figure 4.2B), with a horizontal temperature front occurring at between 23 and 27 km from E1 (feature 3). Although the surface temperature change across the front was small (0.5°C), its narrow width (< 5 km) resulted in strong temperature gradients (> 0.1°C km^{-1}).

Chlorophyll concentrations along both transects (figure 4.2A & B) were low and patchy, ranging from <1 to >2 mg m^{-3}. Concentrations in both the SML and thermocline layers were generally higher than those in the BML. Chlorophyll concentrations increased slightly with distance along each transect, shown most clearly by the surface chlorophyll values (bottom panel of figures 4.2 A and B). For the well-mixed water column along the E1 to S2 transect, chlorophyll values were similar throughout the water column.

Contour plots for 24th June along the E1 to L4 and E1 to S2 transects are presented in figure 4.3A and B respectively. The thermocline at E1 was at ~20 to 30 m depth (feature 1), with a cross-thermocline temperature difference of 2°C. The cross-thermocline temperature difference reduced with distance away from E1, as the BML temperatures increased. The minimum level of stratification along the E1 to L4 transect (figure 4.3A) occurred at a distance of ~18 km from E1 (feature 2) (cross frontal temperature difference of ~0.5°C), whilst the water column along the E1 to S2 transect (figure 4.3B) became well mixed at a distance of 30km from E1 (feature 3).

Chlorophyll concentrations On 24th June (second and bottom panels, figure 4.3A & B) were low in the vicinity of E1 (<1 mg m^{-3}). For both transects, surface chlorophyll concentrations generally increased with distance (figures 4.3A & B, bottom panel), although the increases were more pronounced along the E1 to L4 transect than the E1 to S2 transect. A slight sub-surface chlorophyll maximum (>1 mg m^{-3}) was present over both transects, overlying the thermocline (second panel on figure 4.3). The chlorophyll maximum increased in both vertical extent and intensity along the E1 to L4 transect, with patches of chlorophyll at over 2 mg m^{-3} being observed under low (1°C) levels of stratification (feature 4).

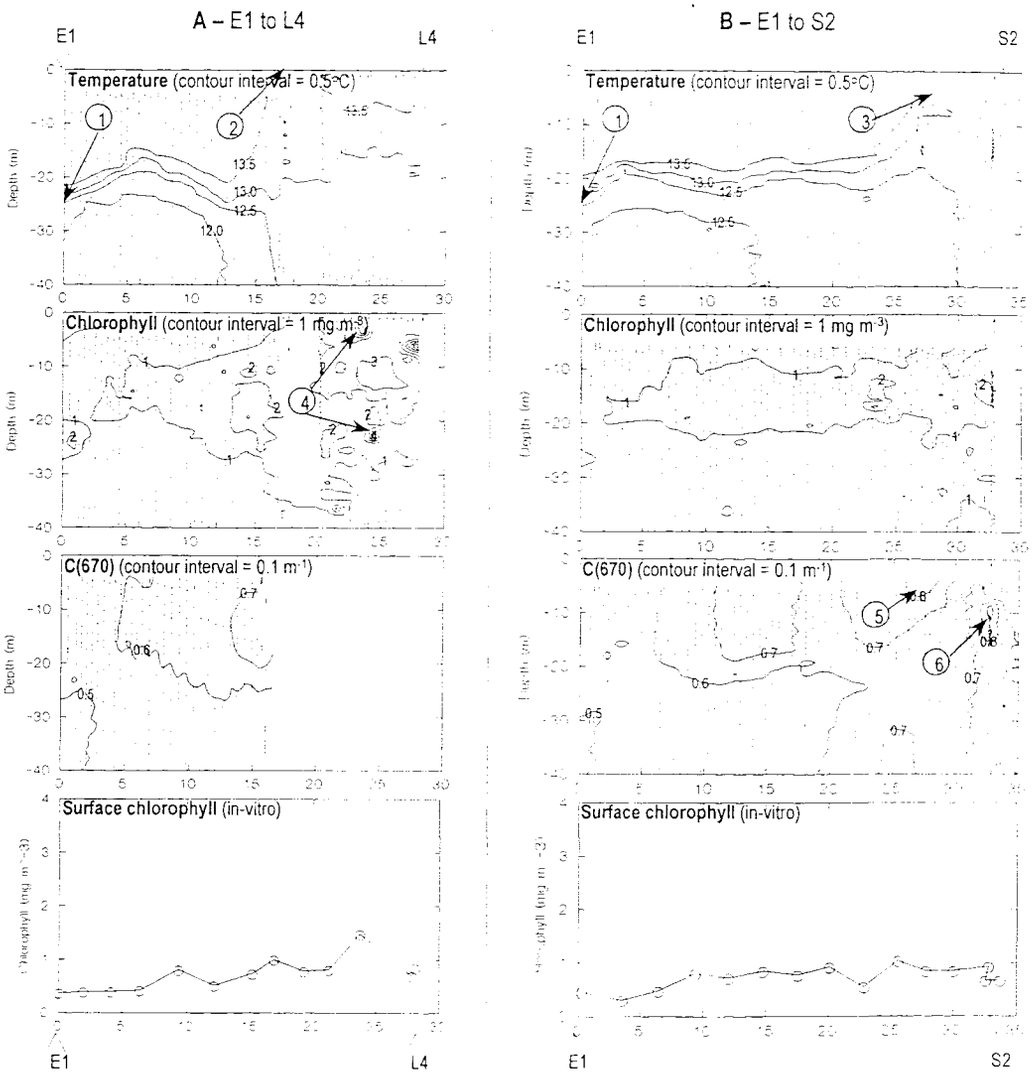

***Figure 4.3** – Temperature, chlorophyll and beam attenuation along two transects on 24th June '97:*
***A** – E1 to L4,*
***B** – E1 to S2.*

Observations of beam attenuation (C(670)) were available on 24th June (third panel, figure 4.3), although reliable data were not collected for the second half of the E1 to L4 transect. Attenuation increased along both transects, from 0.5 m^{-1} at E1 to >0.7 m^{-1} at S2. The highest attenuation coefficients along the E1 to S2 transect (>0.8 m^{-1}) occurred at the surface at 27 km from E1 (feature 5 on the figure), and at ~10 m depth at >31 km from E1 (feature 6). The mean ratios of C(670) to chlorophyll concentration were 0.12, 0.05 and 0.13 in the SML, thermocline and BML layers respectively, with Spearman rank correlations of 0.31, 0.10 and 0.32 in the same respective layers.

The temperature, chlorophyll and attenuation distributions described above (for 10th and 24th June 1997) can be assessed in the context of the meteorological, AVHRR and E1 archive data already presented: The thermocline depths at E1 observed on 10th and 24th June 1997 (20 to 30 m) were typical for E1 at this time of year as shown by the E1 archive data (see figure 4.1). The cross-thermocline temperature difference, however, was lower than average (1-2°C cf. 3°C), and the SML temperature lower than average (13-13.5°C cf. 14°C). These observations can be explained by the higher than average wind mixing that occurred during June 1997, which mixed cooler water from below the SML, thereby reducing both SML temperature and the degree of stratification. This increased wind speed was also used to explain the lower than average June 1997 SST, mentioned in the previous chapter. Along both transects, BML temperatures increased with distance away from E1. Along the E1 to S2 transect, this behaviour can be explained by increasing entrainment of warm surface water into the BML as tidal mixing increased (see figure 3.9, tidal mixing is inversely related to the stratification parameter, S). This increasing entrainment also led to the degree of stratification decreasing with distance from E1. Along the E1 to L4 transect, however, stratification also decreased, even though estimated tidal mixing (as indicated by S, see figure 3.9) decreased. This inconsistency between the predicted values of tidal mixing and the observed temperature distribution along the E1 to L4 transect were discussed previously in relation to SST distribution (see figure 3.19Ci and accompanying text). As for the SST distribution, the inconsistency can be explained by the theory that currents increased in the region of the Eddystone Rocks due to island mixing effects. In support of this theory, it is observed that, on both 10th and 24th June, stratification in the region of the Rocks (20-25 km from E1) was the minimum along the E1 to L4 transect.

The thermal front observed along the E1 to S2 transect on both 10th and 24th June resulted from the increased tidal mixing along the transect eventually overcoming the stabilising force due to net heat flux into the water column. The location of the front corresponded to values of the stratification parameter (S) of 1.9 and 1.7 CGI units on 10th and 24th June respectively. This value is higher than the typical value for tidal fronts (S~1.5), but not unrealistic (Pingree & Griffiths, 1978). The high value of S for the location of the front can be explained by the higher than average wind speeds prevalent in the region during this month: i.e. the additional wind mixing energy reduced the stratification, thereby re-locating the front into regions of lower tidal mixing.

The most likely reason for the low BML chlorophyll concentrations was due to the inhibition of phytoplankton growth due to light limitation. Although no reliable light meter data were available for the June 1997 sampling events, typical values of $K_d(490)$ within the study region during 1997 were ~0.15 m^{-1} (discussed in more detail later).

Estimations of the maximum water column depth at which algal growth can occur using values of $K_d(490)$ are subject to severe limitations; the minimum light level for growth varies by an order of magnitude between and within algal species (Richardson *et al*, 1983), and $K_d(490)$ will be greater than $K_d(PAR)$ (Kirk, 1994). However, using a representative minimum light level for growth of 1 W m^{-2} and a value of $K_d(PAR)$ of 0.15 m^{-1} (Richardson *et al*, 1983), and an incident light level of 90 W m^{-2} (average downwelling irradiance during June 1997 of 180 W m^{-2}, Chapter 3, and a contribution to PAR of 50%, Kirk, 1994), then the maximum depth for growth was 30 m. The average depth of the SML, thermocline and BML at station E1 during the two sampling events for June 1997 were ~10 m, ~25 m and ~50 m respectively. The BML therefore significantly exceeded the approximate maximum depth for algal growth, the thermocline was of marginal depth, and the SML well illuminated.

Following the spring bloom, SML concentrations are generally regulated by nutrient supply, which is typically <1 mmol m^{-3} during June (see figure 4.1). Although well-illuminated, the SML chlorophyll concentrations were low (<1 mg m^{-3}) for station E1 for both sampling events during June 1997. This observation suggests nutrient limitation in the SML during June 1997. Furthermore, the increase in surface chlorophyll concentrations along each of the transects suggests that the increased tidal mixing enhanced the nutrient flux into the SML, and therefore stimulated productivity.

During summer months, a sub surface chlorophyll maximum is a typical feature of the water column at E1 (Holligan & Harbour, 1977). Whilst a sub-surface maximum was not present on 10th June, one had started to form by 24th June. It was estimated above that algal growth in the thermocline was marginal due to the light availability in this layer. It is hypothesised that the development of the feature between the two dates was related to the precise light regime that existed in the thermocline over the same time.

Regions of elevated Chlorophyll concentrations are typical features of tidal fronts (Pingree et al, 1975). There was, however, no evidence for a chlorophyll bloom at the tidal front observed on either of the two dates during June 1997. Three theories for such an absence are suggested: A. The entire water column may have become nutrient depleted following the spring bloom (see figure 4.1C), thereby inhibiting productivity. B. The frontal zone was very narrow (~5 km), and any increase in phytoplankton may therefore have been rapidly dispersed by advection. C. The front was steeply inclined and the vertical temperature gradients low, therefore offering limited vertical stability to the phytoplankton, again inhibiting productivity. It is interesting to note, however, that elevated C(670) values (of up to 0.8 m^{-1}) were observed within the frontal zone on both dates, within the SML to the stratified side of the thermal boundary, and throughout the

watercolumn to the well mixed side. As this feature was not correlated with elevated chlorophyll values, the increased attenuation must have been due to the accumulation of either detrital or inorganic matter. This will have occurred either by production in-situ (by the decay of a previous phytoplankton bloom), by horizontal advection into the region, or by re-suspension from sediments

10th and 29th July 1997 – Mid-Summer Conditions

Contour plots along the E1 to L4 and E1 to S2 transects for 10th July 1997 are presented in figure 4.4A & B respectively. The water column at E1 was strongly stratified, with a cross frontal temperature difference of >3°C, and the thermocline extended from 10 to 28 m depth. Whilst BML temperatures along the E1 to L4 transect were fairly constant (12.25°C +/- 0.25°C), those along the E1 to S2 transect warmed by ~1°C (from ~12.25°C to ~13.25°C). The thermocline depth and extent was fairly constant along the E1 to L4 transect (8 to 20 m, except for 15 to 25 km from E1 where the thermocline widened, marked as feature 1 on the figure). For the E1 to S2 transect, however, the thermocline became shallower with distance from E1, reducing from 10 to 30 m at E1 to <8 m at S2 (feature 2).

Chlorophyll concentrations on 10th June (figure 4.4A & B) were patchy, with concentrations of >5 mg m^{-3} in places. Along both transects, the highest chlorophyll concentrations were observed in the thermocline layer, where concentrations ranged from 2 to 5 mg m^{-3}, compared to typical values of <1 mg m^{-3} in both the SML and BML. The identity of this sub-surface chlorophyll maximum did, however, lose its identity with distance along each transect, with high concentrations extending into the BML. For instance, the 1 mg m^{-3} contour reached 40 m depth at ~11 km along the E1 to L4 transect (marked on the figure as feature 3), and at ~24 km along the E1 to S2 transect (feature 4).

The surface chlorophyll measurements on 10th July (figure 4.3A & B) suggest that SML chlorophyll concentrations were increasing along both transects, from ~0.5 mg m^{-3} at E1, to ~1.5 mg m^{-3} at both L4 and S2. Along the E1 to S2 transect, this observation is reflected in the chlorophyll contour plot, where an increase in concentration occurred throughout the water column at a distance of ~27 km from E1.

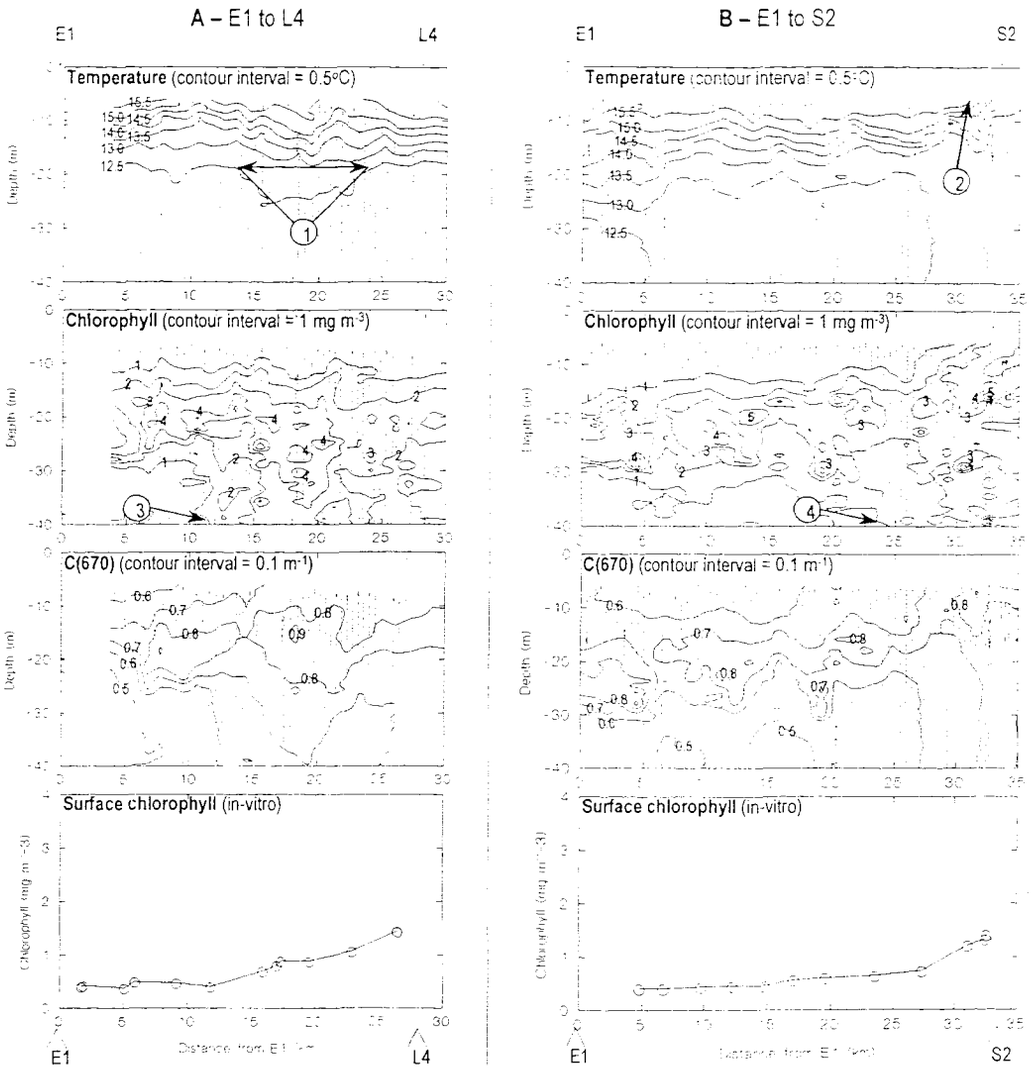

Figure 4.4 – *Temperature, chlorophyll and beam attenuation along two transects on 10th July '97:*
***A** – E1 to L4,*
***B** – E1 to S2.*

Contours of beam attenuation (C(670)) for the two transects on 10th July are also presented in figure 4.4A and B. The general distribution of C(670) was similar to that of chlorophyll, i.e. demonstrated a distinct sub-surface maximum of ~0.8 m^{-1} in the thermocline, with lower values in the SML and BML. Other similarities with the chlorophyll distribution include the loss of identity of the C(670) sub-surface maximum from 10 km along the E1 to L4 transect, and the increase in C(670) throughout the water column at a distance of ~27 km from E1 along the E1 to S2 transect.

A comparison between C(670) and chlorophyll values for the SML, thermocline and BML displayed average ratios of 0.08, 0.04 and 0.07, and Spearman correlation coefficients (r^2) of 0.38, 0.30 and 0.70 respectively. In general, chlorophyll fluorescence measurements were more patchy than for C(670) measurements. As the fluorometer cell size was only ~1 cm across, whereas the transmissometer path was 25 cm long, fluorescence measurements are likely to be more affected by small (e.g. cm) scale variability in phytoplankton abundance, and this is a possible explanation for the patchy fluorescence measurements.

Temperature contour plots for 29th July 1997 along the E1 to L4 and E1 to S2 transects are presented in figure 4.5A & B respectively. At E1 the cross thermocline temperature difference was >4°C, with the thermocline extending from 10 to 20 m depth. Although the degree of stratification was stronger on 29th July than on 10th July, the horizontal patterns of temperature distribution were similar. I.e. along the E1 to L4 transect the thermocline depth was fairly constant with distance from 5 km onwards, with the lowest stratification (broadest thermocline) at ~17 km. Along the E1 to S2 transect, the thermocline shallowed and BML temperatures increased with distance, on both dates.

The chlorophyll distribution on 29th July (figure 4.5 A and B) also showed characteristics that were similar to the 10th July distribution, i.e. elevated sub-surface chlorophyll concentrations (concentrations of 6 mg m^{-3}) were observed in the thermocline layer. Even though the UOR did not adequately sample the SML over most of the transects, low concentrations in this layer are indicated by the low values of the surface chlorophyll measurements (<1 mg m^{-3}). A significant feature of the chlorophyll distribution on 24th July was the high chlorophyll concentrations within the BML (up to 4 mg m^{-3}). These BML concentrations were highest over the first half of each transect. The C(670) distribution (figure 4.5A & B) showed a similar distribution to that of chlorophyll, especially with respect to the intense sub-surface maximum, reaching values of 1.2 m^{-1}. There was less evidence, however, of elevated C(670) values in the BML on 29th June compared with 10th June..

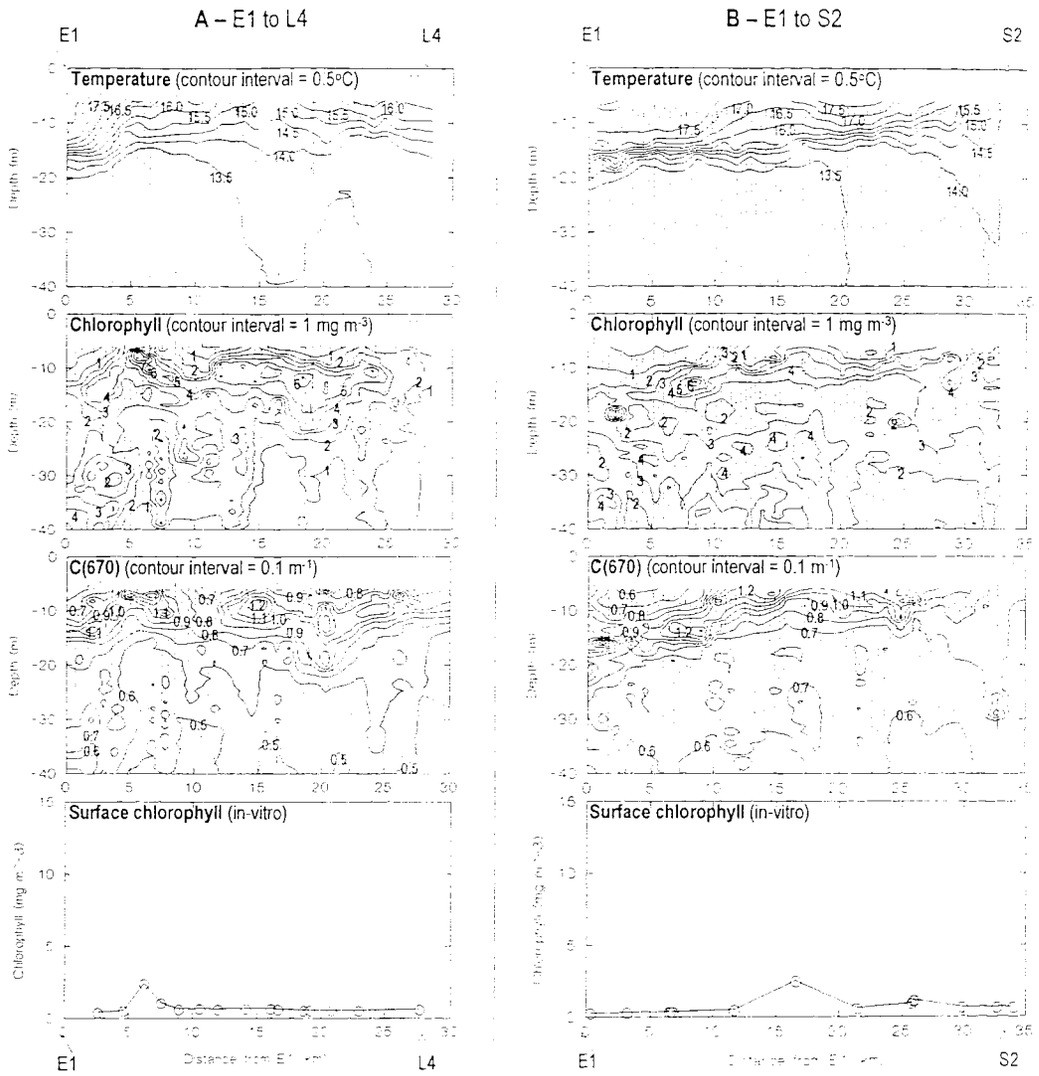

Figure 4.5 – *Temperature, chlorophyll and beam attenuation along two transects on 29th July '97:*
***A** – E1 to L4,*
***B** – E1 to S2.*

By comparing the distributions on 10th and 29th July with those from earlier in the year, several consistent patterns emerge: The watercolumn stratification at E1 was increasing throughout the period from 10th June to 29th July 1997, from 1°C (10th June) to 2°C (24th June), to 3°C (10th July) to 4°C (29th July). Over the same period, the thermocline was shallowing, from 22-32 m (10th June) to 20-30 m (24th June) to 10-25m (10th July) to 10-20m (29th July). Both the increasing stratification and the decreasing thermocline depth resulted from the general trends of increasing heat flux and decreasing wind speeds which were observed in the meteorological data from June to July 1997 (see figures 3.10 and 3.1 respectively). Similarly, the degree of stratification during June 1997 was lower than average (estimated from the E1 archive), whilst the stratification during July 1997 was higher than average. These observations can explained by differences between the 1997 and archive global irradiance and wind speeds (see figure 3.1, irradiance lower than average in June, higher in July, wind speed higher than average in June, lower in July).

The horizontal distribution of temperature along the two transects over the four dates show two consistent features: A. the stratification along the E1 to L4 transect was reduced in an area located between 15 km and 25 km from E1. B. the stratification along the E1 to S2 transect declined steadily with distance from E1 as BML temperatures increased, leading to the water column becoming well mixed at S2 during June. The reduction in stratification along the E1 to L4 transect can be explained by the localised increases in tidal currents in the vicinity of the Eddystone Rocks, caused by island mixing effects. In contrast, the steady reduction in stratification along the E1 to S2 transect can be explained by the gradual increases in mixing caused as tides increase and water depths decrease. The water column did not become well mixed along the E1 to S2 transect during July as the increases in stratification had re-positioned the tidal front to beyond the end of the transect.

The chlorophyll distribution at E1 from 10th June to 29th July 1997 tracks the development of a sub-surface chlorophyll bloom. The thermocline chlorophyll concentrations increased from <1 mg m^{-3} on 10th June, to 1-2 mg m^{-3} on 24th June, to 3-4 mg on 10th and 29th July. These increasing concentrations resulted from either increasing in-situ productivity within the thermocline, or decreasing mixing of phytoplankton out of the thermocline. Both of these processes would have been enhanced by the increasing stability of the water column and the decreasing depth of the thermocline over the period. Assuming a representative value of K_d(PAR) of 0.15 m^{-1} (Richardson *et al,* 1983), an average June PAR of 90 W m^{-2}, and an average July PAR of 120 W m^{-2}, then an approximation for the maximum depth for algal growth was ~30 m depth during June 1997, and ~32 m during July 1997. However, measurements of

$K_d(490)$ at E1 from June and July 1997 produced a spread of values from 0.1 m^{-1} to 0.2 m^{-1}, providing a difference of 10 m in the location of the 1% light level at 490 nm. Assuming that the variability of $K_d(PAR)$ was similar to that of $K_d(490)$, then approximation of the maximum depth for phytoplankton growth using a representative value of $K_d(PAR)$ is not reliable.

On 24th June, the vertical chlorophyll maximum in the vicinity of E1 was generally located in the surface mixed layer overlying the thermocline (depths < 20 m). This region will have been well illuminated compared with the relatively deep thermocline observed on this date. By 10th July, however, the chlorophyll maximum was located at the base of the (now shallower) thermocline (depths < 10 m). The location of sub-surface chlorophyll maxima at the base the thermoclines has been observed previously, and associated, for example, with nutrient exploitation within blooms of the phytoplankton Gyroddinium auroleum that occur in the western English Channel (Holligan et al, 1984b). By 29th July, however, two major changes of chlorophyll distribution had occurred with respect to the 10th July situation. A. BML chlorophyll concentrations had increased from <1 mg m^{-3} to >2 mg m^{-3}, and B. the chlorophyll maximum was now located at the top of the thermocline. One theory is that significant numbers of cells had been transferred from the base of the thermocline into the BML, either by settling or tidal mixing. In addition, the change in position of the sub-surface chlorophyll maxima from the bottom to the top of the thermocline may therefore indicate a change in the most favourable region for growth, i.e. from high nutrient but turbulent conditions to lower nutrient but stable conditions.

11th and 17th September 1997 – Early Autumn Conditions

The temperature distribution on 11th September is sown in figure 4.6 A &B. At E1 the cross-frontal temperature difference was 2.5°C, and the thermocline extended a depth of 20 m to 30 m. With distance along the E1 to L4 and E1 to S2 transects, BML temperatures increased by 1.5°C and 2°C respectively. The degree of stratification correspondingly decreased, to 1.5°C at L4, and becoming well mixed at S2. In addition, the thermocline shallowed with distance along the transects; intersecting the surface at a distance of 25 km from E1 along the E1 to S2 transect. The thermal frontal zone along the E1 to S2 transect was ~10 km wide, and its temperature gradient ~0.2°C km^{-1}. Along the E1 to L4 transect, small-scale disturbance in the temperature field was observed at distances of 15 to 25 km from E1.

Chlorophyll distributions at E1 on 11th September (figure 4.6A & B) showed evidence of a sub-surface chlorophyll maximum of >2 mg m^{-3} located at depth of ~18 m.

Chlorophyll concentrations above the maximum were 1-2 mg m^{-3} whilst those below fell to <1 mg m^{-3}. Along the E1 to L4 transect, the SML chlorophyll concentrations generally increased with distance, reaching a value of 4 mg m^{-3} at L4. Along the E1 to S2 transect, significant local enhancement of

the SML and thermocline chlorophyll concentrations occurred at a position that corresponded to the thermal front. ~25 km from E1 (to 4 mg m^{-3}, cf. 2 mg m^{-3} at E1, 1 mg m^{-3} at S2). The bloom extended ~15km to the stratified side of the front. The C(670) distribution (figure 4.6A & B) showed a similar distribution to that of the chlorophyll distribution, especially with respect to the frontal features observed on the E1 to S2 transect.

The temperature distribution observed on 17th September 1997 is presented in figure 4.7A &B. At E1, the cross-thermocline temperature difference was ~2°C, with the thermocline extending from 15 to 20 m depth. Along the E1 to L4 transect, the stratification first reduced with distance, with the water column becoming well mixed at a distance of ~15 km from E1. The water column re-stratified at a distance of ~25 km from with a cross-thermocline temperature difference of ~1.5°C becoming established by L4. Along the E1 to S2 transect, the stratification decreased with distance throughout, with <1°C temperature difference from 25 km onwards.

The chlorophyll distribution at E1 on 17th September (figure 4.7A & B) was highest in the SML (>2 mg m^{-3}) and declined to <1 mg m^{-3} in the BML. Along the E1 to L4 transect, higher chlorophyll concentrations (>3 and >4 mg m^{-3}) were observed in the thermal frontal zones to either side of the well mixed region. In the well mixed region itself, BML chlorophyll concentrations increased to 1-3 mg m^{-3} (cf. <1 mg m^{-3} to either side). Along the E1 to S2 transect, SML chlorophyll concentrations were similar throughout (2-4 mg m^{-3}), although BML concentrations increased with distance, from <1 mg m^{-3} at E1 to >2 mg m^{-3} at S2.

Several features of the temperature distribution observed earlier in the year were again present on 11th and 17th September. The thermocline was deepest and strongest at E1, reflecting the lowest rates of tidal mixing (feature 1 on figure 4.6). Along the E1 to L4 transect, the water column structure was disturbed in the vicinity of the Eddystone Rocks (15 to 25 km from E1, feature 2 on figure 4.6), reflecting island mixing effects. Along the E1 to S2 transect, the thermocline depth and intensity of stratification declined with distance towards S2, reflecting increasing tidal mixing, and on 11th September a distinct tidal front was present (23 km from E1, corresponding to S ~1.9, feature 3 on figure 4.6).

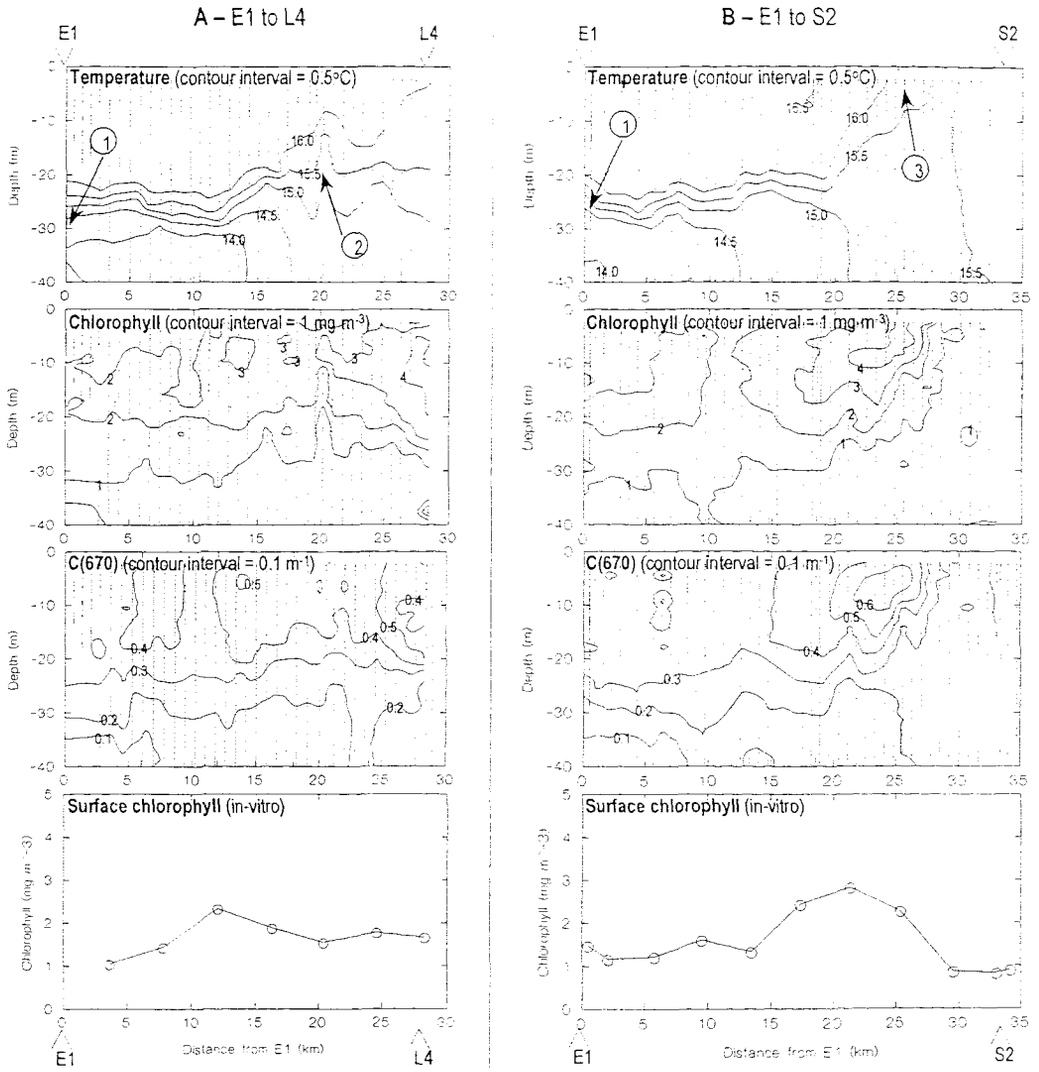

Figure 4.6 – *Temperature, chlorophyll and beam attenuation along two transects on 11th September '97:*
***A** – E1 to L4,*
***B** – E1 to S2.*

The degree of stratification at E1 on 11th September was lower than that on 29th July (2°C cf. 4°C) and the thermocline was located deeper in the water column (20-30 m cf. 10-20 m). These differences reflected reductions in heat flux (figure 3.10) and increases in wind speeds (figure 3.1) that occurred between June and September. By 17th September, the stratification across both transects had declined slightly from the 10th September conditions, especially in the region of the Eddystone Rocks. The thermocline, however, was located higher up in the water column on 17th than 11th September. These changes will have resulted from the balance between atmospheric forcing and tidal mixing that occurred between the two dates.

At E1, the intensity on the sub-surface chlorophyll maximum had declined by 11th September compared to 29th July (>2 mg m^{-3} cf. >4 mg m^{-3}). The bloom did, however, cover a greater depth range on 11th September, extending through most of the SML, compared to the narrow bloom confined to the thermocline on 29th July. Both the lower stratification and the increased mixing conditions on 11th September will have resulted in increased nutrient flux into the SML than on 29th July, thereby enhancing productivity and resulting in higher chlorophyll concentrations. By 17th September, SML chlorophyll concentrations had increased further, and stratification declined, suggesting that the autumn phytoplankton bloom was occurring during this September period.

On 11th September, chlorophyll concentrations in the frontal zone were higher than those observed at the same position on July 10th (figure 4.2B), but not as high as those reported for other positions along the Channel front in the summer. Pingree *et al*, (1976), for example, reported isolated occurrences of >100 mg m^{-3}, but concentrations <20 mg m^{-3} are more typical. Observations of the bloom extending into the thermocline chlorophyll maximum have been reported by several authors (e.g. Pingree et al, 1975). However, no sub-surface thermocline maximum was observed to the stratified side of the front on the 11th September 1997. The relatively low light level associated with the time of year and the relatively large depth of the thermocline could explain its absence. By 17th September, no elevation of SML chlorophyll concentrations were apparent along the E1 to S2 transect. It is interesting to note, however, that frontal chlorophyll blooms were apparent to either side of the well mixed zone along the E1 to L4 transect. The main difference between the frontal zones along the transects on 17th Septemberwas that the horizontal temperature gradients were higher along the E1 to L4 transect than along the E1 to S2 transect (~0.1°C km^{-1} cf. negligible). It is possible, therefore, that a certain degree of horizontal stability is required for chlorophyll blooms to maintain their identity.

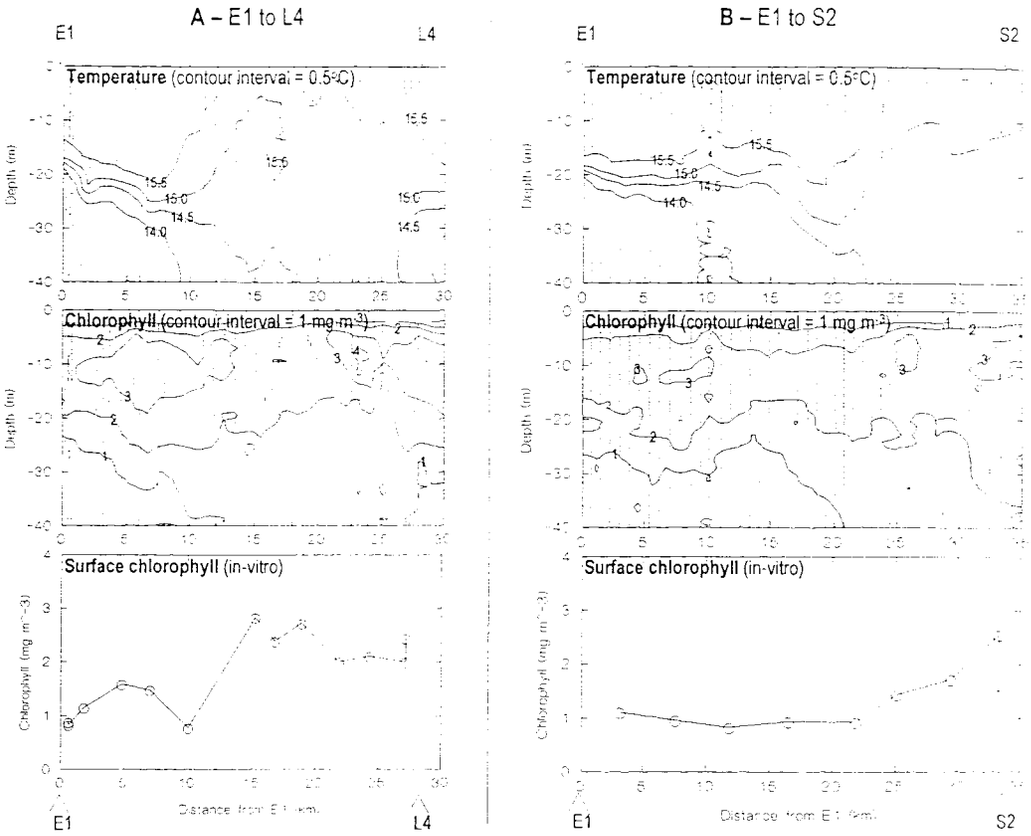

Figure 4.7 – *Temperature, chlorophyll and beam attenuation along two transects on 17th September '97:*
***A** – E1 to L4,*
***B** – E1 to S2.*

23rd September – Late Autumn Conditions

By 23rd September (figure 4.8A & B), the water column stratification had broken down over both of the transects. Temperatures increased slightly with distance towards S2 and L4, as was the case with the satellite SST transects collected during the autumn (see, for example, figure 3.21Ci & ii).

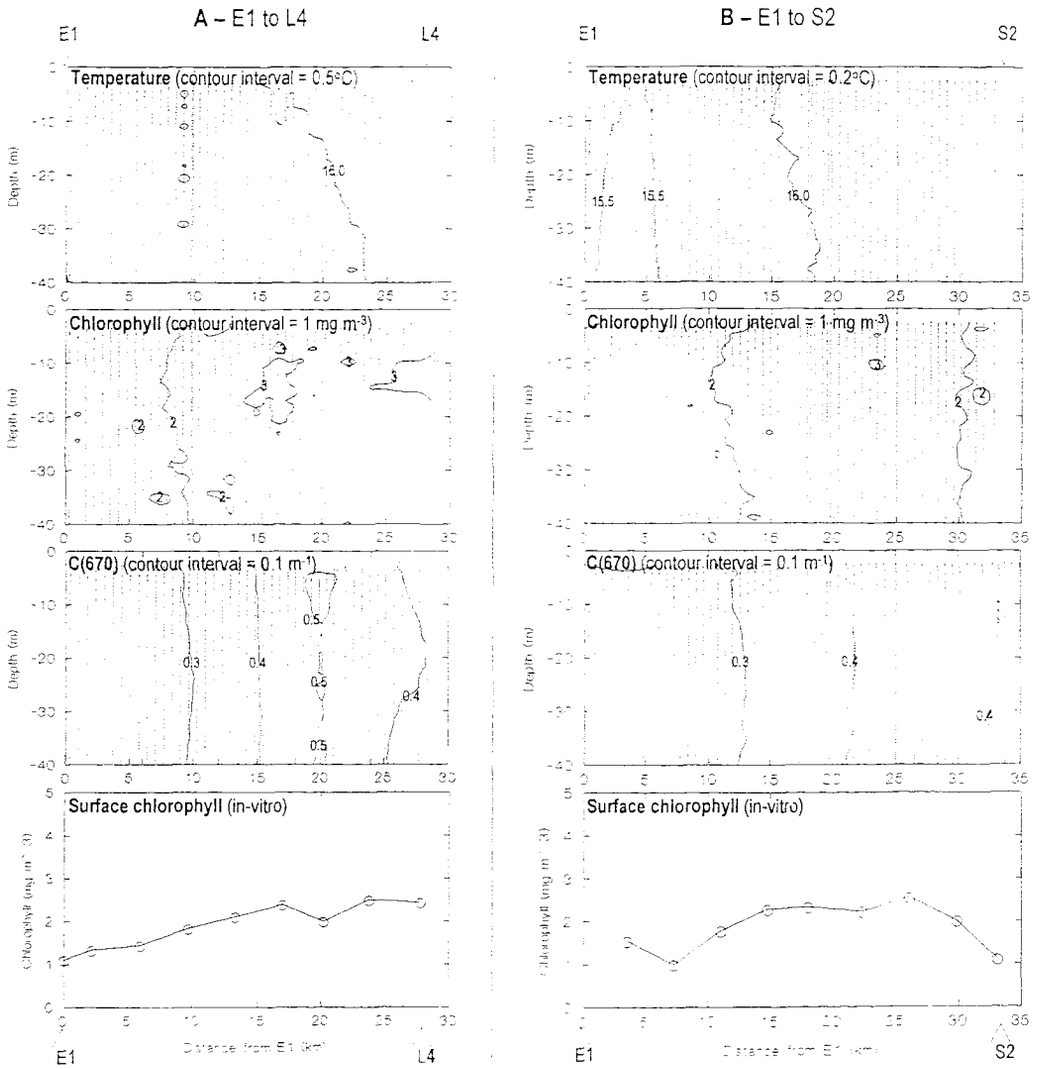

Figure 4.8 – *Temperature, chlorophyll and beam attenuation along two transects on 23rd September '97:*
***A** – E1 to L4 (A),*
***B** – E1 to S2 (B).*

Chlorophyll concentrations (figure 4.8A & B) were fairly homogenous with respect to depth. The concentrations were fairly high (between 1 and 3 mg m^{-3}), but it is more likely that this reflects the fact that the thermocline had broken down recently and redistributed existing chlorophyll, than significant in-situ production was occurring within the well-mixed water column. C(670) distribution along each of the transects was also constant with respect to depth.

Bio-Optical Data from June to September 1997

The availability and use of data collected by satellite ocean colour sensors such as SeaWiFS is set to increase. This provides a need for more information concerning the links between physical/biological/bio-optical processes. During the course of this study, high-quality underwater optical data was collected using the UOR. Due to the lack of availability of ocean colour data contemporaneous with other data presented in this thesis, the optical data has assumed secondary importance. The data presented here concerns the relationships between biological and optical distributions. This is useful in its own right as it provides an insight into the system that is not available from biological measurements alone. Furthermore, it has significance for the future analysis of ocean colour images of the study region.

The Ratio Between C(670) and Chlorophyll Concentration.

To investigate the relationships between beam attenuation measured at 670 nm (C(670)) and chlorophyll concentrations, UOR data for each sampling event were sub divided in the vertical using the SML, thermocline, and BML depths. The results of the comparisons of C(670) and chlorophyll concentration are presented in table 4.3. Although the correlation were generally low, several trends emerged, as discussed below.

During June and early July, the arithmetic mean ratios of beam attenuation to chlorophyll concentration in the SML and BML were similar (~0.1 m^2 mg^{-1}). The ratio in the thermocline, however, was ~0.05 m^2 mg^{-1}. At the end of July, the thermocline ratio was similar to that observed earlier in the year, and the SML and BML ratios had decreased to a similar value (~0.05 m^2 mg^{-1}). In early September, the ratios for all three layers were similar, and double that of the mid-summer value.

Date	Layer	Ratio C(670)/Chl (m^2 mg^{-1})	Spearman r^2	Date	Layer	Ratio C(670)/Chl (m^2 mg^{-1})	Spearman r^2
24th Jun	SML	0.12	0.31	11th Sep	SML	0.12	0.83
	Thermocline	0.05	0.10		Thermocline	0.12	0.93
	BML	0.13	0.32		BML	0.10	0.40
10th Jul	SML	0.08	0.38	17th Sep	SML	0.13	0.21
	Thermocline	0.04	0.30		Thermocline	0.12	0.30
	BML	0.07	0.70		BML	0.12	0.61
11th Jul	SML	0.10	0.52	23rd Sep	SML	0.17	0.71
	Thermocline	0.04	0.10		Thermocline	-	-
	BML	0.07	0.37		BML	-	-
29th Jul	SML	0.05	0.78				
	Thermocline	0.04	0.27				
	BML	0.05	0.76				

***Table 4.3** – Comparisons of C(670) and chlorophyll concentration for the sampling events during 1997.*

Beam attenuation coefficient is controlled by the nature and quantity of organic and inorganic substances either dissolved or suspended in the water column (Kirk, 1994). Beam attenuation is the sum of the scattering and absorption properties of optically active in-water constituents, and is an inherent optical property (i.e. independent of ambient light conditions). C(670) has been shown to vary proportionally with both chlorophyll concentration and suspended particulate matter (SPM) concentration (McKee *et al*, 1999), although log-linear relationships between C(λ) and chlorophyll concentration have also been proposed (Voss et al, 1992). Phytoplankton and their associated materials are often the only or highly dominant optically active in-water constituents. Under these conditions, therefore, the ratio of beam attenuation to chlorophyll concentration will be low, and the correlation coefficients high. The addition of optically active constituents unrelated to phytoplankton will result in high beam attenuation to chlorophyll ratios, and low correlation coefficients. In addition to the source of optically active material, the phytoplankton themselves can alter attenuation to chlorophyll ratios. Pingree et al (1982), for instance, state that fluorescence yields can vary by up to an order of magnitude with changes in physiological state or species composition of phytoplankton. Similarly, McKee et al (1999) determined that beam attenuation coefficients per unit chlorophyll are also strongly dependent on phytoplankton species composition.

The observed relationships between C(670) and chlorophyll concentration listed in Table 4.3 can be explained in relation to the theoretical relationships between beam attenuation and chlorophyll described above. During June, for instance, the high C(670) vs. [chlorophyll] ratios in the BML (0.07 to 0.13 m^2 mg^{-1}) could indicate the presence of inorganic or detrital SPM. This SPM could result from either; re-suspension of sediment from the sea-bed, or settling of detritus from the thermocline. Enhanced BML gradients due to re-suspended matter in tidally energetic regions have been observed by McKee *et*

al (1999). The high SML ratio, however, is unlikely to have resulted from inorganic or detrital SPM, as there are no obvious sources of such material to this layer. A more likely cause is the difference in phytoplankton species between the thermocline and SML. The theory that the observed changes in the C(670) vs. chlorophyll ratio were due to differences in species composition is supported by Holligan & Harbour (1977), who observed that, at E1 during the summer , flagellates were dominant in the SML whilst dinoflagellates dominant in the thermocline.

On 29th July, the similarity of BML and thermocline ratios can be explained by a large number of cells sinking out of the thermocline, which was also responsible for the high observed BML chlorophyll concentration discussed earlier. The similarity of the SML and thermocline concentrations can be explained by the failure of the UOR to adequately sample the SML due to the shallow position of the thermocline, also discussed earlier.

For station E1, Holligan & Harbour (1977) observed an autumn bloom of diatoms replaces the summer flagellate and dinoflagellate populations. A similar change in phytoplankton species during 1997 may have caused the change in the C(670) to chlorophyll ratio between July 1997 and September 1997. There are no observations of phytoplankton species during 1997, however, to support this theory. The ratio had increased further by 23rd September, following the erosion of the thermocline. This is likely to have resulted from the mixing of non-phytoplankton SPM throughout the watercolumn, or the increase of phytoplankton degradation products produced in-situ upon the ending of the autumn bloom.

Diffuse attenuation of the downwelling light field (K_d) is calculated from the depth distribution of downwelling irradiance. The water column K_d is often described using a single value. As for beam attenuation, K_d is also controlled by the nature and quantity of organic and inorganic substances either dissolved or suspended in the water column (Kirk, 1994). $K_d(\lambda)$ is also affected, however, by the characteristics of the ambient light field, and is therefore an apparent optical property (Kirk, 1994).

Many studies have examined the relationship between K_d(PAR) and chlorophyll concentrations (see review of Schanz et al, 1997). The chlorophyll specific diffuse attenuation coefficient, K_c(PAR), can range from 0.005 to 0.021 $m^2\ mg^{-1}$ chl (Atlas & Bannister, 1980). K_c(PAR) has been shown to be dependent on species composition (Atlas & Bannister, 1980), and on the physiological state of the phytoplankton (Osborne & Geider, 1986). In addition to downwelling irradiance at the sea surface, diffuse attenuation at different wavelengths controls the underwater light intensity and spectral

distribution. It is this light field which is utilised by phytoplankton in primary production.

$K_d(490)$ measurements made during the field surveys were compared with depth-averaged chlorophyll concentrations, where the depth range used for the averaging was the same as that used for K_d determination. On 10th June the average $K_d(490)$ vs. chlorophyll ratio was 0.04 m^2 mg^{-1} and r^2 was 0.6. On 29th July, the ratio was 0.03 m^2 mg^{-1}, and r^2 was 0.1. On 11th September, the ratio was 0.08 m^2 mg^{-1}, and r^2 was 0.7.

The three-fold increase in the ratio between July and September can be accounted for by a change in species composition. Atlas & Banister (1981), for instance, observed a four-fold difference in $K_c(PAR)$ with changes in species composition

The difference between the observed values of the $K_d(490)$ Vs. chl ratio, and $K_c(PAR)$ can be explained firstly by the dependence on wavelength of chlorophyll absorption; the chlorophyll specific absorption coefficient at 490 nm is about twice that of the PAR waveband (Bricaud et al, 1995). Secondly, substances other than chlorophyll associated with phytoplankton also absorb at 490 nm, therefore contributing the overall $K_d(490)$ value.

Comparison between 10th and 11th July – Changes from One Day to the Next

Two sampling events were carried out on consecutive days, 10th and 11th July 1997. The hydrographic characteristics for these events along the first 15 km of the E1 to S2 transect are shown in figure 4.9A & B. The temperature distributions for 10th and 11th July (figure 4.9A & B respectively) were strikingly similar. A shallow thermocline (extending from ~10 to 30 m depth) with a temperature difference of ~2.8°C was present throughout. BML temperatures increased slightly with distance away from E1, indicating increased tidal mixing. Between 5 and 10 km from E1, the base of the thermocline domed upwards by approx. 5 m.

There were, however, small but significant differences between the 10th and 11th July sections. The SML had deepened over the 24 hour period (by ~3 m). Furthermore, the base of the thermocline had shallowed, and the horizontal extent of the dome described above had increased by ~2 km, and migrated towards E1 by ~2 km. The 12.5°C isotherm, for example, had receded by ~2.5 km towards E1. These changes each acted to increase the cross-thermocline temperature gradient.

The differences in the SML temperature between the surveys will have been due to surface processes, the most likely of which being differences in heat flux. The air temperature for the period between 0 and 6 GMT on 10th July were, on average, higher than the SML temperatures observed during the sampling event on the same day. Over the same period on 11th July, however, the air temperatures were constantly lower than the SML temperatures. This indicates that the overnight heat flux into the watercolumn on 11th July was negative, and some degree of convective overturn would have resulted. This mixing will have caused the deepening of the depth of the base of the SML that was observed on 11th July relative to the 10th July. Other processes that may have caused similar observations include; horizontal advection or differences in wind mixing. The latter of these is unlikely, as the meteorological data do not indicate any large differences in wind mixing over the few hours preceding the observations.

The differences below the thermocline will have resulted from tidal processes, either mixing or advection. The tidal ellipse at E1 (see figure 3.6) has an orientation of 79°, which is similar to orientation of the E1 to S2 transect (63°), and a major axis length of 8 km.. High water at Devonport on 10th June (08:53 GMT) was 37 min. earlier than high water on 11th June. The transect shown for 10th June was therefore collected from 3.1 to 4.1 hours after high water, whilst that for 11th June was collected from 3.7 to 4.7 hours after high water. Over 0.6 hr at maximum ebb tidal current, the water column will have moved ~1 km towards E1, which explains some of the observed difference of the position of the 12.5°C isotherm. On 10th July, the boat was travelling from S2 to E1 (right to left on figure 4.6), in the same direction as the ebb tide. This would have tended to increase the apparent width of the thermocline dome. Conversely, on 11th July, the boat was heading into the tide, from E1 to S2, thereby reducing the apparent width of the dome. However, the horizontal extent of the dome increased between 10th to 11th July, indicating that tidal advection along the E1 to S2 axis could not have been responsible. Another possibility, increased tidal mixing due to the state of the S2 tide can also be discounted as the tidal range was ~10% lower on the 11th than 10th July. Whilst horizontal advection perpendicular to the transect cannot be discounted, the most likely cause was that the ebb tide on 10th July had been flowing for ~40 minutes less than for 11th July, and had therefore transferred less energy into the BML, resulting in less doming of the thermocline.

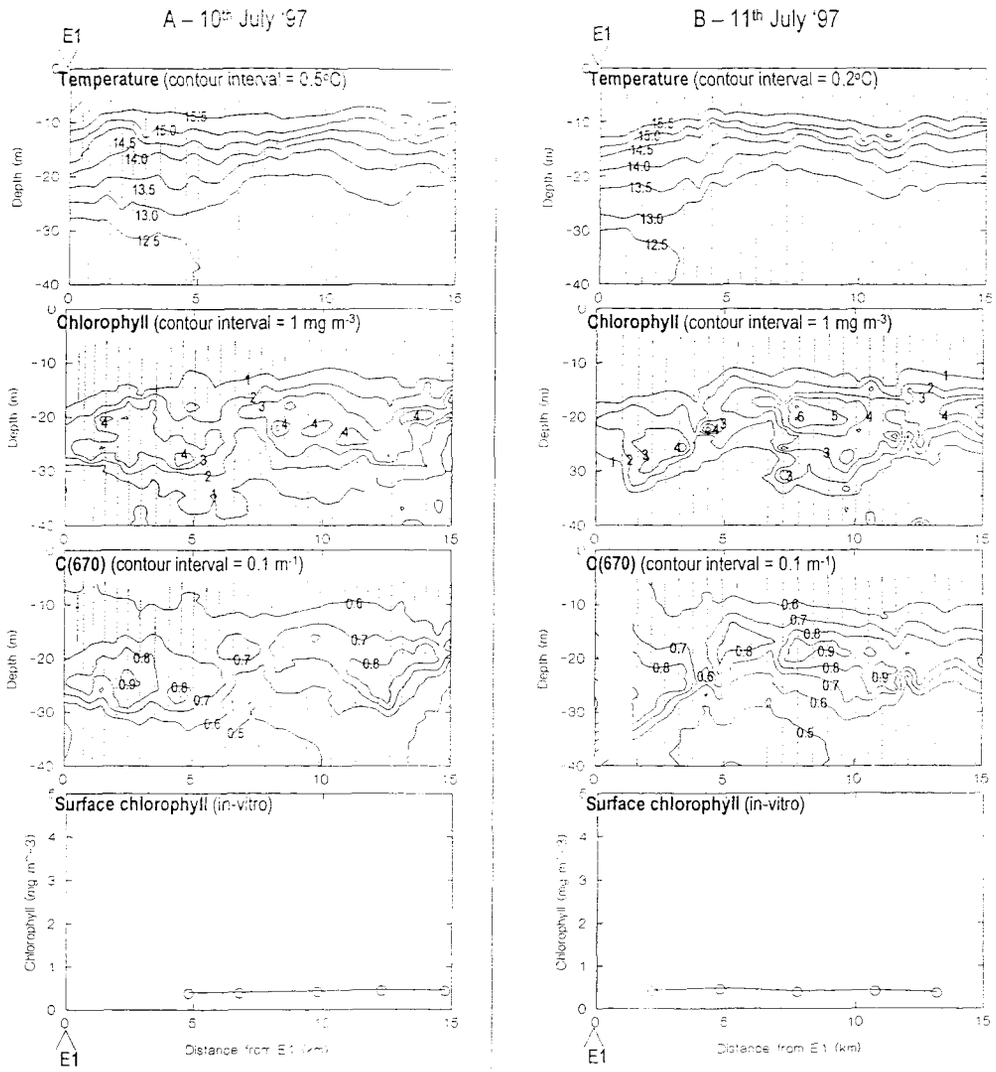

***Figure 4.9** – Temperature and chlorophyll distribution along the first 15 km of the E1 to S2 transect:*
***A** – 10th July '97.*
***B** – 11th July '97.*

The chlorophyll distributions for both dates are presented in figure 4.9A & B. A well-developed thermocline chlorophyll maximum was observed for both events, with typical concentrations of 4 mg m^{-3}. The maximum was located towards the base of the thermocline. The doming of the thermocline identified earlier was associated with two characteristics of the chlorophyll distribution: Firstly, chlorophyll concentrations at the edge of the dome nearest to E1 declined sharply (to ~1 mg m^{-3}). Secondly, the chlorophyll maximum in the area of the dome extended down into the BML, suggesting that cells were being mixed out of the domed thermocline at a higher rate than to either side.

The processes responsible for the observations described above are not clear. It is true, however, that the stratification in the domed region was stronger, the thermocline shallower, and the mixing within the BML more intense than the waters to either side, each of which may have implications on phytoplankton distributions.

Significant changes in the chlorophyll distribution had occurred between 10th and 11th June observations. Thermocline chlorophyll concentrations had increased overall (by ~0.5 mg m^{-3}), and were less horizontally variable. In addition, the features described in relation to the doming of the thermocline had become more pronounced. It is not clear, however, the degree to which these changes were due to in-situ production, or horizontal advection.

4.4 PlyMBODy Observations

Temperature, salinity and chlorophyll measurements were made from the PlyMBODy instrument during 1997 using a CTDF sensor mounted at 3.5 m below the water line (i.e. 3.5 m depth assuming PlyMBODy remained vertical).

During 1997, the buoy was first deployed on 8th August, recovered on 21st August, re-deployed on 5th September, and maintained in-situ on; 16th September, 29th September, 13th October, 31st October and 14th November. PlyMBODy was finally recovered on 29th November 1997 (dates courtesy of Mr M. Pinkerton, PML). In-situ maintenance (carried out by scuba divers) consisted of a visual check of system integrity, and a thorough clean of all scientific instrumentation.

The data as supplied consisted of calibrated measurements of temperature, salinity and chlorophyll concentration at intervals of ~10 min. The Author then averaged these data to calculate hourly, daily and monthly means for each of the measured fields. The daily mean values for each field from 8th August to 26th November are presented in figure 4.10

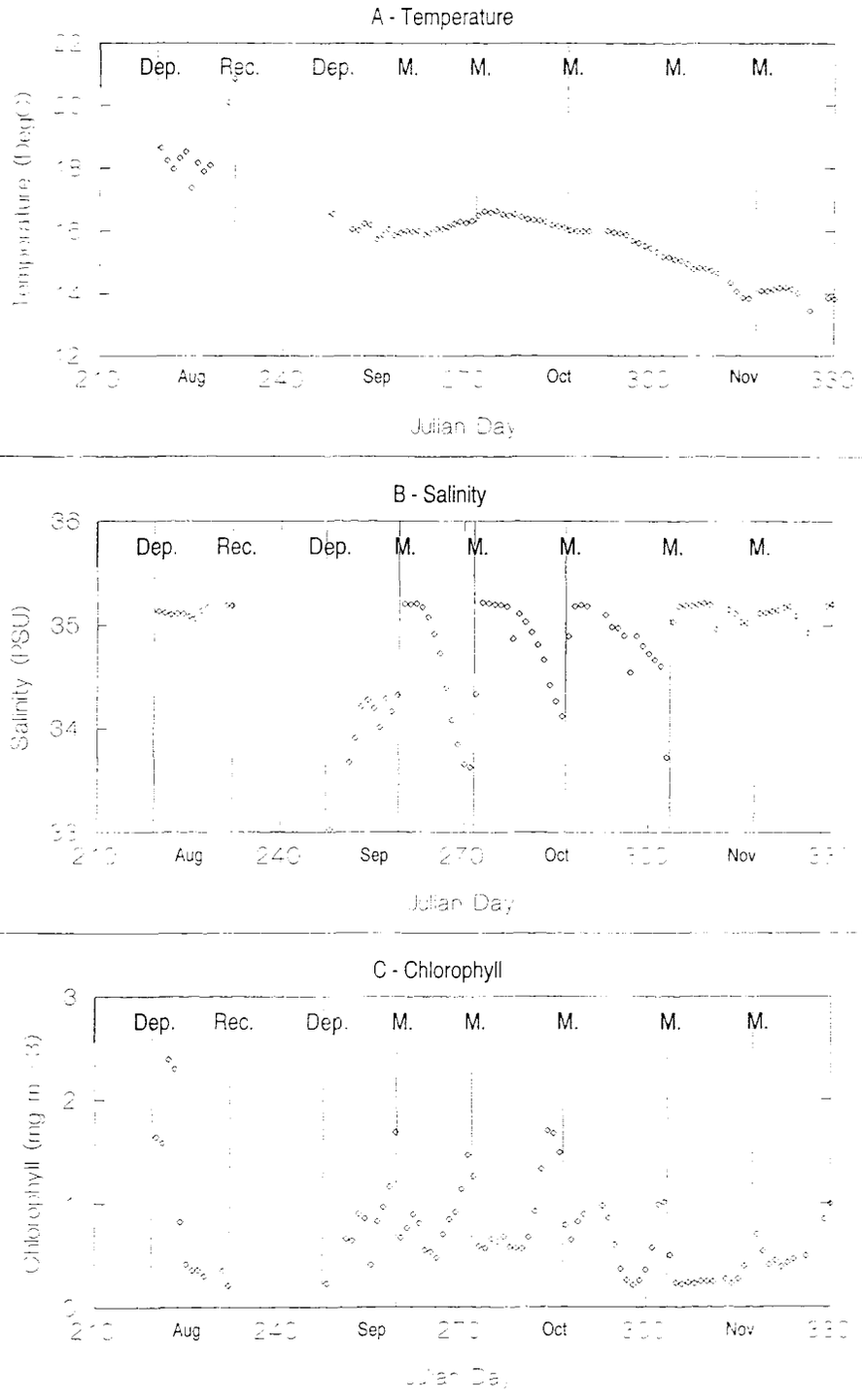

Figure 4.10 – *Daily average PlyMBODy measurements over ~4 months (August to November 1997). Also marked are dates of PlyMBODy deployment (Dep.), recovery (Rec.) and maintenance (M.)*

A – *temperature,*

B – *salinity,*

C – *chlorophyll.*

Figure 4.10 shows that the salinity and chlorophyll values changed markedly upon in-situ maintenance of the buoy system. Step increases in salinity of over 1 PSU, and decreases in chlorophyll of over 1 mg m^{-3}, were typical. These salinity and chlorophyll distributions can be accounted for by considering the effect on salinity and chlorophyll measurement due to the bio-fouling of the buoy's conductivity and fluorescence sensors. The gradual build-up of biological material on the sensors' surfaces (due to algal growth or trapped detritus) is likely to have caused an increase in fluorescence and a decrease in conductivity measurements. This is reflected by the apparent decrease in salinity and increase in chlorophyll with time following sensor cleaning. PlyMBODy's salinity and chlorophyll measurements are therefore inappropriate for the analysis of salinity and chlorophyll distributions over monthly or seasonal scales.

Figure 4.10 also indicates that sensor cleaning had little effect on the temperature measurement. This suggests that the buoy's thermometer measurements were less affected by bio-fouling than for the other sensors. In addition, the Spearman correlation between daily mean PlyMBODy temperature and available AVHRR SST for the PlyMBODy-containing pixel from August to November 1997 was 0.90. This suggests that the PlyMBODy measurements showed a similar distribution to that presented in Chapter 3 for temperature over this period.

8th to 11th August 1997 – Variability Caused by Tidal Processes

Temperature, salinity and chlorophyll distributions, as measured by PlyMBODy over a three-day period (8th to 10th August 1997), are shown in figure 4.11. Temperature (figure 4.11A) ranged between 17 and 19°C, and the variability was characterised by a series of well-defined minima. The time interval between each minimum was ~12 hours. The salinity distribution (figure 4.11B) was very similar to that of temperature in both the timing and relative magnitude of the variation, ranging between 34.05 and 34.15 PSU. The chlorophyll distribution displayed an inverse pattern to temperature and salinity (i.e. temperature minima were related to chlorophyll maxima and vice-versa), ranging between 0.5 to 4.5 mg m^{-3} (excepting the four points from Julian Day 222.8 to 223.0 where values were anomalously high).

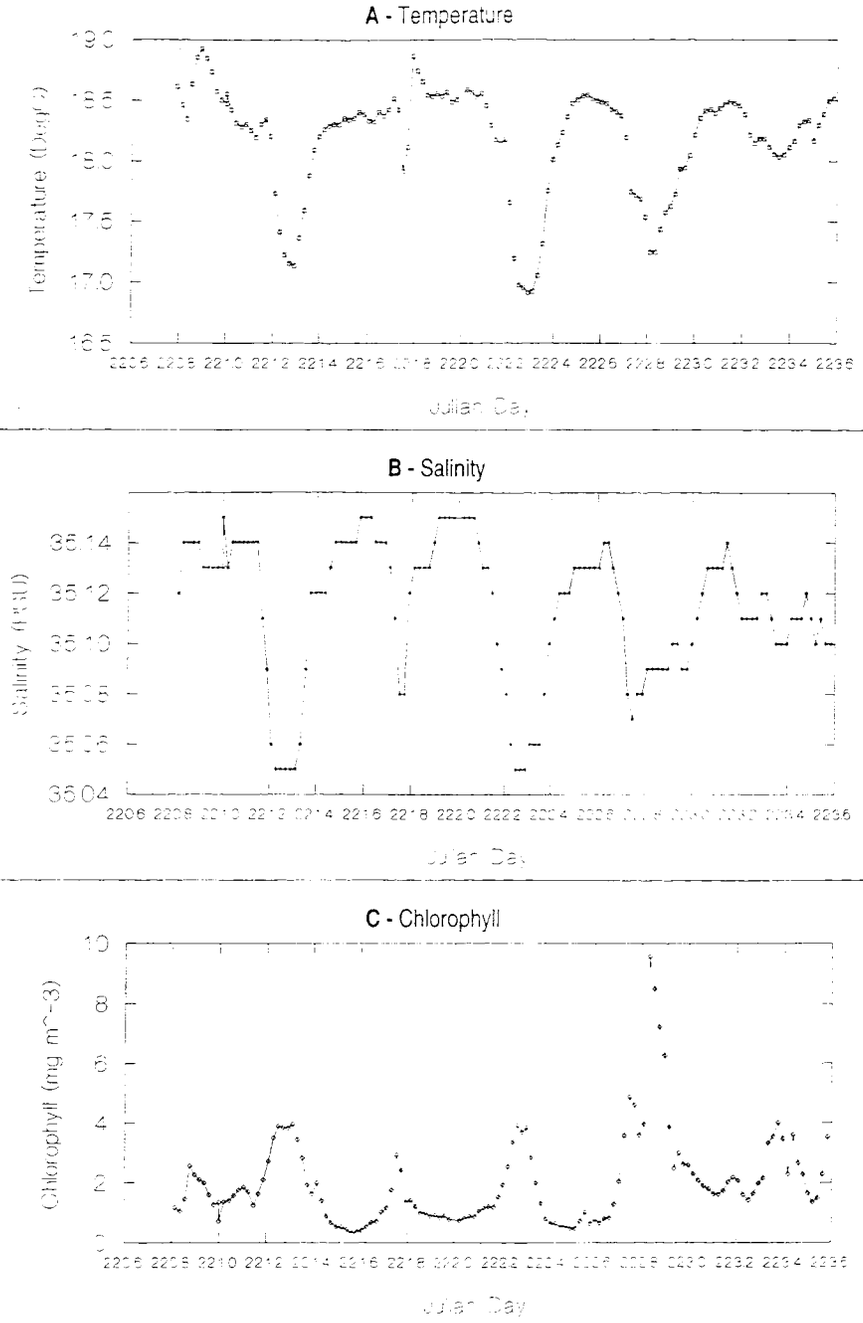

Figure 4.11 – *Hourly variability over a 3-day period (8th to 11th August '97) at PlyMBODy:*
A – *temperature,*
B – *salinity,*
C – *chlorophyll.*

Due to the frequency of the variability of temperature, salinity and chlorophyll observed in figure 4.11 (~12 h), it is likely to have been caused by processes associated with the M2 tide (frequency of 12.2 h). The M2 tidal ellipse at the buoy site was presented in

figure 3.6. The ellipse is highly rectilinear (b/a = 0.1) with its major axis orientated from East to West (104°), and with a length of 7.5 km. A reasonable explanation for the variability observed in figure 4.11 is therefore as follows: The watermass to the west was relatively warm, salty and low in chlorophyll, whilst the one to the east was cool, fresh and high in chlorophyll. The front between them occurred within the tidal ellipse, which was advected across the buoy site with a period of 12 hours. Holligan & Harbour (1977) recorded a similar event at station E1 during August 1975; associating tidal advection from west to east with an increase in surface temperature from 16.2 to 17.4°C, and a decrease in chlorophyll from >2 mg m^{-3} to <0.5 mg m^{-3}.

Due to its stability, salinity is often used as a passive index of mixing. If one considers salinity values to be affected only by mixing, then it can be used as a predictor variable for advection. The Pearson correlation coefficient (r^2) between another variable and salinity therefore provides an estimate of the percentage of that variable which may be attributed to mixing. For the 3-day period (8th to 11th August), 73% of the temperature variability and 42% of the chlorophyll variability can be attributed to advection. Whilst these figures may be underestimates due to sensor limitations (e.g. bio fouling of the fluorescence and conductivity sensors, daytime inhibition of fluorescence etc) it is probable that factors such as algal growth and diurnal heating and mixing also affected the distribution. Meteorological variability over the 3-day period (8th to 11th August) was presented in figure 3.4A. Downwelling irradiance varied from 0 to 800 W m^{-2}, wind speeds varied from 0 to 13 m s^{-1}, and air temperatures varied from 15 to 25°C. Although the magnitude of the atmospheric forcing was substantial, it appears that horizontal advection was the dominant process in causing the observed distributions of water temperature, salinity and chlorophyll.

25th to 28th September – Variability Caused by Diurnal Processes

The distribution of temperature, salinity and chlorophyll for a 3-day period (25th to 28th September 1997) are presented in figure 4.12. Temperature ranged between 16.2 and 16.4°C with a frequency of 24 h. The coolest temperatures occurred at ~07:00 GMT (e.g. Julian days 269.3, 270.3, 271.3, and the warmest temperatures occurred at ~17:00 GMT (e.g. Julian day 269.7). The corresponding salinity (figure 4.12B) decreased from 34.1 to 33.3 PSU over the 3 days, but showed no evidence of diurnal variability. Chlorophyll concentrations (Figure 4.12C) increased by 0.5 mg m^{-3} over the 3 days. Overlaying this trend, however, was a 24-hour pattern of increasing fluorescence between 10:00 and 16:00 GMT, and decreasing fluorescence between 16:00 and 10:00 GMT.

The frequency of both the temperature and chlorophyll variability on 25th to 28th September (~24 h) suggests that their distributions were controlled by processes associated with diurnal variability of atmospheric forcing. Meteorological variability for the 3-day period (25th to 28th September) were presented in figure 3.4. Downwelling irradiance and air temperatures increased during the daytime for each date, causing positive heat flux, and correspondingly in-water temperature, to increase during the daytime. In contrast, downwelling irradiance and air temperatures decreased during the night for each date, causing heat flux, and correspondingly water temperature, to decrease throughout the night. The lack of correlation between temperature and salinity over the 3-day period suggests that vertical processes, rather than horizontal advection, were responsible for the observed temperature distribution. In Chapter 3, AVHRR SST images for August 1977 (figure 3.20) and September 1997 (figure 3.21) were presented. The horizontal temperature gradients in the region of PlyMBODy in September were significantly lower than those in August. This is a possible explanation why a strong advective signal was observed at PlyMBODy during August 1997, but was insignificant at PlyMBODy during September 1997.

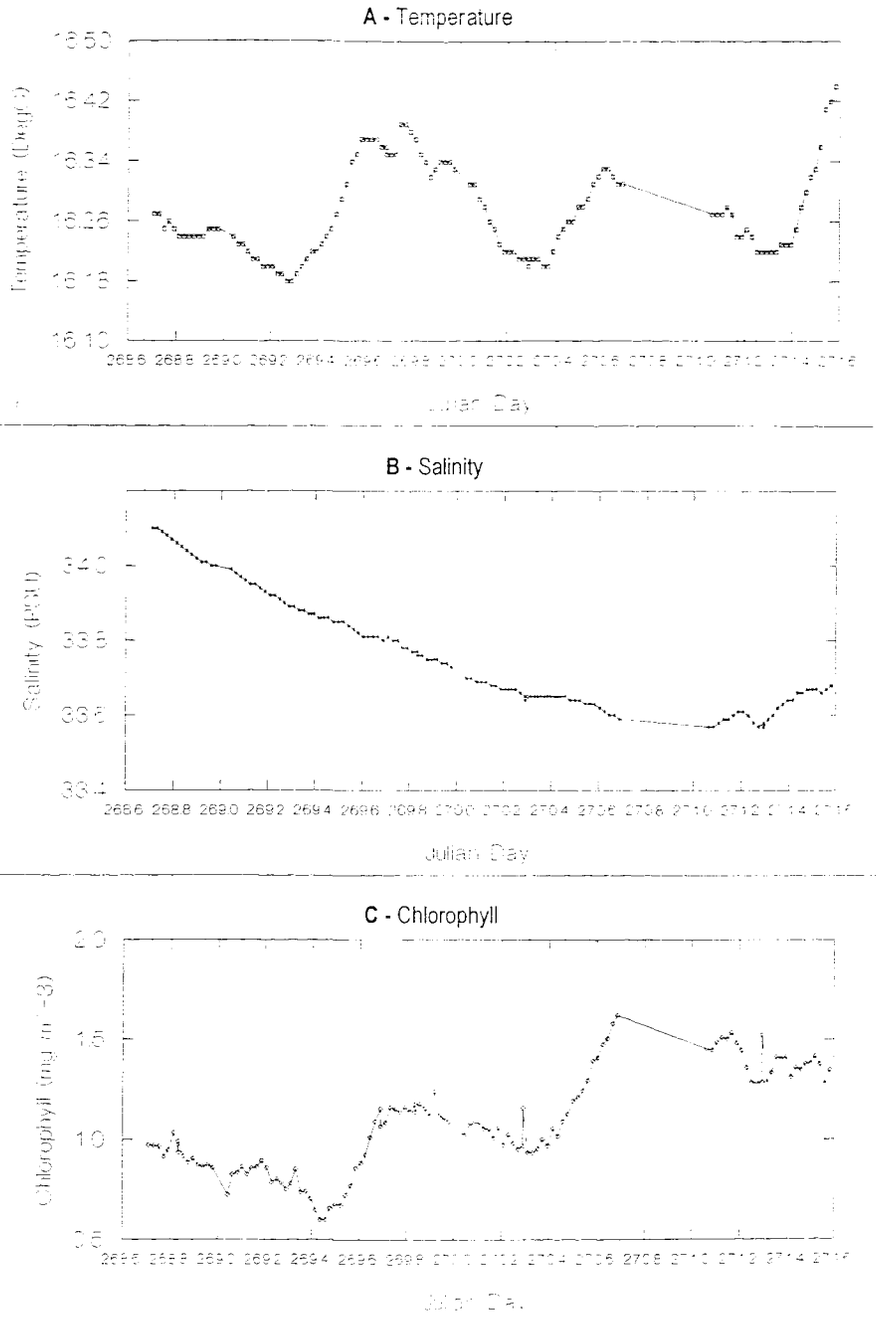

Figure 4.12 – *Hourly variability over a 3-day period (25th to 28th September '97) at PlyMBODy:*
A – *temperature,*
B – *salinity,*
C – *chlorophyll.*

As discussed earlier, the decrease in salinity over the 3-day period (25th to 28th September) can be accounted for by increasing bio-fouling of the conductivity sensor. Bio fouling of the fluorometer also explains the trend of increasing chlorophyll

concentration over the 3-day period. The diurnal signal of chlorophyll variability observed over the 3 days is typical of photochemical quenching of phytoplankton fluorescence, leading to a decrease fluorescence per unit chlorophyll with an increase in illumination (Prezlin & Ley, 1980). This process therefore resulted in artificially lower chlorophyll estimates during the daytime than during the night.

4.5 Conclusions

The findings of the field study are consistent with the analysis of the remote sensed data. The link between the temporal and spatial gradients of SST and the vertical structure of the water column appears to be confirmed by the field observations

- As well as strong temporal and spatial gradients of SST, the study region is also characterised by gradients of stratification and chlorophyll distribution. The field observations were typical of those previously documented for the region.
- The increases in tidal mixing along the E1 to S2 transect resulted in the reduction in the shallowing of the progressive erosion of the thermocline layer. A well-defined tidal front was formed during the early summer and the autumn. During mid-summer, the entire transect was thermally stratified.
- The local current modification caused by the Eddystone Rocks caused increased mixing along the E1 to L4 transect, resulting in small scale (~1 km) horizontal variability in its vicinity.
- Substantial chlorophyll maxima developed in the thermocline layer during mid-summer. Over this period, the degree of stratification was high, and the thermocline shallow.
- Chlorophyll concentrations increased at the tidal front during the autumn. No increases were observed, however, during early summer.
- Chlorophyll distribution was similar in the vicinity of the Eddystone Rocks to the distribution over a similarly stratified sections of the E1 to S2 transect.
- Stratification had broken down over both of the transects by 23rd September, resulting in the re-distribution of chlorophyll throughout the water column.
- Changes in the temperature distribution occurred over periods as short as 24 h. Changes in the surface mixed layer temperature could be related to meteorological

forcing, and changes in the deep mixed layer to tidal advection and mixing. The processes responsible for simultaneous changes in chlorophyll distribution were not clear over this time period.

- Significant intra-daily variation of temperature, chlorophyll and salinity was observed. When strong horizontal gradients existed in the study region, tidal advection created typical patterns of variation in each of the fields. When diurnal variation of heat flux was high, diurnal variation of temperature resulted.

- Changes in phytoplankton speciation were indicated by differences in the relationship between chlorophyll and light attenuation. These changes occurred over vertical, horizontal and seasonal scales.

Combined Conclusions, Chapters 3 And 4:

The extent to which meteorology and tides can be shown empirically to control shelf-sea temperature distribution was discussed in chapters 3 and 4. Here, the meteorological, tidal and water temperature signals were analysed separately for each of the scales of interest. This effective de-coupling of both the forcing (tides and meteorology) and resultant (water temperature) fields using scales of variability allowed the observed temperature distributions to be described using arguments based on vertical processes:

- The seasonal variability of water temperature was accounted for in terms of seasonal variability of solar irradiance, air temperature and wind mixing.

- The differences between 1997 and climatological water temperature distributions were accounted for in terms of differences between 1997 and climatological solar irradiance, air temperature and wind mixing.

- The sub-seasonal variability of water temperature over periods of >1 month was accounted for by variability over similar scales of solar radiance, air temperature and wind mixing.

- The variability of water temperature over periods of >1 day were accounted for by diurnal variability of solar irradiance and air temperature.

- The differences in water temperature variability over the above temporal scales but at different sites in the study region was accounted for by differences in water depth and tidal current at each of the sites.

- The horizontal variability of water temperature, including the occurrence of a frontal zone within the study region at various times of the year, was accounted for by horizontal variations in tidal mixing and water depth.

- The significance of the vertical variability of water temperature in regulating each of the above scales of variability was clearly identified, in terms of the intensity of stratification.

- Several aspects of the observed temperature distributions could not, however, be explained using arguments based on vertical processes forced by meteorology and tides, and separate explanations were proposed. These are as follows:

- The temperature distribution during the first two months of 1997 was too warm to be explained using arguments based on vertical heat flux. This anomaly was accounted for by warm water advecting horizontally into the study region during this period.

- The distribution of water temperature over periods of <1 day showed evidence of variability with a frequency of ~12 hrs. This anomaly was accounted for by horizontal advection of water with the semi-diurnal (M2) tide.

- The horizontal distribution of water temperature over part of the study region (e.g. the E1 to L4 transect) did not vary in accordance with the predicted value of the stratification parameter (S). This anomaly was accounted for by modifications to the current structure caused by the local bathymetry in the vicinity of the Eddystone Rocks.

5. Model Simulations

5.1 Design and Selection of the Model Simulations

The Prestidge-Taylor physical/biological model provides simulations of variables that can be compared directly with the observations presented in previous chapters. These are; the depth of thermocline and the temperature, nutrient and chlorophyll concentration for the SML, thermocline and BML layers. Simulations for specific time periods are achieved by running the model with contemporaneous periods of meteorological observations. Similarly, the model represents specific geographical locations by using realistic estimates of the water depth and tidal current parameters for these locations.

Resolution

The Prestige-Taylor model is forced by hourly meteorological data, resulting in simulations with a corresponding time-step of 1 hour. Furthermore, the vertical extent of each water column layer is calculated to the nearest whole meter. By combining model simulations from multiple runs, 'spatial' simulations are produced, where each run has differing tidal and depth parameters. The maximum resolution of the spatial simulations therefore corresponds to the maximum spatial resolution of the available tidal and depth data. Both the tidal and depth data were mapped onto a 1 km^2 grid, and missing cells estimated using spatial interpolation techniques. The maximum spatial resolution of model simulations was therefore 1 km. The maximum temporal range of model simulations was 1982 to 1997, corresponding to the range of available meteorological data, whereas the maximum spatial range was chosen arbitrary to cover the study region.

To perform individual (1 year) model runs for each 1 km^2 grid cell covering the study region, for the 15-year time period, over 50 000 individual model runs would have been required. To reduce this number, the model was only run to provide simulations consistent with the observational data that was presented in the previous two chapters. If required, the model outputs were averaged over intervals that were similar to those used for the observational data (e.g. daily and monthly means). Table 5.1 presents a summary

of the simulations presented in this chapter, the represented scale of variability, and the observational data type against which they are compared. In several cases, simulations are presented where no appropriate observational data are available. These are used primarily to elucidate qualitative links between the physical and biological simulations.

Each model run is a year in length, from 1st January to 31st December. The meteorological database, however, consisted of continuous data from 1st January 1982 to 31st December 1997. For simulation presented in this thesis, 16 individual model runs were performed (one for each year from 1982 to 1997), and the data concatenated into a single time series. Model temperature and nutrients were initialised to the inter-annual average temperature and nutrient concentrations from the E1 archive data set prior to each model run (i.e. on 1st January for each year of the simulation) to ensure that errors due to advection during winter did not accumulate over the 16 year period (as discussed later). The chlorophyll concentrations for the 1st January of each year used the simulated concentrations from 31st December of the previous year. The chlorophyll concentration was, however, invariably at the minimum level permitted by the model on 31st December.

Simulation Range	Averaging Interval	Scale of Variability	Simulation Variable	Comparison Data
01/01/82 to 31/12/97	Monthly (30-day) averaged over period	**Seasonal (inter-annual)**	Thermocline depth Temperature Chlorophyll Nutrient	E1 Archive E1 Archive E1 Archive E1 Archive
01/01/97 to 31/12/97	Monthly (30-day)	**Seasonal (1997)**	Thermocline depth Temperature Chlorophyll Nutrient	UOR AVHRR UOR None
4/7/97 to 3/8/97, 27/9/97 to 27/10/97	Daily (24-hr)	**Sub-Seasonal**	Thermocline depth Temperature Chlorophyll Nutrient	None AVHRR None None
8/8/97 to 11/8/97 25/9/97 to 28/9/97	None (hourly)	**Diurnal**	Thermocline depth Temperature Chlorophyll Nutrient	None PlyMBODy PlyMBODy None
E1 to L4 transect, E1 to S2 transect	~1 km	**Spatial**	Thermocline depth Temperature Chlorophyll Nutrient	UOR UOR UOR None

Table 5.1 *– Summary of model simulations presented in this chapter, their averaging interval, represented scale of variability, and the observational data types against which they are compared.*

Statistics

The data-processing methods used for the sampling and modelling procedures allowed each discrete space-time observation to be paired with an individual simulation point (within the limitations of the model's temporal and spatial resolution and range). Sets of observations could therefore be compared with model simulations without the need for either averaging or interpolation (although such techniques were often useful). To provide a quantitative measure of correlation between corresponding sets of observed and simulated data, the non-parametric Spearman rank correlation was calculated. Correlation values presented in this chapter are calculated as the square of the correlation coefficient (or coefficient of determination, termed 'r^2').

The difference in magnitude between the simulated and observed values for each observation-simulation pair was also calculated. By plotting all deviations for a set of observation-simulation pairs on a temporal or spatial scale (e.g. time in h), the trends in the performance of the model could be observed over the relevant scale.

It should be noted that a single model parameter set was used for all simulations presented in this thesis, as described in Chapter 2.

5.2 Model Simulations of Seasonal (Inter-Annual) Variability

The simulations from running the model over a 15-year period (1982 to 1997) for station E1 are presented in this section. Monthly mean values for each year were calculated by averaging the hourly model output. The mean monthly values and standard deviations from 1982 to 1997 were then calculated by using the monthly averages for all of the years.

Contour Plots of Temperature, Chlorophyll and Nutrient Distribution

The simulations of temperature, nutrient and chlorophyll are presented in the form of contour plots in figure 5.1. Visually, the distribution of each of the fields is similar to the data from the E1 archive, presented previously in figure 4.1. Obvious differences include; the summer time thermocline is too shallow, summer time nutrient concentrations are too high lower down in the water column, summertime chlorophyll concentrations are too high at the surface.

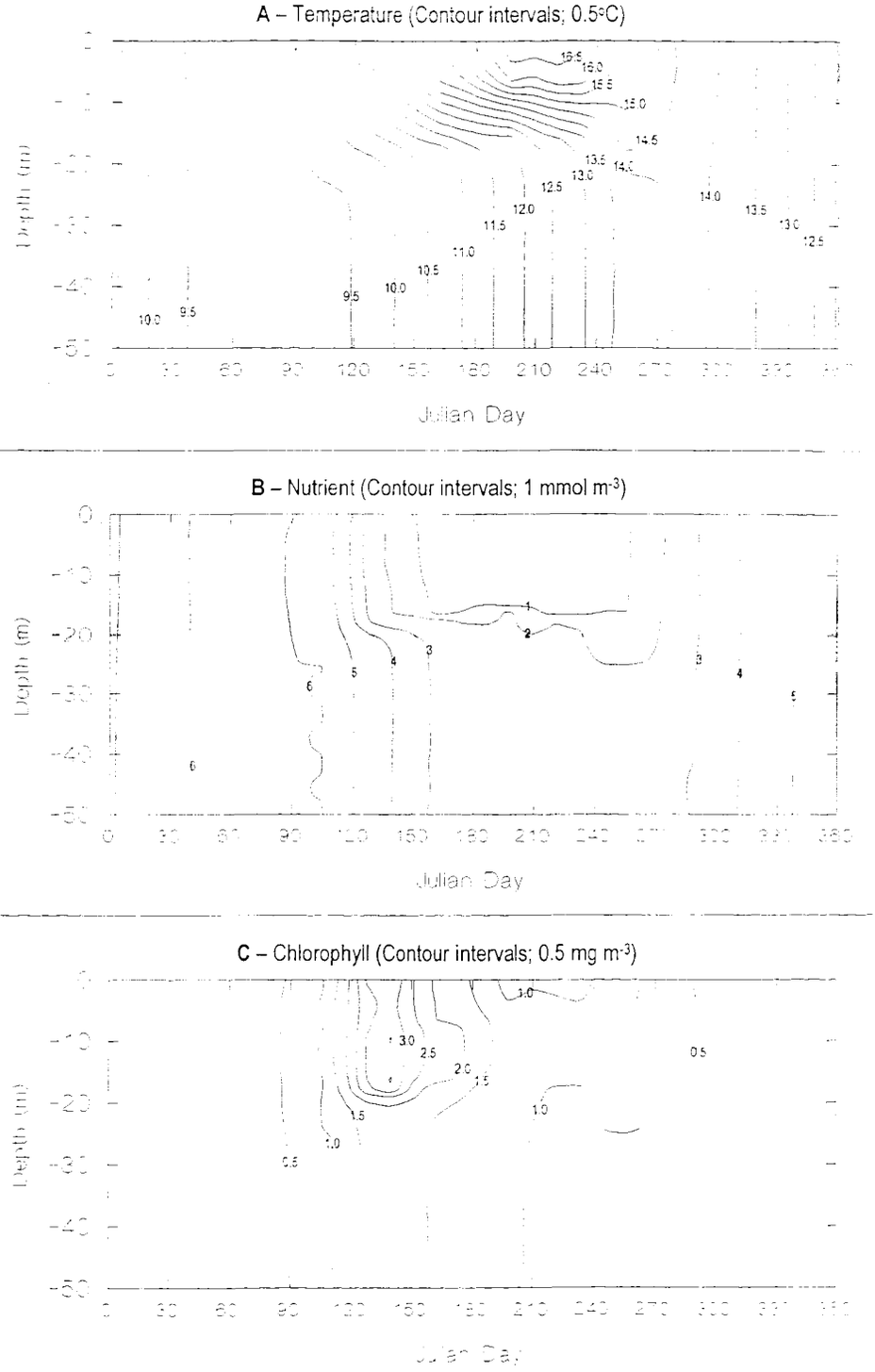

Figure 5.1 - *Model simulation of mean annual distributions at sampling station E1. The simulation time period was from 1982 to 1997.*

***A**: Temperature.* ***B:** Nutrient Concentration.* ***C:** Chlorophyll Concentration*

It must be noted that direct comparisons with archived data sets are limited by the fact that they may not cover the same period as the simulation. For instance, the E1 archive data set was compiled from observations made between 1974 to 1987, whereas the model simulation was run using meteorological observations from 1982 to 1997. Long term trends of temperature, nutrient and phytoplankton have been observed for the NW European continental shelf. For example, Radach et al (1990) showed an increase in yearly average water temperature of 1°C in 23 years, a change that was associated with strong increases in both nutrient and phytoplankton concentrations. In addition, Colebrook & Taylor (1984) identified correlated fluctuations in temperature, salinity and zooplankton distribution with wavelengths of 4, 6 and 11 years in the Western Atlantic.

Temperature – Correlation of Simulations Vs the E1 Archive

The seasonal temperature distribution at E1 simulated by the model correlated closely with the E1 archive (figure 5.2). The value of r^2 was > 0.97 for both the SML and BML. The ability of such models to simulate mean temperature distributions have been demonstrated previously, as described in the introduction. The model performance did, however, show trends with time. At the start of the year (Jan and Feb), simulations and observations were very similar, reflecting the fact that the model was initialised to the mean conditions. After stratification had become established SML simulations overestimated the observations by as much as 0.7°C (May). The overestimate reduced throughout the summer, with reasonable SML predictions during August and September. Overestimates became apparent again, however, over the latter part of the year for both SML and BML.

By setting the initial conditions to the average conditions, advective effects, such as those described in chapter 3, were accounted for at the start of the year. No correction could be made, however, later in the year, which accounts for the increasing deviation between the simulation and the observations after stratification had broken down in October, and advection had become dominant (Pingree & Pennycuick, 1975).

To assess whether the model simulated the correct degree of variability between years, the inter-annual standard deviation of monthly average temperature was calculated, and compared to that of the E1 archive. The results of this analysis are presented in figure 5.3. The model predicted the intra-annual variability of the seasonal SML temperature cycle with a high degree of relative accuracy ($r^2 = 0.76$). On average, the model underestimated the absolute archive variability, possibly because the simulation covered a shorter time span than the archive, and was therefore not entirely representative. The

most significant underestimates of the intra-annual variability of SML temperature (by up to 0.8°C) occurred during July and August, which were also the months for which SML temperatures were overestimated (figure 5.2) and the thermocline depth underestimated (figure 5.1). July and August were also the months of lowest mean wind speed (figure 3.1)

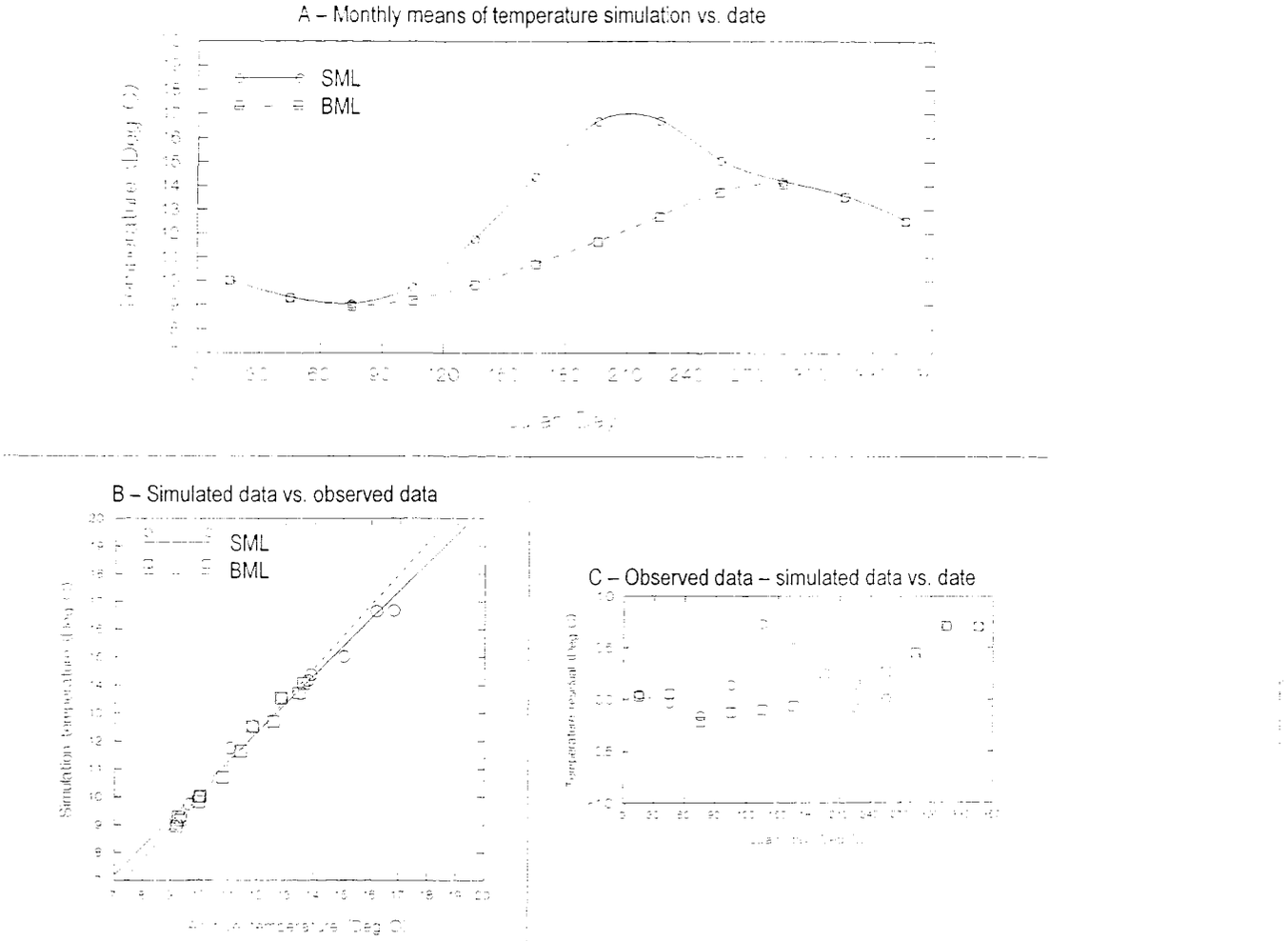

Figure 5.2 – ***A:*** *Monthly means of temperature simulation for station E1 (1982 to 1997) vs. date.*
B: *Monthly means of temperature simulation (above) vs. monthly means of E1 archive temperature data (1970 to 1984). Least squares best-fit line overlaid.*
C: *Difference between monthly means of archive data and monthly means of simulated data, plotted vs. date.*

Monthly average BML temperatures show little inter-annual variability (<0.5°C), and no obvious trend of inter-annual variability within the seasonal cycle. The correlation between the simulation and archive values was correspondingly poor (figure 5.3). The simulated variability during January was unrealistically low due to the use of identical initial conditions for each year.

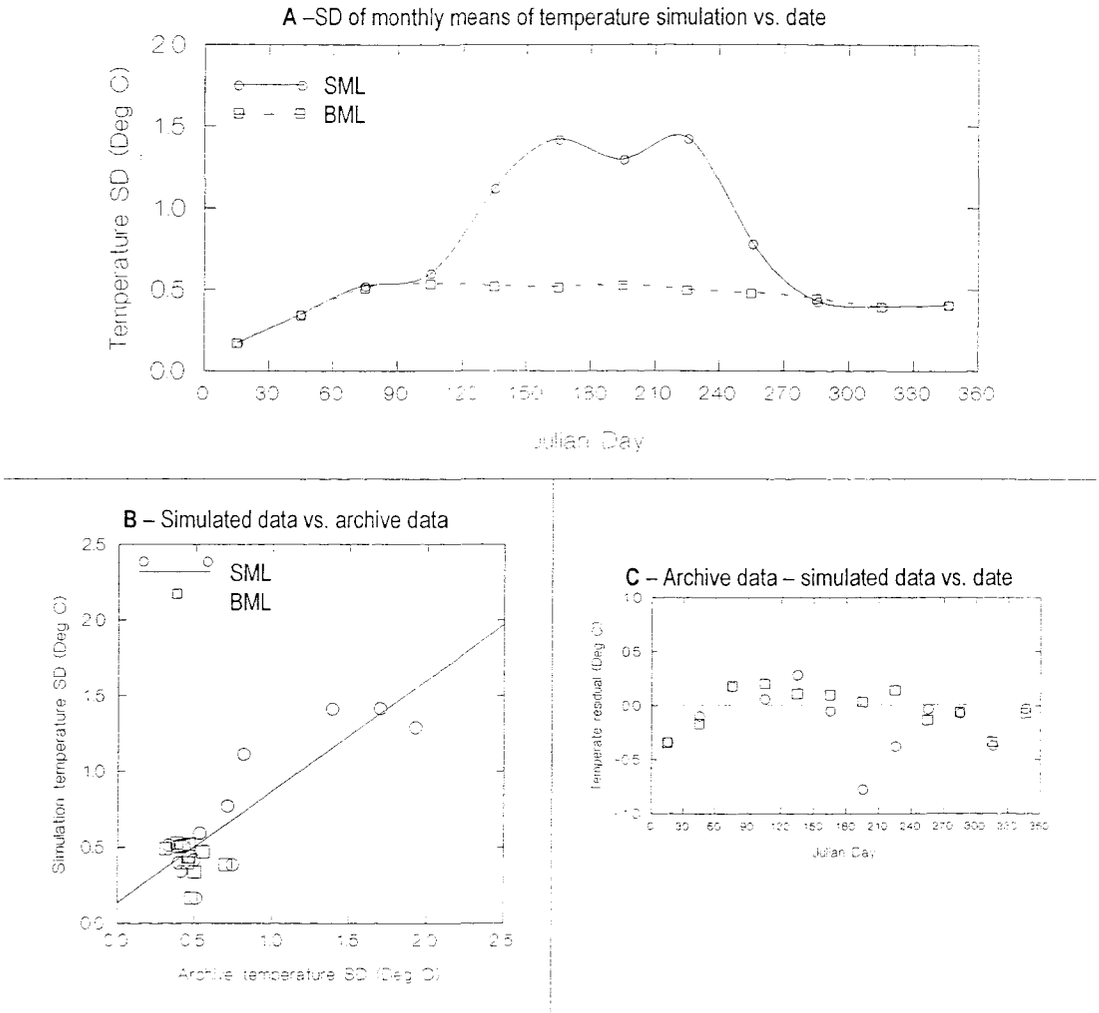

Figure 5.3 – ***A:*** *SD of monthly means of temperature simulation for station E1 (1982 to 1997) vs. date.*
B: *SD of monthly means of temperature simulation (above) vs. SD of monthly means of E1 archive temperature data (1970 to 1984). Least squares best- fit line overlaid.*
C: *Difference between SD of monthly means of archive data and SD of monthly means of simulated data, plotted vs. date*

Nutrient – Correlation of Simulations Vs the E1 Archive

The model also provided a realistic simulation of the average monthly nutrient distribution (figure 5.4). For the comparison, the archive nutrient (nitrate + nitrite) concentration was calculated as the sum of nitrite plus nitrate concentrations. The values of r^2 were 0.73 for the SML, and 0.71 for the BML. The model, however, significantly overestimated summer BML concentrations, generally by a factor of 2. Several physical and biological factors may have caused this difference. Physical factors include; an underestimate in mixing of nutrients into the upper layers, or too rapid re-generation of nutrients from the sediment. Biological factors include; too rapid recycling of nutrients due to sinking of phytoplankton from above, or too little in-situ productivity in the BML.

The most significant deviations between the predicted and observed nutrient occurred during April and May, in both the SML and BML (by ~1 mg m^{-3} and 2 mg m^{-3} respectively). This period corresponded to the reduction of nitrate due to utilisation by phytoplankton during the spring bloom. The model overestimates of nutrient during this period suggest that either the timing of the spring bloom was delayed, or the rate of utilisation per unit of chlorophyll was too low.

The simulation also overestimated BML nutrient concentration during the summer, by ~ 1 mg m^{-3}. The model assumes that nutrients are supplied proportionally to the sediment/BML nutrient gradient, meaning that the supply will be greatest during summer. It is likely, however, that some new nutrient is transported to E1 due to the advection of nutrient rich Atlantic waters. As the rate of advection is greatest during the winter, it is unlikely that the model adequately represents the seasonal distribution of nutrient supply, leading to the observed summer overestimates in the BML.

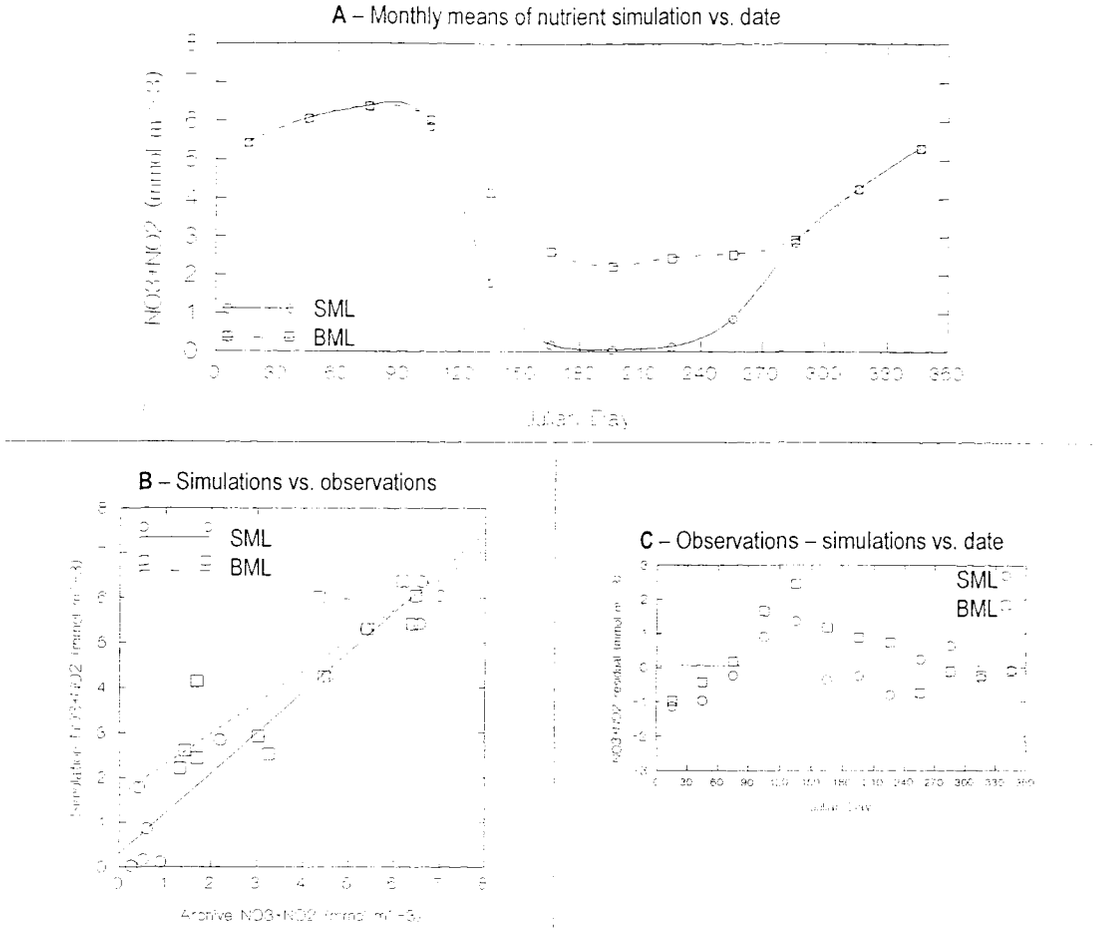

Figure 5.4 – ***A:*** *Monthly means of nutrient simulation for station E1 (1982 to 1997) vs. date.*
B: *Monthly means of nutrient simulation vs. monthly means of E1 archive nutrient (nitrate + nitrite) data (1970 to 1984). Least squares best-fit line overlaid.*
C: *Difference between monthly means of archive data and monthly means of simulated data, plotted vs. date.*

Chlorophyll – Correlation of Simulations Vs the E1 Archive

The simulation (figure 5.5) showed the classical features of chlorophyll distribution for shelf seas (e.g. Holligan & Harbour, 1977), with well-defined spring and autumn chlorophyll blooms separated by minima during the summer and autumn. Numerical comparison with E1 archive data provides r^2 values of 0.39 and 0.26 for the SML and BML respectively). The model predicted the spring phytoplankton bloom during May, whereas the archive suggested that the maximum bloom occurred in April. This difference in phase will have contributed to the low correlation coefficients (r) which were of borderline significance (assuming significant where r>0.5), even though the simulated pattern of chlorophyll variability was qualitatively realistic.

It is reasonable to assume that the delayed onset of the simulated spring bloom allowed enhanced nutrient concentrations to persist for longer into the year, and may therefore have contributed to the overestimate of the model simulation of spring nutrient concentrations identified previously. The model simulation produced a slight (0.5 mg m^{-3}) underestimate of SML nutrient concentration during June and July. It is likely that this error was caused by the fact that the model predicted a later spring bloom than observed, correspondingly depleting nutrients later.

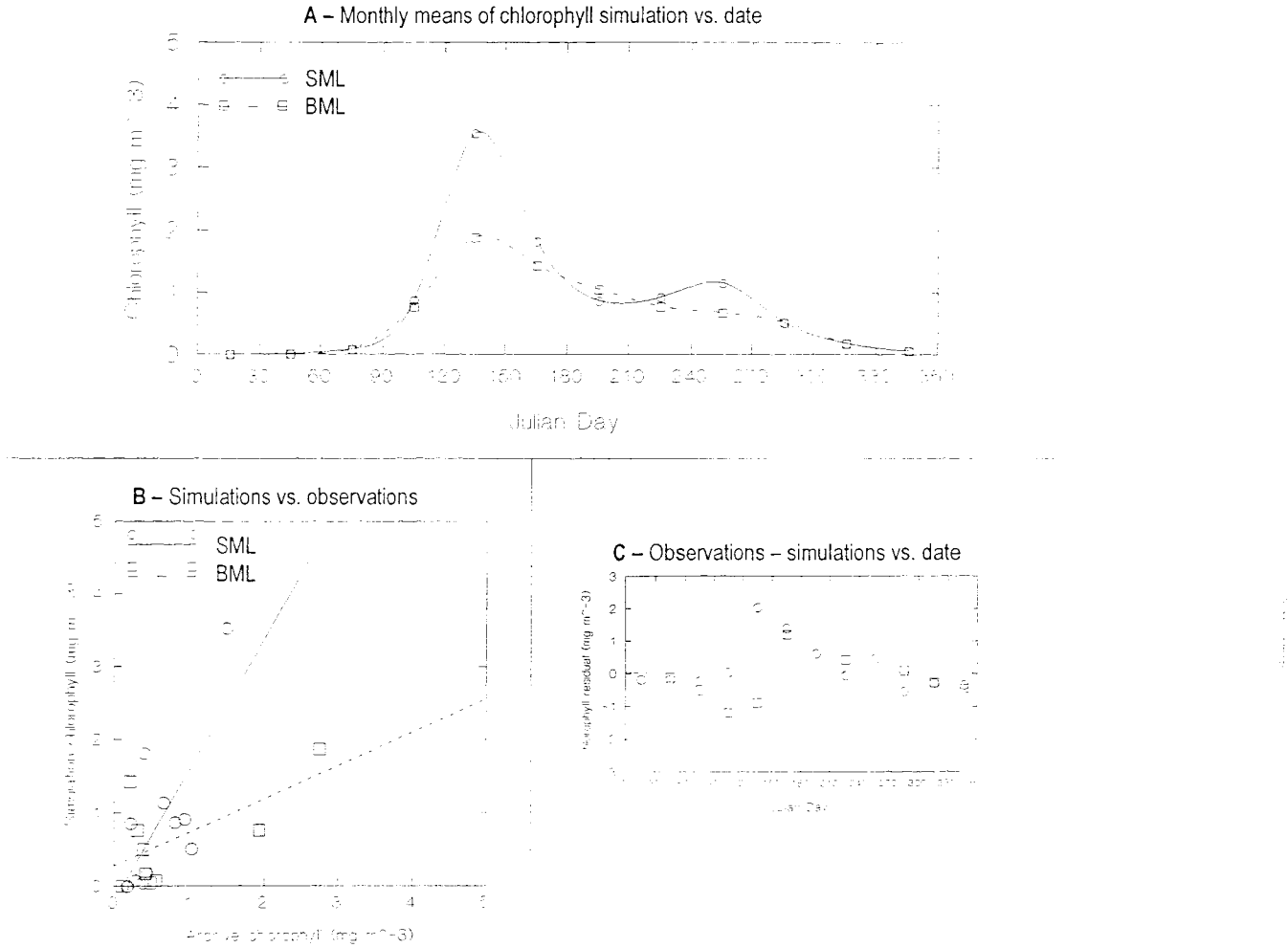

Figure 5.5 – ***A:*** *Monthly means of chlorophyll simulation for station E1 (1982 to 1997) vs. date.*
B: *Monthly means of chlorophyll simulation vs. monthly means of E1 archive chlorophyll data (1970 to 1984). Least squares best-fit line overlaid.*
C: *Difference between monthly means of archive data and monthly means of simulated data, plotted vs. date.*

Whilst the model tended to overestimated summer SML chlorophyll, it generally underestimated BML concentrations. Underestimates of BML chlorophyll suggests that the model failed to

adequately simulate either the rate, or depth, at which nutrients are regenerated. For instance, if the model overestimated regeneration rate, then underestimates of BML chlorophyll would result. Overestimates of regeneration in the SML or thermocline layers would also tend to reduce BML chlorophyll concentrations. Such upper layer regeneration overestimates could result from underestimates of phytoplankton sinking rates, or overestimates of regeneration rates. The relationship between the rates & depths of regeneration and the fluxes of nutrients that fuel productivity is complex. It is likely, however, that regeneration errors will effect the timing of productivity events to some extent.

5.3 Model Simulations of Seasonal (1997) Variability

The simulations presented here were from 1997 model runs for stations E1, L4 and S2. The hourly model outputs were averaged for each month of the year.

Temperature – Correlations of SML simulations Vs 1997 AVHRR SST data.

The model simulations of SML temperature during 1997 for each of the three stations (E1, L4 and S2, figure 5.6) were compared with the monthly average AVHRR SST data that were presented in Chapter 3, figure 3.13. 1997 temperature predictions were very similar to the observations, with r^2 values of >0.97 for each station. For E1 and S2, the predictions did, in general, underestimate the observations. This inconsistency can be explained by the sampling bias inherent in satellite temperature observations. Clear skies, especially during summer, tend to be during periods of warmer weather, which will be reflected by warmer SST values (Robinson, 1985).

The difference between the observations and predictions are presented in figure 5.6C. The model performance against observations changed throughout the year. There is evidence that, during January and February, the water column temperature is dominated by advection. This aspect was as discussed in Chapter 3. To account for this, the initial water column temperatures were set high to compensate. This compensation can be justified by the fact that the chosen temperature was the average January temperature from the E1 archive, and also the initialisation temperature used for the model runs used for the inter-annual simulations presented earlier. The temperature compensation is, however, responsible for the overestimates of temperature during January and February.

From March to June, temperature predictions increased with respect to the observations for all stations. During July the pattern for each station was different; the residual increased for L4 and S2, suggesting that stratification was overestimated, but diminished for E1, suggesting an underestimate. During August, the residuals for E1 and S2 were substantial and negative (suggesting underestimated stratification), whilst L4 values are similar for both observations and predictions. After stratification had broken down (October onwards), the residuals for E1 were more negative than for S2, and S2 more negative than for L4. These differences reflect either that advection is significantly affecting SML temperature, or those inaccuracies in predictions of stratification during the summer affected the heat balance later on during the year.

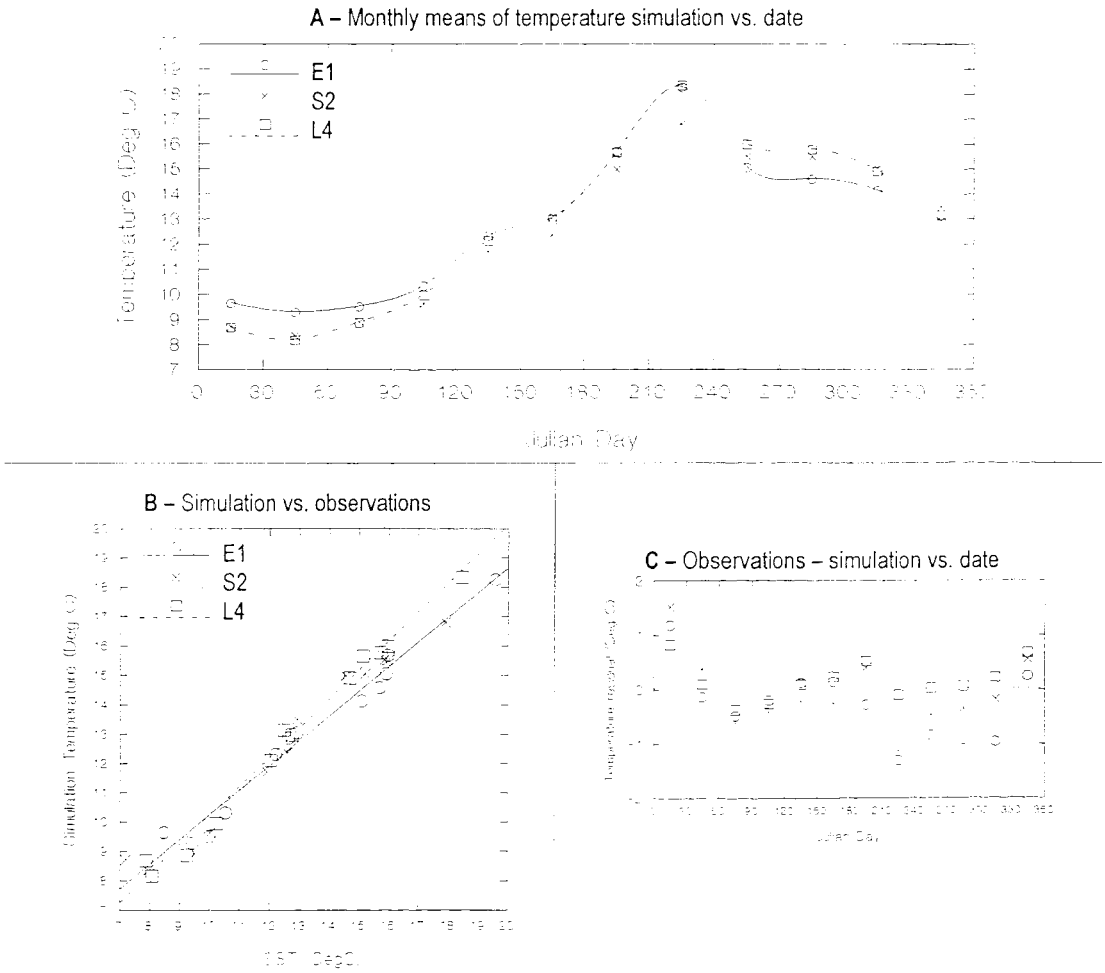

Figure 5.6 – ***A:*** *Monthly means of temperature simulation for stations E1, L4 and S2 for 1997.*
B: *Monthly means of temperature simulation vs. monthly means of AVHRR SST data for stations E1, S2 and L4 for 1997. Least squares best-fit line overlaid.*
C: *Difference between monthly means of AVHRR data and monthly means of simulated data, plotted against date.*

The observations (figure 3.13, Chapter 3) showed that L4 had summer time temperatures that fell between S2 and E1. For the simulations (figure 5.6), however, L4 and E1 temperatures were very close. The SST observations were previously used to propose a tendency of stratification of E1>L4>S2. However, the model simulation suggests an order of E1=L4>S2. That the model overestimates SML temperature with respect to E1 and S2 is supported by the similarity between monthly SST values and model predictions; the simulation for L4, is closer to the SST observations than for E1 or S2. If one assumes that there is an inherent SST overestimate in the AVHRR data, then it follows that there is also an overestimate in the L4 SML predictions. There is evidence, as discussed in Chapter 3, that the turbulence at station L4 is enhanced by island

mixing effects due to the proximity of the Eddystone Rocks. As the model does not account for such effects, the mixing at L4 is correspondingly underestimated.

Simulations of Nutrient and Chlorophyll Distributions

The above discussion highlighted the subtle differences between the seasonal cycle of SML temperature at stations E1, L4 and S2. Unfortunately, the observational data set did not contain appropriate data to resolve the seasonal cycle of either chlorophyll or nutrient for the 1997 annual cycle for the sampling stations. Model simulations, however of chlorophyll and nutrients, however, are presented in figure 5.7, but these cannot be validated against observations. Of the three stations, L4 is the one for which the spring bloom and nutrient depletion developed the earliest (during April). The model predicted that L4 stratified the earliest due to a lower tidal mixing allowing the spring bloom to develop. It is recognised, however, that the degree of mixing at L4 estimated by the model may have been significantly underestimated.

During May, both E1 and L4 were well stratified, forming higher chlorophyll concentrations than at S2, where the mixing was greater. During the summer, SML nutrients were depleted at all stations, leading to low SML chlorophyll concentrations. For the BML at L4, significant chlorophyll concentrations existed due to the shallow depth of the station (50 m) allowing significant light and therefore in-situ productivity to occur in the BML. During the summer, the highest SML chlorophyll concentration occurred at S2. This was due to higher tidal mixing at S2 increasing the nutrient supply to the SML. S2 was also the station with the lowest BML nutrient concentration, reflecting the enhanced upward flux.

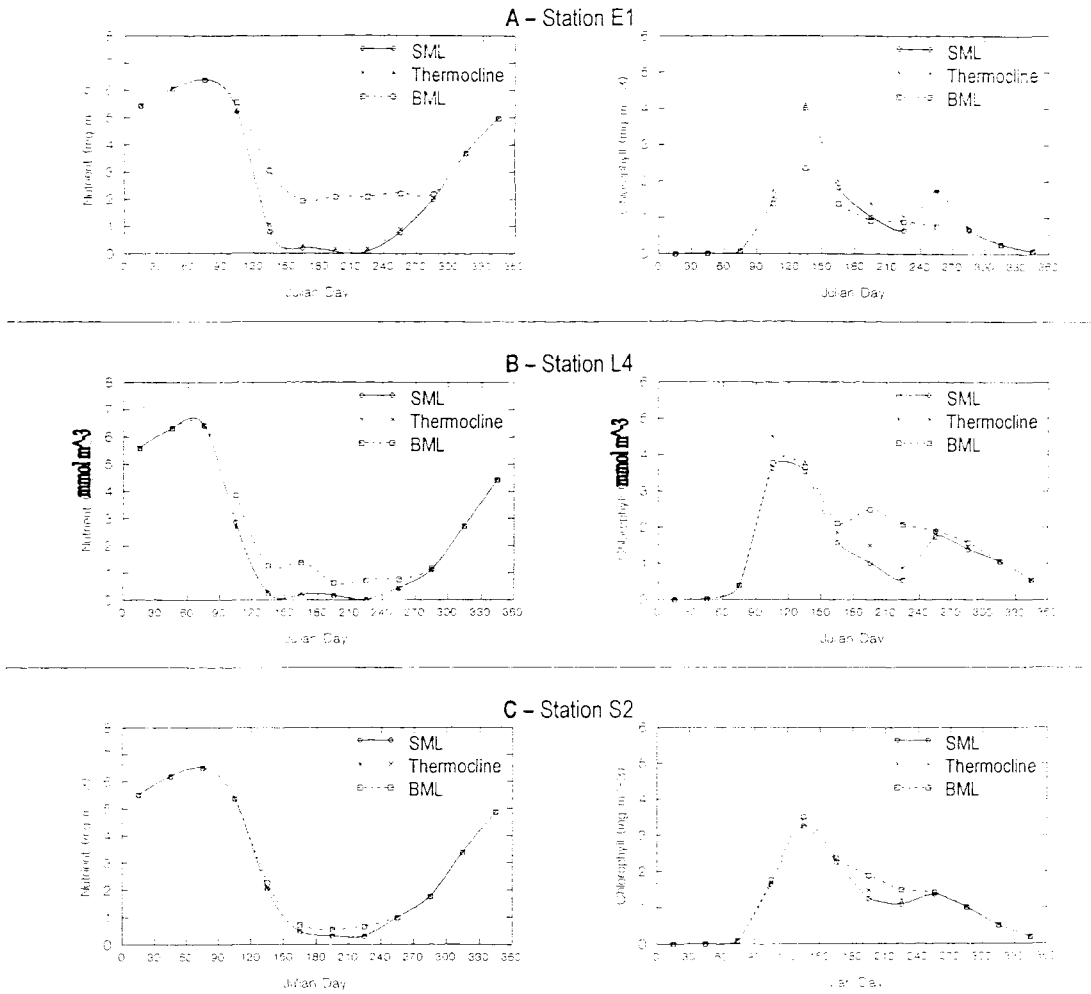

***Figure 5.7** – Monthly means of nutrient and chlorophyll simulations for 1997*
***A:** Station E1.* ***B:** Station L4.* ***C:** Stations S2*

5.4 Model Simulations of Sub-Seasonal Variability.

The simulations presented here are from 1997 model runs. Sub-seasonal variability is presented firstly in terms of the temperature deviation from the underlying seasonal trend, as defined in Chapter 3. Secondly, daily model estimates of temperature, chlorophyll and nutrients for the whole of 1997 are presented. Daily values represent model outputs at midnight, thereby allowing comparison with night-time AVHRR SST measurements. Thirdly, month-long simulations of temperature, chlorophyll and nutrient are examined in more detail. The daily values used here are also at midnight.

Temperature – Deviation from the Underlying Seasonal Trend; Comparison of SML Simulations Vs. AVHRR SST Data

Sub-seasonal variability in SML temperature was determined using the procedure explained in Chapter 3, designed to remove variability caused by the underlying seasonal trend. The distribution of intra-monthly variability for each station is presented in figure 5.8. This figure can be compared directly with the intra-monthly SST variability shown in figure 3.14, (Chapter 3). The distributions on each figure are significantly different, in both magnitude and trend, hence no quantitative comparisons have been attempted. The reasons for the differences are not certain, but the sampling bias and uneven coverage of the AVHRR SST measurements may be culpable. The simulation does, however, reflect the major features described in Chapter 3 with respect to differences in stratification at E1 and S2. For instance, the variability at E1 during April is higher than at S2, suggesting an earlier onset of stratification. Similarly, the variability at E1 is lower than S2 during August, suggesting stronger summer time stratification. Finally, the variability at E1 is higher than at S2 during September, suggesting that E1 re-stratifies on more occasions during this month than at S2.

The intra-monthly SML temperature variability increases confidence that the model predicts that E1 is more likely to stratify than S2. The similarity between E1 and L4 (figure 5.8), however, provides more evidence that the model does not predict that E1 stratifies more readily than L4. This question is investigated in more detail later.

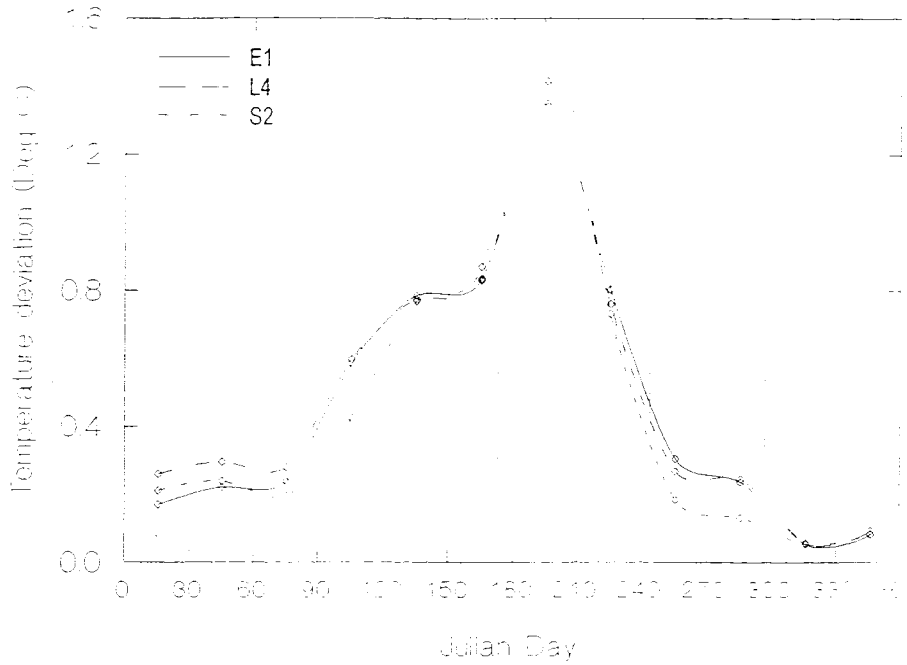

Figure 5.8 *– Deviation of the simulated surface mixed layer (SML) temperature from the simulated underlying trend at sampling stations E1, L4 and S2 during 1997. Hourly deviations have been averaged into monthly mean values.*

Temperature – Daily SML values for 1997; Correlation of simulations Vs Discrete AVHRR Measurements

The comparisons presented above each represented the monthly average values of a number of simulated and observed data points. As mentioned in the introduction, the comparison of averages can be misleading due to the non-contemporaneous nature of the observations and simulations. Satellite SST measurements, however, allow simulations to be tested against a large number of discrete data points covering the entire seasonal cycle. A temperature simulation of midnight SML temperatures is presented in figure 5.9. Model output at midnight has been used as it is consistent with the night time satellite SST measurements presented in figure 3.11 (Chapter 3). The comparison of the SML temperature simulation and the SST measurements at E1 during 1997 (figure 5.9B) returned an r^2 value of 0.94. This is a lower coefficient than for the monthly means, but the large number of data points (~200) result in a higher confidence level.

The magnitude of the simulation error (figure 5.9C) shows the same trends against time as for the monthly mean simulation at E1, although the error of a few of the individual

points exceeded the mean values. The simulation was generally accurate to within +/- 1°C.

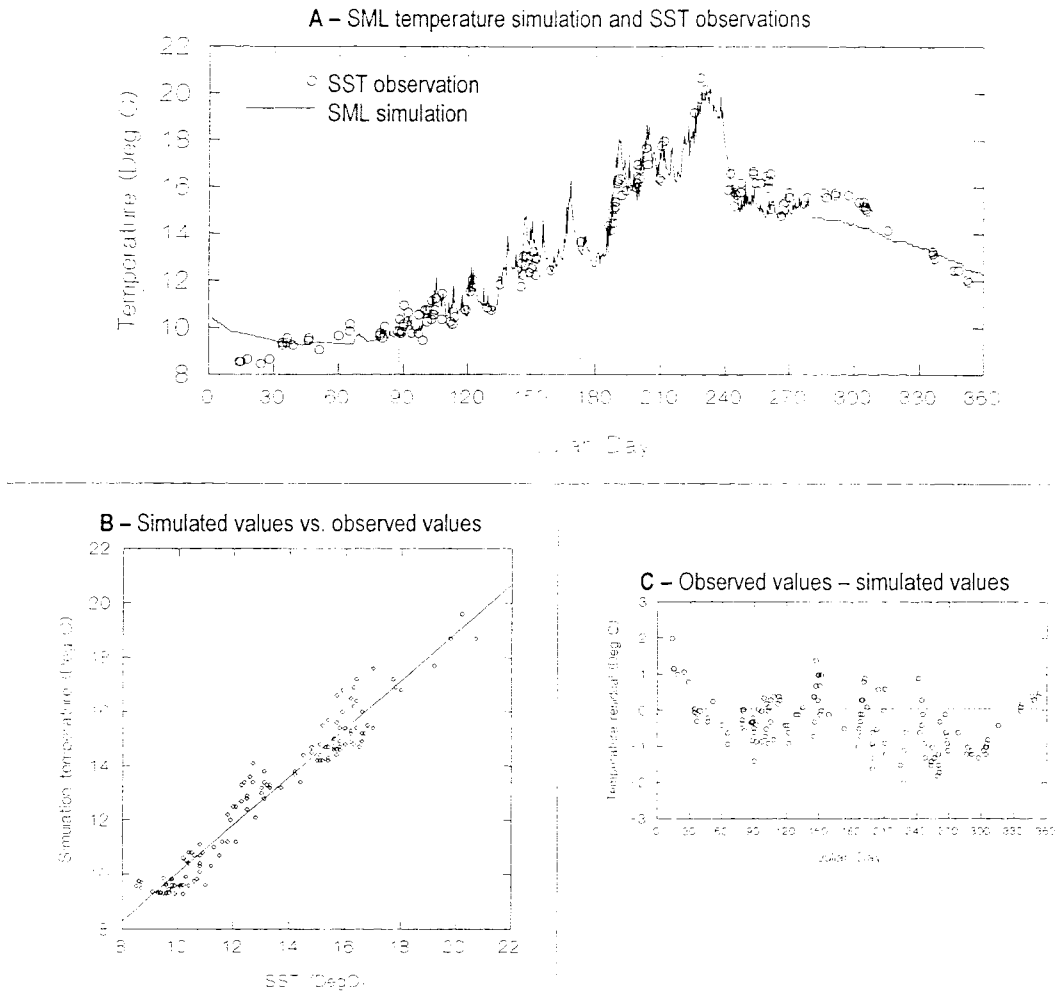

Figure 5.9 – ***A:*** *Discrete (Hourly) values of temperature from the simulation for station E1 for 1997. Discrete AVHRR SST measurements from 1997 have been overlaid.*
B: *Discrete values of temperature from the simulation vs. corresponding AVHRR SST measurements.*
C: *AVHRR SST measurements – simulated temperature values, plotted against date.*

Simulations of Thermocline Depth, Chlorophyll and Nutrients – Daily Values for 1997

Simulations of thermocline depths, nutrients and chlorophyll at E1 for 1997 are presented in figure 5.10. Each of the simulations predicts a high degree of short time-scale variability. Thermocline depths indicate that the stratification during March, April and October was intermittent. Once established, it deepened on several occasions for periods of a few days at a time (e.g. days 125 to 135, 175 to 180) in response to increased mixing from the surface. These periods of deepening caused a decrease in SML temperature (figure 5.9A), and an increase in SML and thermocline nutrient concentrations (figure 5.10B). These nutrient pulses caused a corresponding increase in chlorophyll concentration (figure 5.10C). The model predicted that nutrient concentration in the thermocline would be higher than in the SML, especially during periods where the thermocline depth deepened.

During the summer, chlorophyll concentrations in the thermocline were generally lower than in the SML, even when the thermocline nutrients concentration was high. Only during July and August, where both SML and thermocline nutrient concentration was minimal, did a thermocline chlorophyll maximum occur, reaching 1 mg m^{-3} compared to the SML concentration of 0.5 mg m^{-3}. It would therefore seem that, when the thermocline deepened, the phytoplankton in this layer became light limited, which would be increased due to self-shading by the extra chlorophyll in the SML. Only when the nutrient supply due to mixing decreased and the thermocline rose could a sub-surface chlorophyll maximum become established.

To assess the performance of the model against discrete observations, data collected by the UOR in the vicinity of E1 is used. This data, the corresponding model simulations, and the difference between the simulations and observations are presented in tables 5.2A-C.

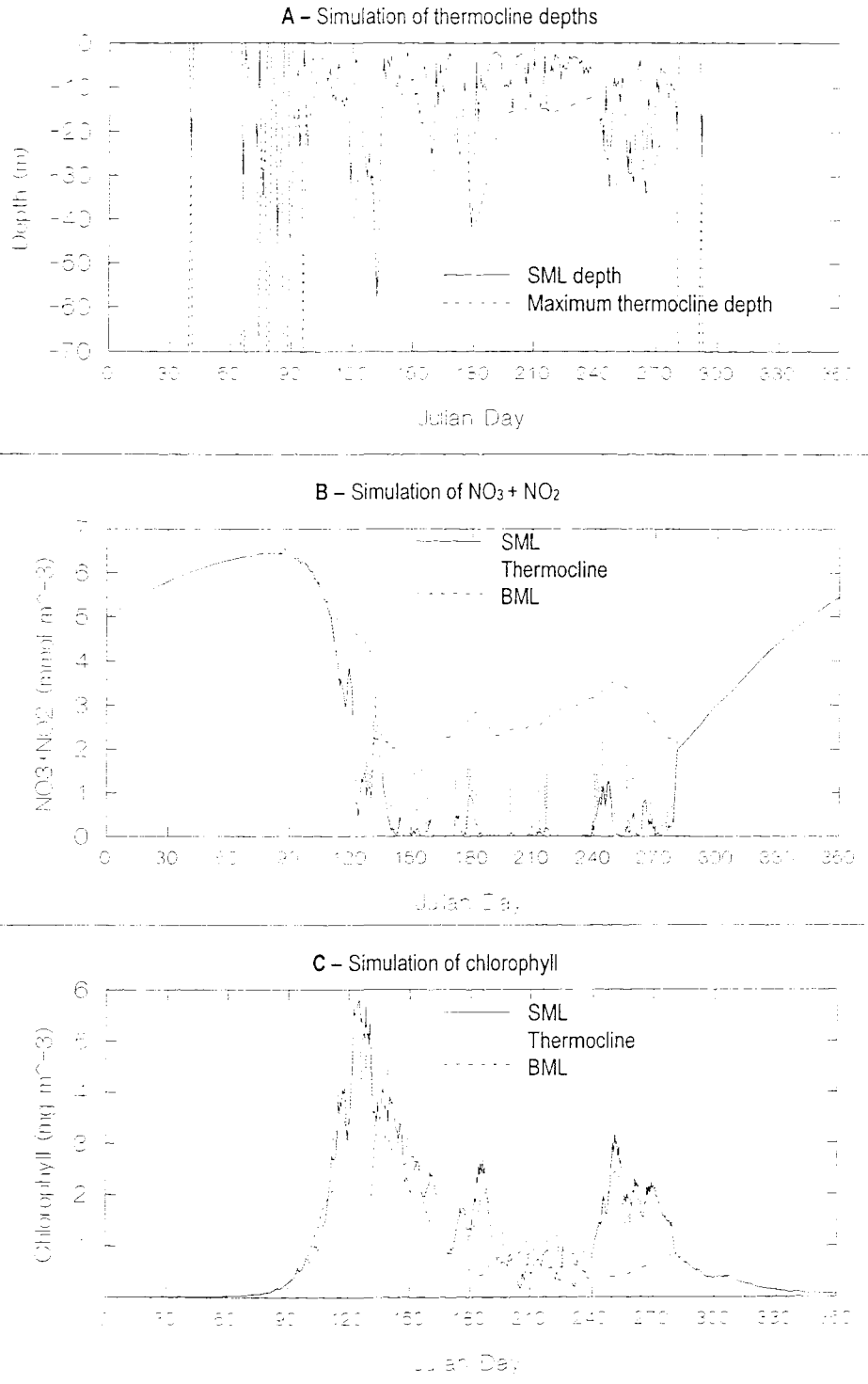

Figure 5.10 *- Simulations at station E1. The model run was for 1997, and 2 outputs per day (00:00 GMT and 12:00 GMT) have been plotted.* ***A:*** *Thermocline depths.* ***B:*** *NO_3 + NO_2.* ***C:*** *Chlorophyll.*

Date	Surface mixed layer (SML) (°C)			Thermocline (°C)			Deep Mixed Layer (°C)		
	Observed	Simulated	Difference	Observed	Simulated	Difference	Observed	Simulated	Difference
10/06/97	12.9	12.6	0.3	12.4	12.3	0.1	11.8	11.4	0.4
24/06/97	13.8	13.5	0.3	12.8	13.1	-0.3	11.9	11.7	0.2
10/07/97	15.7	17.9	-2.2	13.7	13.8	-0.1	12.4	12.3	0.1
11/07/97	15.8	17.0	-1.2	13.7	12.0	-1.7	12.4	12.3	0.1
29.07/97	17.8	17.2	0.6	15.6	16.3	-0.7	13.1	12.7	0.4
11/09/97	16.4	15.3	1.1	15.2	14.9	0.3	14.0	14.0	0.0
17/09/97	16.1	14.8	1.3	15.2	14.6	0.6	14.1	14.2	-0.1
23/09/97	15.5	14.8	0.7	15.5	14.6	0.9	15.5	14.4	0.9
Average	**13.8**	**13.7**	**0.1**	**12.7**	**12.4**	**0.5**	**11.7**	**11.4**	**0.3**

***Table 5.2** – Comparison between simulations and in-situ observations at E1 during 1997. **A:** Temperature.*

Date	Thermocline start (m)			Thermocline end (m)			Thermocline width (m)		
	Observed	Simulated	Difference	Observed	Simulated	Difference	Observed	Simulated	Difference
10/06/97	22	15	7	30	28	2	8	13	-5
24/06/97	18	8	10	27	27	0	9	9	0
10/07/97	8	2	6	30	21	9	22	19	3
11/07/97	10	3	7	32	20	12	22	17	5
29.07/97	10	4	6	32	15	17	22	11	11
11/09/97	20	10	10	30	30	0	10	20	10
17/09/97	18	10	8	23	33	10	5	23	-18
23/09/97	(0)	11	-	(72)	34	-	-	23	-
Average	**13**	**7**	**6**	**26**	**22**	**4**	**12**	**14**	**-2**

***Table 5.2** – Comparison between simulations and in-situ observations at E1 during 1997. **B:** Thermocline Depth.*

Date	Surface mixed layer (mg m^{-3})			Thermocline (mg m^{-3})			Deep Mixed Layer (mg m^{-3})		
	Observed	Simulated	Difference	Observed	Simulated	Difference	Observed	Simulated	Difference
10/06/97	0.8	2.2	-1.4	1.0	2.2	-1.2	0.4	1.2	-0.8
24/06/97	0.6	1.7	-1.1	1.0	1.8	-0.8	0.1	0.7	-0.6
10/07/97	0.3	1.1	-0.8	1.9	1.6	0.3	0.3	0.7	-0.4
11/07/97	0.2	1.0	-0.8	2.0	1.5	0.5	0.2	0.7	-0.5
29/07/97	0.1	0.5	-0.4	3.1	0.8	2.3	2.5	0.9	1.6
11/09/97	1.9	2.7	-0.8	1.7	2.1	-0.4	0.6	0.4	0.2
17/09/97	2.3	2.1	0.2	2.0	1.9	0.1	0.8	0.5	0.3
23/09/97	1.4	1.8	-0.4	1.4	1.7	-0.3	1.4	0.6	0.8
Average	**0.8**	**1.5**	**-0.7**	**1.6**	**1.5**	**0.1**	**0.7**	**0.6**	**0.1**

***Table 5.2** – Comparison between simulations and in-situ observations at E1 during 1997. **C:** Chlorophyll.*

Comparison of discrete SML temperature observations and have been discussed previously with respect to satellite SST measurements. The fit between simulations and field observations (table 5.1A) was similar to that of the SST data over the same period (average error 0.9°C compared with 0.8°C), but worse than the fit over the entire year (average error 0.5°C). The fit between thermocline and BML temperature simulations (average error 0.5°C) and field observations (average error 0.2°C) was better than for SML temperatures, which follows the trend of the their short time-scale variability.

Simulations of the minimum thermocline depth (table 5.2B) underestimated the observations for each sampling event, by a maximum of 10 m.. It is interesting to note

that the two shallowest predictions of the thermocline (2 an 3 m on 10th and 11th July) were associated with large overestimates of SML temperature (by up to 2.2°C). It is likely that the temperature of the SML was overestimated due to its unrealistically small volume. The depth of the base of the thermocline was also generally underestimated. Underestimates of both the minimum and maximum thermocline depths suggest that the model generally underestimated the strength of surface vertical mixing for times corresponding to the sampling events. Predictions of thermocline width produced a similar average value to the observations (table 5.2B). This finding is significant because it suggests that, assuming accurate temperature predictions, the average temperature gradient was, on average, predicted correctly. Compared with discrete observations, however, significant differences were apparent in the in the prediction of thermocline width (average error 7 m).

The chlorophyll simulation generally overestimated observed SML chlorophyll concentrations (table 5.2C). This feature of the model was noted earlier on comparison with the E1 archive data. Simulations of the thermocline and BML were, on average, more representative, although errors for individual sampling events were significant. The intensity of the thermocline chlorophyll maximum observed on 10th, 11th and 29th July was underestimated by the model.

Assessment of the performance of model simulations based on a small number of field measurements, as described above, has several significant limitations. The degree of small temporal scale variability, especially for the SML as shown in figures 5.9 and 5.10 means that the precise time used to match the simulation with the observation is crucial. Changes in this time within hours or days may provide very different values of simulation accuracy. In this context, it is of note that the meteorological fields were measured some distance from E1, and there is therefore some temporal error in the timing of the atmospheric forcing. A separate limitation concerns the sampling bias of the field measurements. These were made during the day time, and only when weather predictions were good. If the wind strength was more than ~10 m s^{-1} immediately preceding the sampling event, then it was cancelled. Details of the prevailing weather conditions for each event are described in appendix 6. The descriptions of model performance made above are only, therefore, representative of low wind day time conditions.

Temperature – SML Values for Two Months During 1997; Correlation of Simulations Vs AVHRR SST Observations.

To highlight the features temperature variability over temporal scales of less than 1 month, month long sections of the overall (1982 to 1997) simulations of SML temperature are presented (figure 5.11). The data are daily spot values from 00:00 GMT. Night time simulation values are used to facilitate comparison with the night time AVHRR SST observations. Maximum resolution (hourly) data for the same periods are presented later.

The variability for the summer month, (4th July to 3rd August, figure 5.11A), is similar to that observed in satellite SST observations, described in Chapter 3 (figure 3.15A). Against the background trend of increasing temperatures, periods of depressed temperatures occur which relate to windy, dull meteorological events. Conversely, periods of elevated temperatures relate to calm, bright periods. During the autumn month (27th September to 27th October, figure 5.11B), there was little small scale variability, and no observable response to meteorological conditions.

To measure the accuracy of the model predictions with respect to AVHRR SST observations, the difference between simultaneous SST observations and model predictions (+/- 30 min.) were calculated. These are presented in figure 5.11C. During the summer month, there were 3 time periods during which good AVHRR coverage was available; days 185 to 193, 199 to 204 and 209 to 213. During the first two of these, temperatures were increasing as the weather became brighter and calmer. For both periods, the simulations underestimated the observations when the water was cool, then overestimated the observations when the water was warm. It is clear, therefore, that the model overestimated the amplitude of the SML response to the meteorological events in both cases, by up to 3°C. The amplitude was overestimated to the greatest extent at S2, followed by L4, then at E1. This is reflected in the values of r^2, which was the smallest at S2 ($r^2 = 0.37$), but increased at L4 ($r^2 = 0.61$), and at E1 ($r^2 = 0.63$). During the winter month, SST observations were more evenly dispersed, but the lack of variability in either the observations or simulations resulted in low correlations between them, and produced no trends in the temperature residuals.

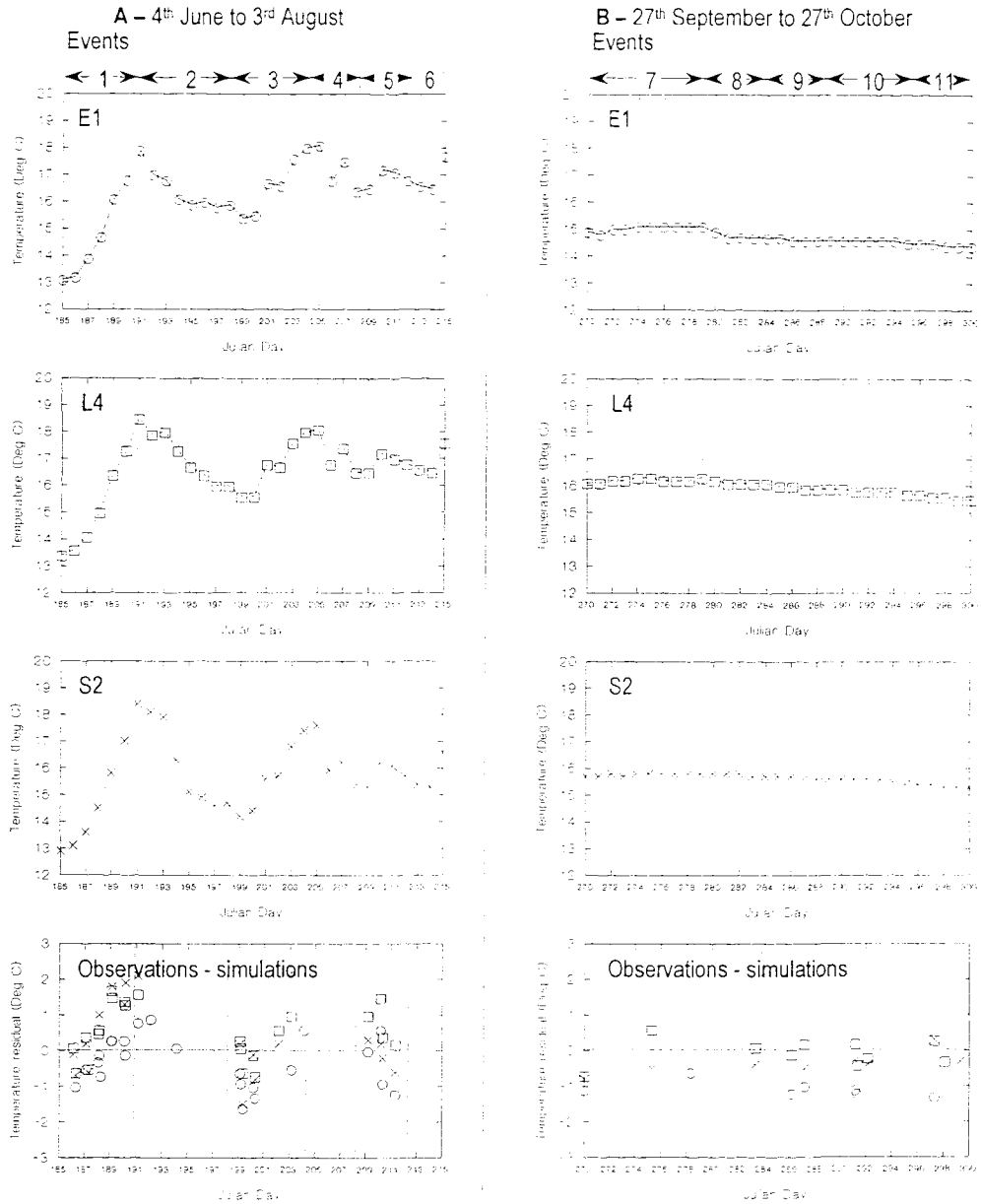

Figure 5.11 *– 30 day simulations of temperature at stations E1, L4 and S2. The model run was for 1997, and one output per day (00:00 GMT) has been plotted. The correlation between simulations and AVHRR SST data from 1997 produced r^2 values of 0.63 (n=23) for E1, 0.61 (n=21)for L4 and 0.37 (n=19) for S2. Corresponding differences between observations and simulations are also presented.*

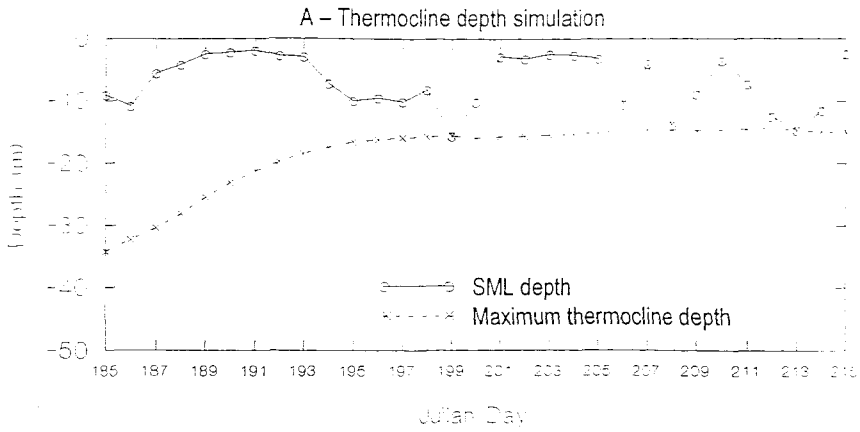

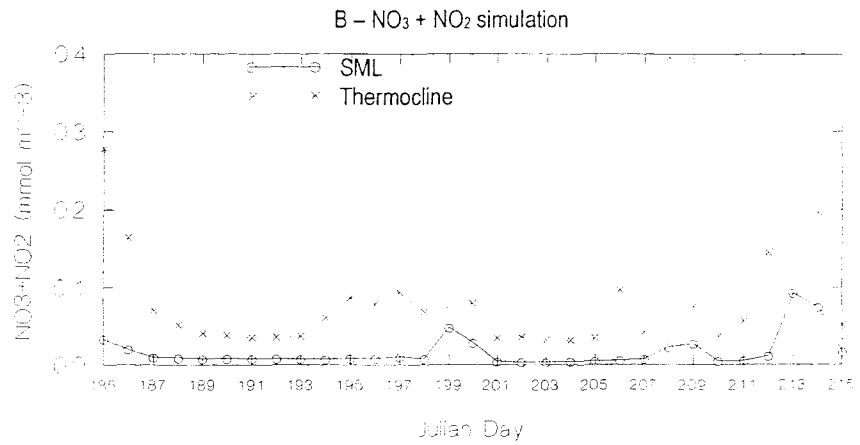

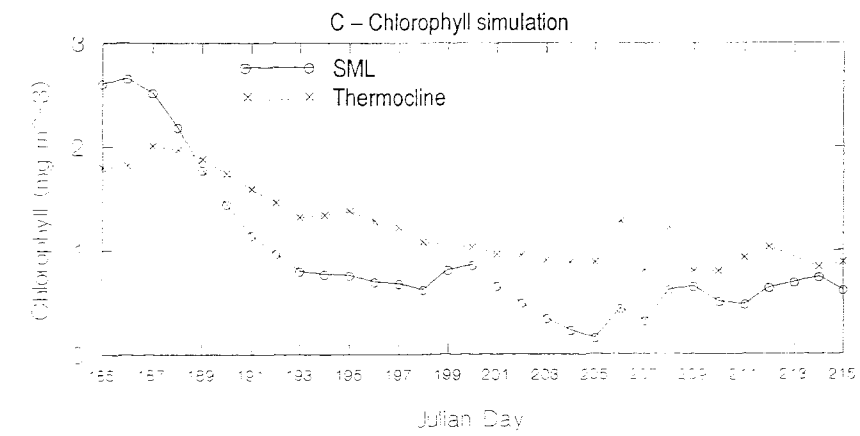

Figure 5.12 *- 30 day simulations at station E1 between 4th July and 3rd August 1997. One output per day (00:00 GMT) has been plotted.* ***A:*** *Thermocline depth.* ***B:*** *NO_3 + NO_2.* ***C:*** *Chlorophyll.*

Simulations of Thermocline Depth, Nutrient and Chlorophyll Response to Meteorological events.

The synoptic-scale atmospheric forcing which caused the observed and modelled changes in SML temperature described above, also affected the simulated thermocline depth, nutrient distribution and chlorophyll distribution (figure 5.12). During the dull, windy, cool periods, decreased surface potential energy due to increased wind speeds and decreased heat exchange caused the SML to deepen and the thermocline to thin. The depth of the base of the thermocline, however, was unaffected. As the potential energy increased due to lower wind speeds and increased heat flux, a shallow thermocline and broad thermocline were re-established. During two days of the month, day 199 and day 213, the thermocline has eroded entirely, and the water column consisted of two layers. This behaviour is typical of 3-layer bulk models, generally in simulations of shallow, tidally energetic waters (Ridderinkhof, 1992). In this case, however, a 2-layer water column is predicted at E1, in response to synoptic atmospheric forcing under conditions of strong thermal stratification.

The periods of decreased surface potential energy were associated with increased nutrient concentrations in the thermocline. As potential energy increased, the nutrients declined. A close inverse correlation can be observed between the width of the thermocline and its nutrient concentration (figure 5.12B). Note that thermocline values are missing on days 199 and 213 when the simulation returned a 2-layer water column. This suggests that the flux of nutrients into the thermocline was similar regardless of the surface potential energy, and that the elevated concentrations resulted from the fact that the volume within which they were distributed had decreased. Variability in nutrient concentration also occurred in the SML in response to the synoptic atmospheric forcing. The nutrient increases were most evident when the simulation returned a 2-layer water column, as direct exchange now occurred between the SML and BML. A significant increase also occurred on day 208, where the thermocline was very thin (~1 m) and displayed elevated nutrient concentrations. It appears that variability in the width of the thermocline has important implications for the supply of nutrients to the SML when the water column is strongly stratified.

The response of chlorophyll concentrations to synoptic atmospheric forcing is not as clear as for temperature, thermocline depths or nutrient concentrations. Due to the time taken for cells to build up to bloom concentrations, and to die following a bloom, the amplitude of mesoscale variability is damped. Mesoscale variability can also be strongly masked by the underlying seasonal signal. Both these features are displayed on the simulation of chlorophyll distribution shown in figure 5.12C. The high concentrations,

which are rapidly decreasing until about day 193, are associated with the decay of a larger bloom which peaked on day 183 (see figure 5.10C). Between day 193 and day 198, chlorophyll concentrations in both the SML and thermocline were fairly steady at concentrations of ~0.8 and ~1.2 mg m^{-3} respectively. These significant concentrations must have been sustained by a background rate of nutrient supply, probably due to regeneration following the bloom. Whilst chlorophyll concentrations in the thermocline did not increase as a result of the elevated nutrient concentrations between days 193 and 201, those in the SML did respond to elevated nutrients between days 198 and 201. Over the 5 following days, SML chlorophyll declined gradually to a yearly low of 0.2 mg m^{-3} on day 205. SML chlorophyll concentrations recovered to ~0.5 mg m^{-3} during the next period of low potential energy. The model predicts that chlorophyll concentrations do respond to synoptic atmospheric forcing, but the precise response is not always clear. For studying mesoscale variability, it may be more revealing to simulate rate variables such as nutrient fluxes or net primary productivity rather than the integrated properties such as nutrient and chlorophyll concentration.

5.5 Simulations of Intra-Daily Variability

The model time step in current configuration is 1 hour. When this full resolution data is plotted for the months corresponding to those described above, clear diurnal patterns are observed in SML temperature distribution, as shown in figure 5.13 (for the PlyMBODy site). The amplitude of the diurnal variability was greater for the 4th July to 3rd August period than the 27th September to 27th October period (maximum of 2.5°C and 0.6°C respectively). Diurnal temperature variations of >1°C amplitude have previously been both observed and simulated for the open ocean (Large et al, 1994). The higher maximum amplitude simulated for July/August 1997 can be justified as shelf sea

SMLs are generally thinner than oceanic SMLs, and therefor more prone to changes in heating due to their lower total heat capacity. This theory also explains the differences in amplitude between the July/August and September/October periods.

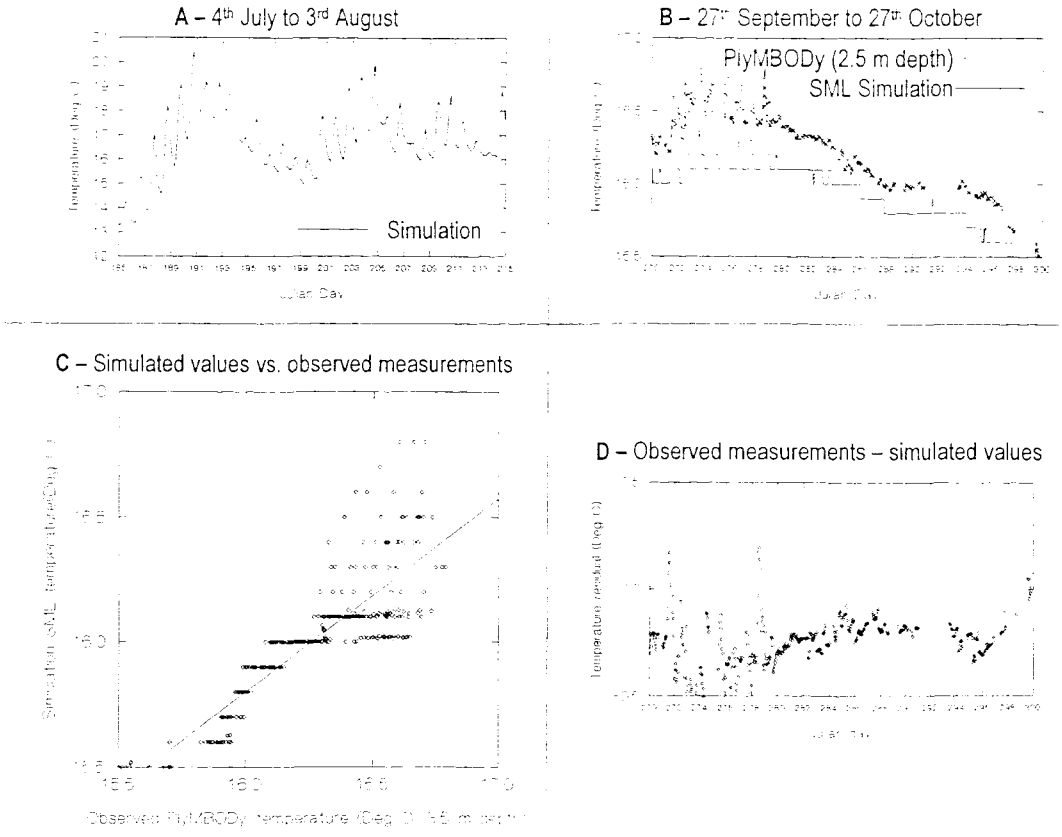

Figure 5.13 *- 30 day simulations of SML temperature for the PlyMBODy site. The model run was for 1997, and 24 outputs per day (hourly) have been plotted.*

A *- 4th July to 3rd August*

B *- 27th September to 27th October (with hourly mean PlyMBODy temperature measurements overlaid)*

C *–Simulated SML temperature vs. hourly mean PlyMBODy temperature (at ~3.5 m depth) from27th September to 27th October 1997. Resulting r^2 = 0.81 (n=279).*

D *–Difference of PlyMBODy measurements and simulated values.*

It is interesting to note that, during June/July 1997, the amplitude of the diurnal variability was altered depending on the phase of the synoptic variability (figure 5.13A). The warming phase of the synoptic variability was associated with clear skies (see figure 3.3, Chapter 3), leading to large diurnal variations in air temperature, therefore large variations in SML temperature. Conversely, during the cooling phase, skies tended to be cloudy, minimising the diurnal temperature difference. There was also differences in mixed layer depth associated with the synoptic variability (see figure 5.12), which would also affect the diurnal variability.

The plots in figure 5.13 are from simulations at the PlyMBODy site. Fortunately, the temperature record for the autumn month is fairly complete for this period. There are no corresponding measurements, however, for the summer month. Whilst AVHRR SST measurements are night time only, and cannot be made under cloudy conditions, the

PlyMBODy measurements are made at regular (~10 min.) intervals. The PlyMBODy system is also more accurate and sensitive than AVHRR. The advantages provided by PlyMBODy are demonstrated by the plot of simulated values vs. PlyMBODy observations, as shown in figure 5.13C. Whilst the comparison of simulations over the same period with AVHRR SST indicated insignificant correlations, the comparison with PlyMBODy data produced a significant correlation with an r^2 of 0.81.

During the start of the autumn month, diurnal fluctuations in the simulation of SML temperature were present. The fluctuations were also apparent in the PlyMBODy data. An analysis of the temperature residuals (figure 5.13D), suggests that the model overestimated the amplitude of the diurnal variability, which is a characteristic explored in more detail later. Following day 280, however, the fluctuations in both the simulation and observations suddenly became negligible. This is an indication that the water column was stratified prior to this point, and that stratification broke down immediately afterwards, as confirmed by figure 5.12A. If the amplitude of diurnal temperature variability is used as an indicator of stratification, then it is likely that there was less stratification on days 270 and 271, a point that is also confirmed by figure 5.12A.

3-Day Simulations of SML Temperature and Chlorophyll at the PlyMBODy Site

In Chapter 4, two, 3-day periods of buoy data were presented, highlighting variability at the PlyMBODy site in response to tidal advection (figure 4.10) and diurnal heating (figure 4.11). Model simulations corresponding to these periods are presented in figure 5.14.

During the first period (8th August to 11th August), it was suggested that tidal advection was responsible for most of the intra-daily variability (+/- 1.5°C) of temperature. The model simulation, however, predicts that there would have been a great deal of variability caused by diurnal heating effects (+/- 1°C). The observations were characterised by temperature minima at ~07:00 GMT and ~20:00 GMT, corresponding to maximum extent of the ebb tide. From the model simulation, 07:00 GMT falls within the night time temperature depression, whilst 20:00 GMT falls within the day time elevation. One would expect, therefore, the 07:00 GMT tidal signal to be reinforced, whilst the 07:00 GMT signal would be diminished. This theory appears to be reflected, to some extent, by the observations.

The correlation between the simulation and the observations for the August period is low (figure 5.14C, r^2=0.32). This is explained by the fact that model is not designed to simulate the advective effects which dominated the temperature variability during this period. This is highlighted by the simulation error plot (figure 5.14D), as positive temperature residuals coincide with tidally induced temperature depressions (at 07:00 and 18:00 GMT). It was indicated earlier, however, that the model appeared to overestimate the amplitude of diurnal temperature variability under stratified conditions. It is likely that this is the case here also, as the temperature residuals were generally negative during the night, and positive during the day. Due to the interference of the tidal signal, however, the magnitude of the overestimate cannot easily be determined.

The second period, 25th to 28th September, the pattern of variability in the PlyMBODy temperature data did not appear to be influenced to a significant extent by tidal advection (see Chapter 4, and figure 4.11). The temperature variability due to diurnal heating was, however, clearly apparent (+/- 0.1°C). The corresponding simulation is presented in figure 5.14B. Under these conditions, the simulated variability was an order of magnitude less than that predicted for the highly stratified conditions during August. Although the amplitude of variability approached the limits of model sensitivity, a relatively good correlation was obtained against the observations (r^2=0.68).

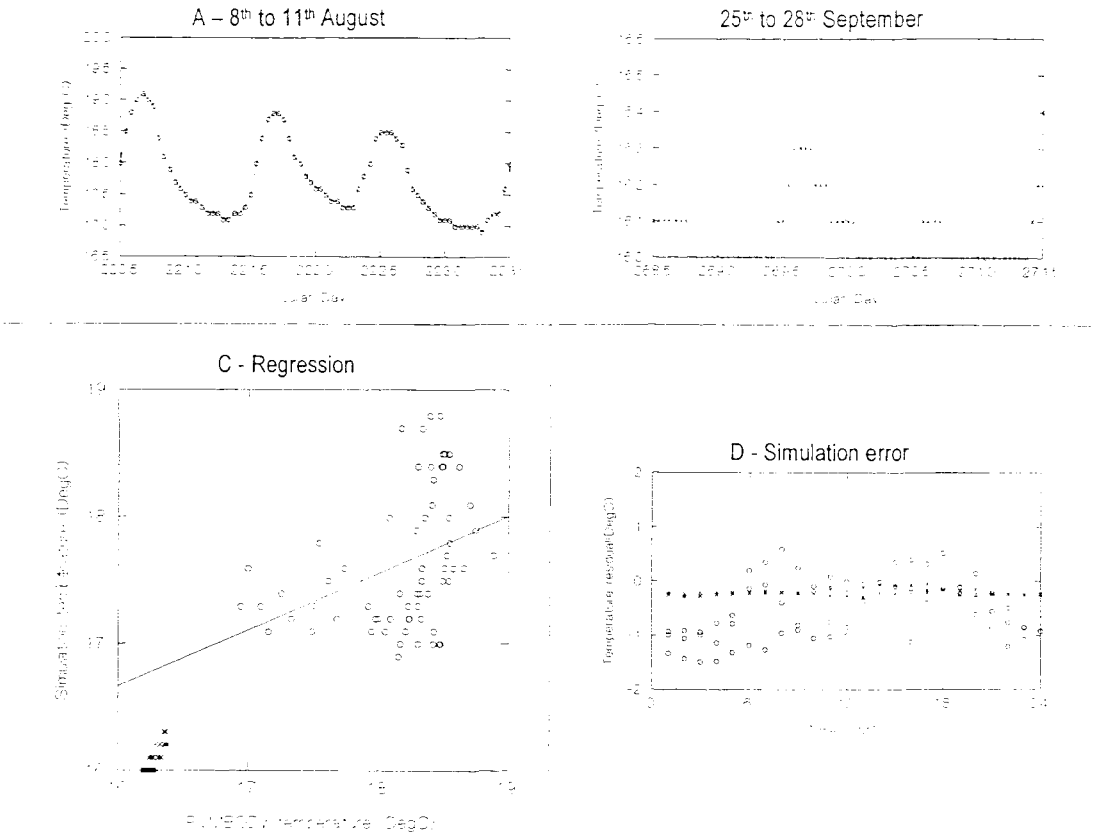

Figure 5.14 *– 3-day simulations of temperature at the PlyMBODy site. The model run was for 1997, and 24 outputs per day (hourly) have been plotted.*
A: *8th to 11th August.* ***B:*** *25th to 28th September.*
C: *Simulated SML temperature vs. observed PlyMBODy temperature (at ~3.5 m depth).*
D: *Difference of PlyMBODy measurements and simulated values.*

Observations of diurnal chlorophyll concentration at PlyMBODy were described in Chapter 4 (see figure 4.10 & 4.11). Between 8th and 11th August, the chlorophyll distribution was characterised by maximum chlorophyll concentrations at the maximum extent of the ebb tide, and vice versa. The comparison between simulated and observed chlorophyll over this period (not plotted) returned a low value of r^2 ($r^2 = 0.12$). The failure of the model to simulate the chlorophyll observations can be used as evidence that advection was the most significant factor controlling the distribution. (as suggested in Chapter 4). This assertion relies on the assumption that the model provided a realistic simulation of the vertical processes controlling chlorophyll concentration over this period, which has not been determined.

For the period between 25th and 28th September, it was suggested (in Chapter 4) that the diurnal variability of chlorophyll concentrations were due to photochemical quenching of fluorescence response, which is related to ambient light levels (Prezlin & Ley, 1980). This explanation is supported by the failure of the model to predict the observed variability (the correlation resulted in a negative relationship), as the model takes no account of such sensor inaccuracies. This assertion again relies on the assumption that the model provided a realistic simulation of the vertical processes

The predicted and observed diurnal cycle of SML temperature suggests that variability in atmospheric forcing over a 24-hr. period can significantly alter water column temperature structure. A simulation of thermocline depth over the period from 8th to 11th August is presented in figure 5.15A. SML depth increases during the day time, and decreases at night. The amplitude of the variation ranged from 3 m (days 220/221, and 221/222) to 7 m (day 222/223). The increased amplitude on day 222/223 is due to decreases in surface potential energy caused by higher wind speeds (up to 12 m s^{-1}) between 12:00 and 20:00 GMT on day 222 (see figure 3.4). Variability in synoptic atmospheric forcing rather than the diurnal cycle of heating therefore caused the apparent increase in amplitude on this date. The cycle of SML depth was not symmetrical, it decreased gradually throughout the night, but increased rapidly at dawn.

The diurnal mixing effect caused a slight but appreciable response in both the nutrient and chlorophyll concentrations as shown in figures 5.15B & C.. On days 220/221 and 221/222, the nutrient concentration in the thermocline increased throughout the night from a minimum of 0.02 mg m^{-3} at 17:00 GMT to a maximum of 0.05 mg m^{-3} at 07:00 GMT. SML nutrient concentrations remained constant at 0.02 mg m^{-3} throughout. The largest increase in thermocline nutrient concentration (to 0.15 mg m^{-3}) occurred on day 222/223, where the width of the thermocline decreased due to the wind mixing described earlier.

Thermocline chlorophyll concentrations (figure 5.15C) were more than double those of the SML (>0.8 mg m^{-3} compared with <0.4 mg m^{-3}). On days 220/221 and 221/222, thermocline concentrations increased from ~10:00 GMT, and throughout the rest of the day and the following night, presumably in response to the elevated nutrient concentrations. At about 07:00 GMT, however, the sudden decrease in SML depth mixed low chlorophyll water from the thermocline, decreasing average thermocline concentrations. The amplitude of the diurnal cycle of chlorophyll was small, at ~0.1 to 0.2 mg m^{-3}. SML chlorophyll concentrations did not vary significantly with the diurnal cycle. This result is different to that obtained by Taylor & Stephens (1993), who simulated a diurnal cycle of chlorophyll variability with amplitude of up to 0.5 mg m^{-3}.

This model, however, was only 1-layer, and therefore could not simulate the apparent buffering effect of the thermocline layer apparent in figure 5.15A.

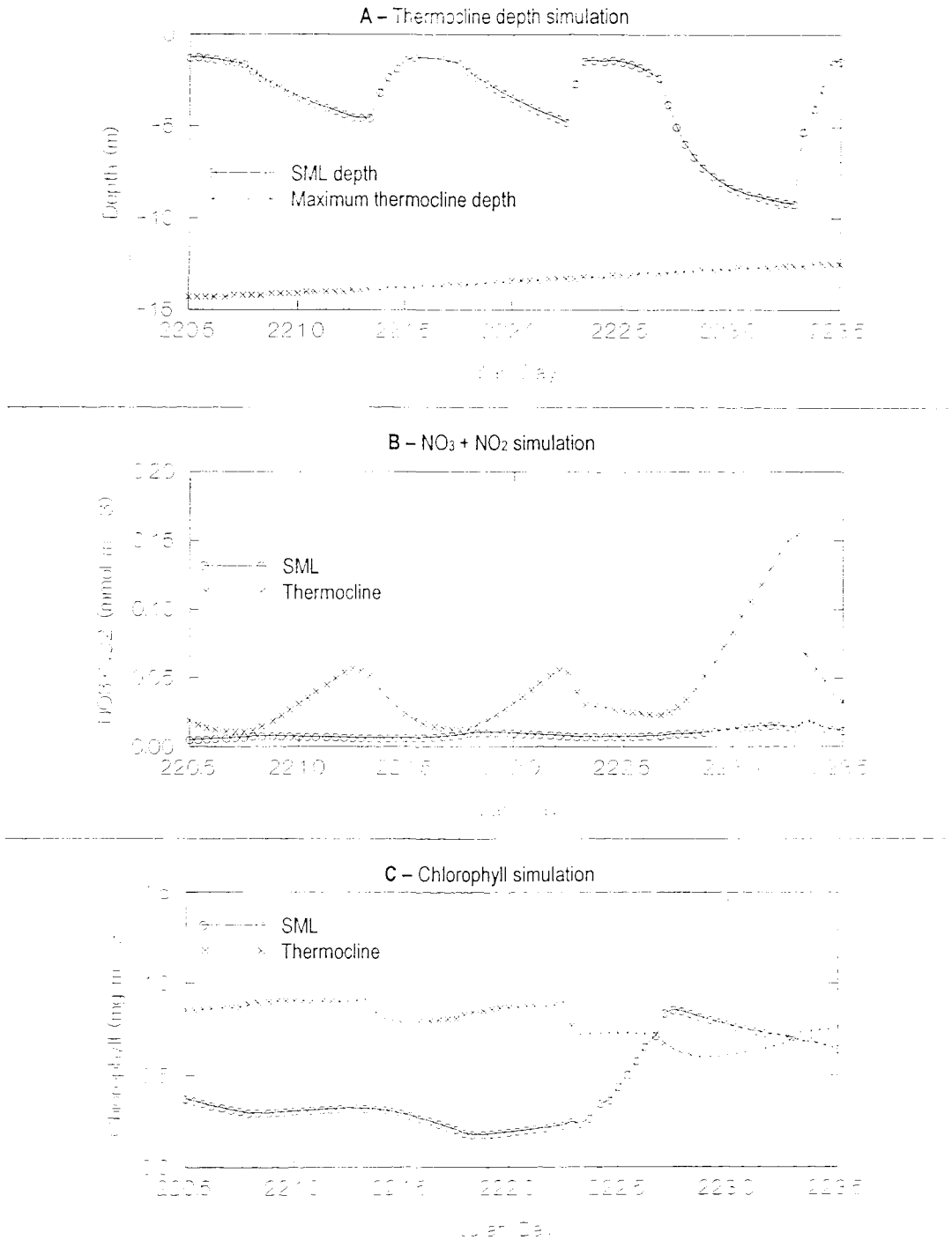

Figure 5.15 *- 3 day simulations at station E1 between 8th August to 11th August 1997. The model run was for 1997, and 24 outputs per day (hourly) have been plotted.*
A: *Thermocline Depth.* ***B:*** *$NO_3 + NO_2$.* ***C:*** *Chlorophyll*

5.6 Simulations of Horizontal Variability

SML Temperature – Comparison with Satellite SST

In Chapter 3, SST distributions along the E1 to L4 and E1 to S2 transects were presented from several images collected during 1997 (see figures 3.17 to 3.22). These observations were simulated by running the model for a number of positions along each transect. The characteristics of each point are shown in table 5.3. The simulations are presented in figure 5.16.

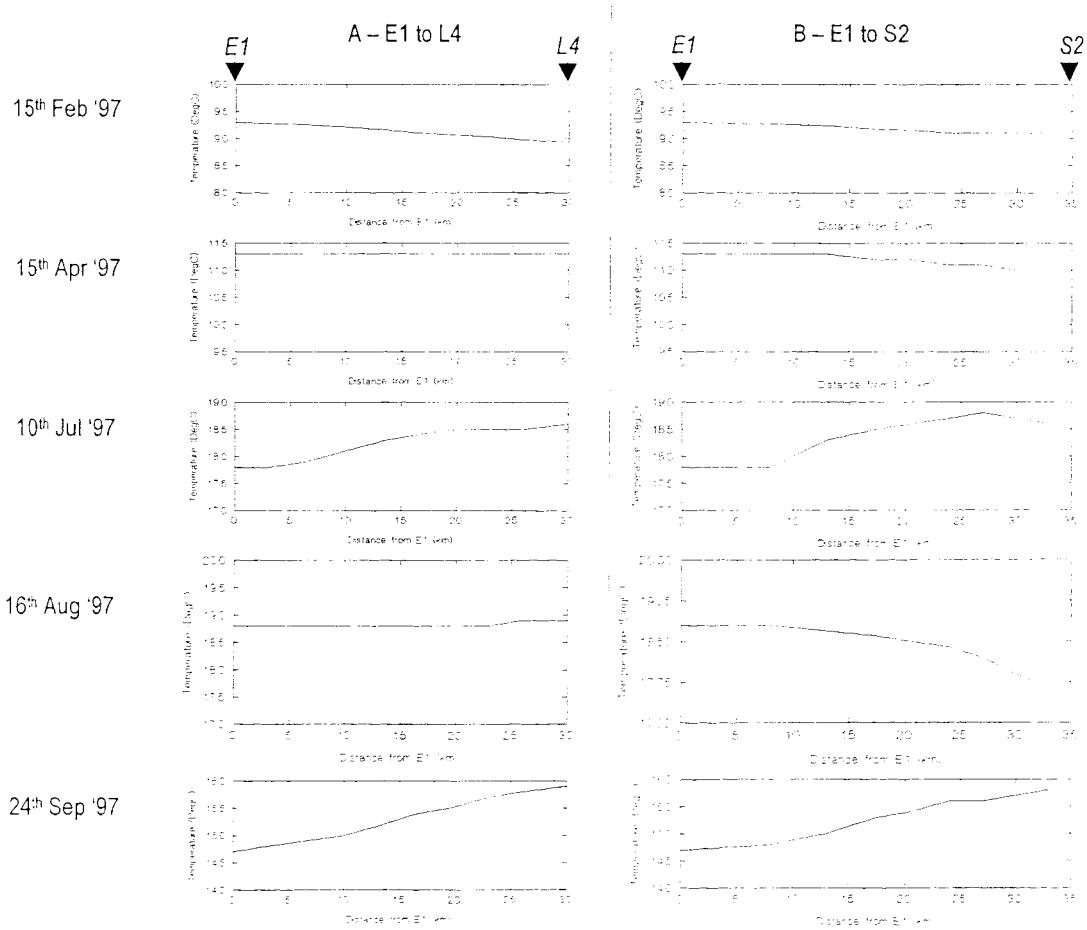

Figure 5.16 *- Simulations of SML temperature along the transects on 5 occasions during 1997.*
A: *The E1 to L4 transect..* ***B:*** *The E1 to S2 transect..*

E1 to L4			E1 to S2		
Distance from E1 (km)	Water Depth (m)	Tidal current (mm s^{-2})	Distance from E1 (km)	Water Depth (m)	Tidal current (m s^{-2})
0 (E1)	72	271	0 (E1)	72	271
2.5	71	266	8.0	70	275
5.5	69	260	12.0	68	282
8.5	66	254	17.5	64	292
11.5	63	247	20.5	63	302
14.0	60	240	24.0	60	311
16.5	58	232	27.0	60	327
19.5	56	224	29.5	60	342
22.0	54	215	31.5	60	356
25.5	52	206	33.0 (S2)	60	369
28.5 (L4)	50	196			

***Table 5.3** – Water depth and tidal current at points along the E1 to L4 and E1 to S2 transect.*

The simulation for the 15th January shows the temperature distribution that is expected if vertical processes alone control the temperature distribution. As the water column had shown little evidence of stratification by this date (see figure 5.16), the SML temperature distribution was inversely related to depth along each transect, reflecting the total heat capacity of the water column. Temperatures therefore fell with distance along both the E1 to L4 transect (by ~1°C) and the E1 to S2 transect (by ~0.5°C). The SST observations on 15th February showed a far larger decrease (of ~1.8°C) over both the transects. The reason that the model did not simulate the magnitude of the observed temperature gradients was that advective processes were significant during this period (as discussed in Chapter 3), but were not included in the model..

On 15th April 1997, the simulations indicated a very uniform temperature distribution along both the E1 to L4 transect, and a reduction of temperature by 1°C along the E1 to S2 transect. An analysis of the simulated water column structure for the transects indicated that a degree of thermal stratification was present, with a SML-BML temperature difference of 1.3°C at E1 and L4, and 0.8°C at S2. Following the onset of stratification, horizontal temperature distribution was controlled by vertical mixing in addition to heat flux. Along the E1 to L4 transect, the tendency for vertical mixing to increase in response to shallower depths was countered by the tendency for vertical mixing to decrease in response to lower tides (see figure 5.16). The degree of stratification was therefore horizontally similar. Along the E1 to S2 transect, however, the reduction in depth and increase in tide tend to increase vertical mixing, reducing the stratification and causing the temperatures to fall. The SST observations for 15th April 1997 described in Chapter 3 also show a 0.8°C temperature reduction along the E1 to S2 transect, which, as explained above, is likely to have resulted from a reduction in stratification. SS along the E1 to L4 transect fell by ~0.4°C, suggesting a lower reduction in stratification.

On 10th July, the simulation predicted an unexpected distribution of SML temperature along the E1 to S2 transect (figure 5.16). Between E1 and a distance of 27 km from E1, temperatures rose from 17.8 to 18.8°C. The temperature then fell to 18.5°C at S2. If the stratification parameter (S) is taken as an index of tidal mixing, then mixing increases between E1 and S2 (see figure 3.9). On 10th July 1997, at a distance of 27 km from E1, there was a threshold of mixing (S~1.9) responsible for the highest SML temperature. At S<1.9, increased mixing of water from below reduced the surface temperature. This positive relationship between S and SST is the one expected for shelf seas (e.g. Pingree, 1980). At values of S>1.9 the water depth increased, and the tides decreased, allowing the width of the thermocline to increase (from 5 m to 20 m). As the width of the thermocline increased, the strength of the temperature gradient across it decreased. The decreased gradient allowed a greater exchange of water between the thermocline and SML, producing the simulated decrease in temperature.

The corresponding SST observations over the E1 to S2 transect on 10th July (see figure 3.19) show that temperatures along the E1 to S2 transect were fairly constant until ~30km from E1, whereupon they started to fall. The observations and simulation agree with respect to the reduction of temperature at the end of the transect, but the temperature distributions differ before this point. Observations were collected on the same date (10th July) using the UOR. These showed that the depth of the base of the thermocline did reduce with distance along the E1 to S2 transect (the first 15 km is presented in figure 4.9). No change in thermocline temperature gradient was observed, however, as the depth of the top of the thermocline was reduced simultaneously. As the temperature gradient did not change, the surface mixing and therefore the SML temperatures remained constant.

The simulation along the E1 to L4 transect on 10th July also showed an SML temperature increase with distance (figure 5.16A). Analysis of the simulated thermocline depth for the transect again showed that the depth of the base of the thermocline reduced with distance, and was therefore responsible for the temperature increase. As the values of tidal current decrease with distance along the transect, thermocline depths must have been shallowing due to the decrease in water depth.

On 16th August, the simulated temperature distributions along the E1 to S2 transect had reversed (figure 5.16),. The simulation was now similar to the observed distribution of SST described in Chapter 3, and consistent with the theory that increased vertical mixing reduce SML temperatures. The average wind strength over the four days preceding 10th July and 16th August was similar (5 m s^{-1}), but the downwelling solar irradiance was different (300 W m^{-2} and 210 W m^{-2} respectively). The difference in

irradiance caused a difference in surface potential energy between the two dates, with 10th July higher than 16th August. This increase in potential energy caused the relationship between SML temperature and S to change from positive to negative. It should be noted that the simulated SML temperature distribution for 16th August was far more typical than the simulation for 10th July throughout the stratified period of 1997. S2 temperatures only exceeded those of E1 on four days, 10th to 13th June.

The simulation for the E1 to L4 transect on 16th August produced a fairly homogenous horizontal distribution of SML temperature. The SST observations, however, showed that SST decreased by over 2°C. The model calculates tidal mixing on a similar basis to calculations of S (i.e. h/u^3). It was shown in Chapters 3 and 4 that the degree of mixing indicated by the calculated values of S are underestimates due to the influence of the Eddystone Rocks. It is reasonable, therefore, that the failure of the model to simulate the SST distribution on 16th August result from errors in the calculation of tidal mixing.

The simulations for both transects on the 24th September reflect the overall heat balance of the simulated water column after stratification had broken in the Autumn. The differences in between the simulated and observed (see figure 3.21) distribution reflect either, inaccuracies in the simulations during the stratified period, or advective effects which are likely to be significant in the study region on this date period.

Simulations of Early Summer Conditions (10th June 1997)

Observations of temperature and chlorophyll structure along the E1 to L4 and E1 to S2 transects on for a variety of sampling events during 1997 were described in detail in Chapter 4. By simulating the water column at several points along each transect (see table 5.3), a number of the observed fields could be reproduced. The include; SML depth, maximum thermocline depth, SML, thermocline and BML temperature, SML, thermocline and BML chlorophyll. The simulations for each field are presented individually.

Due to the number of fields being compared, and the number of sampling events considered, it is not appropriate here to produce detailed a detailed numerical analysis of model performance on each occasion, as provided earlier. Instead, the comparisons will be qualitative, highlighting the features of the observed horizontal distribution that the model appeared to simulate adequately, and those that it did not. As the model simulations for each point along the transects provided an inherently temporal simulation, it is difficult to de-couple the processes causing the horizontal variability. This point is especially pertinent where the model failed to simulate the observed

distributions, as past errors in the modelling the salient processes will be manifest in any current simulation even if the processes are now modelled correctly.

The first sampling event presented in Chapter 4 was from 10th June 1997. The observed data (figure 4.2) is showed that a tidal front occurred along the E1 to S2 transect, as a result of progressively stronger tidal mixing eventually overcoming thermal stratification. The stratification along the E1 to L4 transect also diminished with distance from E1, but never broke down entirely. The simulation of this event (figure 5.17) correctly predicted the presence of a tidal front along the E1 to S2 transect, and the lessening of stratification along the E1 to L4 transect. Over both transects, the predicted location and width of the mixed layer was correct. The simulation also correctly predicted the reduction in BML temperature with distance, and the horizontal variation in temperature difference across the thermocline. The correct prediction of both the width of the thermocline and the temperature difference across it indicates that the prediction of the thermocline temperature gradient was accurate.

The model failed, however, in several respects. The predicted location of the tidal front was too far from E1 by ~8 km.. Furthermore, the thermocline to the stratified side of the front decreased in width until a 2-layer water column resulted, instead of widening and becoming bifurcated as suggested by the observations. The simulation of a narrow thermocline under conditions of low thermal stratification, represented as a 2-layer system, is a characteristic of 3-layer bulk models that has been noted previously (Ridderinkhof, 1992). The model did not reproduce the strong

horizontal SML temperature gradient, indeed the simulated gradient was negligible. The spacing between the model points, and the horizontal resolution of the input data (water depth and tidal speed) ensured that the model was not able to reproduce the type of small scale horizontal variability that was observed along the E1 to L4 transect, in the vicinity of the Eddystone Rocks.

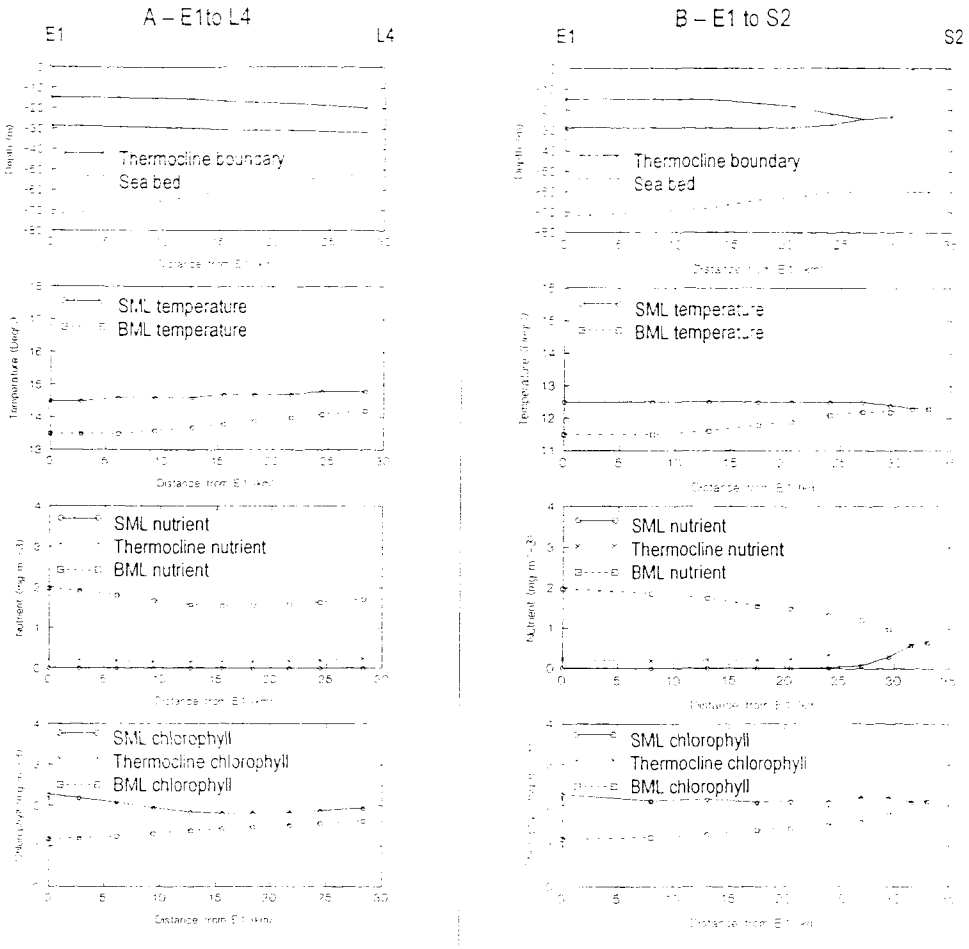

Figure 5.17 *- Simulations of thermocline depth, temperature, nutrient and chlorophyll along the transects on 10th June 1997.* ***A:*** *The E1 to L4 transect.* ***B:*** *The E1 to S2 transect.*

As described in Chapter 4, the tidal front on 10th July was not characterised by well defined horizontal chlorophyll gradients. Similarly, the model simulation for the E1 to S2 transect returned low horizontal variability. The simulated vertical distribution at E1 correctly predicted that SML and thermocline chlorophyll concentrations were approx. twice the BML level, but the absolute concentrations for the simulation were higher than those observed. The model also failed to predict the slight increases in concentration towards the end of each transect, with the concentrations over the E1 to L4 simulation undergoing a decline with distance.

Simulations of Mid Summer Conditions (29th July 1997)

The observations on 29th July represented a highly stratified water column with little horizontal variability in hydrographic structure (Chapter 4, figure 4.5). The depths of the thermocline decreased slightly with distance along each transect, and the cross-thermocline temperature difference reduced, indicating increased mixing from the bottom. The SML temperature plotted on the water column summary plot was inaccurate due to the failure of the UOR to sample this layer. The model simulation for this event is presented in figure 5.18. The simulation of the E1 to S2 did predict a decrease in thermocline depth, but its magnitude was insufficient (4 m over the transect, compared with the observed 8 m decrease). The width of the thermocline, although constant horizontally (~10 m) was adequately reproduced for both the E1 to S2 and the E1 to L4 transects.

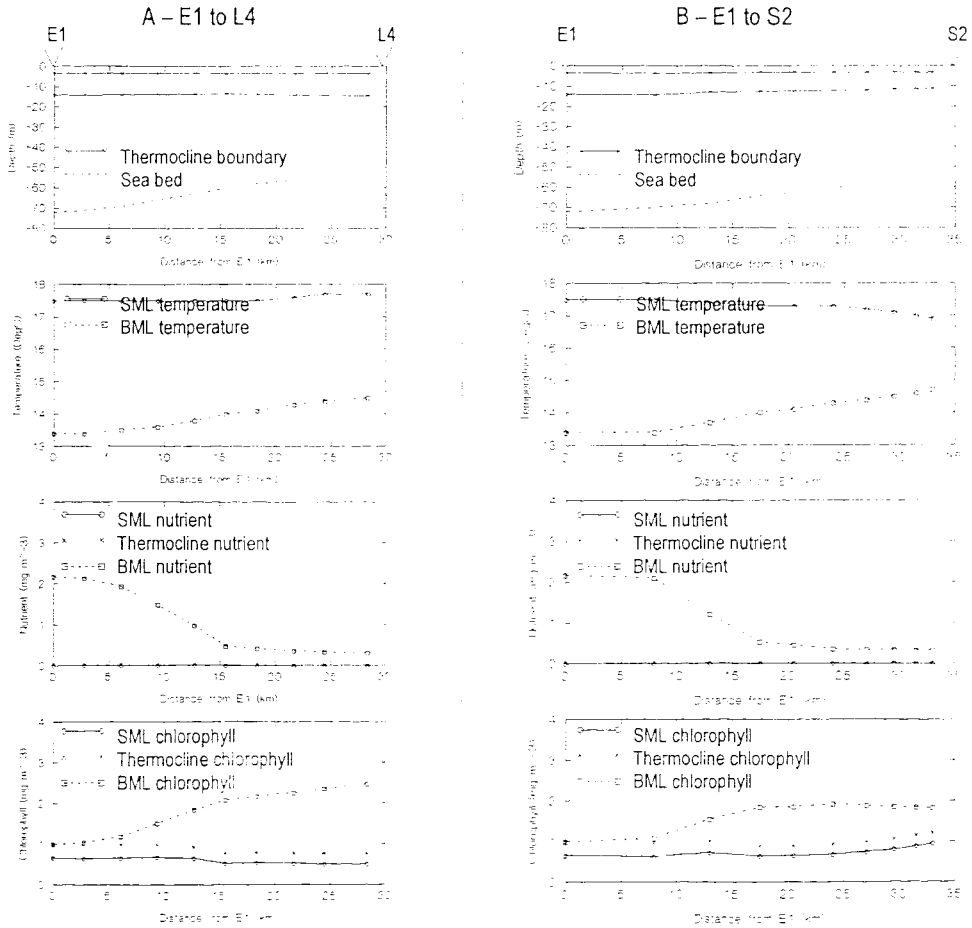

Figure 5.18 *- Simulations of thermocline depth, temperature, nutrient and chlorophyll along the transects on 29th July 1997. A: The E1 to L4 transect. B: The E1 to S2 transect.*

The model correctly simulated the increase in BML temperature with distance from E1, but it is difficult to assess whether the simulation of SML temperature was realistic, as the observations were inadequate. It is likely that the decrease in SML temperature along the E1 to S2 transect was correct, but the increase along the E1 to L4 transect appears erroneous, even allowing for inaccuracies in the observations. The model failed to provide a realistic simulation of the mixed layer depth, which was too shallow, especially at E1 (4 m compared with the observed 12 m). An analysis of whether the thermocline was still too shallow at S2 is not possible due to the limitations of the observations.

The chlorophyll observations made during the sampling event indicated that BML concentrations were higher than SML concentrations. The simulations reproduce this feature but, on analysis of the nutrient distributions, it appears that the model predicted a substantial amount of in-situ productivity within the BML. This theory is indicated by the increasing BML concentrations with decreasing depth, and therefore higher light levels. Another indication is the reduction of nutrients that corresponds with increased BML chlorophyll concentration. In reality, he elevated BML concentrations result from the sinking of phytoplankton cells from the pronounced thermocline chlorophyll bloom. The model simulates some enhancement of thermocline chlorophyll concentrations, but they do not reach the level indicated by the observations (1 mg m^{-3} compared with 4 mg m^{-3}). It is the lack of attenuation by chlorophyll in the thermocline that lets sufficient light penetrate the BML for substantial in-situ productivity to occur in the BML.

Simulations of Early Autumn Conditions (11th September 1997)

The observations on 11th September indicated the reappearance of the tidal front along the E1 to S2 transect, with an associated SML bloom of phytoplankton to the stratified side. Again there was clear evidence of increased tidal mixing with distance along both transects (Chapter 4, figure 4.6). The model simulations of this event are presented in figure 5.19. The model correctly simulated the presence of the tidal front, and also decreased thermocline depths, and increased BML temperatures consistent with increased mixing from the bottom. The simulation failed, however, by predicting a 2-layer water column for water columns with low stratification, and did not predict a cross frontal temperature gradient, both of which were inaccuracies described for the front on 10th June. The predicted SML depth was also too shallow, which appears to be a general feature of many of the simulations.

The simulation of horizontal SML chlorophyll did not predict the bloom at the front. Thermocline depth and nutrient simulations suggested that sufficient stability and

elevated nutrients existed at the front, so it is unclear why a bloom did not result. The model did, however, correctly predict that SML chlorophyll concentration was higher than BML and thermocline concentrations when stratification was well established, and that concentrations were lower to well mixed side of the front.

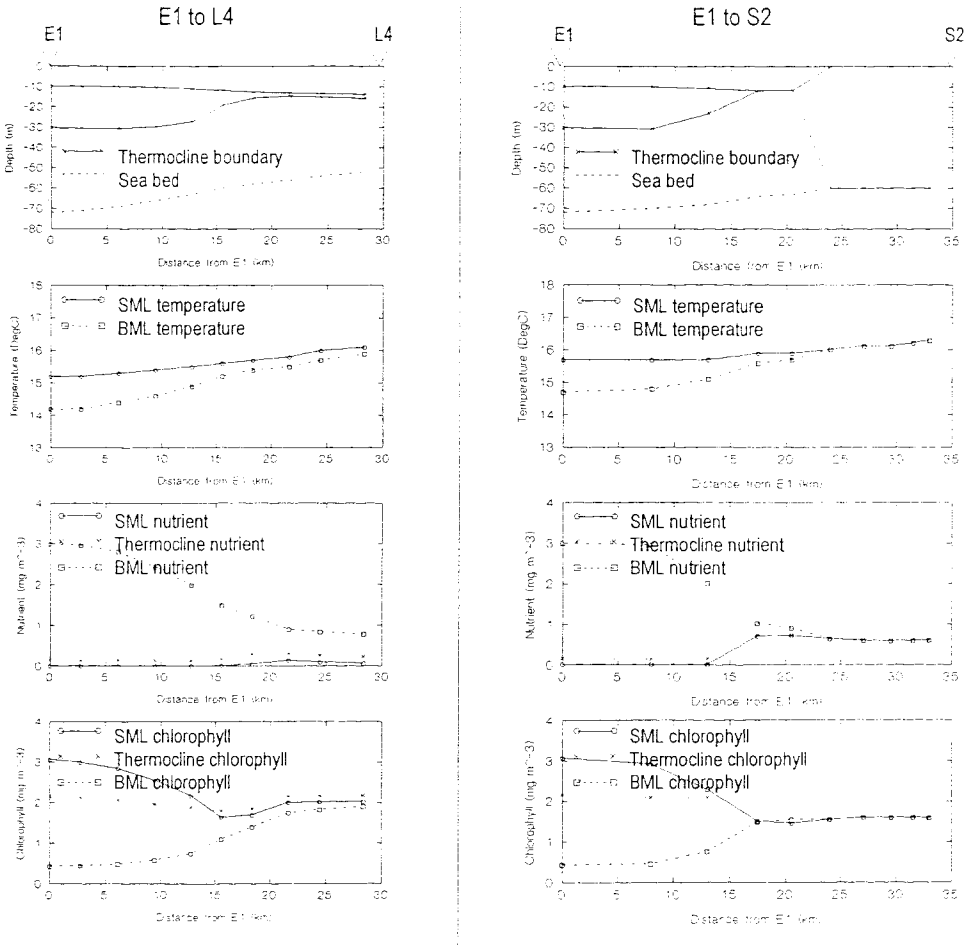

Figure 5.19 *- Simulations of thermocline depth, temperature, nutrient and chlorophyll along the transects on 11th September 1997.* ***A:*** *The E1 to L4 transect.* ***B:*** *The E1 to S2 transect.*

Simulations of Late Autumn Conditions (23rd September 1997)

The observations for 23rd September showed that the stratification had broken down over both of the transects (Chapter 4, figure 4.8). The model simulations for this event are presented as figure 5.20. The model also predicted a breakdown of stratification except close to E1, where the stratification was weak. The temperature simulation was accurate in terms of horizontal variability over both transects, reflecting the overall heat balance of the water column immediately following stratification breakdown.

The horizontal variation in the chlorophyll simulation is dominated by the transition from stratified to well mixed waters. As the prediction of stratification was unrealistic, the simulations of chlorophyll concentration also fail against the observations. If one considers only the well-mixed section of the simulation, the model predicts that in-situ production is taking place, indicated by the negative relationship between chlorophyll and nutrient concentration. The in-situ productivity appears to be light limited, as chlorophyll increases and nutrients decrease with depth along both transects. As the simulation had not predicted the phytoplankton bloom at the tidal front on 11th September, the elevated chlorophyll concentrations in this region following the breakdown of stratification were not reproduced.

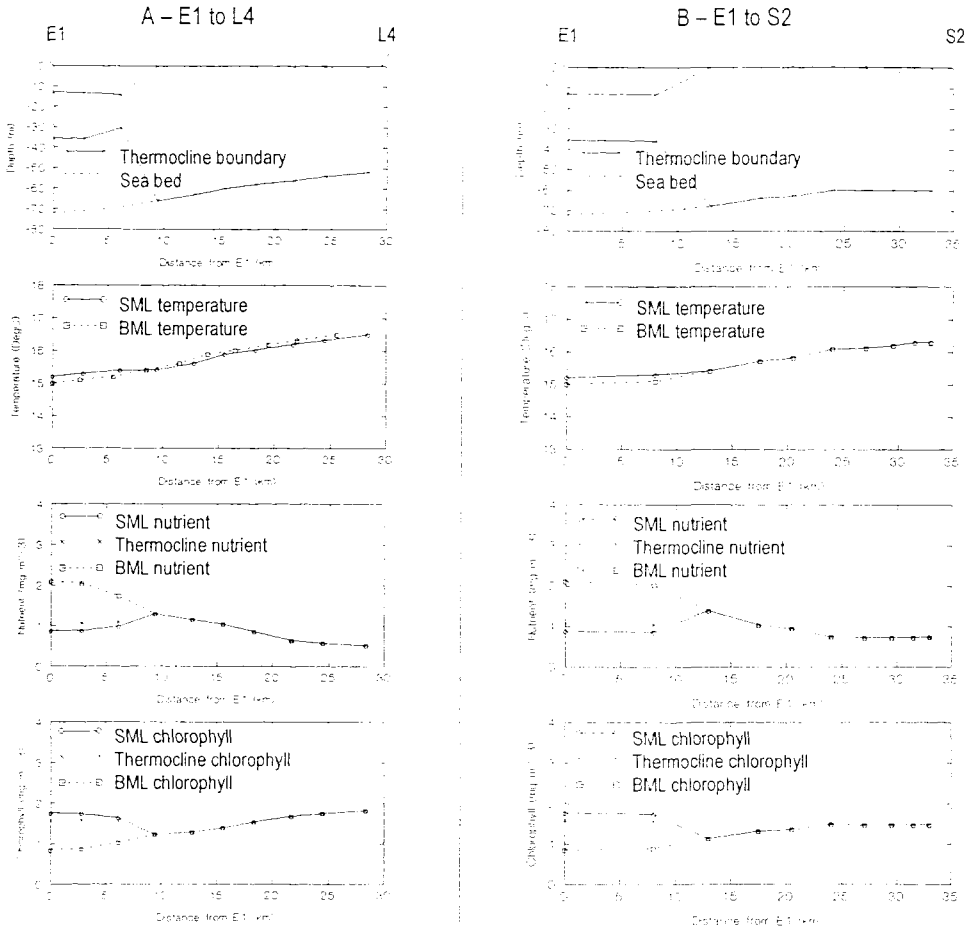

Figure 5.20 - *Simulations of thermocline depth, temperature, nutrient and chlorophyll along transects on 26th September 1997.* ***A:*** *The E1 to L4 transect.* ***B:*** *The E1 to S2 transect.*

Simulations of Spatial Variability – Changes from One Day to the Next (10th and 11th July 1997)

Observations from two sampling events on subsequent days (10th and 11th July) showed slight, but significant differences along the first 15 km of the E1 to S2 transect. (Chapter 4, figure 4.9). The water column on these dates was highly stratified, and characterised by a depression ('dome') in the thermocline depth between approx. 5 and 10 km from E1. Between the two days, SML depth had increased, the depth of the base of the thermocline had decreased, and the dome had moved towards E1.

The model simulations for the 10th and 11th July over the first 15 km of the E1 to S2 transect are presented in figure 5.21. It is clear that the horizontal spacing of the simulations (~5 km) was of a much lower resolution than the observations (~0.5 km). The spacing of the simulations reflects the resolution of the tidal and depth data used to drive the model. With the current tidal and depth data, the model is not an appropriate tool for reproducing small horizontal scale features such as the doming of the thermocline observed on 10th and 11th July. The model did, however, reproduce several of the differences between the two days that were identified from the observations. The simulation of the depth of the base of the thermocline predicted a decrease from 10th to 11th July (by 3 m at E1, compared to the observed decrease of 3 m). The increase in the depth of the SML was also predicted (by 2 m at E1, compared to the observed decrease of 2 m).

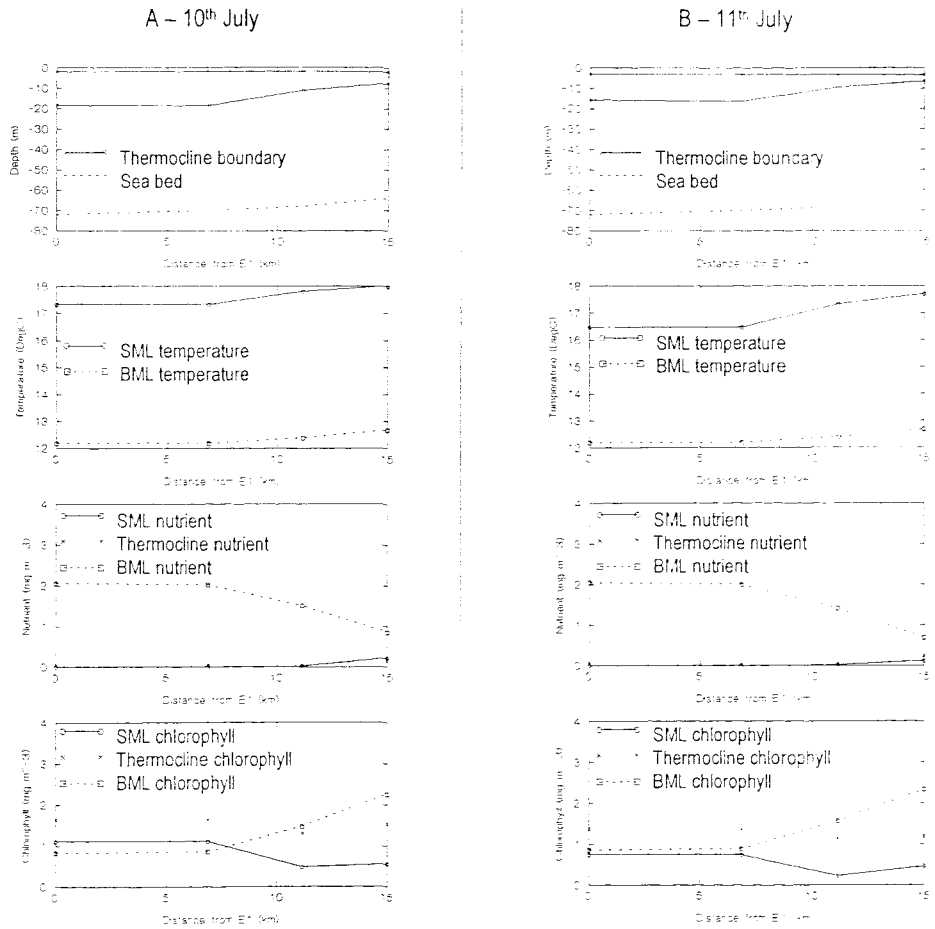

***Figure 5.21** - Simulations of thermocline depth, temperature, nutrient and chlorophyll along a portion of the E1 to S2 transect. **A:** 10th July 1997. **B:** 11th July 1997 (B).*

The model's general trend of underestimating SML depth was apparent on both the 10th and 11th July simulations. This characteristic may be responsible for another of the model's trends; the overestimation of the amplitude of diurnal variability. The deepening of the SML by 2 m between the days caused the volume of the SML to increase by 100%. This increase was supplied by cooler water from the thermocline, thereby cooling the SML. Simulated temperatures had dropped by 1°C (from 17.5 to 16.5) between 10th and 11th June. A similar deepening was shown by the observations, but, due to the increased depth of the SML, the change in volume was only ~20%, and no significant cooling occurred.

The model provides a valuable insight into an assumption made in Chapter 4 to explain the reduction in the depth of the base of the thermocline. Here, it was assumed that the thermocline depth had shallowed due to increasingly energetic bottom mixing. The model simulation predicted the shallowing of the thermocline, but using constant bottom mixing energy. An analysis of the model simulations over the preceding few days identified that the thermocline had been shallowing throughout, as the potential energy of the surface layer increased. The theory that, under a constant energy of tidal mixing, the depth of the base of the thermocline is controlled by the surface potential energy, appears to be supported by the observations.

The observations showed that a substantial thermocline phytoplankton bloom had occurred on 10th July, and its magnitude increased by 11th July. The model also predicted a thermocline bloom at E1 on 10th July (1.7 mg m^{-3} in the thermocline compared to 1.1 mg m^{-3} in the SML and 0.8 mg m^{-3} in the BML). However, chlorophyll concentrations were lower at E1 on 11th July. The model also predicted a strong increase in BML chlorophyll concentrations with distance along the track, associated with a fall in both SML and thermocline concentrations. In reality, this feature did not occur. As the BML chlorophyll concentrations were inversely related to BML nutrient concentrations and water depth, it is likely that the increased chlorophyll resulted from in-situ productivity. The processes behind the prediction of a reduction in thermocline and SML chlorophyll with distance along the transect are not clear, as nutrient concentrations appear to increase slightly with distance. The prediction of a reduction in chlorophyll with increased SML nutrients was described previously, to the stratified side of the tidal front on 11th September. One possibility is that the rate of exchange of water between the layers is greater than the rate of productivity for thin layers, thereby preventing the build up of elevated chlorophyll concentrations.

5.7 Conclusions

Model Performance

A summary of model performance vs. observed data for each of the scales of interest is presented in Table 5.4. It is clear that the model provided realistic simulations of the observed variability over a variety of the scales, but performed less well over several others.

Implications of the Model Simulations

In chapters 3 and 4, various theories were proposed concerning the processes responsible for the characteristic distributions of temperature and chlorophyll observed within the study region over each of the scales of interest. In many cases, the analysis of model performance was used to support these theories. Several examples are as follows;

- The simulations of seasonal variability of water temperature at E1 in response to meteorological forcing were accurate. This supports the theory that vertical processes of mixing and heating dominate the seasonal temperature cycle at E1.
- The model provided a realistic simulation of the seasonal distribution of chlorophyll distribution at E1, suggesting that biological distributions over this scale are also affected by vertical processes.
- The ability of the model to provide a good representation of the seasonal pattern for both an individual year and the multiple year average suggest that inter-annual temperature variability is controlled by inter-annual variability in atmospheric forcing.
- The model simulated the average 1997 seasonal distribution of temperature at E1, L4 and S2 to a high degree of accuracy. The success of the model suggests that vertical processes are dominant throughout the study region.
- The model provided realistic qualitative simulations of sub-seasonal and diurnal temperature variability. This suggests that vertical processes are highly significant over these scales also.
- In terms of spatial variability, the model correctly predicted the occurrence and location of the tidal front between E1 and S2. This supports the theory that tidal fronts within the study region result from horizontal gradients of vertical mixing.

The analysis of model performance was also revealing with respect to physical forcing processes on occasions where the model failed to realistically simulate the observed variability:

- As horizontal advective effects were not included in the model design, inaccuracies in model simulations during January and February 1997 support the theory that horizontal advection was significant during this period.

- Similarly, the failure of the model to simulate observed diurnal patterns of temperature variability for 8th to 11th August 1997 supports the theory that tidal advection controlled the temperature distribution over this period. In addition, the failure of the model to simulate observed diurnal patterns of chlorophyll variability for 25th to 28th September 1997 supports the theory that instrumental artefacts (i.e. photochemical quenching of fluorescence) were responsible for the observed variability. This second assertion must be treated with caution as there was no evidence that the model realistically simulated chlorophyll variability over this scale.

- The model predicted that, for the three stations, the tendency to stratify was E1=L4>S2, whereas the observations suggested that the order was E1>L4>S2. This feature supports the theory that island mixing effects due to the Eddystone Rocks are significant additional source of mixing at L4, as such effects are not included in the model design.

- Similarly, poor simulations along the E1 to L4 transect (generally overestimates of stratification) support the theory that island mixing effects are significant along this transect.

Scale of Variability	Variable	Model performance
Seasonal (inter-annual)	Thermocline depth	Simulations were qualitatively reasonable but were generally underestimates
	Temperature	Simulations were accurate, r^2>0.98, +/- 1°C. Overestimates occurred for the SML during early summer
	Nutrient	Simulations were accurate, r^2 up to 0.93, +/- 2 mg m^{-3}. Overestimates occurred during early spring, underestimates during late spring.
	Chlorophyll	Simulations were reasonable, r^2 up to 0.5, +/- 2 mg m^{-3}. Underestimates occurred during early spring, overestimates during late spring.
Seasonal (1997)	Thermocline depth	Simulations were qualitatively reasonable but were underestimates
	Temperature	Simulations were accurate. Monthly average, r^2>0.97, +/- 1°C. Discrete observations, r^2>0.94, +/- 2°C.
	Chlorophyll	Simulations were qualitatively reasonable. During the summer, SML concentrations were overestimated and thermocline concentrations underestimated.
Sub-Seasonal	Temperature	Simulations were reasonable for E1 and L4, r^2>0.6, +/- 2°C. The amplitude of the variability was overestimated.
Diurnal	Temperature	Simulations were reasonable when vertical processes were dominant, but poor otherwise. The amplitude of the variability was overestimated.
	Chlorophyll	Simulations were unreasonable due to horizontal processes and sensor artefacts.
Spatial	Thermocline depth	Simulations were qualitatively reasonable but generally underestimates. Predictions of the location and presence of tidal fronts were accurate.
	Temperature	Simulations were qualitatively realistic in most cases, especially for the BML. For the SML, horizontal gradients were underestimated, especially at tidal fronts.
	Chlorophyll	Simulations of horizontal gradients were poor in most cases. Simulations failed to predict chlorophyll blooms at tidal fronts
Vertical	Thermocline depth	SML depth was consistently underestimated. A better reproduction of thermocline width and maximum depth was achieved.
	Temperature	Vertical temperature profiles were reproduced with consistent accuracy within the limitations of the thermocline depth simulation
	Nutrient	The nutricline was reproduced accurately within the limitations of the thermocline depth simulation
	Chlorophyll	Sub surface chlorophyll maxima were reproduced, but with insufficient intensity. SML concentrations were consistently too high.

***Table 5.4** – A summary of model performance against observations for each of the listed scales of variability.*

6. Spectral Analysis and Conclusions

6.1 Techniques for the Spectral Analysis of Observed and Simulated Data

In the previous chapter, it was suggested that the performance of the Prestidge-Taylor model differed strongly between various spatial and temporal scales of variability, where each of the identified scales was selected to represent some dominant feature of the external physical forcing. This final chapter examines whether the analysis of data within the frequency domain (spectral analysis) provides a further test for the hypothesis that model performance differs between scales of variability. Firstly, the frequency responses of model simulations to the external physical forcing are examined, where the frequency response of a system is defined as its amplitude response to variation in input signals, as a function of frequency. Secondly, characteristics of the simulated frequency distributions are compared with observed data covering similar frequency ranges.

Time series measurements of natural systems are often analysed by using spectral analysis techniques such as the Discrete Fourier Transform (DFT) (e.g. Jenkins & Watts, 1987). Fourier theory states that any signal in the time domain can be decomposed into several frequency components made up of simple harmonic signals (sine and cosine waves) of varying amplitude and phase. The discrete Fourier transform is expressed as shown in equation 6.1.

$$H[k] = \frac{1}{N}\sum_{n=0}^{N-1} x[n]e^{-i2\pi kn/N} \qquad (6.1)$$

Where: $H[k]$ is the Fourier component at frequency index k, $x[n]$ is the signal value at time index n, and N is the number of data points in the series.

Furthermore, the Fourier components at a given frequency provide a complete description of the time-domain variability at that frequency, as shown in equation 6.2.

$$x[n] = A\cos\left(n/T + \phi\right) \quad (6.2)$$

Where: $x(n)$ is the variable(e.g. air temperature) at time index n, and A, T and ϕ are the amplitude, period and phase respectively of the Fourier component at period T.

The inverse Fourier transform converts data from the frequency domain into the time domain. The inverse transform is expressed in equation 6.2.

$$x[n] = \sum_{k=0}^{N-1} X[k] e^{-i2\pi kn/N} \quad (6.2)$$

Where: $X[k]$ is the Fourier component at frequency index k, $x[n]$ is the signal amplitude at time index n, and N is the number of data points in the series.

By taking the Fourier transform, filtering in the frequency domain (i.e. setting non-required components to zero), and then taking the inverse Fourier transform on the filtered data, time series data may be accurately filtered.

The DFT data presented in this chapter were produced using the Matlab software package using the 'fft' routine as described in the MathWorks Signal Processing Toolbox Users Guide (Anon, 1999).

In this chapter, data in the frequency domain are represented as plots of Fourier component amplitude vs. frequency or period (1/frequency). In certain circumstances, velocity vector ('feather') plots are used, which allow both the amplitude and phase of Fourier components to be visualised on a single axis. Plots were generated using the Matlab software package.

6.2 Spectral Features of The Meteorological Data

The formulation of the DFT is based on the characteristics of a discrete complex signal. In order to produce accurate analysis of the DFT, the following assumptions are made (Beckwith et al, 1993):

- the signal has been sampled in N intervals of time,
- the intervals of time are uniform and equal to Δt,
- the signal is periodic within the sampling period.

The meteorological data set for Plymouth (with irradiance from Camborne), as described in Chapter 2, provides a series that satisfies each of these assumptions: the data covers 16 years (1982 to 1997), has a uniform and equal sampling period of 1 hour, and is periodic on both diurnal and seasonal time scales (as discussed in Chapter 3).

Due to the number of data records for each field ($\sim 1.4 \times 10^5$), the computationally efficient Fast Fourier Transform algorithm (FFT, Cooley & Tukey, 1965) was required. One limitation of the FFT is that the number of data points in the signal to be processed must be an exact factor of two. The closest factor of two to the size of the meteorological data set is 2^{17}. A subset of 2^{17} points was extracted from the time series for each meteorological field, with the subset running from 1st Jan 1993 at 00:00 GMT to 14th Dec 1997 at 08:00GMT. Before calculating the FFT from each time series, the series mean and linear trend were removed from each data point (de-trending).

Time-series subsets, after de-trending, for downwelling irradiance, air temperature and wind speed, plotted against time, are included in Appendix 12A. The corresponding frequency series of Fourier component amplitudes, plotted against period, are also included in Appendix 12A. Significant features of each frequency representation include; dominant waveforms with diurnal and annual periods, and elevated amplitudes at the fundamental harmonic frequencies of each dominant waveform. Each of these features is discussed in the following section with particular reference to air temperature data, whose time and frequency series are presented in figure 6.1.

Cyclic meteorological variability at sub-seasonal scales (e.g. with periods of several days) was described in both chapters 3 and 5. No sub-seasonal signature is apparent, however, in the DFT plots for the meteorological data. Due to the stochastic nature of the meteorological signals over sub-seasonal scales, the DFT technique is an inappropriate method for the identification of their variability, and such scales are excluded from the following spectral analysis.

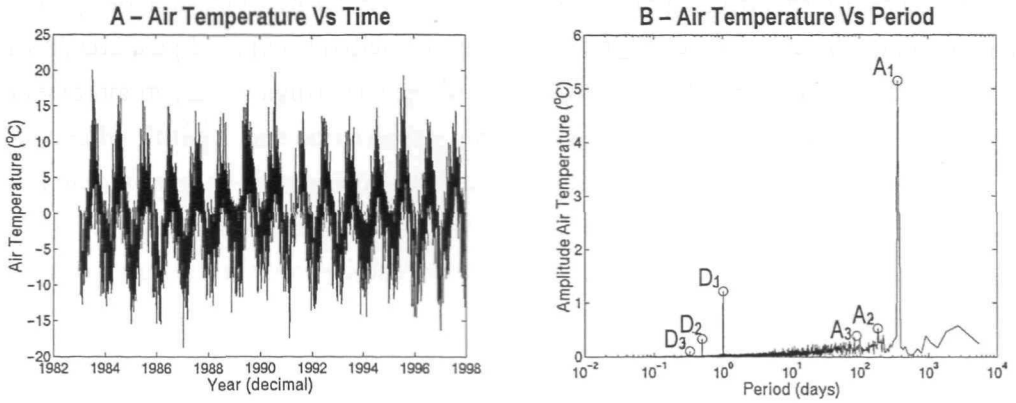

***Figure 6.1** –Air temperature data from 1st Jan 1993 to 14th December 1997. The data is presented as both a time series (A) as measured, and the corresponding DTF frequency series (B). The peaks labelled on the frequency series (A_{1-3}, D_{1-3}) are discussed in the text.*

Peak Label	Period (day)	Amplitude (°C)	ϕ (rad)
A_1	364.1	5.15	2.49
A_2	182.0	0.52	-1.13
A_3	121.0	0.19	-0.66
D_1	1.000	1.22	-1.59
D_2	0.500	0.33	1.96
D_3	0.333	0.11	1.41

***Table 6.1** – Spectral characteristics of the peaks labelled in Figure 6.1*

The Frequency Spectrum of Air Temperature – Characteristics of the Annual Waveform

The frequency series of air temperature, presented in Figure 6.1 displays a major peak in amplitude at a period of 364.1 days, labelled A_1 (see Table 6.1). This peak results from the annual variability of air temperature, as discussed in Chapter 3. The difference between the DFT period (364.1 days) and the expected period (365.25 days) is result of the mathematics behind the FFT; the frequency bin with a period of 364.1 days is the closest bin to the 'real' period of 365.25 days.

The spectral coefficients of A_1 (see table 6.1) can expressed as cosine a wave as shown in equation 6.3.

$$P_1(h) = 5.15\cos\left(\frac{2\pi h}{364.1\times 24} + 2.49\right) \qquad (6.3)$$

Where $P_1(h)$ is the air temperature in °C at h hours measured from the start of the time series

The amplitude of A_1 (5.15°C) gives a summer to winter temperature difference of ~10°C, and the phase (2.49 radians from the start of the year) locates the maximum air temperature in early August. The spectral coefficients of A_1 are similar to those obtained by fitting a sine curve (using the DFT technique) with a period of 12 months to the monthly average air temperature data presented in Chapter 3, figure 3.1 C. The spectral coefficients for the monthly average air temperature are expressed in equation 6.4, and represent an underestimate of 1.4% in amplitude, and an advancement of 7 days in phase, compared with the non-averaged spectral coefficients. Differences of similar relative magnitudes were returned on comparison between averaged and non-averaged spectral coefficients for downwelling irradiance and wind speed.

$$P_1(m) = 5.08\cos\left(\frac{2\pi m}{12} + 2.61\right) \qquad (6.4)$$

Where $P_1(m)$ is the air temperature in °C at m months, measured from the start of the time series

As the waveform representing the annual variability of air temperature is not a perfect sinusoid, its description in the frequency domain consists of multiple spectral components, with each component located at a fundamental harmonic frequency of the waveform (where harmonic frequencies are those that occur at integer multiples of the waveform frequency). The first three of these components are annotated on figure 6.1 as peaks A_1, A_2 and A_3. In the case of air temperature, the signal amplitude decreases rapidly with increasing harmonics, indicating that the first harmonic frequency contains the majority of the variance attributable to the annual cycle.

Each of the frequency representations for the meteorological fields presented in Appendix 12A displays annual waveforms with similar harmonic characteristics to air temperature (annotated as $A_{1\text{-}3}$ on the plots). Differences in amplitudes and phases between each spectrum represent the difference in amplitude and shape of the annual waveform between each meteorological field.

Frequency Spectrum of Air Temperature – Characteristics of the Diurnal Waveform

The dominant spectral signature of the diurnal waveform of the air temperature data presented in figure 6.1 is a sinusoid with a peak in the frequency representation at a period of 1.0001 days. This peak is labelled D_1 on figure 6.1 B.

Amplitude peaks at the second and third harmonic frequencies of D_1 are also labelled (D_2 and D_3). These harmonics are attributable to deviations from pure sinusoidal of the diurnal waveform.

6.3 Frequency Response of the Model in Response to Meteorological Forcing

The time-domain features of the data set simulated by the Prestidge-Taylor model simulation from 1982 to 1997 for the study region were discussed in Chapter 5. The model simulation for station E1 from 1982 to 1997 meets the assumptions for valid DFT analysis as described in Beckwith et al (1993): i.e. the data has a uniform and equal sampling interval of 1 hour, and the signals contain periodic waveforms (as discussed in Chapter 5). The time-series and frequency representation for each field of the simulated E1 data set are presented in Appendix 12B. Due to the constraints imposed by the FFT algorithm, the time period used was 1st Jan 1993 to 14th Dec 1997.

Four simulated fields; SML and BML water column temperature, and SML and BML chlorophyll, display spectral characteristics that are typical of the simulated fields as a whole, and the frequency representations of these two fields are discussed in greater detail. The time domain and frequency domain plots for SML and BML water column temperature simulations are presented in figure 6.2, and similar plots for chlorophyll simulations are presented in figure 6.3.

As the scope of the Prestidge-Taylor model did not include the spring-neap tidal cycle, there is no response in the DFT plots with a 14 day period

The spectral characteristics of each of the model simulations presented in figures 6.2 and 6.3 are broadly similar to the spectral characteristics of the air temperature data presented in figure 6.1. For instance, figures 6.2 and 6.3 each show that waveforms with both annual and diurnal frequencies were present in the simulated water temperature and chlorophyll data, within both the SML and the DML. In addition, each simulated waveform was associated with a number of amplitude peaks, corresponding to their harmonic frequencies (labelled A_{1-3} and D_{1-3} for annual and diurnal waveforms respectively). These characteristics were also apparent in the frequency series for each of the meteorological forcing fields (presented in appendix 12A) and simulated data fields (presented in appendix 12B).

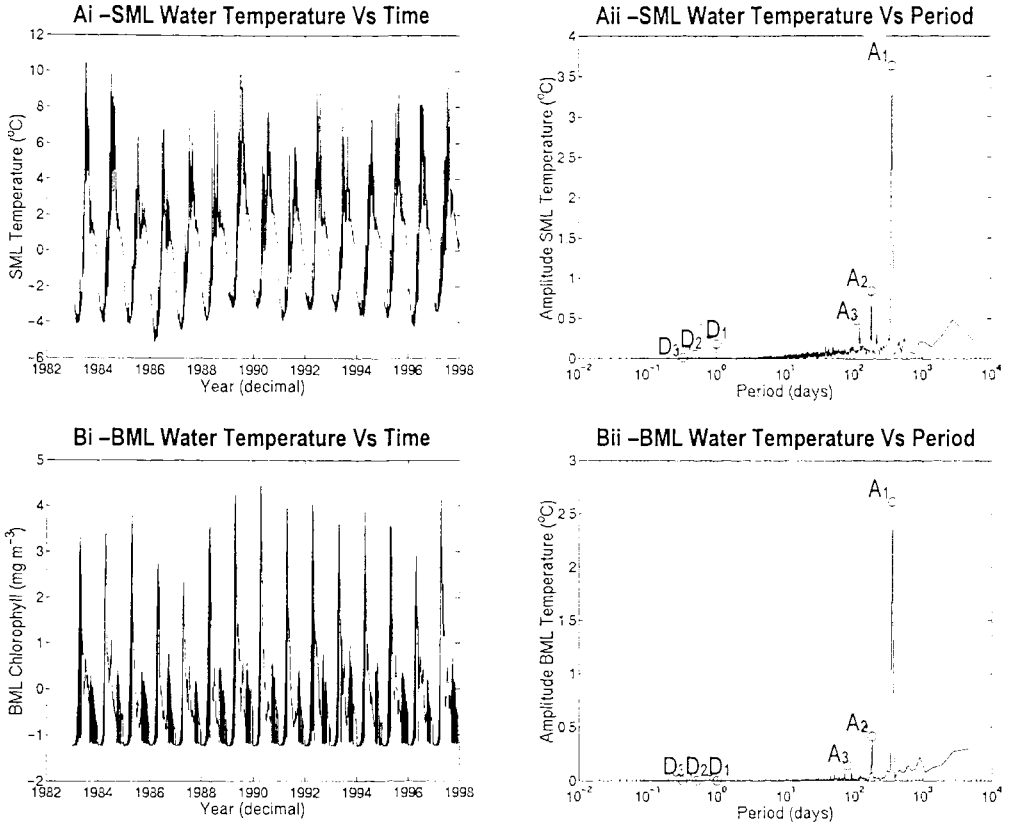

***Figure 6.2** –Simulations of water column temperature from 1st Jan 1993 to 14th December 1997 for the SML (Ai, Aii) and the BML (Bi, Bii), for station E1. The data are presented as both time series (Ai, Bi), and the corresponding DTF frequency series (Aii, Bii). The peaks labelled on the frequency series (A_{1-3}, D_{1-3}) are discussed in the text.*

Whilst there were certain similarities between the spectral characteristics of the variability simulated by the model and the variability of the meteorological forcing, there were also significant differences. For instance, for the SML chlorophyll data presented in figure 6.3, the amplitude of the second harmonic of the annual waveform was ~0.5 times greater than the first harmonic, whilst the second harmonic of annual air temperature was 10 times smaller in amplitude than the first harmonic (see table 6.1). In addition, many more harmonics of the annual SML chlorophyll waveform had noticeable above-baseline amplitudes than for the annual air temperature waveform. The annual variability of SML chlorophyll therefore had a far more complex frequency signature than the annual variability of air temperature. This indicates that the model had introduced significant distortions within the annual frequency response of SML chlorophyll to meteorological forcing. The frequency responses for many other model fields presented in Appendix 1[illegible]B show similar distortions of the annual cycle.

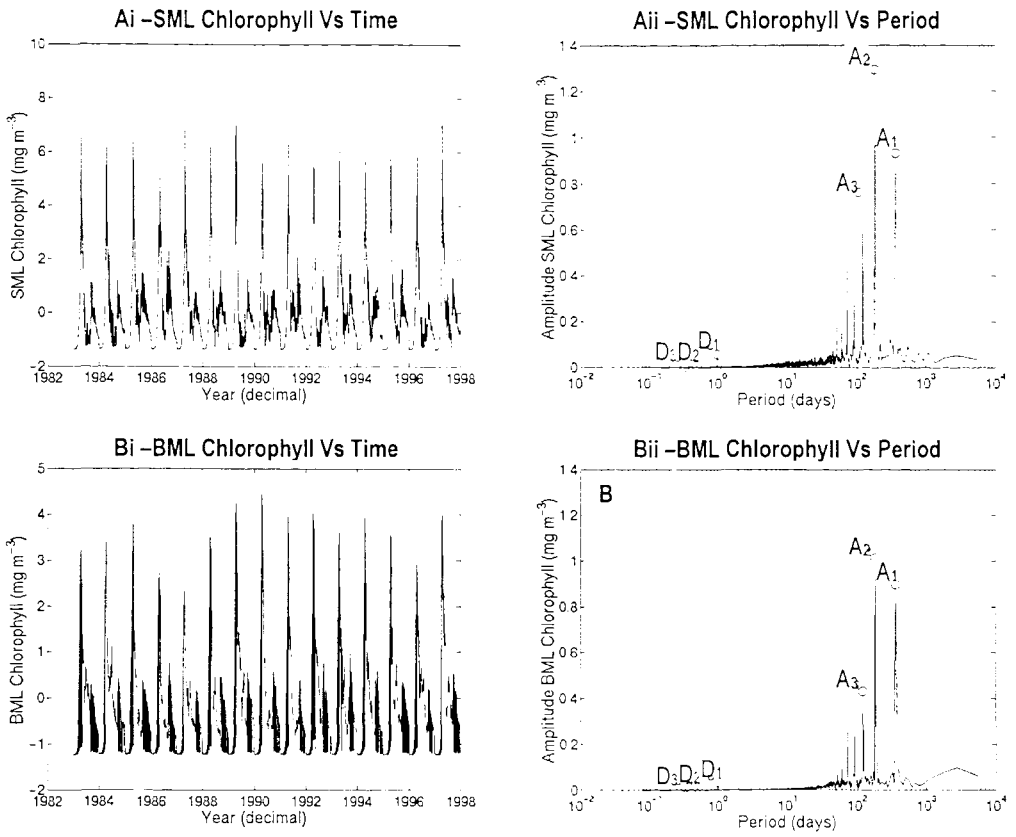

***Figure 6.3** –Simulations of chlorophyll from 1st Jan 1993 to 14th December 1997 for the SML (Ai, Aii) and the BML (Bi, Bii), for station E1. The data are presented as both time series (Ai, Bi), and the corresponding DTF frequency series (Bi, Bii). The peaks labelled on the frequency series (A_{1-3}, D_{1-3}) are discussed in the text.*

Simulations of water column temperatures (figure 6.2), however, are an exception, as the spectral characteristics of their annual waveforms are similar in complexity to those of air temperature.

A second significant difference between the frequency characteristics of the simulations and the meteorology was that the ratios of amplitudes between the annual and diurnal waveforms for both water temperature and chlorophyll were greater for the simulations than for air temperature. For instance, the ratio of first annual harmonic amplitude to first diurnal harmonic amplitude for SML water temperature was 20.2, whilst the same ratio for air temperature was 4.2. This suggests that the diurnal frequency response of SML water temperature to meteorological forcing is lower in comparison with the annual frequency response. This observation is apparent in all of the simulated fields

presented in appendix 12B. The model therefore displayed a greater amplitude response to the annual waveform of the meteorological forcing than to the diurnal waveform.

Differences between the spectral characteristics of the SML and the BML for a given simulation were also apparent. For example, the amplitudes of the Fourier components related to both the annual and diurnal waveforms were generally lower in the BML water temperature signal than in the SML (figure 6.2). This observation was also true for chlorophyll simulations (figure 6.3) and also for each of the simulated fields presented in appendix 12B. The amplitude response to meteorological forcing was therefore greater in the SML than the BML.

The frequency response of the model to meteorological forcing for station E1 from 1983 to 1997 can therefore be summarised as follows:

- The model responds to both annual and diurnal variability in meteorological forcing. The response is apparent across all simulated fields.
- The amplitude response of the model to meteorological forcing is greater in the SML than in the BML.
- The amplitude response of the model to meteorological forcing is greater for the annual cycle than the diurnal cycle.
- The shape of the annual waveform is heavily distorted (i.e. non-sinusoidal) for most simulated fields in comparison with the annual waveform for the meteorological fields.

6.4 Comparison between the Spectral Characteristics of the Simulated and Observed Marine Data

The previous sections in this chapter highlighted the frequency domain characteristics of the meteorological data from 1983 to 1997, and the corresponding frequency response of the Prestidge-Taylor physical/biological model for station E1. The aim of this section is to compare the frequency distributions of the model simulations to the frequency distributions of 'real' water column temperature and chlorophyll distributions as estimated from the observational data presented in Chapters 3 and 4.

It is obvious that the observational data presented in Chapters 3 and 4 are insufficient to estimate a complete hourly time series of water column temperature and chlorophyll for the study region from 1983 to 1997. The analysis must therefore be confined by the availability of the observational data and derived products.

The waveforms with periods of 1 year (annual) and 1 day (diurnal) are of primary interest, as these dominated the frequency spectra of both the meteorological and modelled signals. By using a combination of AVHRR, PlyMBODy and E1 archive data sets, some degree of water temperature and chlorophyll frequency information for both annual and diurnal waveforms can be extracted.

Frequency Spectra of Mean Monthly Water Column Temperature and Chlorophyll for Station E1: Comparison Between Simulations and Observations

In Chapter 3, the AVHRR data from 1997 for station E1 was used to calculate mean monthly values of nighttime SST. In Chapter 5, the validity of the comparison between AVHRR-derived SST and model simulations of SML water temperature was discussed.

As the process of averaging in the time domain acts as a high-pass frequency filter, the 12-point DFT of the monthly average SST provides a good representation of the frequency characteristics of the 'real' annual water temperature variability during at E1 during 1997 (within the measurement limitations of the AVHRR technique). Furthermore, the 12-point DFT of model-simulated monthly mean SML temperature for 1997 has been taken to allow a direct frequency-domain comparison with the SST data. This comparison is presented in Figure 6.4, where the Fourier components of observed and simulated water temperature are displayed as vector plots, displaying both harmonic amplitude and phase.

As identified earlier in the chapter, the frequency distribution of (hourly) simulated SML water temperature (from 1983 to 1997) was dominated by the first harmonic of the annual waveform. Figure 6.4 shows that this feature, also dominates the frequency spectra from 1997, for both (monthly mean) simulated SML temperature (labelled S_1) and observed SST temperature (labelled O_1).

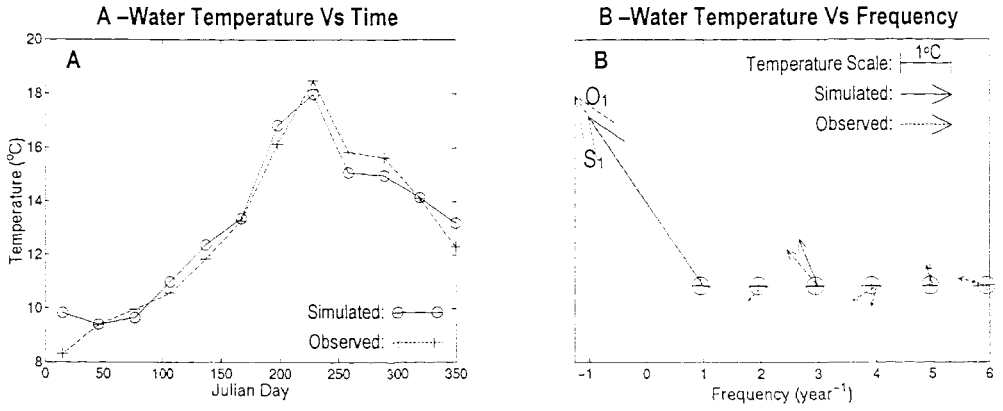

Figure 6.4 – *Comparison between monthly means of the simulated SML water temperature and monthly means of the AVHRR-derived SST temperature; both for station E1 during 1997. The data are presented as a time series of temperature (A), and a frequency series vector plot of amplitude and phase (B). The arrows labelled S_1 and O_1 on the vector plot are discussed in the text.*

Figure 6.4 also highlights the similarity between the observed and modelled frequency coefficients for the first harmonic of the annual waveform. For instance, the phase difference between the simulated and observed data ($S_1 - O_1$) was +0.012 radians (less than 1 day), and the ratio of modelled to observed amplitude was 0.89 (indicating the model underestimated the amplitude of the annual cycle by 11 % compared with the observations).

As described in Chapter 4, the archive of data collected between 1974 and 1987 at station E1 was used to calculate monthly mean values of water column temperature, nutrient and chlorophyll. The validity of the comparison between this archived data set and the average monthly mean values from the model simulation between 1982 and 1997 was discussed in Chapter 5.

A 12-point DFT of both the archive data and the comparable model data was taken, with the results for SML and BML water column temperature presented in Figure 6.5, alongside the original time series. As expected, the frequency distribution of the multi-year average annual cycle of SML temperature (figure 6.5 Aii) was very similar to the distribution for a single year (figure 6.4 B).

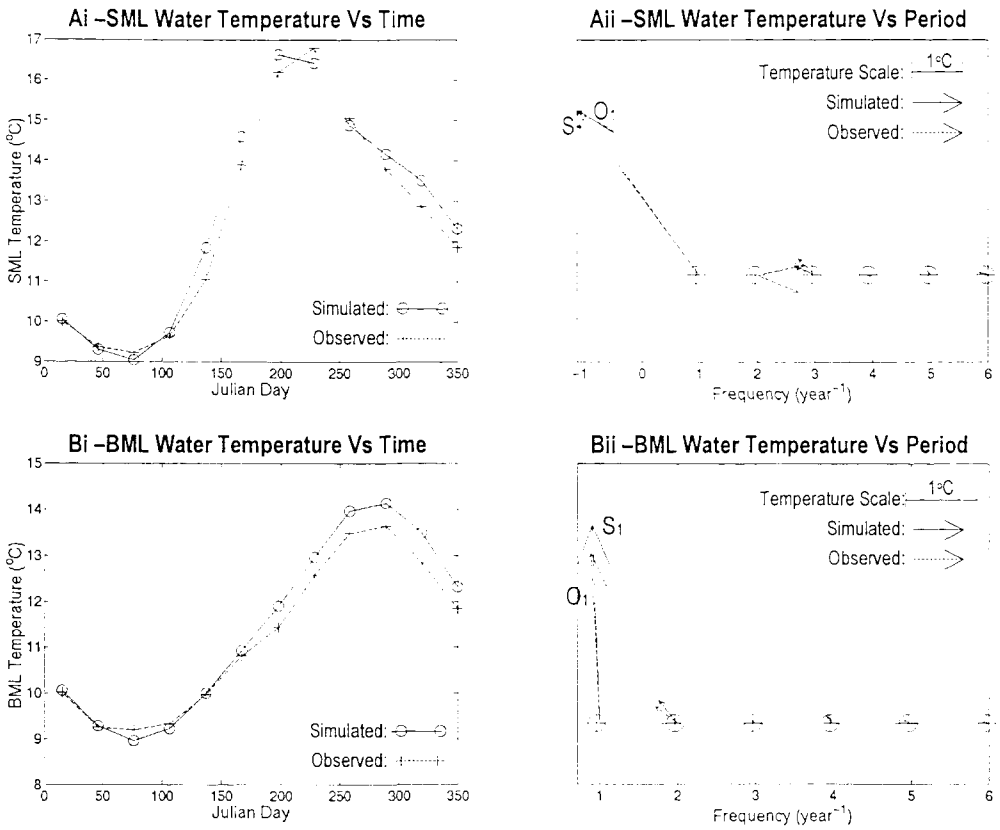

Figure 6.5 - *Comparison between monthly means of the simulated water column temperature between 1982 and 1997 and monthly means of the E1 archive water column temperature between 1974 and 1987; both for station E1. Plots are presented for the SML (Ai, Aii) and the BML (Bi, Bii), as both time series of temperature (Ai, Bi), and frequency series vector plots of amplitude and phase (Aii, Bii). The arrows labelled S_1 and O_1 on the vector plot are discussed in the text.*

The first harmonics of the multi-year average annual cycle of SML temperature are labelled on the figure (6.5 Aii) as O_1 and S_1 for the observed and simulated data respectively. The first harmonic for BML temperature has been similarly annotated (figure 6.5 Bii). The difference between the phase of S_1 and O_1 was +0.015 radians for the SML, and -0.013 for the BML. Both of these phase differences represent a time difference of less than 1 day. The ratio between the amplitudes of S_1 and O_1 was 1.01 and 1.16 for the SML and BML respectively, indicating that the model overestimated the amplitude of the annual cycle by 1% for the SML and 16% for the BML, compared with the observations.

Figure 6.6 presents the multi-year average annual cycle of chlorophyll, as compiled from the E1 archive and model simulation data sets. As the annual chlorophyll waveform is distinctly non-sinusoidal, the amplitude peak at its first harmonic frequency does not dominate its frequency signature (figures 6.6 Aii and Bii); in fact, the signal amplitude at the second harmonic is greater than that at the first, for both simulated and observed data. The first three harmonics of the annual chlorophyll waveform are labelled on figures 6.6 Aii and Bii as $O_{1\text{-}3}$ and $S_{1\text{-}3}$ (where 'O' represents the observed data, and 'S' represents the simulated data).

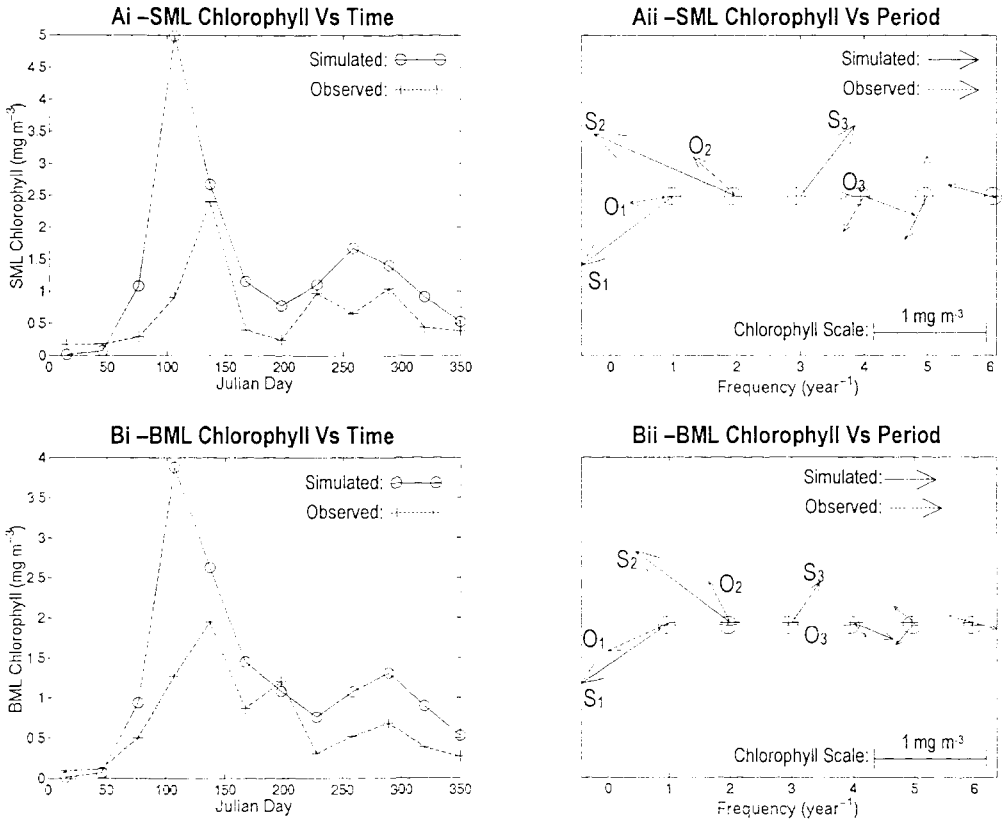

***Figure 6.6** - Comparison between monthly means of the simulated chlorophyll between 1982 and 1997 and monthly means of the E1 archive chlorophyll between 1974 and 1987; both for station E1. Plots are presented for the SML (Ai, Aii) and the BML (Bi, Bii), as both time series of chlorophyll (Ai, Bi), and frequency series vector plots of amplitude and phase (Aii, Bii). The arrows labelled $S_{1\text{-}3}$ and $O_{1\text{-}3}$ on the vector plot are discussed in the text.*

The data presented in figure 6.6 can be used to calculate numerical comparisons between the simulated and observed components of the annual cycle of chlorophyll:

- For the SML, the differences in phase; S_1 - O_1, S_2 - O_2, S_3 - O_3, were; 0.50 radians (-28 days), 0.38 radians (-11 days), and 0.92 radians (-18 days) respectively.
- For the SML, the ratios of amplitudes; S_1:O_1, S_2:O_2, S_3:O_3, were; 2.63, 2.94, and 1.81 respectively.
- The differences in phase between simulations and observations were similar for the BML to those for the SML.
- The ratios of amplitudes for the BML were again similar to those for the SML.
- The model, therefore, significantly overestimated the amplitude of each of these features (i.e. 1st, 2nd and 3rd harmonics) of the annual chlorophyll waveform (by up to 3-fold) compared with the observations. In addition, the model phase-shifted each of these features forwards in time by up to 1 month.

Frequency Spectra of Hourly Water Temperature and Chlorophyll for PlyMBODy: Comparison Between Simulations and Observations

Sections of the PlyMBODy data collected during 1997 were presented in Chapter 4, and comparisons with model simulations for the PlyMBODy location (forced with hourly meteorological data from 1997) were presented in Chapter 5. These earlier discussions identified cyclic patterns in the observed water temperature and chlorophyll signals over periods of the order of 1 day. In the following section, DFTs of the PlyMBODy data are compared with corresponding DFTs from the model simulations. Two time ranges are assessed, a 3-day period from 8th to 11th August 1997, and a 20-day period from 17th September to 7th October 1997. The time interval of both PlyMBODy and modelled data was 1 hr, and all series were high-pass filtered (2-day) using the inverse DFT technique, and de-trended prior to analysis.

The de-trended PlyMBODy temperature data from 8th to 11th August 1997, and corresponding model SML temperature data, are presented in figure 6.7, both as time plots, and frequency spectra of amplitude vs. period.

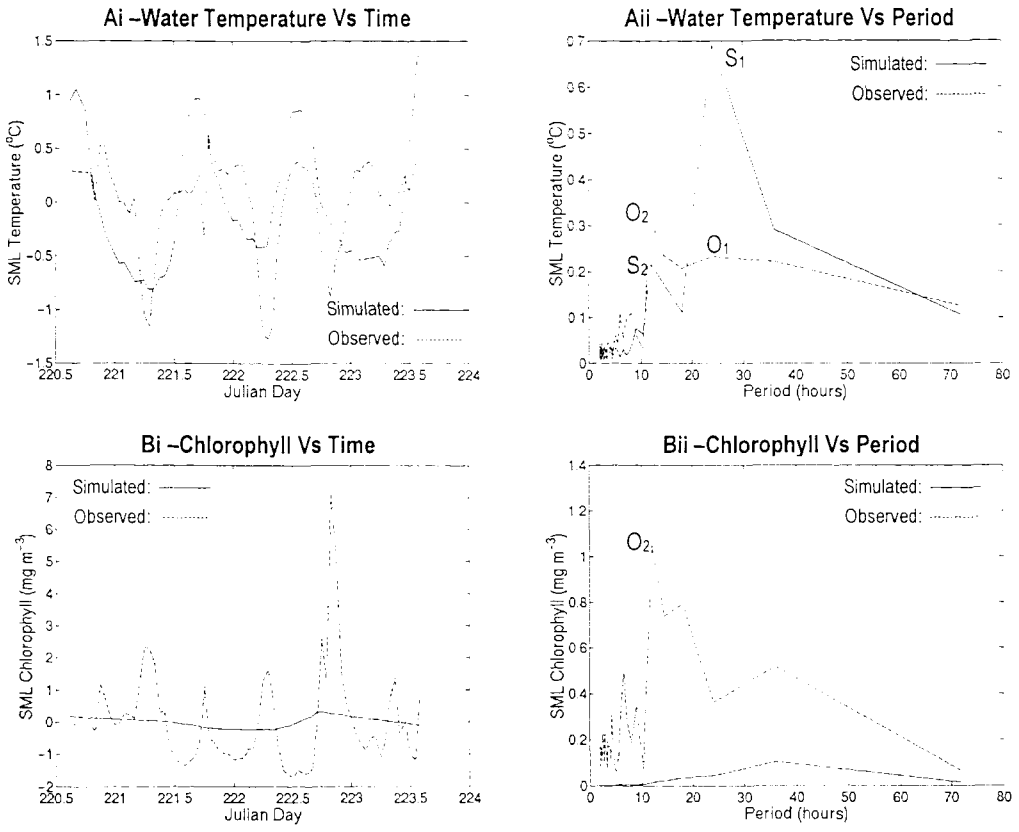

***Figure 6.7** – SML water temperature (A) and chlorophyll (B); Comparison between simulations for the PlyMBODy site, and PlyMBODy observations. Time period is 8th August to 11th August 1997. Data are presented as time plots (Ai, Bi) and frequency spectra (Aii, Bii).*

The model SML temperature signal presented in figures 6.7Ai and Aii contains a strong diurnal waveform (period of 24 hours), identified by its first and second harmonic frequencies (labelled S_1 and S_2 on figure 6.7 B). The PlyMBODy temperature signal also contains peaks with periods of 24 and 12 hours (labelled O_1 and O_2 on figure 6.7 B). However, at greater resolution (generated by zero-padding the data series before taking the DFT), the location of the O_2 peak falls at a period of 12-13 hrs (12.5 for a 288-point DFT), whilst the O_1, S_1 and S_2 peaks remain stationary. This suggests that suggest that the amplitude peak at O_2 is not simply the second harmonic of the amplitude peak at O_1:

In Chapters 4 and 5, it was suggested that the variability of the PlyMBODy data from the 8th – 11th August 1997 was caused by advection due to the semi-diurnal tidal cycle (with a period of ~12.4 hrs). The results of the spectral analysis, presented above, reinforce this theory.

Whilst the peak at O_2 was probably due to tidal advection, it is still likely that the peak at O_1 was due to the diurnal cycle of meteorological forcing. If this is assumed to be the case, then a comparison with the simulated data (peak S_1) suggests that the model overestimated the amplitude of the diurnal cycle by 3 fold by comparison with the observations (the amplitude ratio of S_1:O_1 being 3.0).

Chlorophyll data from 8th to 11th August are also presented in figure 6.7. The PlyMBODy data show a significant amplitude peak at a period of ~12 hrs, which one may assume is due to tidal advection. Neither the observations nor simulations, however, show a periodic 24 hr signal, suggesting that the amplitude response of chlorophyll to meteorological forcing over the time interval was negligible.

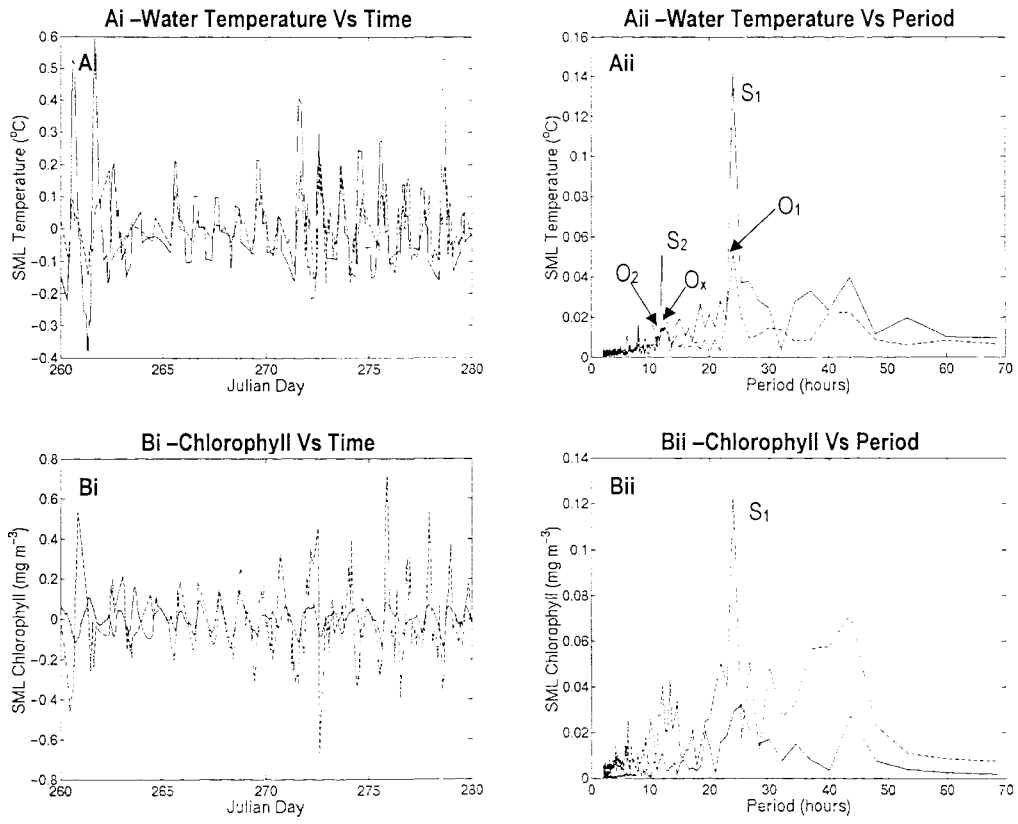

***Figure 6.8** - Comparison between SML water temperature simulated for the PlyMBODy site, and PlyMBODy water temperature observations. Observations and simulations are for 17th September to 7th October 1997. Data are presented as time plots (A) and frequency spectra (B).*

Although the data presented in figure 6.7 suggested that the model had over-estimated the amplitude of the observed diurnal SML temperature, it is useful to run a similar

comparison over a longer time range, and one that is not so contaminated by extraneous signals. Therefore, the PlyMBODy and model data for a 20-day time interval (17th September 1997 to 7th October 1997) are presented in figure 6.8.

The amplitude peaks with a period of 24 hours dominate the PlyMBODy and modelled frequency series of water temperature presented in figure 6.8. These are labelled S_1 and O_1 for the simulations and observations respectively. For this time series (17th September to 7th October 1997), the affect of the semi-diurnal tide is far less apparent than for the 8th to 11th August series: the observed data displays a small amplitude peak (0.018°C) with a period of ~12.5 hours (labelled O_x on the figure). Also, due to the greater resolution of the DFT (which is restricted by the number of data points), an additional peak with similar magnitude is also resolved with a period of 12.0 hours (labelled O_2). It is reasonable to assume, therefore that peak O_x is due to tidal advection, whilst peak O_2 is the second harmonic of the diurnal waveform.

The comparison between the modelled and observed frequency representation of the diurnal waveform shows that the model overestimated the amplitude of the first harmonic by almost 3 fold (the amplitude ration of S_1:O_1 being 2.7). In addition, the phase difference between S_1 and O_1 was 0.43 radians, indicating that the model retarded the timing of the diurnal waveform by 1.6 hrs.

Chlorophyll data for the 17th September to 7th October interval are also plotted, as shown in figures 6.8 Bi and Bii. The simulations show a distinct peak with an amplitude of ~0.12 mg m^{-3} and a period of 24 hrs (marked as S_1 on the figure). This is clear evidence that the model simulated a significant chlorophyll response in response to diurnal meteorological forcing. For the chlorophyll observations, there is a suggestion of an amplitude peak between 20 and 30 hrs, but, as the peak amplitude was close to the level of the baseline noise, its presence cannot be confirmed.

Due to the spring-neap tidal cycle, one may anticipate the occurrence of an amplitude peak at a period of ~14 days within the PlyMBODy temperature and chlorophyll signals. However, as the spring-neap tidal cycle is outside the scope of the model, this feature has not been investigated, and any potential signal has been removed by high-pass filtering of the PlyMBODy data.

6.5 Analysis of Model Performance - Conclusions from both the Time Domain and Frequency Domain

The null hypothesis of this thesis, as stated in Chapter 1 was:

"The ability of a given shelf-sea physical-biological model to simulate temperature and chlorophyll distributions at one scale of variability will be the same as its ability over all of the scales of variability defined by the 'scope' of the model."

Also in Chapter 1, the 'scope' of the model was clearly defined as 'covering only the environment and processes that the model was designed to simulate, and limited to the scales of variability resolved by the model'. The analysis of the model's frequency response to meteorological forcing identified two scales in particular – annual and diurnal variability – that clearly fell within the scope of the model. In addition, observational data was presented that also resolved annual and diurnal variability, and could be compared directly with model simulations in both the temporal and frequency domains.

For the annual variability of water temperature, the comparison between modelled vs. observed data is summarised as:

- In the time domain, the Spearman rank correlation (r^2) between simulated and observed temperature was greater than 0.94 for both 1997 and multi-year data.
- In the frequency domain, the amplitude ratio of the first harmonic of the annual waveform of simulated/observed temperature was between 0.89 and 1.16.
- The phase difference between the first harmonic of the simulated and observed temperature was generally less than 1 day (0.27% of the annual period).
- The annual chlorophyll waveform was more complex than that of temperature. The general shape of the simulated waveform was qualitatively similar to that of the observed waveform (over the first 3 harmonics of the annual waveform). The numerical comparisons suggested that the model overestimated the amplitude of the annual waveform by up to 3-fold, and advanced its timing by up to 1 month.

For the diurnal variability, the comparison between modelled vs. observed data is summarised as:

- In the time domain, the Spearman rank correlation (r^2) between the simulated and observed temperature was 0.43. The time series contaminated by tidal advection had been ignored, as tidal advection falls outside of model scope.

- In the frequency domain, the amplitude ratio of the first harmonic of the diurnal waveform of simulated/observed temperature was ~3.

- The phase difference between the first harmonic of the simulated and observed temperature was 1.6 hrs (6.7% of the diurnal period).

- The small amplitudes of the responses, and the limited availability of observational data hampered comparisons between simulated and observed chlorophyll over diurnal scales. However, a distinct peak in the simulated chlorophyll had no corresponding peak in the observations, suggesting that the model had overestimated the diurnal variability of chlorophyll concentrations.

The difference in the temperature rank correlation between annual and diurnal scales (>0.94 and 0.43 respectively) certainly suggests a difference in model performance between the scales. However, rank correlation provides no information on magnitude or phase differences between two variables. This information is provided by the frequency analysis, which shows that the amplitude ratios between annual and diurnal scales differed greatly, from ~1 for the annual cycle, to 3 for the diurnal cycle. In addition, the validity of a direct magnitude comparison between simulations and observations is supported by the small phase differences between the simulations and observations (0.27% of the annual period, and 6.7% of the diurnal period). This suggests that each waveform resulted from the same physical forcing, i.e. meteorology.

Given the differences in the model vs. observed signals over annual and diurnal scales for both time and frequency domain analysis, then the null hypothesis is proved void:

The ability of a given shelf-sea physical-biological model to simulate temperature and chlorophyll distributions at one scale of variability is not the same as its ability over all of the scales of variability defined by the 'scope' of the model

The dismissal of the null hypothesis does, however, rely on the acceptance of the following assumptions, but only applied to frequencies of 1 $year^{-1}$ and 1 day^{-1}:

- The observations provide an accurate estimate of the amplitude of the 'real' variability.

- The amplitudes of variability within the 'real' system due to processes outside the scope of the model are insignificant compared with the amplitudes of the response to meteorological forcing. The variability due to tidal advection, for instance, has been shown to cause significant variability, but *not* at frequencies of the annual or diurnal cycles.

- The frequency response of the 'real' system to meteorological forcing at a single scale is deterministic. This supports the generalisations that were made using short sections of data.

- The vertical processes of heating and mixing dominate the variability of the system. This assumption is supported by the analysis of data presented in this thesis, and also by other studies of the region (e.g. Pingree, 1980).

6.6 Implications of the Void Null Hypothesis

In Chapter 5, it was suggested that one consistent feature of the model was that it significantly underestimated the depth of the thermocline. It is argued that this feature was, in part, responsible for the overestimate of the amplitude of diurnal SML temperature variability, Due to the lowered heat capacity of the modelled SML layer, it heated too rapidly during the day, and cooled too rapidly during the night.

The exact extent to which the amplitude overestimate of the diurnal variation of SML temperature affected cross-thermocline mixing cannot be estimated without the aid of direct measurements that resolve thermocline depth over diurnal scales. Nevertheless, due to the direct affect of temperature structure on vertical mixing calculations, errors in cross-thermocline mixing over diurnal scales are likely to be significant. As the relationship between nutrients and chlorophyll are non-linear with respect to vertical mixing rates, one must expect that mixing errors over diurnal scales will result in magnitude errors in chlorophyll and nutrients over annual scales. Unfortunately, the estimation of model accuracy in simulations of diurnal and annual variability were limited by the availability of observational data. It can be argued, however, that such a validation is not of critical interest, considering that the parameterisation of the model's biological compartment can be optimised, to a large extent, thus artificially correcting for shortcomings of the underlying model.

Given the uncertainty of the model's representation of the physical variability over diurnal scales, it is argued that, in its current form, the model is not an appropriate

diagnostic tool for the prediction of chlorophyll and nutrient concentrations over any scale of variability. This finding is specifically extended to the estimation of diurnal vertical nutrient fluxes that, as proposed by Taylor & Stephens (1993) and Large *et al* (1994) for example, provide a crucial flux of nutrients to sustain chlorophyll productivity in stratified waters during summer months, and also to the estimation of seasonal-scale nutrient fluxes that are implicit in the timing of the spring and autumn chlorophyll blooms (e.g. Pingree *et al*, 1977a).

As this thesis has demonstrated, if a model is validated only with respect to longer scales of variability, then misleading conclusions may be drawn: amplitude errors of the type described will be smoothed as the data is averaged, resulting in a good fit for annual variability even when the small-scale dynamics are poorly characterised. The Prestidge-Taylor model appears to be of this type. Many shelf-sea models have been presented that use hourly meteorological forcing to draw conclusions about annual cycles with no reference to validation at shorter scales, including those of Elliott & Li (1995), Lenhardt *et al* (1995) and Ruardij *et al* (1997). Questions may be asked about the validity of the simulations of these models (especially with respect to nutrient and chlorophyll distributions) over all scales, including those scales for which the fit between the simulations and observations appear reasonable.

6.7 Conclusions

In order to verify and improve physical/biological models, observational/numerical studies are required that introduce procedures for the comparison of model output with observational databases (Baretta *et al*, 1998, Lynch *et al*, 1995). This thesis has investigated a number of basic procedures, including time-domain analysis, and frequency-domain analysis.

In general, observational/numerical studies of shelf-seas are limited by the scope and availability of observational data sets (Lynch *et al*, 1995, and Smith, 1993). To counter these limitations, this project has used archived observational data, and supplemented these with data collected from a disparate range of modern observational platforms, including satellite (AVHRR, SeaWiFS), towed-undulator (UOR), and remote-buoy (PlyMBODy). The result has been a large and consistent observational database that resolves a wide range of temporal and spatial scales for a well-defined study region. This thesis has concentrated on the use of the database for the rigorous examination of the performance of an established physical-biological model.

The potential for variability in meteorological and tidal forcing and resultant (vertical) physical water-column processes to control the annual distributions of temperature, chlorophyll and nutrients (nitrate + nitrite) in shelf seas has been investigated by numerous studies over the past several decades. Examples specific to the Western English Channel area, and the study region in particular, include the works of Pingree (1980) and Holligan (1981).

The observational data presented in Chapters 4 and 5 showed the presence within the study region of many features identified for the shelf-sea waters of the western English Channel by earlier studies. Similarly, the application of the Prestidge-Taylor model confirmed that many of the temperature features could be explained numerically through the theory that vertical processes forced by meteorology and tides control shelf-sea temperature distribution, and that many of the chlorophyll features could be explained by the theory that the availability of light and nutrients control phytoplankton growth in shelf seas.

❑ *Seasonal Cycle of Temperature and Chlorophyll*

- Water temperature distributions from the project database for station E1 displayed the characteristic annual cycle of water-column stratification in the spring and convective mixing in the autumn. The timings of these events, both for 1997 and for the E1 data archive, fell within the environmental range for E1 presented by Maddock & Swann (1977). The hourly water column temperature simulations of the Prestidge-Taylor model for E1 were numerically accurate (rank correlation, amplitude and phase) over seasonal scales for both 1997 and the longer time-scale archive. This suggests that, over the seasonal cycle, vertical processes in response to meteorological forcing dominantly controlled temperature distributions at station E1. Many other studies have reported similar conclusions for other shelf-sea areas using both seasonal meteorological forcing (e.g. James, 1977), and hourly meteorological forcing (e.g. Ruardij *et al*, 1997).

- Surface water temperature distributions from the project database identified the occurrence of significant horizontal advection through the study region during the winter months, at a rate consistent with that proposed for the western English Channel by Taylor & Stephens (1983). This finding was able to explain the inconsistency between observed and calculated winter temperatures at E1 noted previously by Pingree & Pennycuick (1975). For the model, the advective signal was affectively cancelled out by restoring the model variables to climatic mean

conditions at the start of each simulated year. This procedure allowed the avoidance of cumulative errors over long model runs.

- For 1997, the project database did not cover the spring bloom of phytoplankton. The data archive for E1, however, confirmed the existence of a spring phytoplankton bloom immediately following the onset of seasonal stratification, and an autumn bloom immediately preceding the destruction of stratification. This pattern has been reported previously for station E1 by Holligan & Harbour (1977), and can be explained by vertical processes following Svedrup's (1953) theory. Although the chlorophyll simulations of the Prestidge-Taylor model were numerically inaccurate over seasonal scales (rank correlation, amplitude and phase), general simulated pattern of spring and spring and autumn blooms was represented. The ability of 1-D models to simulate spring and spring and autumn blooms has been demonstrated previously by, for example, Agoumi *et al* (1985) and Ruardij *et al* (1997). To further develop the Prestidge Taylor model, it is important to understand why its seasonal chlorophyll simulations differed by such a degree from the observations. Possible explanations include; theoretical limitations due to model scope (e.g. the omission of advection and the assumption of a single chlorophyll species), biological initialisation/parameterisation errors, the model's poor representation of the physical dynamics at diurnal scales, or even uncertainty of the observational database measurements. Further study is required to investigate each of these areas.

- The project database identified the presence of a sub-surface chlorophyll maxima at station E1 during the summer months, for both 1997 and the longer time-scale archive. This feature has been identified previously for E1, and explained using vertical processes control (Holligan & Harbour, 1977). The model's chlorophyll simulations, however, did not contain a clear sub-surface chlorophyll bloom, which is an omission that is typical of simple 1-D physical/biological models, such as Agoumi *et al* (1985), see also Sharples & Tett, (1994). The reason behind the inability of the Prestidge-Taylor model to simulate this feature is another issue pertinent for further investigation, with focus on model limitations concerning theoretical scope, parameterisation, initialisation, and dynamics at diurnal scales.

❑ *Spatial Distribution of Temperature and Chlorophyll*

- During the summer months, two geographic areas could be identified within the study region; thermally stratified waters (of which station E1 was typical), and a

frontal zone of SML temperature gradient (of which station S2 was typical). The location of the frontal zone fell within the range of tidal mixing energy expected for a tidal front (as suggested by Pingree & Griffiths, 1978), with the stratified waters corresponding with areas of lower tidal energy. On some occasions, the water column became well-mixed for the most tidally-energetic waters. From satellite images, the gradient zone was identified as a northwards extension of the Ushant tidal front, whose characteristics have been extensively studied previously (see Pingree, 1980 for a review). The temperature simulations of the Prestidge-Taylor model accurately identified the differences between these two zones, as highlighted by the differences between the temperature simulations for stations E1 and S2. Less well simulated, however, was the temperature variability along transects between E1 and S2. It can be argued that, since the model is a simple 1-D 3-layer bulk model, the analysis of horizontal temperature structure does not fall within the model's scope. More complex multi-layer models, such those of Franks & Chen (1996) and Sharples & Simpson (1996), provide better representations of horizontal temperature distributions.

- At the tidal front that existed in the study region during 1997, significant enhancement of chlorophyll concentration was identified to the stratified side of the frontal interface. Such features have been identified previously for the western English Channel by, for example, Pingree *et al* (1977b). It has been shown that models that assume that the availability of light and nutrients is controlled by vertical mixing can explain such chlorophyll elevations numerically (for example, Tett, 1981). The Prestidge-Taylor model, however, did not predict frontal chlorophyll elevations in the simulations of horizontal chlorophyll distributions, and, for similar reasons to those proposed above for temperature distributions, such simulations may be considered outside of the scope of the model. The model did, however, simulate differences in annual chlorophyll cycles between stations E1 and S2 that were consistent with the difference in tidal mixing energy between the two locations.

- In the waters adjacent to the Eddystone Rocks, temperature distributions were identified that were consistent with island mixing. Such features have been identified previously for other shelf-sea regions by, for example, Simpson & Tett (1986). The observed vertical chlorophyll distributions in areas affected by island mixing were similar to those in areas of similar stratification (e.g. within the zone of the tidal front). This suggests that the light and nutrient regime resulting from island mixing is similar to the regime existing within tidal fronts. As the tidal data used for

model parameterisation did not resolve the enhanced tidal energies in the Eddystone location, the Prestidge-Taylor model was unable to provide any evidence of tidal mixing effects.

❑ *Temperature and Chlorophyll Distributions over Sub-Seasonal Scales*

- The observational database showed evidence of surface temperature variability over scales of both 1-day and ~10 days. Both the 1-day and 10-day variability were directly related to changes in meteorological forcing over the same scales. The chlorophyll data contained some evidence of chlorophyll variability over 1-day scales. Sub-seasonal variability of water column temperature and chlorophyll has been less extensively studied than the annual cycle, both due to the lower amplitude of the response, and due to the operational difficulty in collecting measurements that are resolved over these shorter scales, but examples include Kiorbe & Neilsen (1990) and Taylor & Stephens (1993) for several-day and diurnal variability respectively. The Prestidge-Taylor model predicted significant temperature and chlorophyll variability in response to meteorological forcing over scales of both 1-day and several days. However, by using spectral techniques to compare model simulations with database observations, it became clear that the model significantly overestimated the amplitude response of surface temperature variability to diurnal meteorological forcing.

This thesis has detailed the collection and processing of a consistent observational database for a given study region that resolved shelf-sea temperature and chlorophyll distributions over a range of temporal and spatial scales.

The characteristic features of temperature and chlorophyll distributions contained within the observational data have been identified by many previous studies. These distributions can mainly be explained the frequency response of vertical water-column processes forces to meteorological and tidal forcing. It is therefore appropriate to further study such features using a simple 1-dimensional physical/biological model.

The novel feature of this work has been the use of the database in the identification of the differences in performance between various scales of observed variability of an established 1-dimensional physical/biological model. Specifically, both time and

frequency domain analyses were used to identify significant differences between performance at seasonal and diurnal scales:

- Whilst the simulations of both annual and diurnal waveforms of SML water temperature were in phase with observed waveforms, the simulation of the annual waveform was significantly more accurate in terms of amplitude and rank correlation than the diurnal simulations.

- The errors in temperature simulations over diurnal scales either result from, or lead to, significant uncertainty in the stability structure of water column simulations, and therefore mixing rates between the layers.

- Amplitude errors in mixing rates over diurnal scales will lead to amplitude errors in nutrient and chlorophyll concentrations over seasonal scales, therefore bringing into doubt the validity of all nutrient and chlorophyll simulations made by the model.

In addition to the uncertainty of model simulations over diurnal scales, the model did not identify several characteristic features of the study region's temperature and chlorophyll distributions. These include features that clearly fell outside of the scope of the model, (e.g. those due to horizontal advection and island mixing). Limitations of model scope cannot be used to dismiss the failure of the model to simulate certain features, such as the summer sub-surface chlorophyll maximum, where non-optimal parameterisation and/or initialisation may be implicated.

Following the pioneering works of, for instance Pingree *et al* (1975, 1977a, 1977b, 1978), Holligan (1981), and Tett (1980) it has become established that the response of vertical processes to tidal and meteorological forcing are dominant factors in the control of shelf-sea temperature and chlorophyll distributions, especially over seasonal and spatial scales. What is less well understood, however, is the degree to which variability in physical (meteorological) forcing over smaller temporal scales (e.g. the diurnal cycle) affects the temperature, chlorophyll and nutrient distributions over larger temporal scales (e.g. the annual cycle). Several models have suggested that the annual distributions of shelf-sea temperature and chlorophyll are strongly influenced by the cumulative affects of variability over sub-seasonal scales (e.g. Ruardij *et al,* 1997, Elliot & Li, 1995, Sharples & Tett, 1994). On first inspection, tools such as the Prestidge-Taylor model seem to provide ideal methods for the estimation of the significance of such affects, which are difficult to estimate using traditional observational methods. However, such models must be validated over these smaller-scales prior to their application.

Of great current relevance is the diagnostic use of simple physical/biological shelf-sea models to address questions about the role of shelf-seas processes in climate change. Climate change in general is likely to alter the amplitude of meteorological forcing, e.g. increased frequency and intensity of storm events, as well as the underlying mean values, e.g. increased mean air temperature (IPCC, 1995). Given the importance affects of bio-chemical fluxes on climate change, and the muli-frequency characteristics of the predicted changes, models that have been validated against multiple scales of variability are required. Given the limitations of the Prestigde-Taylor model identified in this chapter, this model is not, in its present state, an appropriate tool for such detailed diagnostic applications.

Efforts to improve the performance of a given model with respect to observational databases often concern the widening of model scope to incorporate as many processes of the 'real' system as possible (e.g. Varela *et al*, 1990), or the optimisation of 'free' parameters to force a best-fit with the available observations (e.g. Fasham *et al*, 1995). The results of this project, however, suggest that an examination of model performance at multiple scales of variability using simple correlation, amplitude and phase comparisons, may provide alternative focus for model improvement without the need for increasing model complexity, as is the case with the Prestidge-Taylor model.

Index of Appendices

Appendix 1 – Tidal Ellipse Characteristics for the Study Region

M2 major axis (cm/s)

North (dec.) \ East (dec.)	-4.50	-4.42	-4.33	-4.25	-4.17	-4.08	-4.00	-3.92	-3.83
50.33	18.0	19.0	20.2	21.1	12.3	---	---	---	
50.29	20.2	21.8	23.4	25.7	30.8	31.2	26.5	16.5	
50.25	23.2	25.2	26.4	28.4	31.9	34.3	36.9	36.4	
50.21	26.1	28.3	29.7	31.6	34.7	39.4	47.8	67.2	
50.17	28.0	30.1	32.1	34.4	37.5	42.2	49.8	60.4	
50.12	30.3	32.2	34.3	36.5	39.8	44.1	49.3	56.0	
50.08	32.8	34.3	36.2	38.4	41.5	45.3	49.2	53.7	
50.04	35.0	36.4	38.1	40.2	42.9	46.2	49.5	52.9	
50.00									

M2 b/a *1000

North (dec.) \ East (dec.)	-4.50	-4.42	-4.33	-4.25	-4.17	-4.08	-4.00	-3.92	-3.83
50.33	-80	-245	-202	-95	-519	---	---	---	
50.29	-172	-191	-192	-133	-146	-58	-88	-120	
50.25	-191	-205	-194	-151	-160	-136	-116	-54	
50.21	-194	-204	-191	-162	-146	-118	-51	-76	
50.17	-177	-181	-174	-152	-129	-99	-56	-100	
50.12	-153	-158	-153	-134	-113	-86	-52	-58	
50.08	-143	-144	-136	-117	-98	-74	-41	-25	
50.04	-134	-129	-119	-103	-85	-61	-29	-4	
50.00									

M2 phase (deg)

North (dec.) \ East (dec.)	-4.50	-4.42	-4.33	-4.25	-4.17	-4.08	-4.00	-3.92	-3.83
50.33	151.1	152.8	161.1	156.5	177.8	---	---	---	
50.29	155.9	158.8	163.5	165.9	168.3	164.7	161.9	165.6	
50.25	153.9	157.4	161.0	163.7	166.4	165.8	166.2	170.3	
50.21	151.3	155.0	159.1	162.8	166.3	169.9	172.2	170.3	
50.17	150.5	154.2	158.1	161.7	165.1	168.4	170.5	173.4	
50.12	149.2	152.7	156.4	160.2	163.8	167.0	169.9	173.5	
50.08	147.8	151.3	154.9	158.6	162.0	165.3	168.3	171.5	
50.04	146.5	149.8	153.2	156.6	159.9	163.2	166.3	169.5	
50.00									

M2 phase (deg)

North (dec.) \ East (dec.)	-4.50	-4.42	-4.33	-4.25	-4.17	-4.08	-4.00	-3.92	-3.83
50.33	151.1	152.8	161.1	156.5	177.8	---	---	---	
50.29	155.9	158.8	163.5	165.9	168.3	164.7	161.9	165.6	
50.25	153.9	157.4	161.0	163.7	166.4	165.8	166.2	170.3	
50.21	151.3	155.0	159.1	162.8	166.3	169.9	172.2	170.3	
50.17	150.5	154.2	158.1	161.7	165.1	168.4	170.5	173.4	
50.12	149.2	152.7	156.4	160.2	163.8	167.0	169.9	173.5	
50.08	147.8	151.3	154.9	158.6	162.0	165.3	168.3	171.5	
50.04	146.5	149.8	153.2	156.6	159.9	163.2	166.3	169.5	
50.00									

Mean M2 Tidal Stream Amplitude (cm/s)

North (dec.) \ East (dec.)	-4.50	-4.42	-4.33	-4.25	-4.17	-4.08	-4.00	-3.92	-3.83
50.33	11.7	13.0	13.6	13.7	9.6	---	---	---	
50.29	13.4	14.6	15.7	16.9	20.4	20.1	17.2	10.8	
50.25	15.5	17.0	17.7	18.8	21.2	22.6	24.2	23.5	
50.21	17.5	19.1	19.9	21.0	22.9	25.8	31.4	43.6	
50.17	18.7	20.1	21.4	22.8	24.6	27.5	32.2	39.4	
50.12	20.0	21.3	22.7	24.0	26.0	28.7	31.8	36.2	
50.08	21.6	22.6	23.8	25.1	27.0	29.3	31.7	34.5	
50.04	23.0	23.9	24.9	26.2	27.8	29.8	31.8	34.0	
50.00									

Mean Cube M2 Tidal Stream Amplitude (x10^3 (cm/s)^3)

North (dec.) \ East (dec.)	-4.50	-4.42	-4.33	-4.25	-4.17	-4.08	-4.00	-3.92	-3.83
50.33	2.5	3.1	3.7	4.1	10.1	---	---	---	
50.29	3.6	4.6	5.7	7.4	12.8	13.2	8.1	2.0	
50.25	5.5	7.1	8.2	10.1	14.3	17.7	21.9	20.9	
50.21	7.8	10.1	11.6	13.9	18.4	26.7	50.1	132.0	
50.17	9.6	12.0	14.6	17.9	23.1	32.7	53.6	96.2	
50.12	12.1	14.6	17.7	21.2	27.5	37.3	52.0	76.3	
50.08	15.3	17.6	20.7	24.6	31.1	40.3	51.6	67.1	
50.04	18.6	20.9	24.0	28.2	34.2	42.7	52.5	64.1	
50.00									

Appendix 2 – List of Reliable AVHRR SST Overpasses

Notes

Filename is assigned by RSDAS.

WEC stands for Western English Channel (standard RSDAS PACE region); 46°N to 52°N, 8°W to 2°W.

ROI stands for Region of Interest, and is the study region; 50°00'N to 50°20'N, 4°30'W to 3°50'W.

Filename	Date	Time GMT	% WEC clear	%ROI clear
13jan970244pa:	13-Jan-97	2:44	13.1	19.4
14jan970706pa:	14-Jan-97	7:06	11.9	16.9
18jan970330pa:	18-Jan-97	3:30	8.1	14
28jan970321pa:	28-Jan-97	3:21	12.0	17.3
03feb970215pa:	3-Feb-97	2:15	12.4	22.8
03feb970356pa:	3-Feb-97	3:56	8.1	16
05feb970334pa:	5-Feb-97	3:34	28.1	31.8
05feb970725pa:	5-Feb-97	7:25	42.7	49.6
08feb970302pa:	8-Feb-97	3:02	18.9	30.3
15feb970326pa:	15-Feb-97	3:26	32.8	41.8
15feb970706pa:	15-Feb-97	7:06	30.8	30.6
20feb970412pa:	20-Feb-97	4:12	26.1	30.6
01mar970233pa:	1-Mar-97	2:33	24.3	42.1
06mar970319pa:	6-Mar-97	3:19	40.0	55.6
06mar970650pa:	6-Mar-97	6:50	11.5	18.4
20mar970227pa:	20-Mar-97	2:27	49.5	56.5
20mar970407pa:	20-Mar-97	4:07	48.0	57.8
21mar970216pa:	21-Mar-97	2:16	13.1	23.5
21mar970357pa:	21-Mar-97	3:57	12.2	19.8
22mar970346pa:	22-Mar-97	3:46	37.0	52.5
22mar970740pa:	22-Mar-97	7:40	31.0	42.1
28mar970240pa:	28-Mar-97	2:40	35.6	39.6
28mar970709pa:	28-Mar-97	7:09	34.0	38.9
29mar970229pa:	29-Mar-97	2:29	59.4	78.6
29mar970410pa:	29-Mar-97	4:10	56.8	73.3
29mar970646pa:	29-Mar-97	6:46	49.6	55.4
30mar970218pa:	30-Mar-97	2:18	34.3	44.1
30mar970359pa:	30-Mar-97	3:59	41.3	55.3
31mar970207pa:	31-Mar-97	2:07	13.5	20.7
31mar970348pa:	31-Mar-97	3:48	52.7	68.1
31mar970743pa:	31-Mar-97	7:43	52.9	69.1
01apr970337pa:	1-Apr-97	3:37	38.3	44.8
02apr970326pa:	2-Apr-97	3:26	36.5	54.3
02apr970659pa:	2-Apr-97	6:59	32.2	49
04apr970304pa:	4-Apr-97	3:04	38.9	53
04apr970755pa:	4-Apr-97	7:55	23.8	31.8
07apr970231pa:	7-Apr-97	2:31	8.3	23.1
07apr970649pa:	7-Apr-97	6:49	11.3	21.8
09apr970350pa:	9-Apr-97	3:50	16.1	20.4
10apr970339pa:	10-Apr-97	3:39	51.8	55.8
10apr970724pa:	10-Apr-97	7:24	59.9	70.2

Filename	Date	Time GMT	% WEC clear	%ROI clear
11apr970328pa:	11-Apr-97	3:28	66.5	81.2
11apr970702pa:	11-Apr-97	7:02	58.7	74
13apr970306pa:	13-Apr-97	3:06	55.5	69.1
13apr970758pa:	13-Apr-97	7:58	34.7	51
14apr970255pa:	14-Apr-97	2:55	53.3	64.6
14apr970736pa:	14-Apr-97	7:36	34.7	53.3
15apr970244pa:	15-Apr-97	2:44	56.6	69.7
15apr970714pa:	15-Apr-97	7:14	47.1	63.8
18apr970211pa:	18-Apr-97	2:11	19.6	31.4
18apr970352pa:	18-Apr-97	3:52	49.1	62.4
18apr970749pa:	18-Apr-97	7:49	46.8	64.1
22apr970308pa:	22-Apr-97	3:08	19.2	22.1
23apr970257pa:	23-Apr-97	2:57	18.6	33.6
24apr970246pa:	24-Apr-97	2:46	16.3	15.4
29apr970332pa:	29-Apr-97	3:32	22.9	38.2
30apr970321pa:	30-Apr-97	3:21	13.1	14.6
01may970310pa:	1-May-97	3:10	49.3	66
02may970259pa:	2-May-97	2:59	60.0	69.6
02may970742pa:	2-May-97	7:42	48.7	62.6
11may970301pa:	11-May-97	3:01	9.9	10.6
14may970228pa:	14-May-97	2:28	45.1	58.5
14may970409pa:	14-May-97	4:09	43.3	50.7
15may970217pa:	15-May-97	2:17	22.4	31.3
15may970358pa:	15-May-97	3:58	27.4	28.5
16may970347pa:	16-May-97	3:47	14.1	13.4
25may970208pa:	25-May-97	2:08	8.6	10.8
25may970349pa:	25-May-97	3:49	51.6	67.2
25may970738pa:	25-May-97	7:38	34.8	49.8
26may970338pa:	26-May-97	3:38	61.6	75.3
26may970716pa:	26-May-97	7:16	53.9	59.6
27may970327pa:	27-May-97	3:27	38.3	43.9
27may970654pa:	27-May-97	6:54	21.7	24.7
29may970306pa:	29-May-97	3:06	63.5	75.7
29may970751pa:	29-May-97	7:51	57.8	68.8
30may970255pa:	30-May-97	2:55	43.6	52.8
31may970244pa:	31-May-97	2:44	48.7	60.9
31may970707pa:	31-May-97	7:07	47.2	63.5
01jun970232pa:	1-Jun-97	2:32	44.1	62.5
01jun970413pa:	1-Jun-97	4:13	35.2	49
01jun970645pa:	1-Jun-97	6:45	33.3	55.4
07jun970308pa:	7-Jun-97	3:08	17.0	27.7

Filename	Date	Time GMT	% WEC clear	%ROI clear
08jun970257pa:	8-Jun-97	2:57	16.2	28.5
09jun970246pa:	9-Jun-97	2:46	16.6	18.5
22jun970345pa:	22-Jun-97	3:45	9.2	14.6
05jul970303pa:	5-Jul-97	3:03	44.0	43.1
05jul970740pa:	5-Jul-97	7:40	35.9	53.1
06jul970252pa:	6-Jul-97	2:52	28.2	43.6
06jul970718pa:	6-Jul-97	7:18	33.2	47.5
07jul970241pa:	7-Jul-97	2:41	38.1	58.2
07jul970421pa:	7-Jul-97	4:21	27.5	56.4
07jul970656pa:	7-Jul-97	6:56	28.3	50.4
08jul970229pa:	8-Jul-97	2:29	32.6	46.7
08jul970410pa:	8-Jul-97	4:10	36.4	53.4
09jul970218pa:	9-Jul-97	2:18	17.6	30.5
09jul970359pa:	9-Jul-97	3:59	36.9	48.4
10jul970348pa:	10-Jul-97	3:48	33.8	44.4
11jul970338pa:	11-Jul-97	3:38	14.4	24.8
13jul970316pa:	13-Jul-97	3:16	5.3	14.9
18jul970220pa:	18-Jul-97	2:20	15.9	26.4
18jul970401pa:	18-Jul-97	4:01	41.2	48.2
18jul970755pa:	18-Jul-97	7:55	37.5	46.5
19jul970350pa:	19-Jul-97	3:50	48.8	56.7
19jul970733pa:	19-Jul-97	7:33	39.1	49.1
22jul970318pa:	22-Jul-97	3:18	50.2	67
23jul970307pa:	23-Jul-97	3:07	6.1	13.4
28jul970352pa:	28-Jul-97	3:52	16.2	26.5
29jul970341pa:	29-Jul-97	3:41	28.9	39.6
29jul970714pa:	29-Jul-97	7:14	14.3	26.8
30jul970652pa:	30-Jul-97	6:52	10.6	17.5
13aug970418pa:	13-Aug-97	4:18	25.3	43.8
14aug970226pa:	14-Aug-97	2:26	21.3	16.5
14aug970407pa:	14-Aug-97	4:07	19.0	22.5
15aug970356pa:	15-Aug-97	3:56	15.3	21.7
15aug970741pa:	15-Aug-97	7:41	14.2	24.7
16aug970345pa:	16-Aug-97	3:45	37.2	40.3
16aug970719pa:	16-Aug-97	7:19	19.3	26.2
18aug970323pa:	18-Aug-97	3:23	7.2	14.7
29aug970303pa:	29-Aug-97	3:03	10.0	14.2
01sep970411pa:	1-Sep-97	4:11	12.1	68.5
02sep970219pa:	2-Sep-97	2:19	4.8	10.7
04sep970338pa:	4-Sep-97	3:38	23.1	33.1
04sep970702pa:	4-Sep-97	7:02	22.3	33.3
06sep970316pa:	6-Sep-97	3:16	19.3	31.9
10sep970232pa:	10-Sep-97	2:32	32.4	36.5
10sep970413pa:	10-Sep-97	4:13	24.2	24
13sep970340pa:	13-Sep-97	3:40	15.4	20
16sep970307pa:	16-Sep-97	3:07	29.7	44.9
17sep970717pa:	17-Sep-97	7:17	8.5	12.2
18sep970245pa:	18-Sep-97	2:45	22.5	30.6
18sep970425pa:	18-Sep-97	4:25	12.5	21.3
18sep970655pa:	18-Sep-97	6:55	26.7	34.3
23sep970331pa:	23-Sep-97	3:31	18.6	17.3
24sep970320pa:	24-Sep-97	3:20	33.9	32.4
25sep970309pa:	25-Sep-97	3:09	34.5	37.6
25sep970741pa:	25-Sep-97	7:41	20.2	26
26sep970719pa:	26-Sep-97	7:19	17.7	27

Filename	Date	Time GMT	% WEC clear	%ROI clear
27sep970427pa:	27-Sep-97	4:27	9.3	20.7
27sep970657pa:	27-Sep-97	6:57	15.6	19.2
05oct970722pa:	5-Oct-97	7:22	27.3	34.9
10oct970712pa:	10-Oct-97	7:12	21.8	31.6
13oct970312pa:	13-Oct-97	3:12	10.9	15.1
14oct970301pa:	14-Oct-97	3:01	8.2	15.7
18oct970358pa:	18-Oct-97	3:58	23.9	36.9
18oct970737pa:	18-Oct-97	7:37	24.7	34
19oct970347pa:	19-Oct-97	3:47	34.7	38.6
24oct970705pa:	24-Oct-97	7:05	10.2	13.5
25oct970241pa:	25-Oct-97	2:41	14.9	15.2
27oct970400pa:	27-Oct-97	4:00	11.7	15.4
29oct970338pa:	29-Oct-97	3:38	22.9	39.7
29oct970655pa:	29-Oct-97	6:55	17.5	20.5
31oct970316pa:	31-Oct-97	3:16	11.2	13.9
31oct970751pa:	31-Oct-97	7:51	30.3	28.7
01nov970305pa:	1-Nov-97	3:05	30.1	42.2
01nov970729pa:	1-Nov-97	7:29	23.8	36.4
02nov970254pa:	2-Nov-97	2:54	9.8	20.1
02nov970707pa:	2-Nov-97	7:07	9.3	11.9
19nov970734pa:	19-Nov-97	7:34	12.9	24.8
02dec970406pa:	2-Dec-97	4:06	8.9	20.2
02dec970749pa:	2-Dec-97	7:49	13.9	17.6
03dec970355pa:	3-Dec-97	3:55	18.0	32
03dec970727pa:	3-Dec-97	7:27	16.7	34.9
04dec970344pa:	4-Dec-97	3:44	12.1	20.7
12dec970357pa:	12-Dec-97	3:57	16.9	20.8
12dec970729pa:	12-Dec-97	7:29	16.0	26.5
14dec970335pa:	14-Dec-97	3:35	7.8	15
14dec970645pa:	14-Dec-97	6:45	14.4	23.7
18dec970657pa:	18-Dec-97	6:57	20.3	23.3
19dec970240pa:	19-Dec-97	2:40	16.8	22.1
19dec970420pa:	19-Dec-97	4:20	15.9	21.8

Appendix 3 – Standard Boat Track Logistics

Parameter	Value	Parameter	Value
Track length	100 km	Position of S1	50°15'N, 4°11'W
Number of bottle casts	4	Position of S2	50°10'N 3°58' W
Total time taken	8 hr 15 min	Position of E1	50°02'N 4°22'W
Steaming along track	6 hr	Position of L4	50°15'N 4°13'W
Steaming to start point	45 min	Position of PlyMBODy	50°13'N 4°05'W
Steaming from end point	45 min	Distance S1 to S2	24 km
Time for each bottle cast	15 min	Distance S2 to E1	33 km
		Distance E1 to L4	29 km

Appendix 4 - R.V. Squilla; Ship's Data

Type	Specification	Type	Specification
Length	19.5 m	*Gantry*	Fixed stern A-frame, SWL 10 T
Breadth	5.7 m	*Winch*	Twin drum traction winch, SWL 3 T
Draft	3.0 m	*Winch storage*	500 m of 14 mm cable
Displacement	73 T	*Laboratory*	15 m^2
Endurance	5 days at 10 kts	*Navigation*	Shipmate DGPS navigator
Propulsion	326 BHP diesel, variable pitch prop.		Shipmate RS2500 plotter
Crew	4		FUSO 200 and 814 echosounders
Cranage	Starboard Hi-Ab crane, SWL 1 T, extension 4 m		Racian 41XXX radar

Appendix 5 – Field Programme Sampling Events Track Plots

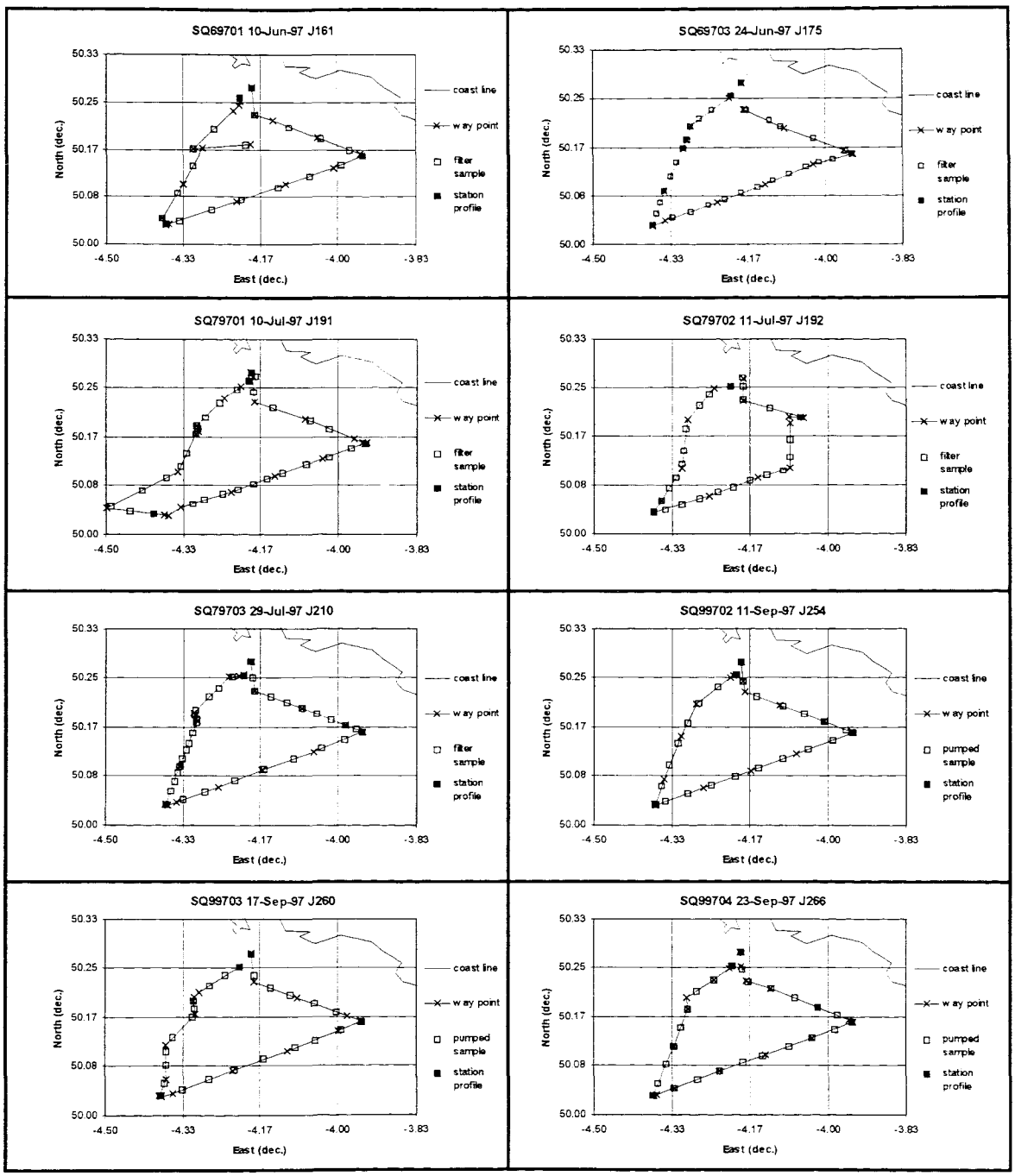

Appendix 6 – Field Programme Sampling Events Scientific Log

Cruise	*Time*	*Longitude*	*Latitude*	*Depth*	*Activity*	*Comment*
SQ69701	Normal track. L5 meter net. E1 meter net.					
10-Jun-97	08 30	Sutton Harbour			Depart	
	09 31	50o 16.56' N	4o 11.18' W	52.0	S1 station	Water bottles
	09 44	50o 16.56' N	4o 11.11' W	52.0	Leg 1	UOR deployed
	10 05	50o 13.62' N	4o 10.69' W		Leg 1	
	10 15	50o 13.03' N	4o 08.44' W		Leg 1	
	10 43	50o 11.26' N	4o 02.60' W	62.0	Leg 1	
	11 12	50o 09.51' N	3o 57.13' W	62.0	Leg 1	UOR recovered
	11 17	50o 09.36' N	3o 56.88' W	62.0	S2 station	Water bottles
	11 27	50o 09.32' N	3o 56.87' W	62.0	Leg 2	UOR deployed
	11 45	50o 08.01' N	4o 00.54' W	66.0	Leg 2	
	12 15	50o 06.36' N	4o 06.73' W	71.0	Leg 2	
	12 45	50o 04.57' N	4o 13.12' W	73.0	Leg 2	
	13 26	50o 02.08' N	4o 21.95' W	74.0	Leg 2	UOR recovered
	13 30	50o 02.03' N	4o 22.25' W	74.0	E1 station	Water bottles
	14 00	50o 02.75' N	4o 22.79' W	74.0	Leg 3	UOR deployed
	14 30	50o 06.30' N	4o 20.11' W	71.0	Leg 3	
	15 00	50o 10.11' N	4o 17.45' W	61.0	Leg 3	
	15 03	50o 10.51' N	4o 11.27' W	61.0	Leg 3	UOR recovered
	15 25	50o 10.07' N	4o 18.72' W	60.0	Leg 3	UOR deployed
	16 00	50o 14.07' N	4o 13.45' W	54.0	Leg 3	
	16 05	50o 14.64' N	4o 12.68' W	53.0	Leg 3	UOR recovered
	16 10	50o 15.04' N	4o 12.65' W	53.0	L4 station	
	15 20	Sutton Harbour			Return	
SQ69703	Normal track. L5 meter net.					
24-Jun-97	Wind - W 1 to 2. Sea - slight. Sky - overcast.					
	7:20	Sutton Harbour			Depart	
	8:17	50o 16.54' N	4o 10.80' W	52.0	S1 station	Water bottles
	8:30	50o 16.54' N	4o 10.85' W	52.0	Leg 1	UOR deployed
	8:43	50o 13.90'N	4o 10.60' W	58.0	Leg 1	A/C
	9:17	50o 11.95' N	4o 05.40' W	59.0	Leg 1	
	9:43	50o 09.61' N	3o 57.55' W	62.0	Leg 1	
	9:51	50o 09.29' N	3o 56.61' W	63.0	Leg 1	UOR recovered
	9:51	50o 09.29' N	3o 56.61' W	63.0	S2 station	Water bottles
	10:00	50o 09.25' N	3o 56.47' W	63.0	Leg 2	UOR deployed
	10:00	50o 09.25' N	3o 56.47' W	63.0	Leg 2	A/C
	10:30	50o 08.20' N	4o 01.69' W	66.0	Leg 2	
	11:00	50o 06.19' N	4o 07.83' W	71.0	Leg 2	
	11:30	50o 04.28' N	4o 14.06' W	73.0	Leg 2	
	12:00	50o 02.44' N	4o 20.77' W	73.0	Leg 2	
	12:10	50o 01.89' N	4o 22.32' W	74.0	Leg 2	UOR recovered
	12:10	50o 01.89' N	4o 22.32' W	74.0	E1 station	Water bottles
	12:15	50o 01.91' N	4o 22.33' W	74.0	Leg 3	UOR deployed
	12:15	50o 01.91' N	4o 22.33' W	74.0	Leg 3	A/C
	12:45	50o 05.48' N	4o 20.86' W	70.0	Leg 3	
	13:15	50o 09.85' N	4o 18.37' W	60.0	Leg 3	
	13:25	50o 10.70' N	4o 17.89' W	59.0	Leg 3	UOR recovered
	13:57	50o 12.19' N	4o 17.39' W	59.0	Leg 3	UOR deployed

Cruise	*Time*	*Longitude*	*Latitude*	*Depth*	*Activity*	*Comment*
	14:30	50o 15.07' N	4o 12.44' W	52.0	Leg 3	UOR recovered
	14:30	50o 15.07' N	4o 12.44' W	52.0	L4 staton	Water bottles
	16:00	Sutton Harbour			Return	
SQ79701 10-Jul-97	Normal track. E1 meter net. L5 meter net. 09:00: Wind - E 3 to 4. Sea - slight. Sky - overcast. 12:00: Wind - E 5 to 6. Sea - moderate. Sky - mainly clear.					
	8:00	Sutton Harbour			Depart	
	8:59	50° 16.56' N	4° 11.24' W	51.5	S1 station	Water bottles
	9:09	50° 16.59' N	4° 11.19' W	51.7	Leg 1	UOR deployed
	9:30	50° 13.64' N	4° 10.76' W	58.1	Leg 1	
	10:00	50° 11.81' N	4° 04.28' W	61.7	Leg 1	
	10:30	50° 09.83' N	3° 57.90' W	63.0	Leg 1	
	10:38	50° 09.46' N	3° 56.75' W	62.0	Leg 1	UOR recovered
	10:43	50° 09.35' N	3° 56.55' W	62.0	S2 station	Water bottles
	10:50	50° 09.37' N	3° 56.30' W	62.9	Leg 2	UOR deployed
	11:20	50° 07.74' N	4° 02.07' W	68.0	Leg 2	
	11:50	50° 06.06' N	4° 08.16' W	72.0	Leg 2	
	12:20	50° 04.38' N	4° 13.78' W	73.0	Leg 2	
	12:53	50° 02.83' N	4° 20.33' W	74.0	Leg 2	
	13:03	50° 01.98' N	4° 21.99' W	74.0	Leg 2	UOR recovered
	13:08	50° 02.01' N	4° 22.39' W	74.0	E1 station	Water bottles
	13:45	50° 02.72' N	4° 29.92' W	74.0	Leg 3	UOR deployed
	14:15	50° 06.38' N	4° 20.77' W	71.0	Leg 3	
	14:45	50° 10.27' N	4° 18.30' W	60.0	Leg 3	
	14:48	50° 10.56' N	4° 17.93' W	60.0	Leg 3	UOR recovered
	15:16	50° 11.19' N	4° 18.26' W	59.6	Leg 3	UOR deployed
	15:45	50° 13.97' N	4° 14.60' W	52.1	Leg 3	
	15:58	50° 15.13' N	4° 12.55' W	52.0	Leg 3	UOR recovered
	15:58	50° 15.13' N	4° 12.55' W	52.0	L4 station	Water bottles
	17:00	Sutton Harbour			return	
SQ79702 11-Jul-97	Track in reverse direction. Reduced length due lack of time. Wind - ESE 1 to 2. Sea - slight. Sky - overcast.					
	9:10	Sutton Harbour			depart	
	10:14	50° 15.14' N	4° 12.52' W	55.9	L4 station	Water bottles
	10:21	50° 15.16' N	4° 12.55' W	55.9	Leg 3	UOR deployed
	10:30	50° 14.91' N	4° 14.62' W	56.1	Leg 3	
	10:58	50° 11.72' N	4° 18.04' W	60.1	Leg 3	
	11:33	50° 06.75' N	4° 18.76' W	73.0	Leg 3	
	12:00	50° 03.38' N	4° 21.39' W	74.0	Leg 3	
	12:09	50° 02.28' N	4° 22.35' W	75.8	Leg 3	UOR recovered
	12:09	50° 02.28' N	4° 22.35' W	75.8	E1 station	Water bottles
	12:19	50° 02.20' N	4° 22.31' W	75.6	Leg 2	UOR deployed
	12:50	50° 03.90' N	4° 15.32' W	73.3	Leg 2	
	13:20	50° 05.77' N	4° 09.01' W	71.8	Leg 2	
	13:39	50° 06.77' N	4° 04.97' W	68.5	Leg 2	AC
	14:10	50° 11.35' N	4° 05.00' W	61.0	Towing	
	14:15	50° 12.03' N	4° 05.13' W	60.0	Towing	UOR recovered
	14:15	50° 12.03' N	4° 05.13' W	60.0	PlyMBODy	Water bottles
	14:28	50° 11.93' N	4° 03.29' W	60.0	Leg 1	UOR deployed
	14:55	50° 13.70' N	4° 10.87' W	55.3	Leg 1	
	15:10	50° 15.93' N	4° 10.99' W	50.0	Leg 1	UOR recovered
	16:10	Sutton Harbour			Return	

Cruise	*Time*	*Longitude*	*Latitude*	*Depth*	*Activity*	*Comment*
SQ79703	Normal track. L5 meter net.					
29-Jul-97	09:00: Wind - ESE 1 to 2. Sea - calm. Sky - clear. 12:00: Wind - SSE 1 to 2.					
	8:20	Sutton Harbour			depart	
	9:22	50o 16.55' N	4o 11.15' W	48.9	S1 station	Water bottles
	9:29	50o 16.54' N	4o 11.32' W	49.4	Leg 1	UOR deployed
	9:50	50o 13.58' N	4o 10.76' W	55.4	Leg 1	
	10:20	50o 11.78' N	4o 04.63' W	60.8	Leg 1	
	10:50	50o 10.12' N	3o 59.02' W	62.0	Leg 1	
	11:06	50o 09.43' N	3o 56.81' W	61.6	Leg 1	UOR recovered
	11:09	50o 09.43' N	3o 56.81' W	61.6	S2 station	Water bottles
	11:15	50o 09.39' N	3o 56.96' W	61.4	Leg 2	UOR deployed
	11:45	50o 07.43' N	4o 03.10' W	63.5	Leg 2	
	12:15	50o 05.57' N	4o 09.78' W	72.9	Leg 2	
	12:46	50o 03.88' N	4o 15.35' W	72.5	Leg 2	
	13:15	50o 02.32' N	4o 20.85' W	75.5	Leg 2	
	13:20	50o 02.06' N	4o 22.01' W	76.0	Leg 2	UOR recovered
	13:26	50o 02.09' N	4o 22.33' W	76.8	E1 station	Water bottles
	13:33	50o 02.14' N	4o 22.14' W	76.0	Leg 3	UOR deployed
	14:00	50o 06.00' N	4o 20.41' W	72.9	Leg 3	
	14:30	50o 10.55' N	4o 18.14' W	63.4	Leg 3	UOR recovered
	15:03	50o 11.37' N	4o 18.64' W	62.9	Leg 3	UOR deployed
	15:33	50o 14.96' N	4o 13.99' W	55.0	Leg 3	
	15:40	50o 15.07' N	4o 12.83' W	55.0	Leg 3	UOR recovered
	15:45	50o 15.14' N	4o 12.20' W	55.0	L4 station	Water bottles
	16:45	Sutton Harbour			return	
SQ99702	Normal track					
11-Sep-97	09:00: Wind - SE 1 to 2. Sea - slight. Sky - overcast. 12:00: Wind - SW 1 to 2.					
	8:00	Sutton Harbour			depart	
	9:06	50o 16.58' N	4o 11.19' W	50.1	S1 station	Water bottles
	9:16	50o 16.59' N	4o 11.22' W	50.1	Leg 1	UOR deployed
	9:30	50o 14.64' N	4o 10.96' W	53.5	Leg 1	
	9:37	50o 13.56' N	4o 10.73' W	57.0	Leg 1	
	10:00	50o 12.27' N	4o 06.24' W	60.0	Leg 1	
	10:30	50o 10.61' N	4o 00.58' W	62.0	Leg 1	
	10:48	50o 09.55' N	3o 57.12' W	61.8	Leg 1	UOR recovered
	10:52	50o 09.47' N	3o 56.81' W	61.8	S2 station	Water bottles
	10:58	50o 09.40' N	3o 56.85' W	61.5	Leg 2	UOR deployed
	11:32	50o 07.31' N	4o 04.14' W	68.3	Leg 2	
	12:00	50o 05.57' N	4o 09.92' W	72.8	Leg 2	
	12:30	50o 03.77' N	4o 15.97' W	74.6	Leg 2	
	13:02	50o 02.01' N	4o 22.10' W	76.0	Leg 2	UOR recovered
	13:06	50o 02.13' N	4o 22.15' W	76.1	E1 station	Water bottles
	13:13	50o 02.18' N	4o 22.09' W	76.0	Leg 3	UOR deployed
	13:30	50o 04.65' N	4o 21.02' W	74.3	Leg 3	
	14:00	50o 09.01' N	4o 18.87' W	64.5	Leg 3	
	14:24	50o 12.35' N	4o 16.88' W	61.0	Leg 3	
	14:49	50o 15.00' N	4o 12.62' W	54.4	Leg 3	UOR recovered
	14:54	50o 15.20' N	4o 12.19' W	54.4	L4 station	Water bottles
	16:00	Sutton Harbour			return	
SQ99703	Normal track. L5 meter net.					
17-Sep-97	Wind - E light. Sea - slight. Sky - clear.					
	8:00	Sutton Harbour			depart	
	9:05	50o 16.55' N	4o 11.22' W	51.2	S1 station	Water bottles
	9:15	50o 16.39' N	4o 11.18' W	51.6	Leg 1	UOR deployed

	9:33	50o 13.63' N	4o 10.75' W	56.8	Leg 1	
	10:00	50o 11.99' N	4o 05.21' W	60.2	Leg 1	
	10:30	50o 10.10' N	3o 58.85' W	62.0	Leg 1	
	10:39	50o 09.57' N	3o 57.03' W	60.1	Leg 1	UOR recovered
	10:42	50o 09.49' N	3o 56.96' W	60.1	S2 station	Water bottles
	10:47	50o 09.47' N	3o 57.04' W	59.0	Leg 2	UOR deployed
	11:00	50o 08.51' N	3o 59.89' W	60.0	Leg 2	
	11:30	50o 06.54' N	4o 06.48' W	68.0	Leg 2	
	12:00	50o 04.59' N	4o 13.55' W	70.8	Leg 2	
	12:31	50o 02.24' N	4o 21.39' W	71.6	Leg 2	
	12:38	50o 01.91' N	4o 22.85' W	72.2	Leg 2	UOR recovered
	12:41	50o 02.00' N	4o 22.87' W	72.2	E1 station	Water bottles
	12:47	50o 02.00' N	4o 23.12' W	72.2	Leg 3	UOR deployed
	13:00	50o 03.70' N	4o 22.20' W	71.0	Leg 3	
	13:30	50o 07.22' N	4o 22.23' W	67.7	Leg 3	
	13:54	50o 10.27' N	4o 18.40' W	59.7	Leg 3	UOR recovered
	14:23	50o 11.63' N	4o 18.60' W	58.9	Leg 3	UOR deployed
	14:26	50o 12.02' N	4o 18.53' W	58.7	Leg 3	
	14:30	50o 12.51' N	4o 17.86' W	58.1	Leg 3	
	15:04	50o 15.15' N	4o 12.66' W	51.5	Leg 3	UOR recovered
	15:06	50o 15.15' N	4o 12.66' W	51.5	L4 station	Water bottles
	16:10	Sutton Harbour			Return	
SQ99704	Normal track					
23-Sep-97	Wind - E 4 to 5. Sea - slight to moderate. Sky - mostly clear.					
	8:15	Sutton Harbour			depart	
	9:13	50o 16.58' N	4o 11.18' W	51.0	S1 station	Water bottles
	9:22	50o 16.57' N	4o 11.28' W	51.3	Leg 1	UOR deployed
	9:30	50o 15.15' N	4o 11.15' W	55.5	Leg 1	
	9:44	50o 13.65' N	4o 10.57' W	57.6	Leg 1	
	10:00	50o 12.89' N	4o 07.40' W	58.6	Leg 1	
	10:30	50o 10.96' N	4o 01.44' W	61.5	Leg 1	
	10:54	50o 09.68' N	3o 57.26' W	61.1	Leg 1	UOR recovered
	10:57	50o 09.52' N	3o 56.89' W	61.1	S2 station	Water bottles
	11:03	50o 09.49' N	3o 56.87' W	61.1	Leg 2	UOR deployed
	11:30	50o 07.83' N	4o 02.17' W	67.0	Leg 2	
	12:00	50o 06.12' N	4o 08.07' W	72.2	Leg 2	
	12:30	50o 04.49' N	4o 13.85' W	74.4	Leg 2	
	13:00	50o 02.68' N	4o 19.69' W	75.0	Leg 2	
	13:11	50o 02.00' N	4o 21.97' W	75.5	Leg 2	UOR recovered
	13:14	50o 01.93' N	4o 22.37' W	75.7	E1 station	Water bottles
	13:20	50o 01.96' N	4o 22.48' W	75.5	Leg 3	UOR deployed
	14:00	50o 07.03' N	4o 19.74' W	71.0	Leg 3	
	14:30	50o 10.80' N	4o 18.01' W	62.0	Leg 3	
	14:37	50o 11.99' N	4o 18.08' W	60.0	Leg 3	
	15:00	50o 13.81' N	4o 14.68' W	54.2	Leg 3	
	15:13	50o 14.98' N	4o 12.64' W	53.2	Leg 3	UOR recovered
	15:17	50o 15.13' N	4o 12.39' W	53.1	L4 station	
	16:30	Sutton Harbour			Return	

Appendix 7 – Field Programme Sampling Events Water Sampling Logs.

Date	Time gmt	Depth (m)	Vial
SQ69701	8:40	pump	10.06.97 u1
10-Jun-97	9:05	pump	10.06.97 u2
	9:25	pump	10.06.97 u3
	9:45	pump	10.06.97 u4
	10:05	pump	10.06.97 u5
	10:20	pump	10.06.97 u6
	10:40	pump	10.06.97 u7
	11:00	pump	10.06.97 u8
	11:20	pump	10.06.97 u9
	11:42	pump	10.06.97 u10
	12:00	pump	10.06.97 u11
	12:20	pump	10.06.97 u12
	12:35	pump	10.06.97 u13
	13:00	pump	10.06.97 u14
	13:23	pump	10.06.97 u15
	13:45	pump	10.06.97 u16
	14:05	pump	10.06.97 u17
	14:25	pump	10.06.97 u18
	14:43	pump	10.06.97 u19
	15:15	pump	10.06.97 u20
	8:35	5	10.06.97 p1
	""	40	10.06.97 p2
	""	pump	10.06.97 u1
	10:20	40	10.06.97 p3
	""	5	10.06.97 p4
	""	pump	10.06.97 u6
	12:35	40	10.06.97 p5
	""	5	10.06.97 p6
	""	pump	10.06.97 u13
	15:15	40	10.06.97 p7
	""	5	10.06.97 p8
	""	pump	10.06.97 u20
SQ69703	8:27	pump	24.06.97 u1
24-Jun-97	8:45	pump	24.06.97 u2
	9:05	pump	24.06.97 u3
	9:15	pump	24.06.97 u4
	9:30	pump	24.06.97 u5
	9:45	pump	24.06.97 u6
	10:00	pump	24.06.97 u7
	10:15	pump	24.06.97 u8
	10:25	pump	24.06.97 u9
	10:35	pump	24.06.97 u10
	10:45	pump	24.06.97 u11
	10:55	pump	24.06.97 u12
	11:05	pump	24.06.97 u13
	11:15	pump	24.06.97 u14
	11:25	pump	24.06.97 u15
	11:35	pump	24.06.97 u16
	11:45	pump	24.06.97 u17
	11:55	pump	24.06.97 u18

Date	Time gmt	Depth (m)	Vial
	12:15	pump	24.06.97 u19
	12:25	pump	24.06.97 u20
	12:35	pump	24.06.97 u21
	12:45	pump	24.06.97 u22
	12:55	pump	24.06.97 u23
	13:05	pump	24.06.97 u24
	13:15	pump	24.06.97 u25
	13:25	pump	24.06.97 u26
	13:55	pump	24.06.97 u27
	14:05	pump	24.06.97 u28
	14:15	pump	24.06.97 u29
	14:32	pump	24.06.97 u30
	8:27	40	24.06.97 p1
	""	5	24.06.97 p2
	""	pump	24.06.97 u1
	10:00	40	24.06.97 p3
	""	5	24.06.97 p4
	""	pump	24.06.97 u7
	12:15	40	24.06.97 p5
	""	5	24.06.97 p6
	""	pump	24.06.97 u19
	14:32	40	24.06.97 p7
	""	5	24.06.97 p8
	""	pump	24.06.97 u30
SQ79701	8:11	pump	10.07.97 u1
10-Jul-97	8:23	pump	10.07.97 u2
	8:41	pump	10.07.97 u3
	9:03	pump	10.07.97 u4
	9:15	pump	10.07.97 u5
	9:47	pump	10.07.97 u6
	10:00	pump	10.07.97 u7
	10:15	pump	10.07.97 u8
	10:30	pump	10.07.97 u9
	10:45	pump	10.07.97 u10
	10:55	pump	10.07.97 u11
	11:05	pump	10.07.97 u12
	11:15	pump	10.07.97 u13
	11:25	pump	10.07.97 u14
	11:37	pump	10.07.97 u15
	11:45	pump	10.07.97 u16
	12:30	pump	10.07.97 u17
	12:47	pump	10.07.97 u18
	13:00	pump	10.07.97 u19
	13:10	pump	10.07.97 u20
	13:20	pump	10.07.97 u21
	13:30	pump	10.07.97 u22
	13:45	pump	10.07.97 u23
	14:02	pump	10.07.97 u24
	14:15	pump	10.07.97 u25
	14:25	pump	10.07.97 u26

Date	Time gmt	Depth (m)	Vial
	14:40	pump	10.07.97 u27
	14:55	pump	10.07.97 u28
	15:10	pump	10.07.97 u29
	8:05	40	10.07.97 p1
	""	5	10.07.97 p2
	""	pump	10.07.97 u1
	9:45	40	10.07.97 p3
	""	5	10.07.97 p4
	""	pump	10.07.97 u6
	12:15	40	10.07.97 p5
	""	5	10.07.97 p6
	""	1	10.07.97 p7
	15:05	40	10.07.97 p8
	""	5	10.07.97 p9
	""	pump	10.07.97 u29
SQ79702	9:18	pump	11.07.97 u1
11-Jul-97	9:35	pump	11.07.97 u2
	9:45	pump	11.07.97 u3
	10:05	pump	11.07.97 u4
	10:20	pump	11.07.97 u5
	10:30	pump	11.07.97 u6
	10:40	pump	11.07.97 u7
	10:50	pump	11.07.97 u8
	11:00	pump	11.07.97 u9
	11:15	pump	11.07.97 u10
	11:26	pump	11.07.97 u11
	11:35	pump	11.07.97 u12
	11:45	pump	11.07.97 u13
	11:56	pump	11.07.97 u14
	12:05	pump	11.07.97 u15
	12:15	pump	11.07.97 u16
	12:25	pump	11.07.97 u17
	12:35	pump	11.07.97 u18
	12:47	pump	11.07.97 u19
	12:59	pump	11.07.97 u20
	13:25	pump	11.07.97 u22
	13:43	pump	11.07.97 u23
	13:55	pump	11.07.97 u24
	14:05	pump	11.07.97 u25
	14:11	pump	11.07.97 u26
	9:16	40	11.07.97 p1
	""	5	11.07.97 p2
	""	pump	11.07.97 u1
	11:15	40	11.07.97 p3
	""	5	11.07.97 p4
	""	pump	11.07.97 u10
	13:25	40	11.07.97 p5
	""	5	11.07.97 p6
	""	pump	11.07.97 u22
SQ79703	8:26	pump	29.07.97 u1
29-Jul-97	8:41	pump	29.07.97 u2
	8:50	pump	29.07.97 u3
	9:00	pump	29.07.97 u4
	9:10	pump	29.07.97 u5

Date	Time gmt	Depth (m)	Vial
	9:20	pump	29.07.97 u6
	9:30	pump	29.07.97 u7
	9:40	pump	29.07.97 u8
	9:50	pump	29.07.97 u9
	10:00	pump	29.07.97 u10
	10:15	pump	29.07.97 u11
	10:26	pump	29.07.97 u12
	10:40	pump	29.07.97 u13
	10:57	pump	29.07.97 u14
	11:14	pump	29.07.97 u15
	11:35	pump	29.07.97 u16
	11:55	pump	29.07.97 u17
	12:10	pump	29.07.97 u18
	12:30	pump	29.07.97 u19
	12:42	pump	29.07.97 u20
	12:49	pump	29.07.97 u21
	12:55	pump	29.07.97 u22
	13:00	pump	29.07.97 u23
	13:05	pump	29.07.97 u24
	13:10	pump	29.07.97 u25
	13:15	pump	29.07.97 u26
	13:22	pump	29.07.97 u27
	13:29	pump	29.07.97 u28
	13:37	pump	29.07.97 u29
	13:55	pump	29.07.97 u30
	14:05	pump	29.07.97 u31
	14:16	pump	29.07.97 u32
	14:24	pump	29.07.97 u33
	14:35	pump	29.07.97 u34
	14:45	pump	29.07.97 u35
	8:26	40	29.07.97 p1
	""	5	29.07.97 p2
	""	pump	29.07.97 u1
	10:12	40	29.07.97 p3
	""	5	29.07.97 p4
	""	pump	29.07.97 u11
	12:30	40	29.07.97 p5
	""	5	29.07.97 p6
	""	pump	29.07.97 u19
	14:45	40	29.07.97 p7
	""	5	29.07.97 p8
	""	pump	29.07.97 u35
SQ99702	8:14	pump	11.09.97 u1
11-Sep-97	8:30	pump	11.09.97 u2
	8:45	pump	11.09.97 u3
	9:02	pump	11.09.97 u4
	9:16	pump	11.09.97 u5
	9:30	pump	11.09.97 u6
	9:45	pump	11.09.97 u7
	9:55	pump	11.09.97 u8
	10:10	pump	11.09.97 u9
	10:25	pump	11.09.97 u10
	10:40	pump	11.09.97 u11
	10:55	pump	11.09.97 u12

Date	Time gmt	Depth (m)	Vial
	11:10	pump	11.09.97 u13
	11:25	pump	11.09.97 u14
	11:40	pump	11.09.97 u15
	11:55	pump	11.09.97 u16
	12:10	pump	11.09.97 u17
	12:25	pump	11.09.97 u18
	12:40	pump	11.09.97 u19
	12:55	pump	11.09.97 u20
	13:10	pump	11.09.97 u21
	13:25	pump	11.09.97 u22
	13:40	pump	11.09.97 u23
	13:58	pump	11.09.97 u24
	8:10	40	11.09.97 p1
	""	5	11.09.97 p2
	""	pump	11.09.97 u1
	9:55	40	11.09.97 p3
	""	5	11.09.97 p4
	""	pump	11.09.97 u8
	12:10	40	11.09.97 p5
	""	5	11.09.97 p6
	""	pump	11.09.97 u17
	13:58	40	11.09.97 p7
	""	5	11.09.97 p8
	""	pump	11.09.97 u24
SQ99703	8:13	pump	17.09.97 u1
17-Sep-97	8:29	pump	17.09.97 u2
	8:43	pump	17.09.97 u3
	8:56	pump	17.09.97 u4
	9:10	pump	17.09.97 u5
	9:24	pump	17.09.97 u6
	9:44	pump	17.09.97 u7
	9:58	pump	17.09.97 u8
	10:14	pump	17.09.97 u9
	10:25	pump	17.09.97 u10
	10:43	pump	17.09.97 u11
	10:59	pump	17.09.97 u12
	11:12	pump	17.09.97 u13
	11:26	pump	17.09.97 u14
	11:43	2	17.09.97 p7
	11:57	pump	17.09.97 u15
	12:12	pump	17.09.97 u16
	12:24	pump	17.09.97 u17
	12:36	pump	17.09.97 u18
	12:52	pump	17.09.97 u19
	13:08	pump	17.09.97 u20
	13:23	pump	17.09.97 u21
	13:39	pump	17.09.97 u22
	13:52	pump	17.09.97 u23
	14:08	pump	17.09.97 u24
	8:13	40	17.09.97 p1
	""	5	17.09.97 p2
	""	pump	17.09.97 u1
	9:44	40	17.09.97 p3
	""	5	17.09.97 p4

Date	Time gmt	Depth (m)	Vial
	""	pump	17.09.97 u7
	11:43	40	17.09.97 p5
	""	5	17.09.97 p6
	""	2	17.09.97 p7
	14:08	40	17.09.97 p8
	""	5	17.09.97 p9
	""	pump	17.09.97 u24
SQ99704	8:22	pump	23.09.97 u1
23-Sep-97	8:33	pump	23.09.97 u2
	8:45	pump	23.09.97 u3
	9:00	pump	23.09.97 u4
	9:15	pump	23.09.97 u5
	9:30	pump	23.09.97 u6
	9:45	pump	23.09.97 u7
	10:00	pump	23.09.97 u8
	10:15	pump	23.09.97 u9
	10:30	pump	23.09.97 u10
	10:45	pump	23.09.97 u11
	11:02	pump	23.09.97 u12
	11:15	pump	23.09.97 u13
	11:30	pump	23.09.97 u14
	11:45	pump	23.09.97 u15
	12:00	pump	23.09.97 u16
	12:16	pump	23.09.97 u17
	12:30	pump	23.09.97 u18
	12:45	pump	23.09.97 u19
	13:00	pump	23.09.97 u20
	13:15	pump	23.09.97 u21
	13:30	pump	23.09.97 u22
	13:45	pump	23.09.97 u23
	14:00	pump	23.09.97 u24
	14:19	pump	23.09.97 u25
	8:17	40	23.09.97 p1
	""	5	23.09.97 p2
	""	pump	23.09.97 u1
	10:00	40	23.09.97 p3
	""	5	23.09.97 p4
	""	pump	23.09.97 u8
	12:16	40	23.09.97 p5
	""	5	23.09.97 p6
	""	pump	23.09.97 u17
	14:19	40	23.09.97 p8
	""	5	23.09.97 p9
	""	pump	23.09.97 u25

Appendix 8 – Uor Wing Angle Programme

```
                        GENERAL INFORMATION
                        -------------------
Minimum Depth:    3
Maximum Depth:   40
Present Depth:    0
Crank angle   : 121

Speed in sectors 1 - 30 when climbing.                    total (sec)
Sectors  1  2  3  4  5  6  7  8  9 10 11 12 13 14 15
Times    5  2  2  2  2  2  3  3  4  5  6  7  8  9 10

Sectors 16 17 18 19 20 21 22 23 24 25 26 27 28 29 30
Times   10  9  8  7  6  5  4  3  3  2  2  2  2  2  5  140
sec

Speed in sectors 1 - 30 when diving.
Sectors  1  2  3  4  5  6  7  8  9 10 11 12 13 14 15
Times    5  2  2  2  2  2  3  3  4  5  6  7  8  9 10

Sectors 16 17 18 19 20 21 22 23 24 25 26 27 28 29 30
Times   10  9  8  7  6  5  4  3  3  2  2  2  2  2  5  140
sec

                      Hit any key to return to Menu
                        PML Servo Controller IEB.96
                      ---------------------------------
```

Appendix 9 – UOR Instrument Calibration Coefficients

Instrumentation deployed in the UOR for each sampling event from June to September 1997 is listed in Table 1. Table 1 indicated that 3 sensor cylinders were used during these sampling events. The calibration coefficients for depth and temperature for each cylinder are listed in Table 2a (temperature) and 2b (depth). In addition, two logger cylinders were used, and the calibration coefficients listed in Table 3a (JA10) and 3b (JA6). Light meter calibrations in table 4a and 4b were supplied by Mr G. Moore. A combined pitch and roll calibration coefficient was determined from a number of calibration exercises, which are not listed here. The combined logger / sensor coefficients used for each event are listed in tables 5a to f. These coefficients are copied into CALSYS.CMD 'SYSTAT' basic code, listed in appendix 10.

Event	*Date*	*JDAY*	*Sensor*	*Logger*	*Servo*	*T-miss*	*Light*
SQ69701	10-Jun-97	161	JA4	JA10	S3	Chelsea	I/R 002
SQ79701	10-Jul-97	191	JA4	JA10	S3	Chelsea	I/R 002
SQ79702	11-Jul-97	192	JA4	JA10	S3	Chelsea	I/R 002
SQ79703	29-Jul-97	210	JA4	JA6	S2	Chelsea	I/R 002
SQ99702	11-Sep-97	254	ARE1	JA6	S5	SeaTech	I/R 002
SQ99703	17-Sep-97	260	ARE1	JA6	S5	SeaTech	I/R 002
SQ99704	23-Sep-97	266	ARE1	JA6	S5	SeaTech	I/R 002

TABLE 1 - UOR Instrumentation Used During 1997 Sampling Events

ARE 1 Temperature 19/05/97 (LoggerJA6)			
(x^0)*(x^1)	-0.181527	**x^0 (i.e. c)**	**1.6242699**
1/x^1	0.1117588	**x^1 (i.e. m)**	**8.9478379**
Pearson correlation (R^2)			0.9999734
Standard error of temperature (°C)			0.0278528
Standard error of digital counts			0.0031129
Temp JA4 4/8/97			
(x^0)*(x^1)	0.0052648	**x^0 (i.e. c)**	**-0.046555**
1/x^1	0.1130887	**x^1 (i.e. m)**	**8.8426153**
Pearson correlation (R^2)			0.9999883
Standard error of temperature (°C)			0.0279969
Standard error of output (V)			0.0031662

TABLE 2a - temperature coefficients

Depth ARE1 1/8/97			
(x^0)*(x^1)	-0.037528	**x^0 (i.e. c)**	**-2.477235**
1/x^1	-0.015149	**x^1 (i.e. m)**	**-66.00972**
Pearson correlation (R^2)			-0.999976
Standard error of depth (m)			0.2341294
Standard error of output (V)			0.003547
Depth JA4 1/8/97			
(x^0)*(x^1)	-0.011313	**x^0 (i.e. c)**	**-0.740052**
1/x^1	-0.015286	**x^1 (i.e. m)**	**-65.41862**
Pearson correlation (R^2)			-0.999982
Standard error of depth (m)			0.1998242
Standard error of output (V)			0.0030546

TABLE 2b - depth coefficients

JA10 10BIT 27/7/97 signals 1, 4, 5			
(x^0)*(x^1)	35.482101	**x^0 (i.e. c)**	**-0.005371**
1/x^1	6606.1453	**x^1 (i.e. m)**	**0.0001514**
Pearson correlation (R^2)			0.9999969
Standard error of input (V)			0.0038767
Standard error of output (counts)			25.610025
JA10 10BIT 27/7/97 signals 20, 21			
(x^0)*(x^1)	-2.353237	**x^0 (i.e. c)**	**0.0003563**
1/x^1	6604.6463	**x^1 (i.e. m)**	**0.0001514**
Pearson correlation (R^2)			0.999998
Standard error of input (V)			0.0031064
Standard error of output (counts)			20.516492
JA10 12BIT 27/7/97			
(x^0)*(x^1)	22.46398	**x^0 (i.e. c)**	**-0.003426**
1/x^1	6557.7503	**x^1 (i.e. m)**	**0.0001525**
Pearson correlation (R^2)			0.9999949
Standard error of input (V)			0.004924
Standard error of output (counts)			32.290237

TABLE 3a - Logger JA10 coefficients

JA6 10BIT 13/9/97			
(x^0)*(x^1)	8.5922838	**x^0 (i.e. c)**	**-0.001296**
1/x^1	6630.5225	**x^1 (i.e. m)**	**0.0001508**
Pearson correlation (R^2)			0.9999958
Standard error of input (V)			0.0046829
Standard error of output (counts)			31.050344
JA6 12BIT 13/9/97 not signal 3			
(x^0)*(x^1)	10.320389	**x^0 (i.e. c)**	**-0.001571**
1/x^1	6568.5022	**x^1 (i.e. m)**	**0.0001522**
Pearson correlation (R^2)			0.9999994
Standard error of input (V)			0.0018527
Standard error of output (counts)			12.169394
JA6 12BIT 13/9/97 signal 3			
(x^0)*(x^1)	14.72704	**x^0 (i.e. c)**	**-0.002248**
1/x^1	6551.5804	**x^1 (i.e. m)**	**0.0001526**
Pearson correlation (R^2)			0.9999996
Standard error of input (V)			0.0015716
Standard error of output (counts)			10.296187

TABLE 3b - Logger JA6 coefficients

OCR-200 002, 18-Mar-97							
Wavelength (mid, nm)	412.5	443.1	490.7	510.5	555.2	669.9	682.9
Coefficients	5.87E-01	5.87E-01	5.82E-01	3.55E-01	3.55E-01	2.33E-01	2.40E-01
Dark mV	9.40E-01	1.30E+00	9.50E-01	9.20E-01	9.60E-01	8.50E-01	1.18E+00
Imersion correction	1.75E-03	1.74E-03	1.74E-03	1.73E-03	1.73E-03	1.72E-03	1.72E-03
x^0 (i.e. c)	**-9.65E-04**	**-1.33E-03**	**-9.62E-04**	**-5.66E-04**	**-5.89E-04**	**-3.41E-04**	**-4.86E-04**
x^1 (i.e. m)	**1.03E+00**	**1.02E+00**	**1.01E+00**	**6.15E-01**	**6.13E-01**	**4.01E-01**	**4.12E-01**

TABLE 4a - Light meter calibration; $L_u(\lambda)$

OCI-200 002, 18-Mar-97							
Wavelength (mid, nm)	412.5	443.1	490.7	510.5	555.2	669.9	682.9
Coefficients	1.35E+01	1.43E+01	1.43E+01	1.43E+01	1.47E+01	1.44E+01	1.47E+01
Dark mV	7.50E-01	9.60E-01	8.20E-01	1.03E+00	1.16E+00	8.90E-01	8.40E-01
Imersion correction	1.75E-03	1.74E-03	1.74E-03	1.73E-03	1.73E-03	1.72E-03	1.72E-03
x^0 (i.e. c)	**-1.77E-02**	**-2.39E-02**	**-2.04E-02**	**-2.55E-02**	**-2.95E-02**	**-2.20E-02**	**-2.12E-02**
x^1 (i.e. m)	**2.36E+01**	**2.49E+01**	**2.49E+01**	**2.48E+01**	**2.55E+01**	**2.48E+01**	**2.52E+01**

TABLE 4a - Light meter calibration; $E_d(\lambda)$

Channel	*Bit*	*Signal*	*Logg x^0*	*Logg x^1*	*Sens x^0*	*Sens x^1*	*Comb x^0*	*Comb x^1*
1	10	**Depth**	-5.371E-03	1.514E-04	-7.401E-01	-6.542E+01	**-3.887E-01**	**-9.903E-03**
2	12	**Temp**	-3.426E-03	1.525E-04	-4.735E-02	8.844E+00	**-7.764E-02**	**1.349E-03**
3	12	**Cond**	-3.426E-03	1.525E-04			**-3.426E-03**	**1.525E-04**
4	10	**Fluor**	-5.371E-03	1.514E-04			**-5.371E-03**	**1.514E-04**
5	10	**T-miss**	-5.371E-03	1.514E-04			**-5.370E-03**	**1.510E-04**
6	12	**E_d(412)**	-3.426E-03	1.525E-04	-1.771E-02	2.361E+01	**-9.857E-02**	**3.600E-03**
7	12	**E_d(443)**	-3.426E-03	1.525E-04	-2.389E-02	2.488E+01	**-1.091E-01**	**3.794E-03**
8	12	**E_d(490)**	-3.426E-03	1.525E-04	-2.045E-02	2.493E+01	**-1.059E-01**	**3.802E-03**
9	12	**E_d(510)**	-3.426E-03	1.525E-04	-2.552E-02	2.477E+01	**-1.104E-01**	**3.778E-03**
10	12	**E_d(555)**	-3.426E-03	1.525E-04	-2.954E-02	2.547E+01	**-1.168E-01**	**3.883E-03**
11	12	**E_d(665)**	-3.426E-03	1.525E-04	-2.203E-02	2.475E+01	**-1.068E-01**	**3.774E-03**
12	12	**E_d(683)**	-3.426E-03	1.525E-04	-2.121E-02	2.525E+01	**-1.077E-01**	**3.850E-03**
13	12	**L_u(412)**	-3.426E-03	1.525E-04	-9.653E-04	1.027E+00	**-4.483E-03**	**1.566E-04**
14	12	**L_u(443)**	-3.426E-03	1.525E-04	-1.328E-03	1.021E+00	**-4.826E-03**	**1.557E-04**
15	12	**L_u(490)**	-3.426E-03	1.525E-04	-9.624E-04	1.013E+00	**-4.433E-03**	**1.545E-04**
16	12	**L_u(510)**	-3.426E-03	1.525E-04	-5.657E-04	6.148E-01	**-2.672E-03**	**9.376E-05**
17	12	**L_u(555)**	-3.426E-03	1.525E-04	-5.889E-04	6.135E-01	**-2.690E-03**	**9.355E-05**
18	12	**L_u(665)**	-3.426E-03	1.525E-04	-3.406E-04	4.008E-01	**-1.713E-03**	**6.111E-05**
19	12	**L_u(683)**	-3.426E-03	1.525E-04	-4.861E-04	4.119E-01	**-1.897E-03**	**6.282E-05**
20	10	**Pitch**	3.563E-04	1.514E-04			**7.160E+01**	**4.375E-03**
21	10	**Roll**	3.563E-04	1.514E-04			**7.160E+01**	**4.375E-03**

Logg = logger; Sens = sensor; Comb = combined logger and sensor.

TABLE 5a - UOR calibration coefficients used for SQ69701, SQ69703 and SQ79701.

Channel	Bit	***Signal***	Logg x^0	Logg x^1	Sens x^0	Sens x^1	Comb x^0	Comb x^1
1	10	**Depth**	-5.371E-03	1.514E-04	-7.401E-01	-6.542E+01	-3.887E-01	-9.903E-03
2	12	**Temp**	-3.426E-03	1.525E-04	-4.735E-02	8.844E+00	-7.764E-02	1.349E-03
3	12	**Cond**	-3.426E-03	1.525E-04			-5.371E-03	1.514E-04
4	10	**Fluor**	-5.371E-03	1.514E-04			-5.371E-03	1.514E-04
5	10	**T-miss**	-5.371E-03	1.514E-04			-5.370E-03	1.510E-04
6	12	**E_d(412)**	-3.426E-03	1.525E-04	-1.771E-02	2.361E+01	-9.857E-02	3.600E-03
7	12	**E_d(443)**	-3.426E-03	1.525E-04	-2.389E-02	2.488E+01	-1.091E-01	3.794E-03
8	12	**E_d(490)**	-3.426E-03	1.525E-04	-2.045E-02	2.493E+01	-1.059E-01	3.802E-03
9	12	**E_d(510)**	-3.426E-03	1.525E-04	-2.552E-02	2.477E+01	-1.104E-01	3.778E-03
10	12	**E_d(555)**	-3.426E-03	1.525E-04	-2.954E-02	2.547E+01	-1.168E-01	3.883E-03
11	12	**E_d(665)**	-3.426E-03	1.525E-04	-2.203E-02	2.475E+01	-1.068E-01	3.774E-03
12	12	**E_d(683)**	-3.426E-03	1.525E-04	-2.121E-02	2.525E+01	-1.077E-01	3.850E-03
13	12	**L_u(412)**	-3.426E-03	1.525E-04	-9.653E-04	1.027E+00	-4.483E-03	1.566E-04
14	12	**L_u(443)**	-3.426E-03	1.525E-04	-1.328E-03	1.021E+00	-4.826E-03	1.557E-04
15	12	**L_u(490)**	-3.426E-03	1.525E-04	-9.624E-04	1.013E+00	-4.433E-03	1.545E-04
16	12	**L_u(510)**	-3.426E-03	1.525E-04	-5.657E-04	6.148E-01	-2.672E-03	9.376E-05
17	12	**L_u(555)**	-3.426E-03	1.525E-04	-5.889E-04	6.135E-01	-2.690E-03	9.355E-05
18	12	**L_u(665)**	-3.426E-03	1.525E-04	-3.406E-04	4.008E-01	-1.713E-03	6.111E-05
19	12	**L_u(683)**	-3.426E-03	1.525E-04	-4.861E-04	4.119E-01	-1.897E-03	6.282E-05
20	10	**Pitch**	3.563E-04	1.514E-04			7.160E+01	-4.375E-03
21	10	**Roll**	3.563E-04	1.514E-04			7.160E+01	-4.375E-03

Logg = logger; Sens = sensor; Comb = combined logger and sensor.

TABLE 5b - UOR calibration coefficients used for SQ79702

Channel	Bit	***Signal***	Logg x^0	Logg x^1	Sens x^0	Sens x^1	Comb x^0	Comb x^1
1	10	**Depth**	-1.296E-03	1.508E-04	-7.401E-01	-6.542E+01	-6.553E-01	-9.866E-03
2	12	**Temp**	-1.571E-03	1.522E-04	-4.735E-02	8.844E+00	-6.124E-02	1.346E-03
3	12	**Cond**	-2.248E-03	1.526E-04			-2.248E-03	1.526E-04
4	10	**Fluor**	-1.296E-03	1.508E-04			-1.296E-03	1.508E-04
5	10	**T-miss**	-1.296E-03	1.508E-04			-1.296E-03	1.508E-04
6	12	**E_d(412)**	-1.571E-03	1.522E-04	-1.771E-02	2.361E+01	-5.480E-02	3.594E-03
7	12	**E_d(443)**	-1.571E-03	1.522E-04	-2.389E-02	2.488E+01	-6.298E-02	3.788E-03
8	12	**E_d(490)**	-1.571E-03	1.522E-04	-2.045E-02	2.493E+01	-5.962E-02	3.796E-03
9	12	**E_d(510)**	-1.571E-03	1.522E-04	-2.552E-02	2.477E+01	-6.444E-02	3.772E-03
10	12	**E_d(555)**	-1.571E-03	1.522E-04	-2.954E-02	2.547E+01	-6.955E-02	3.877E-03
11	12	**E_d(665)**	-1.571E-03	1.522E-04	-2.203E-02	2.475E+01	-6.092E-02	3.768E-03
12	12	**E_d(683)**	-1.571E-03	1.522E-04	-2.121E-02	2.525E+01	-6.088E-02	3.844E-03
13	12	**L_u(412)**	-1.571E-03	1.522E-04	-9.653E-04	1.027E+00	-2.579E-03	1.563E-04
14	12	**L_u(443)**	-1.571E-03	1.522E-04	-1.328E-03	1.021E+00	-2.932E-03	1.555E-04
15	12	**L_u(490)**	-1.571E-03	1.522E-04	-9.624E-04	1.013E+00	-2.554E-03	1.542E-04
16	12	**L_u(510)**	-1.571E-03	1.522E-04	-5.657E-04	6.148E-01	-1.532E-03	9.360E-05
17	12	**L_u(555)**	-1.571E-03	1.522E-04	-5.889E-04	6.135E-01	-1.553E-03	9.339E-05
18	12	**L_u(665)**	-1.571E-03	1.522E-04	-3.406E-04	4.008E-01	-9.703E-04	6.101E-05
19	12	**L_u(683)**	-1.571E-03	1.522E-04	-4.861E-04	4.119E-01	-1.133E-03	6.271E-05
20	10	**Pitch**	-1.296E-03	1.508E-04			7.160E+01	-4.375E-03
21	10	**Roll**	-1.296E-03	1.508E-04			7.160E+01	-4.375E-03

Logg = logger; Sens = sensor; Comb = combined logger and sensor.

TABLE 5c - UOR calibration coefficients used for SQ79703

Channel	Bit	*Signal*	Logg x^0	Logg x^1	Sens x^0	Sens x^1	Comb x^0	Comb x^1
1	10	**Depth**	-1.296E-03	1.508E-04	-2.477E+00	-6.601E+01	-2.392E+00	-9.955E-03
2	12	**Temp**	-1.571E-03	1.522E-04	1.624E+00	8.948E+00	1.610E+00	1.362E-03
3	12	**Cond**	-2.248E-03	1.526E-04			-2.248E-03	1.526E-04
4	10	**Fluor**	-1.296E-03	1.508E-04			-1.296E-03	1.508E-04
5	10	**T-miss**	-1.296E-03	1.508E-04			-1.296E-03	1.508E-04
6	12	**E_d(412)**	-1.571E-03	1.522E-04	-1.771E-02	2.361E+01	-5.480E-02	3.594E-03
7	12	**E_d(443)**	-1.571E-03	1.522E-04	-2.389E-02	2.488E+01	-6.298E-02	3.788E-03
8	12	**E_d(490)**	-1.571E-03	1.522E-04	-2.045E-02	2.493E+01	-5.962E-02	3.796E-03
9	12	**E_d(510)**	-1.571E-03	1.522E-04	-2.552E-02	2.477E+01	-6.444E-02	3.772E-03
10	12	**E_d(555)**	-1.571E-03	1.522E-04	-2.954E-02	2.547E+01	-6.955E-02	3.877E-03
11	12	**E_d(665)**	-1.571E-03	1.522E-04	-2.203E-02	2.475E+01	-6.092E-02	3.768E-03
12	12	**E_d(683)**	-1.571E-03	1.522E-04	-2.121E-02	2.525E+01	-6.088E-02	3.844E-03
13	12	**L_u(412)**	-1.571E-03	1.522E-04	-9.653E-04	1.027E+00	-2.579E-03	1.563E-04
14	12	**L_u(443)**	-1.571E-03	1.522E-04	-1.328E-03	1.021E+00	-2.932E-03	1.555E-04
15	12	**L_u(490)**	-1.571E-03	1.522E-04	-9.624E-04	1.013E+00	-2.554E-03	1.542E-04
16	12	**L_u(510)**	-1.571E-03	1.522E-04	-5.657E-04	6.148E-01	-1.532E-03	9.360E-05
17	12	**L_u(555)**	-1.571E-03	1.522E-04	-5.889E-04	6.135E-01	-1.553E-03	9.339E-05
18	12	**L_u(665)**	-1.571E-03	1.522E-04	-3.406E-04	4.008E-01	-9.703E-04	6.101E-05
19	12	**L_u(683)**	-1.571E-03	1.522E-04	-4.861E-04	4.119E-01	-1.133E-03	6.271E-05
20	10	**Pitch**	-1.296E-03	1.508E-04			7.160E+01	-4.375E-03
21	10	**Roll**	-1.296E-03	1.508E-04			7.160E+01	-4.375E-03

Logg = logger; Sens = sensor; Comb = combined logger and sensor.

TABLE 5f - UOR calibration coefficients used for SQ99702, SQ99703 and SQ99704

Appendix 10 – Computer Code used for UOR Data Processing

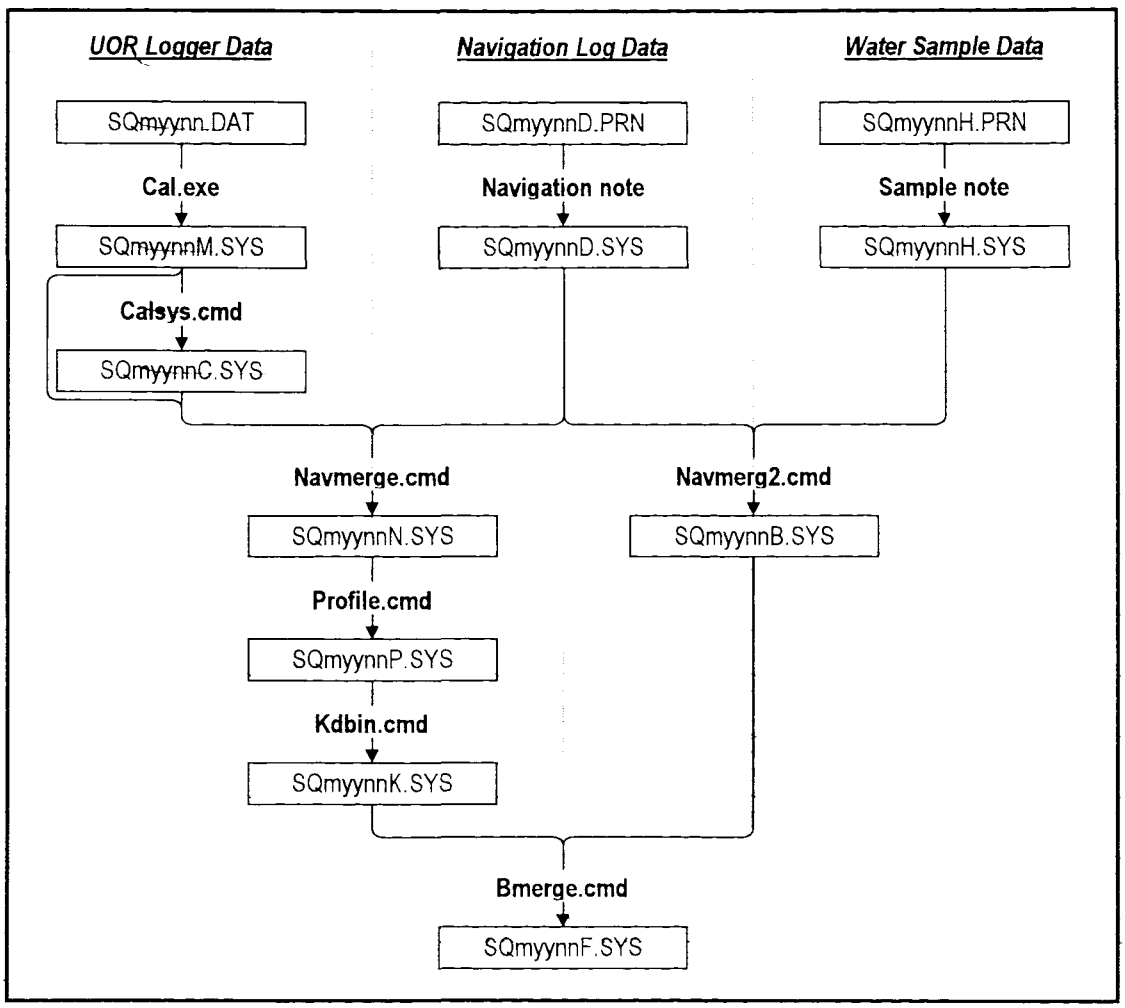

File naming protocol and processing schematic

The 'SYSTAT basic' code for processing UOR data (to Sqmyynnk.SYS) is listed over the following pages. The functionality of Calsys.cmd, Navmake.cmd, Navmerge.cmd, Profile.cmd and Kdbin.cmd are described. Cal.exe is a DOS executable programme written by G.F. Moore. A processing scheme for the water sample data is being developed.

Navigation note - The input file, SQmmyynnD.PRN, must be an ASCII text file with data arranged in space delimited columns with headings as follows; TIMEDEC (decimal time in GMT), EAST (decimal longitude), NORTH (decimal latitude), DEPTH (wter depth in meters). This file can be directly imported into SYSTAT and saved as SYSTAT format.

Samples note - SQmmyynnH.PRN is as for SQmmyynnD.PRN, with headings as follows; TIMEDEC (decimal time in GMT), DEPTH_W (depth from which the water was taken, meters), IVFLUO (chlorophyll concentration determined by *in vitro* fluorescence, mg m^{-3}), HPLC (Chlorophyll-a concentration determined by HPLC, mg m^{-3}.

```
rem  ---------------
rem |
rem |   CALSYS.CMD
rem  ---------------
rem apply calibration coefficients to each logger
channel, calculate the natural logarithm of light data,
and convert pitch and roll into tilt.
DATA
    rem edit**********************************
    USE 'C:\PHDDATA\UOR\SQmyynn\SQmyynnM.SYS'
    SAVE  C:\PHDDATA\UOR\SQmyynn SQmyynnC.SYS'
    rem ***************************************

rem apply calibrations to input channels
rem channels 1-2 = depth (m), temperature (deg C)
    LET DEPT  = -0.3886838826 + 1.009902691* DEPT
    LET TEMP  = -0.07764413079 + 1.001348628 * TEMP
rem channels 3-5 = conductivity (Volts), fluorescence
(Volts),
rem transmission (Volts)
    LET COND  = -0.003425562 + 0.000152491 * COND
    LET FLUO  = -0.005371075 + 0.000151374 * FLUO
    LET TMIS  = -0.005371075 + 0.000151374 * TMIS
rem channels 6-12 = downwelling irradiance (muW cm^-2)
    LET ED412 = -0.098574580 + 0.003599939 * ED412
    LET ED443 = -0.109121554 + 0.003794289 * ED443
    LET ED490 = -0.105859690 + 0.003802249 * ED490
    LET ED510 = -0.110380311 + 0.003777759 * ED510
    LET ED555 = -0.116774085 + 0.003883283 * ED555
    LET ED670 = -0.106813612 + 0.003774282 * ED670
    LET ED700 = -0.107703734 + 0.003850345 * ED700
rem channels 13-19 = upwelling radiance (muW cm^-2 sr^-1
    LET LU412 = -0.004482596 + 0.000156e93 * LU412
    LET LU443 = -0.004825772 + 0.000155725 * LU443
    LET LU490 = -0.004432567 + 0.000154478 * LU490
    LET LU510 = -0.002671834 + 0.000093758 * LU510
    LET LU555 = -0.002690[illegible] + 0.000093547 * LU555
    LET LU670 = -0.001713474 + 0.000061112 * LU670
    LET LU683 = -0.001897221 + 0.000062817 * LU683
rem channels 20-21 = roll (deg), pitch (deg)
    LET ROLL  = 71.6000  + [illegible]4375    * ROLL
    LET PITC  = 71.6000  + [illegible]4375    * PITC
rem end applying calibrations

rem calculate the natural log of the light measurements
    LET LU412L = log(LU412)
    LET LU443L = log(LU443)
    LET LU490L = log(LU490)
    LET LU510L = log(LU510)
    LET LU555L = log(LU555)
    LET LU683L = log(LU683)
    LET ED412L = log(ED412)
    LET ED443L = log(ED443)
    LET ED490L = log(ED490)
    LET ED510L = log(ED510)
    LET ED555L = log(ED555)
    LET ED670L = log(ED670)
rem end calculating logs

rem convert pitch and roll into tilt
    LET TILT = (ACS(1/(((TAN(PITC*0.01745))^2)
           + ((TAN(ROLL*0.01745))^2)+1)^0.5))*57.296
rem end converting

RUN
rem end CALSYS.CMD

rem  ---------------
rem |               |
rem | NAVMAKE3.CMD  |
rem |               |
rem  ---------------

rem this programme takes the way point data and uses
these to create a file which can be merged with the UOR
data file, or similar data files, using the merge
variable TOD_M, which is decimal hours GMT to 2 decimal
places. Also calculated are the grid cell, water bottle
station, track leg and track merge variable, KM_TRAK,
which is distance along the normal track in km.
DATA
    rem edit**********************************
    USE 'C:\PHDDATA\UOR\SQmyynn SQmyynnD.SYS'
    rem ***************************************
SAVE TEMP1

rem calculate change in east, north, depth with time;
d(var)/dt.
    LET NEXTTIME = TIMEDEC
    LET TIMEDEC  = LAG(TIMEDEC)
    LET NEXTEAST = EAST
    LET NEXTNOR  = NORTH
    LET NEXTDEP  = DEPTH
    LET EAST     = LAG(EAST)
    LET NORTH    = LAG(NORTH)
    LET DEPTH    = LAG(DEPTH)
rem delete the first record
    IF CASE = 1 THEN FOR
        LET NEXTEAST = .
        LET NEXTNOR  = .
        LET NEXTDEP  = .
        LET NEXTTIME = .
    NEXT
    LET M_EAST  = (EAST-NEXTEAST)/(TIMEDEC-NEXTTIME)
    LET M_NORTH = (NORTH-NEXTNOR)/(TIMEDEC-NEXTTIME)
    LET M_DEPTH = (DEPTH-NEXTDEP)/(TIMEDEC-NEXTTIME)
rem End calculating d(var)/dt.
DROP NEXTEAST NEXTNOR NEXTTIME NEXTDEP

rem round timedec variable to 2 d.p. New variable called
tod_m. The tod_m variable is used for merging files
w.r.t. time.
    IF (TIMEDEC*100)-INT(TIMEDEC*100)>0.5 THEN,
        LET TOD_M = (INT(TIMEDEC*100)+1)/100
    ELSE,
        LET TOD_M = (INT(TIMEDEC*100))/100
rem end rounding.
RUN
rem Merge navigation file (temp1) with grid file (one),
w.r.t. time. 'One' consists of a single variable:
0=<tod_m>24 with an interval of 0.01.
    USE ONE TEMP1  TOD_M
    SAVE TEMP2
rem End merging
RUN
DATA
    USE TEMP2
    SAVE TEMP3
    HOLD

rem The merged file has missing values of east, north and
depth. These are calculated from the d(var)/dt variables.
I.e. linear interpolation.
    IF EAST <>. THEN FOR
        LET T = TIMEDEC
        LET E = EAST
        LET N = NORTH
        LET ME = M_EAST
        LET MN = M_NORTH
        LET D = DEPTH
        LET MD = M_DEPTH
    NEXT
    ELSE FOR
        LET T=T
        LET E=E
        LET N=N
        LET ME=ME
        LET MN=MN
        LET D=D
        LET MD=MD
    NEXT
    LET EAST = ME*(TOD_M-T)+E
    LET NORTH = MN*(TOD_M-T)+N
    LET DEPTH = MD*(TOD_M-T)+D
rem End linear interpolate

rem Add tidal model data relevant to each record. There
are 64 possible areas.
IF EAST > -4.500 AND EAST <= -4.417 THEN FOR
    IF NORTH<50.3333 AND NORTH>50.2917 THEN,
        LET AREA$='AA'
    ELSE IF NORTH<50.2917 AND NORTH>50.2500 THEN,
        LET AREA$='AB'
    ELSE IF NORTH<50.2500 AND NORTH>50.2083 THEN,
        LET AREA$='AC'
    ELSE IF NORTH<50.2083 AND NORTH>50.1667 THEN,
        LET AREA$='AD'
    ELSE IF NORTH<50.1667 AND NORTH>50.1250 THEN,
        LET AREA$='AE'
    ELSE IF NORTH<50.1250 AND NORTH>50.0833 THEN,
        LET AREA$='AF'
    ELSE IF NORTH<50.0833 AND NORTH>50.0417 THEN,
        LET AREA$='AG'
    ELSE IF NORTH<50.0417 AND NORTH>50.0000 THEN,
        LET AREA$='AH'
    ELSE LET AREA$=''
NEXT
IF EAST > -4.417 AND EAST <= -4.333 THEN FOR
    IF NORTH<50.3333 AND NORTH>50.2917 THEN,
        LET AREA$='BA'
    ELSE IF NORTH<50.2917 AND NORTH>50.2500 THEN,
        LET AREA$='BB'
    ELSE IF NORTH<50.2500 AND NORTH>50.2083 THEN,
        LET AREA$='BC'
    ELSE IF NORTH<50.2083 AND NORTH>50.1667 THEN,
        LET AREA$='BD'
    ELSE IF NORTH<50.1667 AND NORTH>50.1250 THEN,
        ET AREA$='BE'
    ELSE IF NORTH<50.1250 AND NORTH>50.0833 THEN,
        LET AREA$='BF'
    ELSE IF NORTH<50.0833 AND NORTH>50.0417 THEN,
        LET AREA$='BG'
    ELSE IF NORTH<50.0417 AND NORTH>50.0000 THEN,
        LET AREA$='BH'
    ELSE LET AREA$=''
NEXT
IF EAST > -4.333 AND EAST <= -4.250 THEN FOR
    IF NORTH<50.3333 AND NORTH>50.2917 THEN LET
AREA$='CA'
    ELSE IF NORTH<50.2917 AND NORTH>50.2500 THEN,
        LET AREA$='CB'
    ELSE IF NORTH<50.2500 AND NORTH>50.2083 THEN
        LET AREA$='CC'
    ELSE IF NORTH<50.2083 AND NORTH>50.1667 THEN
        LET AREA$='CD'
    ELSE IF NORTH<50.1667 AND NORTH>50.1250 THEN
        LET AREA$='CE'
    ELSE IF NORTH<50.1250 AND NORTH>50.0833 THEN
        LET AREA$='CF'
    ELSE IF NORTH<50.0833 AND NORTH>50.0417 THEN
        LET AREA$='CG'
    ELSE IF NORTH<50.0417 AND NORTH>50.0000 THEN
        LET AREA$='CH'
    ELSE LET AREA$=''
NEXT
IF EAST > -4.250 AND EAST <= -4.167 THEN FOR
    IF NORTH<50.3333 AND NORTH>50.2917 THEN,
        LET AREA$='DA'
    ELSE IF NORTH<50.2917 AND NORTH>50.2500 THEN,
        LET AREA$='DB'
    ELSE IF NORTH<50.2500 AND NORTH>50.2083 THEN,
        LET AREA$='DC'
    ELSE IF NORTH<50.2083 AND NORTH>50.1667 THEN,
        LET AREA$='DD'
    ELSE IF NORTH<50.1667 AND NORTH>50.1250 THEN,
        LET AREA$='DE'
    ELSE IF NORTH<50.1250 AND NORTH>50.0833 THEN,
```

```
        LET AREA$='DF'
    ELSE IF NORTH<50.0833 AND NORTH>50.0417 THEN,
        LET AREA$='DG'
    ELSE IF NORTH<50.0417 AND NORTH>50.0000 THEN,
        LET AREA$='DH'
    ELSE LET AREA$=''
NEXT
IF EAST > -4.167 AND EAST <= -4.083 THEN FOR
    IF NORTH<50.3333 AND NORTH>50.2917 THEN,
        LET AREA$='EA'
    ELSE IF NORTH<50.2917 AND NORTH>50.2500 THEN,
        LET AREA$='EB'
    ELSE IF NORTH<50.2500 AND NORTH>50.2083 THEN,
        LET AREA$='EC'
    ELSE IF NORTH<50.2083 AND NORTH>50.1667 THEN,
        LET AREA$='ED'
    ELSE IF NORTH<50.1667 AND NORTH>50.1250 THEN,
        LET AREA$='EE'
    ELSE IF NORTH<50.1250 AND NORTH>50.0833 THEN,
        LET AREA$='EF'
    ELSE IF NORTH<50.0833 AND NORTH>50.0417 THEN,
        LET AREA$='EG'
    ELSE IF NORTH<50.0417 AND NORTH>50.0000 THEN,
        LET AREA$='EH'
    ELSE LET AREA$=''
NEXT
IF EAST > -4.083 AND EAST <= -4.000 THEN FOR
    IF NORTH<50.3333 AND NORTH>50.2917 THEN,
        LET AREA$='FA'
    ELSE IF NORTH<50.2917 AND NORTH>50.2500 THEN,
        LET AREA$='FB'
    ELSE IF NORTH<50.2500 AND NORTH>50.2083 THEN,
        LET AREA$='FC'
    ELSE IF NORTH<50.2083 AND NORTH>50.1667 THEN,
        LET AREA$='FD'
    ELSE IF NORTH<50.1667 AND NORTH>50.1250 THEN,
        LET AREA$='FE'
    ELSE IF NORTH<50.1250 AND NORTH>50.0833 THEN,
        LET AREA$='FF'
    ELSE IF NORTH<50.0833 AND NORTH>50.0417 THEN,
        LET AREA$='FG'
    ELSE IF NORTH<50.0417 AND NORTH>50.0000 THEN,
        LET AREA$='FH'
    ELSE LET AREA$=''
NEXT
IF EAST > -4.000 AND EAST <= -3.917 THEN FOR
    IF NORTH<50.3333 AND NORTH>50.2917 THEN,
        LET AREA$='GA'
    ELSE IF NORTH<50.2917 AND NORTH>50.2500 THEN
        LET AREA$='GB'
    ELSE IF NORTH<50.2500 AND NORTH>50.2083 THEN,
        LET AREA$='GC'
    ELSE IF NORTH<50.2083 AND NORTH>50.1667 THEN,
        LET AREA$='GD'
    ELSE IF NORTH<50.1667 AND NORTH>50.1250 THEN,
        LET AREA$='GE'
    ELSE IF NORTH<50.1250 AND NORTH>50.0833 THEN,
        LET AREA$='GF'
    ELSE IF NORTH<50.0833 AND NORTH>50.0417 THEN,
        LET AREA$='GG'
    ELSE IF NORTH<50.0417 AND NORTH>50.0000 THEN,
        LET AREA$='GH'
    ELSE LET AREA$=''
NEXT
IF EAST > -3.917 AND EAST <= -3.833 THEN FOR
    IF NORTH<50.3333 AND NORTH>50.2917 THEN,
        LET AREA$='HA'
    ELSE IF NORTH<50.2917 AND NORTH>50.2500 THEN,
        LET AREA$='HB'
    ELSE IF NORTH<50.2500 AND NORTH>50.2083 THEN,
        LET AREA$='HC'
    ELSE IF NORTH<50.2083 AND NORTH>50.1667 THEN,
        LET AREA$='HD'
    ELSE IF NORTH<50.1667 AND NORTH>50.1250 THEN,
        LET AREA$='HE'
    ELSE IF NORTH<50.1250 AND NORTH>50.0833 THEN,
        LET AREA$='HF'
    ELSE IF NORTH<50.0833 AND NORTH>50.0417 THEN,
        LET AREA$='HG'
    ELSE IF NORTH<50.0417 AND NORTH>50.0000 THEN,
        LET AREA$='HH'
    ELSE LET AREA$=''
    NEXT
IF EAST <= -4.500 OR EAST > -3.833 THEN LET AREA$=''

IF EAST > -4.500 AND EAST <= -4.417 THEN FOR
    IF NORTH<50.3333 AND NORTH>50.2917 THEN,
        LET UCUBED=2510
    ELSE IF NORTH<50.2917 AND NORTH>50.2500 THEN,
        LET UCUBED=3625
    ELSE IF NORTH<50.2500 AND NORTH>50.2083 THEN,
        LET UCUBED=5513
    ELSE IF NORTH<50.2083 AND NORTH>50.1667 THEN,
        LET UCUBED=7844
    ELSE IF NORTH<50.1667 AND NORTH>50.1250 THEN,
        LET UCUBED=9630
    ELSE IF NORTH<50.1250 AND NORTH>50.0833 THEN,
        LET UCUBED=12116
    ELSE IF NORTH<50.0833 AND NORTH>50.0417 THEN,
        LET UCUBED=15018
    ELSE IF NORTH<50.0417 AND NORTH>50.0000 THEN,
        LET UCUBED=18558
    ELSE LET UCUBED=.
NEXT
IF EAST > -4.417 AND EAST <= -4.333 THEN FOR
    IF NORTH<50.3333 AND NORTH>50.2917 THEN,
        LET UCUBED=3185
    ELSE IF NORTH<50.2917 AND NORTH>50.2500 THEN,
        LET UCUBED=4888
    ELSE IF NORTH<50.2500 AND NORTH>50.2083 THEN,
        LET UCUBED=7115
    ELSE IF NORTH<50.2083 AND NORTH>50.1667 THEN,
        LET UCUBED=10086
    ELSE IF NORTH<50.1667 AND NORTH>50.1250 THEN,
        LET UCUBED=12207
    ELSE IF NORTH<50.1250 AND NORTH>50.0833 THEN,
        LET UCUBED=14894
    ELSE IF NORTH<50.0833 AND NORTH>50.0417 THEN,
        LET UCUBED=17564
    ELSE IF NORTH<50.0417 AND NORTH>50.0000 THEN,
        LET UCUBED=20903
    ELSE LET UCUBED=.
NEXT
IF EAST > -4.333 AND EAST <= -4.250 THEN FOR
    IF NORTH<50.3333 AND NORTH>50.2917 THEN,
        LET UCUBED=3667
    ELSE IF NORTH<50.2917 AND NORTH>50.2500 THEN,
        LET UCUBED=5690
    ELSE IF NORTH<50.2500 AND NORTH>50.2083 THEN,
        LET UCUBED=8166
    ELSE IF NORTH<50.2083 AND NORTH>50.1667 THEN,
        LET UCUBED=11604
    ELSE IF NORTH<50.1667 AND NORTH>50.1250 THEN,
        LET UCUBED=14870
    ELSE IF NORTH<50.1250 AND NORTH>50.0833 THEN,
        LET UCUBED=17661
    ELSE IF NORTH<50.0833 AND NORTH>50.0417 THEN,
        LET UCUBED=20662
    ELSE IF NORTH<50.0417 AND NORTH>50.0000 THEN,
        LET UCUBED=23981
    ELSE LET UCUBED=.
NEXT
IF EAST > -4.250 AND EAST <= -4.167 THEN FOR
    IF NORTH<50.3333 AND NORTH>50.2917 THEN LET
UCUBED=4066
    ELSE IF NORTH<50.2917 AND NORTH>50.2500 THEN,
        LET UCUBED=7434
    ELSE IF NORTH<50.2500 AND NORTH>50.2083 THEN,
        LET UCUBED=10077
    ELSE IF NORTH<50.2083 AND NORTH>50.1667 THEN,
        LET UCUBED=13891
    ELSE IF NORTH<50.1667 AND NORTH>50.1250 THEN,
        LET UCUBED=17866
    ELSE IF NORTH<50.1250 AND NORTH>50.0833 THEN,
        LET UCUBED=21239
    ELSE IF NORTH<50.0833 AND NORTH>50.0417 THEN,
        LET UCUBED=24601
    ELSE IF NORTH<50.0417 AND NORTH>50.0000 THEN,
        LET UCUBED=28155
    ELSE LET UCUBED=.
NEXT
IF EAST > -4.167 AND EAST <= -4.083 THEN FOR
    IF NORTH<50.3333 AND NORTH>50.2917 THEN,
        LET UCUBED=1014
    ELSE IF NORTH<50.2917 AND NORTH>50.2500 THEN,
        LET UCUBED=12843
    ELSE IF NORTH<50.2500 AND NORTH>50.2083 THEN,
        LET UCUBED=14306
    ELSE IF NORTH<50.2083 AND NORTH>50.1667 THEN,
        LET UCUBED=18352
    ELSE IF NORTH<50.1667 AND NORTH>50.1250 THEN,
        LET UCUBED=23067
    ELSE IF NORTH<50.1250 AND NORTH>50.0833 THEN,
        LET UCUBED=27479
    ELSE IF NORTH<50.0833 AND NORTH>50.0417 THEN,
        LET UCUBED=31050
    ELSE IF NORTH<50.0417 AND NORTH>50.0000 THEN,
        LET UCUBED=34198
    ELSE LET UCUBED=.
NEXT
IF EAST > -4.083 AND EAST <= -4.000 THEN FOR
    IF NORTH<50.3333 AND NORTH>50.2917 THEN,
        LET UCUBED=.
    ELSE IF NORTH<50.2917 AND NORTH>50.2500 THEN,
        LET UCUBED=13150
    ELSE IF NORTH<50.2500 AND NORTH>50.2083 THEN,
        LET UCUBED=17682
    ELSE IF NORTH<50.2083 AND NORTH>50.1667 THEN,
        LET UCUBED=26748
    ELSE IF NORTH<50.1667 AND NORTH>50.1250 THEN,
        LET UCUBED=32747
    ELSE IF NORTH<50.1250 AND NORTH>50.0833 THEN,
        LET UCUBED=37285
    ELSE IF NORTH<50.0833 AND NORTH>50.0417 THEN,
        LET UCUBED=40325
    ELSE IF NORTH<50.0417 AND NORTH>50.0000 THEN,
        LET UCUBED=42678
    ELSE LET UCUBED=.
NEXT
IF EAST > -4.000 AND EAST <= -3.917 THEN FOR
    IF NORTH<50.3333 AND NORTH>50.2917 THEN LET UCUBED=.
    ELSE IF NORTH<50.2917 AND NORTH>50.2500 THEN,
        LET UCUBED=8073
    ELSE IF NORTH<50.2500 AND NORTH>50.2083 THEN,
        LET UCUBED=21935
    ELSE IF NORTH<50.2083 AND NORTH>50.1667 THEN,
        LET UCUBED=50225
    ELSE IF NORTH<50.1667 AND NORTH>50.1250 THEN,
        LET UCUBED=53589
    ELSE IF NORTH<50.1250 AND NORTH>50.0833 THEN,
        LET UCUBED=51945
    ELSE IF NORTH<50.0833 AND NORTH>50.0417 THEN,
        LET UCUBED=51582
    ELSE IF NORTH<50.0417 AND NORTH>50.0000 THEN,
        LET UCUBED=52457
    ELSE LET UCUBED=.
NEXT
IF EAST > -3.917 AND EAST <= -3.833 THEN FOR
    IF NORTH<50.3333 AND NORTH>50.2917 THEN,
        LET UCUBED=.
    ELSE IF NORTH<50.2917 AND NORTH>50.2500 THEN,
        LET UCUBED=1960
    ELSE IF NORTH<50.2500 AND NORTH>50.2083 THEN,
        LET UCUBED=20900
    ELSE IF NORTH<50.2083 AND NORTH>50.1667 THEN,
        LET UCUBED=131902
```

```
    ELSE IF NORTH<50.1667 AND NORTH>50.1250 THEN,
        LET UCUBED=96170
    ELSE IF NORTH<50.1250 AND NORTH>50.0833 THEN,
        LET UCUBED=76172
    ELSE IF NORTH<50.0833 AND NORTH>50.0417 THEN,
        LET UCUBED=67087
    ELSE IF NORTH<50.0417 AND NORTH>50.0000 THEN,
        LET UCUBED=64066
    ELSE LET UCUBED=.
NEXT
IF EAST <= -4.500 OR EAST > -3.833 THEN LET UCUBED=.
rem End tidal.

rem Calculate H over U cubed (Simpson's parameter) using
tidal and depth data.
    LET H_OV_U = LOG((DEPTH*100)/(0.0025*UCUBED))/LOG(10)
rem End calculation

DROP M_EAST M_NORTH M_DEPTH T E N ME MN D MD
RUN

DATA
    USE TEMP3
    SAVE TEMP4

rem Determine the leg, the value of the common distance
variable, KM_TRAK and the positions of possible water
bottle stations by: Define the end positions of each of
the 5 legs on the normal track.
    LET EAST_A = -4.1856
    LET NORT_A = 50.2760
    LET EAST_B = -4.1790
    LET NORT_B = 50.2265
    LET EAST_C = -3.9465
    LET NORT_C = 50.1569
    LET EAST_D = -4.3727
    LET NORT_D = 50.0341
    LET EAST_E = -4.2995
    LET NORT_E = 50.1930
    LET EAST_F = -4.2074
    LET NORT_F = 50.2620

rem define the gradients and intercepts of the five
normal track legs:
    LET GRD_AB = -7.50000
    LET GRD_BC = -0.29935
    LET GRD_CD = 0.28813
    LET GRD_DE = 2.17265
    LET GRD_EF = 0.64061
    LET INT_AB = 16.8845
    LET INT_BC = 48.9765
    LET INT_CD = 51.2940
    LET INT_DE = 59.5262
    LET INT_EF = 52.9473

rem calculate the nearest point on each leg of the normal
track to each measured navigation point using the
following expressions:
rem y1 = mx1 + c1       (1)
rem (y1-y2)/(x1-x2) = -1/m  (2)
rem subst 1 int 2 and rearrange: x1 = (my2-mc+x2)/(1+m^2)
LET EAST_AB=,
    (GRD_AB*NORTH-GRD_AB*INT_AB-EAST)/(1+GRD_AB^2)
LET EAST_BC=,
    (GRD_BC*NORTH-GRD_BC*INT_BC-EAST)/(1+GRD_BC^2)
LET EAST_CD=,
    (GRD_CD*NORTH-GRD_CD*INT_CD-EAST)/(1+GRD_CD^2)
LET EAST_DE=,
    (GRD_DE*NORTH-GRD_DE*INT_DE-EAST)/(1+GRD_DE^2)
LET EAST_EF=,
    (GRD_EF*NORTH-GRD_EF*INT_EF-EAST)/(1+GRD_EF^2)
LET NORT_AB=GRD_AB*EAST_AB+INT_AB
LET NORT_BC=GRD_BC*EAST_BC+INT_BC
LET NORT_CD=GRD_CD*EAST_CD+INT_CD
LET NORT_DE=GRD_DE*EAST_DE+INT_DE
LET NORT_EF=GRD_EF*EAST_EF+INT_EF

rem the distance between the measured and calculated
navigation points is the root of the sum of the squares
(pythagrus)
LET DIST_AB=,
    (((EAST-EAST_AB)*70)^2+(NORTH-NORT_AB)*111)^2)^0.5
LET DIST_BC=,
    (((EAST-EAST_BC)*70)^2+((NORTH-NORT_BC)*111)^2)^0.5
LET DIST_CD=,
    (((EAST-EAST_CD)*70)^2+(NORTH-NORT_CD)*111)^2)^0.5
LET DIST_DE=,
    (((EAST-EAST_DE)*70)^2+(NORTH-NORT_DE)*111)^2)^0.5
LET DIST_EF=,
    (((EAST-EAST_EF)*70)^2+(NORTH-NORT_EF)*111)^2)^0.5


rem determine which is the lowest distance. This will be
the current leg.
IF  DIST_AB < DIST_BC AND DIST_AB < DIST_CD AND,
    DIST_AB < DIST_DE AND DIST_AB < DIST_EF THEN FOR
    LET LEG = 1
    LET EAS_TRAK = EAST_AB
    LET NOR_TRAK = NORT_AB
    LET TRAK_ERR = DIST_AB
    NEXT
IF  DIST_BC < DIST_AB AND DIST_BC < DIST_CD AND,
    DIST_BC < DIST_DE AND DIST_BC < DIST_EF THEN FOR
    LET LEG = 2
    LET EAS_TRAK = EAST_BC
    LET NOR_TRAK = NORT_BC
    LET TRAK_ERR = DIST_BC
    NEXT
IF  DIST_CD < DIST_BC AND DIST_CD < DIST_AB AND,
    DIST_CD < DIST_DE AND DIST_CD < DIST_EF THEN FOR
    LET LEG = 3
    LET EAS_TRAK = EAST_CD
    LET NOR_TRAK = NORT_CD
    LET TRAK_ERR = DIST_CD
    NEXT
IF  DIST_DE < DIST_BC AND DIST_DE < DIST_CD AND,
    DIST_DE < DIST_AB AND DIST_DE < DIST_EF THEN FOR
    LET LEG = 4
    LET EAS_TRAK = EAST_DE
    LET NOR_TRAK = NORT_DE
    LET TRAK_ERR = DIST_DE
    NEXT
IF  DIST_EF < DIST_BC AND DIST_EF < DIST_CD AND,
    DIST_EF < DIST_DE AND DIST_EF < DIST_AB THEN FOR
    LET LEG = 5
    LET EAS_TRAK = EAST_EF
    LET NOR_TRAK = NORT_EF
    LET TRAK_ERR = DIST_EF
    NEXT

rem From the estimated position along the normal track,
calculate the distance elapsed in KM along the track,
assuming clockwise direction
IF LEG=1 THEN LET TRAK_KM=(((EAST_AB-EAST_A
    *70)^2+((NORT_AB-NORT_A)*111)^2)^0.5
IF LEG=2 THEN LET TRAK_KM=.5.514+(((EAST_BC-
    -EAST_B)*70)^2+((NORT_BC-NORT_B)*111)^2)^0.5
IF LEG=3 THEN LET TRAK_KM=23.529+(((EAST_CD-
    -EAST_C)*70)^2+((NORT_CD-NORT_C)*111)^2)^0.5
IF LEG=4 THEN LET TRAK_KM=56.330+(((EAST_DE-
    -EAST_D)*70)^2+((NORT_DE-NORT_D)*111)^2)^0.5
IF LEG=5 THEN LET TRAK_KM=74.697+(((EAST_EF-
    -EAST_E)*70)^2+((NORT_EF-NORT_E)*111)^2)^0.5

rem Calculate distance between record and each station in
terms of kilometers.
    LET DIST_A=,
    (((EAST-EAST_A)*70)^2+(NORTH-NORT_A)*111)^2)^0.5
    LET DIST_C=,
    (((EAST-EAST_C)*70)^2+(NORTH-NORT_C)*111)^2)^0.5
    LET DIST_D=,
    (((EAST-EAST_D)*70)^2+((NORTH-NORT_D)*111)^2)^0.5
    LET DIST_F=,
    (((EAST-EAST_F)*70)^2+((NORTH-NORT_F)*111)^2)^0.5

rem If the distance is less than 2, then mark the record
with the station name.
    IF DIST_A < 2 THEN FOR
        LET STATION$ = "S1<2KM"
        LET STAT_ERR = DIST_A
    NEXT
    IF DIST_C < 2 THEN FOR
        LET STATION$ = "S2<2KM"
        LET STAT_ERR = DIST_C
    NEXT
    IF DIST_D < 2 THEN FOR
        LET STATION$ = "S3<2KM"
        LET STAT_ERR = DIST_D
    NEXT
    IF DIST_F < 2 THEN FOR
        LET STATION$ = "S4<2KM"
        LET STAT_ERR = DIST_F
    NEXT

rem clean up the file
    DROP    EAST_A EAST_B EAST_C EAST_D EAST_E EAST_F
    DROP    NORT_A NORT_B NORT_C NORT_D NORT_E NORT_F
    DROP    DIST_A DIST_C DIST_D DIST_F
    DROP    GRD_AB GRD_BC GRD_CD GRD_DE GRD_EF
    DROP    INT_AB  INT_BC  INT_CD  INT_DE  INT_EF
    DROP    EAST_AB EAST_BC EAST_CD EAST_DE EAST_EF
    DROP    NORT_AB NORT_BC NORT_CD NORT_DE NORT_EF
    DROP    DIST_AB DIST_BC DIST_CD DIST_DE DIST_EF

RUN

DATA
USE TEMP4 (TOD_M    TIMEDEC  EAST     NORTH    EAS_TRAK ,
           NOR_TRAK TRAK_KM  TRAK_ERR DEPTH    AREAS    ,
           UCUBED   H_OV_U   LEG      STATIONS STAT_ERR)
    rem edit**********************************
    SAVE 'C:\PHDDATA\UOR\SQmyymn.SQmyymnW.SYS'
    rem **********************************
RUN
end navmake

rem  ______________
rem |              |
rem |  NAVMERG2.CMD|
rem |______________|
rem This programme navigates each record of UOR data
(created by CALSYS.CMD) using navigation data created by
NAVMAKE.CMD.
DATA
    rem edit**********************************
    USE 'C:\PHDDATA\UOR\SQmyymn.SQmyymnC.SYS'
    rem **********************************
    SAVE TEMP4

rem create standard time stamp (round to 3 d.p.) for UOR
data
    IF (TOD*100)-INT(TOD*100)>0.5 THEN LET,
        TOD_M = (INT(TOD*100)+1)/100
    ELSE LET,
        TOD_M = (INT TOD*100)/ 100
RUN
rem merge navigation and UOR data
    rem edit**********************************
USE TEMP4    'C:\PHDDATA\UOR\SQmyymn.SQmyymnW.SYS' / TOD_M
    rem **********************************
    SAVE TEMP5
RUN
rem clean up file
DATA
    USE TEMP5  TIME     TOD      TOD_M    EAST     ,
      NORTH    EAS_TRAK NOR_TRAK TRAK_KM  TRAK_ERR ,
```

```
      AREA$    DEPTH    UCUBED   H_OV_U   STATION$,
      STAT_ERR LEG      DEPT     TEMP     COND     ,
      TMIS     FLUO     ED412    ED443    ED490    ,
      ED510    ED555    ED670    LU412    LU443    ,
      LU490    LU510    LU555    LU683    ED412L   ,
      ED443L   ED490L   ED510L   ED555L   ED670L   ,
      LU412L   LU443L   LU490L   LU510L   LU555L   ,
      LU683L   PITC     ROLL     TILT)
    rem  edit**********************************
    SAVE 'C:\PHDDATA\UOR\SQmyynn\SQmyynnN.SYS'
    rem  **********************************
    IF TOD = . THEN DELETE
RUN
rem end navmerge.

rem  ____________
rem |
rem | PROFSEN2.CMD
rem |____________|
rem this programme splits the continuous UOR data into
separate depth profiles. Turning points in the real depth
data are unreliable due to noise. A smoothed depth record
is therefore calculated, using a 40 point running mean,
and this variable used to detect turning points. Average
positions, times etc. are calculated for each profile.
EDIT
    rem  edit**********************************
    USE 'C:\PHDDATA\UOR\SQmyynn\SQmyynnN.SYS'
    rem  **********************************
rem
    SERIES
    SAVE TEMP6 / DOUBLE
rem calculate a 40 pt running mean smooth of UOR depth
(to a new file)
    SMOOTH DEPT/MEAN=40
DATA
rem merge smoothed depth file with UOR data
    rem  edit**********************************
    USE 'C:\PHDDATA\UOR\SQmyynn\SQmyynnN.SYS' TEMP6
    rem  **********************************
    SAVE TEMP7
RUN
DATA
    USE TEMP7
    SAVE TEMP8
rem use the smoothed depth variable to split continuous
UOR data into 'up' (climbing) and 'down' (sinking)
sections. Number each profile sequentially.
HOLD
    LET LAGG  = LAG(SMOOTH)
    LET GRAD  = SMOOTH - LAGG
    LET LGRAD = LAG(GRAD)
    IF GRAD < 0 THEN LET UP_DOWN$ = 'DOWN'
    IF GRAD > 0 THEN LET UP_DOWN$ = 'UP'
    IF (GRAD>=0 AND LGRAD<0) OR (GRAD<0 AND LGRAD>0)
THEN LET SELECT = CASE
    IF CASE = 1 THEN DELETE
    LET N=1
RUN
EDIT
    USE TEMP8
    BY SELECT
STATS

rem calculate the mean time, position and stratification
for each profile
    SAVE TEMP9
    STATS SELECT   TOD      EAST     NORTH    EAS_TRAK,
                   NOR_TRAK TRAK_KM  TRAK_ERR DEPTH   ,
                   UCUBED   H_OV_U   / MEAN

rem calculate the number of records for each profile
    SAVE TEMP10
    STATS N /SUM

DATA
rem change name of mean variables, allowing merging.
    USE TEMP9
    SAVE TEMP11
        LET TOD_PROF = TOD
        LET E1       = EAST
        LET N1       = NORTH
        LET E2       = EAS_TRAK
        LET N2       = NOR_TRAK
        LET D1       = DEPTH
        LET U1       = UCUBED
        LET H1       = H_OV_U
        LET T1       = TRAK_KM
        LET T2       = TRAK_ERR

    DROP TOD      EAST     NORTH    EAS_TRAK NOR_TRAK ,
         DEPTH    UCUBED   H_OV_U   TRAK_KM  TRAK_ERR
RUN

rem change name of sum variable, to allow merging.
    USE TEMP10
    SAVE TEMP12
    LET N_RECS = N
    DROP N
RUN

rem merge the mean and sum data files
    USE TEMP11 TEMP12
    SAVE TEMP13
RUN

rem merge the profile statistics file with the UOR data
file.
    USE TEMP8 TEMP13 ! SELECT
    SAVE TEMP14
RUN

DATA
    USE TEMP14
    SAVE TEMP15
HOLD

rem Examine the number of records contained in each
profile. If this is less than 41, then insufficient data
exists, and the records deleted.
    IF N_RECS<41 THEN DELETE
RUN

DATA
    USE TEMP15
    SAVE TEMP 16
HOLD
rem rename the merged variables
        LET EAST     = E1
        LET NORTH    = N1
        LET EAS_TRAK = E2
        LET NOR_TRAK = N2
        LET DEPTH    = D1
        LET UCUBED   = U1
        LET H_OV_U   = H1
        LET TRAK_KM  = T1
        LET TRAK_ERR = T2
rem Count the profiles from the start
    LET L = TEM
    IF L <> SELECT THEN LET PROF_NO = PROF_NO+1
    LET TEM = SELECT

    DROP LAGG     GRAD     LGRAD    N
    DROP E1 N1 E2 N2 D1 U1 H1 T1 T2
    DROP SELECT   L        TEM
RUN

DATA
    USE TEMP16 ,
  (TIME     TOD      TOD_M    TOD_PROF PROF_NO UP_DOWN$,
   N_RECS   EAST     NORTH    EAS_TRAK NOR_TRAK TRAK_KM,
   TRAK_ERR AREA$    DEPTH    UCUBED   H_OV_U  STATION$,
   STAT_ERR LEG      DEPT     TEMP     COND     TMIS    ,
   FLUO     ED412    ED443    ED490    ED510    ED555   ,
   ED670    LU412    LU443    LU490    LU510    LU555   ,
   LU683    ED412L   ED443L   ED490L   ED510L   ED555L  ,
   ED670L   LU412L   LU443L   LU490L   LU510L   LU555L  ,
   LU683L   PITC     ROLL     TILT)

rem  edit**********************************
SAVE 'C:\PHDDATA\UOR\SQmyynn\SQmyynnP.SYS'
rem  **********************************
RUN
rem end PROFILE.CMD

rem  ____________
rem |
rem | KD_BIN2.CMD
rem |____________|
rem This programme calculates difuse attenuation
coefficient values, by regressing the logs of the light
data against depth.
DATA
rem edit**********************************
USE 'C:\PHDDATA\UOR\SQmyynn\SQmyynnP.SYS'
rem **********************************
    SAVE TEMP21
rem Screen data for tilt
    IF TILT > 20 THEN DELETE

rem create new array variables
    DIM Y(12)
    DIM YY(12)
    DIM XY(12)
rem copy all text variables to numerical for averaging.
    IF UP_DOWN$ = 'UP' THEN LET UP_DOWN = 1
    IF UP_DOWN$ = 'DOWN' THEN LET UP_DOWN = -1
    IF STATION$ = 'S1<2KM' THEN LET STATION = 1
    IF STATION$ = 'S2<2KM' THEN LET STATION = 2
    IF STATION$ = 'E1<2KM' THEN LET STATION = 3
    IF STATION$ = 'L4<2KM' THEN LET STATION = 4
    IF AREA$='AA' THEN LET AREA = 1
    IF AREA$='AB' THEN LET AREA = 2
    IF AREA$='AC' THEN LET AREA = 3
    IF AREA$='AD' THEN LET AREA = 4
    IF AREA$='AE' THEN LET AREA = 5
    IF AREA$='AF' THEN LET AREA = 6
    IF AREA$='AG' THEN LET AREA = 7
    IF AREA$='AH' THEN LET AREA = 8
    IF AREA$='BA' THEN LET AREA = 9
    IF AREA$='BB' THEN LET AREA = 10
    IF AREA$='BC' THEN LET AREA = 11
    IF AREA$='BD' THEN LET AREA = 12
    IF AREA$='BE' THEN LET AREA = 13
    IF AREA$='BF' THEN LET AREA = 14
    IF AREA$='BA' THEN LET AREA = 15
    IF AREA$='BH' THEN LET AREA = 16
    IF AREA$='CA' THEN LET AREA = 17
    IF AREA$='CB' THEN LET AREA = 18
    IF AREA$='CC' THEN LET AREA = 19
    IF AREA$='CD' THEN LET AREA = 20
    IF AREA$='CE' THEN LET AREA = 21
    IF AREA$='CF' THEN LET AREA = 22
    IF AREA$='CG' THEN LET AREA = 23
    IF AREA$='CH' THEN LET AREA = 24
    IF AREA$='DA' THEN LET AREA = 25
    IF AREA$='DB' THEN LET AREA = 26
    IF AREA$='DC' THEN LET AREA = 27
    IF AREA$='DD' THEN LET AREA = 28
    IF AREA$='DE' THEN LET AREA = 29
    IF AREA$='DF' THEN LET AREA = 30
    IF AREA$='DG' THEN LET AREA = 31
    IF AREA$='DH' THEN LET AREA = 32
    IF AREA$='EA' THEN LET AREA = 33
    IF AREA$='EB' THEN LET AREA = 34
    IF AREA$='EC' THEN LET AREA = 35
```

```
    IF AREA$='ED' THEN LET AREA = 36
    IF AREA$='EE' THEN LET AREA = 37
    IF AREA$='EF' THEN LET AREA = 38
    IF AREA$='EG' THEN LET AREA = 39
    IF AREA$='EH' THEN LET AREA = 40
    IF AREA$='FA' THEN LET AREA = 41
    IF AREA$='FB' THEN LET AREA = 42
    IF AREA$='FC' THEN LET AREA = 43
    IF AREA$='FD' THEN LET AREA = 44
    IF AREA$='FE' THEN LET AREA = 45
    IF AREA$='FF' THEN LET AREA = 46
    IF AREA$='FG' THEN LET AREA = 47
    IF AREA$='FH' THEN LET AREA = 48
    IF AREA$='GA' THEN LET AREA = 49
    IF AREA$='GB' THEN LET AREA = 50
    IF AREA$='GC' THEN LET AREA = 51
    IF AREA$='GD' THEN LET AREA = 52
    IF AREA$='GE' THEN LET AREA = 53
    IF AREA$='GF' THEN LET AREA = 54
    IF AREA$='GG' THEN LET AREA = 55
    IF AREA$='GH' THEN LET AREA = 56
    IF AREA$='HA' THEN LET AREA = 57
    IF AREA$='HB' THEN LET AREA = 58
    IF AREA$='HC' THEN LET AREA = 59
    IF AREA$='HD' THEN LET AREA = 60
    IF AREA$='HE' THEN LET AREA = 61
    IF AREA$='HF' THEN LET AREA = 62
    IF AREA$='HG' THEN LET AREA = 63
    IF AREA$='HH' THEN LET AREA = 64
rem end copying text variable

rem fill the array variables with log-light data
    LET X    = DEPT
    LET N    = 12
    LET Y(1) = LU412L
    LET Y(2) = LU443L
    LET Y(3) = LU490L
    LET Y(4) = LU510L
    LET Y(5) = LU555L
    LET Y(6) = LU683L
    LET Y(7) = ED412L
    LET Y(8) = ED443L
    LET Y(9) = ED490L
    LET Y(10) = ED510L
    LET Y(11) = ED555L
    LET Y(12) = ED670L
    FOR A = 1 TO 12

rem calculate regression variables YY and XY and XX
        LET YY(A) = Y(A)*Y(A)
        LET XY(A) = Y(A)*DEPT
    NEXT
        LET XX = DEPT*DEPT

rem determine the depth range for the regression
    LET Z_RANGE=11
    IF DEPT<-8 AND DEPT>-19 THEN LET Z_SET=-14
    ELSE IF DEPT<-19 AND DEPT>-50 THEN LET Z_SET=-25
    ELSE DELETE
RUN
DATA
    USE TEMP21
    SAVE TEMP22
    SORT TOD_PROF Z_SET
RUN
    USE TEMP22
EDIT
    BY TOD_PROF Z_SET
STATS
rem calculate regression sigma variables
    SAVE TEMP23
    STATS N X Y(1-12) XX YY 1-12) XY(1-12) / SUM
    SAVE TEMP24
rem calculate averages of other variables
    STATS TOD_PROF EAST     NORTH    Z_SET    DEPT     ,
    EAS_TRAK NOR_TRAK TRAK_KM  TRAK_ERR AREA  DEPTH    ,
    UCUBED   H_OV_U   STATIONS STAT_ERR LEG   TEMP     ,
    COND     FLUO     TMIS     TILT     UP_DOWN  PROF_NO,
    PITC     ROLL     TILT     MEAN

rem merge the statistics files
DATA
    USE TEMP24 TEMP23
    SAVE TEMP25
RUN

rem do the regression
DATA
    USE TEMP25
    SAVE TEMP26
    DIM ZR_U(12)
    DIM ZKD_U(12)
    FOR A = 1 TO 12
rem calculate the slope
        LET ZR_U(A) = ((N*XY(A))-(X*Y(A)))/(
SQR((N*XX)-(X*X))*(N*YY(A))-(Y(A)*Y(A))))
rem calculate the pearson correlation
        LET ZKD_U A= ((N*XY(A))-(X*Y(A)))/((N*XX)-(X*X))
    NEXT

rem if pearson is below a threshold, reject slope value
    FOR A = 1 TO 12
        IF ZR_U(A) < 0.95 THEN LET ZKD_U(A) = .
    NEXT

rem return variable names from array variables
    LET KD_412 = ZKD_U 1
    LET KD_443 = ZKD_U 2
    LET KD_490 = ZKD_U 3
    LET KD_510 = ZKD_U 4
    LET KD_555 = ZKD_U 5
    LET KD_683 = ZKD_U 6
    LET KD_412 = ZKD_U 7
    LET KD_443 = ZKD_U 8
    LET KD_490 = ZKD_U 9
    LET KD_510 = ZKD_U 10
    LET KD_555 = ZKD_U 11
    LET KD_671 = ZKD_U 12
    LET RU_412 = ZR_U(1)
    LET RU_443 = ZR_U(2)
    LET RU_490 = ZR_U(3)
    LET RU_510 = ZR_U(4)
    LET RU_555 = ZR_U(5)
    LET RU_683 = ZR_U(6)
    LET RD_412 = ZR_U(7)
    LET RD_443 = ZR_U(8)
    LET RD_490 = ZR_U(9)
    LET RD_510 = ZR_U(10)
    LET RD_555 = ZR_U(11)
    LET RD_670 = ZR_U(12)
rem rename variables
    LET Z_OBS = Z
    LET  Z_MEAN = DEPT
    IF (TOD_PROF*100-INT(TOD_PROF*100)>0.5 THEN
 LET TOD_M = (INT((TOD_PROF*100)+1.)/100
    ELSE LET TOD_M = (INT(TOD_PROF*100))/100
rem return the text variables to text
    IF UP_DOWN = 1 THEN LET UP_DOWN$ = 'UP'
    IF UP_DOWN = -1 THEN LET UP_DOWN$ = 'DOWN'
    IF STATION = 1 THEN LET STATION$ = 'S1<2KM'
    IF STATION = 2 THEN LET STATION$ = 'S2<2KM'
    IF STATION = 3 THEN LET STATION$ = 'E1<2KM'
    IF STATION = 4 THEN LET STATION$ = 'L4<2KM'
    IF AREA = 1  THEN LET AREA$='AA'
    IF AREA = 2  THEN LET AREA$='AB'
    IF AREA = 3  THEN LET AREA$='AC'
    IF AREA = 4  THEN LET AREA$='AD'
    IF AREA = 5  THEN LET AREA$='AE'
    IF AREA = 6  THEN LET AREA$='AF'
    IF AREA = 7  THEN LET AREA$='AG'
    IF AREA = 8  THEN LET AREA$='AH'
    IF AREA = 9  THEN LET AREA$='BA'
    IF AREA = 10 THEN LET AREA$='BB'
    IF AREA = 11 THEN LET AREA$='BC'
    IF AREA = 12 THEN LET AREA$='BD'
    IF AREA = 13 THEN LET AREA$='BE'
    IF AREA = 14 THEN LET AREA$='BF'
    IF AREA = 15 THEN LET AREA$='BG'
    IF AREA = 16 THEN LET AREA$='BH'
    IF AREA = 17 THEN LET AREA$='CA'
    IF AREA = 18 THEN LET AREA$='CB'
    IF AREA = 19 THEN LET AREA$='CC'
    IF AREA = 20 THEN LET AREA$='CD'
    IF AREA = 21 THEN LET AREA$='CE'
    IF AREA = 22 THEN LET AREA$='CF'
    IF AREA = 23 THEN LET AREA$='CG'
    IF AREA = 24 THEN LET AREA$='CH'
    IF AREA = 25 THEN LET AREA$='DA'
    IF AREA = 26 THEN LET AREA$='DB'
    IF AREA = 27 THEN LET AREA$='DC'
    IF AREA = 28 THEN LET AREA$='DD'
    IF AREA = 29 THEN LET AREA$='DE'
    IF AREA = 30 THEN LET AREA$='DF'
    IF AREA = 31 THEN LET AREA$='DG'
    IF AREA = 32 THEN LET AREA$='DH'
    IF AREA = 33 THEN LET AREA$='EA'
    IF AREA = 34 THEN LET AREA$='EB'
    IF AREA = 35 THEN LET AREA$='EC'
    IF AREA = 36 THEN LET AREA$='ED'
    IF AREA = 37 THEN LET AREA$='EE'
    IF AREA = 38 THEN LET AREA$='EF'
    IF AREA = 39 THEN LET AREA$='EG'
    IF AREA = 40 THEN LET AREA$='EH'
    IF AREA = 41 THEN LET AREA$='FA'
    IF AREA = 42 THEN LET AREA$='FB'
    IF AREA = 43 THEN LET AREA$='FC'
    IF AREA = 44 THEN LET AREA$='FD'
    IF AREA = 45 THEN LET AREA$='FE'
    IF AREA = 46 THEN LET AREA$='FF'
    IF AREA = 47 THEN LET AREA$='FG'
    IF AREA = 48 THEN LET AREA$='FH'
    IF AREA = 49 THEN LET AREA$='GA'
    IF AREA = 50 THEN LET AREA$='GB'
    IF AREA = 51 THEN LET AREA$='GC'
    IF AREA = 52 THEN LET AREA$='GD'
    IF AREA = 53 THEN LET AREA$='GE'
    IF AREA = 54 THEN LET AREA$='GF'
    IF AREA = 55 THEN LET AREA$='GG'
    IF AREA = 56 THEN LET AREA$='GH'
    IF AREA = 57 THEN LET AREA$='HA'
    IF AREA = 58 THEN LET AREA$='HB'
    IF AREA = 59 THEN LET AREA$='HC'
    IF AREA = 60 THEN LET AREA$='HD'
    IF AREA = 61 THEN LET AREA$='HE'
    IF AREA = 62 THEN LET AREA$='HF'
    IF AREA = 63 THEN LET AREA$='HG'
    IF AREA = 64 THEN LET AREA$='HH'
rem delete unwanted variables
DROP    N X Y(1-12) XX YY 1-12) XY(1-12) UP_DOWN ZKD_U 1-
12),
ZR_U(1-12) AREA STATION
RUN
rem clean up the file
DATA
    USE TEMP26,
  (TOD_PROF PROF_NO  UP_DOWN$ Z_SET    Z_MEAN   Z_OBS    ,
   EAST     NORTH    EAS_TRAK NOR_TRAK TRAK_KM  TRAK_ERR ,
   AREA$    DEPTH    UCUBED   H_OV_U   STATIONS STAT_ERR ,
   LEG      DEPT     TEMP     COND     TMIS     FLUO     ,
   PITC     ROLL     TILT     TILT     ,
   KU_412   RU_412   KU_443   RU_443   KU_490   RU_490   ,
   KU_510   RU_510   KU_555   RU_555   KU_683   RU_683   ,
   KD_412   RD_412   KD_443   RD_443   KD_490   RD_490   ,
   KD_510   RD_510   KD_555   RD_555   KD_670   RD_670)
rem  edit*********************************
SAVE 'C:\PHDDATA\DSR_S2myymm.S2myymmR.SYS'
```

Appendix 11 – Model Data; Variables and Parameters

Table of model variables

Meteorological Variables		
q	Heat input to the water surface	W m^{-2}
W	Wind speed	M s^{-1}
I	Light Intensity	W m^{-2}
Site-Specific Variables		
d	Water depth	m
U	Tidal Speed	M s^{-2}
Model Output Variables		
$h_{[n]}$	Thickness of the n^{th} layer	m
$T_{[n]}$	Temperature of the n^{th} layer	°C
P_j	Chlorophyll concentration of the n^{th} layer	mg Chl m^{-3}
$N_{[n]}$	Nutrient concentration of the n^{th} layer	mmol N m^{-3}

Table of model parameters.

All parameters taken from Prestidge & Taylor (1995) except:
*1 Modified from Simpson & Bowers (1981)
*2 Taken from Simpson & Bowers (1981)
*3 A. Taylor (pers. Com.)

Physical Parameters		
δt	Time step of the model	3600 s
g	Acceleration due to gravity	9.810 m s^{-2}
a	Thermal expansion coefficient of sea water	2.1×10^{-4} °C^{-1}
b	Dependence of density on salinity	7.7×10^{-4}
c	Specific heat capacity of sea water	3.9×10^{3} J m^{-3} °C^{-1}
ρ_w	Density of sea water	1.025×10^{3} kg m^{-3}
ρ_a	Density of air	1.25 kg m^{-3}
f_0	Wind mixing efficiency *1	8.0×10^{-2}
f_3	Tidal mixing efficiency *1	8.0×10^{-3}
k_0	Wind drag coefficient *2	6.4×10^{-5}
k_3	Sea bed drag coefficient	2.5×10^{-3}
d_{min}	Minimum depth for stratification	15 m
S_{min}	Minimum salinity difference for stratification	0.05 PSU
e_1	Thermocline diffusion coefficient *3	4.5×10^{-9} m s^{-1}
e_2	Thermocline diffusion coefficient *3	1×10^{-4} m s^{-1}
k_c	Convective mixing penetration efficiency	0.1
Φ_0	Constant variable for mixing efficiency	5 J m^{-1}
ζ_{lw}	Wind potential energy time lag	3 h
C_a	Specific heat capacity of air	1.004×10^{3} J m^{-3} °C^{-1}
e_Q	Air/sea heat exchange coefficient	2.5×10^{-3} °C^{-1}
e_v	Water vapour exchange coefficient	1.45×10^{-3}
A	Albedo	0.06
ϵ	Emissivity of sea surface	0.987
σ	Stephan's constant	5.67×10^{8}

c_1	Latent heat capacity of sea water	2.5008×10^6
$_pI_r$	Proportion of penetrating red light	0.25
$_pI_g$	Proportion of penetrating green light	0.25
k_{r0}	Pure-water attenuation for red light	0.4 m^{-1}
k_{g0}	Pure-water attenuation for green light	0.08 m^{-1}
k_{chl}	Chlorophyll-specific attenuation coefficient	0.16 m^2 mg^{-1} Chl
k_{s1}	Tidal component of sediment attenuation	7.0 s^3 m^{-3}
k_{s2}	Salinity component of sediment attenuation	0.3 m^{-1}
Biological Parameters		
γ	Chlorophyll to nitrate conversion factor	0.510 mmol N mg^{-1} Chl
m	Mean phytoplankton mortality rate	1.5×10^{-6} s^{-1}
δ_m	Amplitude of mortality rate variation	8.7×10^{-7} s^{-1}
ω_m	Phase of mortality rate variation	-2.34 radians
η	Proportion of mortality recycled as nutrient	0.2
T_{max}	Temperature coefficient for growth rate	17°C
α_{max}	Maximum growth rate at T_{max}	2.31×10^{-5} s^{-1}
I_H	Light half-saturation coefficient for growth	9.5 W m^{-2}
N_h	Nutrient half-saturation for growth	0.1 mmol N m^{-3}
ν	Phytoplankton sinking rate	1.0×10^{-5} s^{-1}
P_0	Minimum phytoplankton concentration	0.01 mg Chl m^{-3}
N_{sed}	Sediment nutrient concentration	8.0 mmol N m^{-3}
e_{sed}	Coefficient for sediment/water nutrient exchange	1.5×10^{-5}

Appendix 12A – Meteorological Data; Time and Frequency

Downwelling Irradiance Observations (Camborne), 1983 to 1997

A – Time Series
B – Frequency Series
C – Peak Characteristics

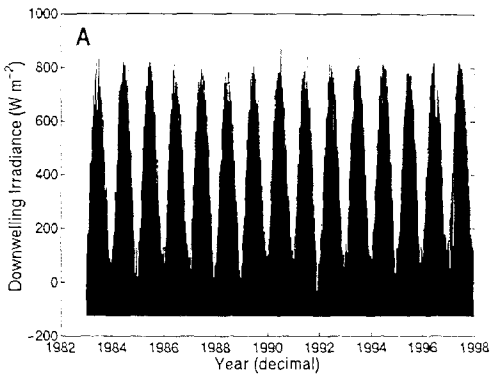

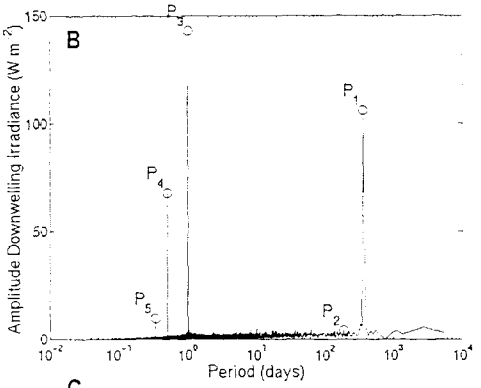

C

	P_1	P_2	P_3	P_4	P_5
T (day)	364.1	182.0	1.000	0.500	0.333
A (W m^{-2})	106.1	4.0	142.9	68.0	9.6
ϕ (rad)	-3.08	0.77	-1.38	2.72	-0.12

Air Temperature Observations (Plymouth), 1983 to 1997

A – Time Series
B – Frequency Series
C – Peak Characteristics

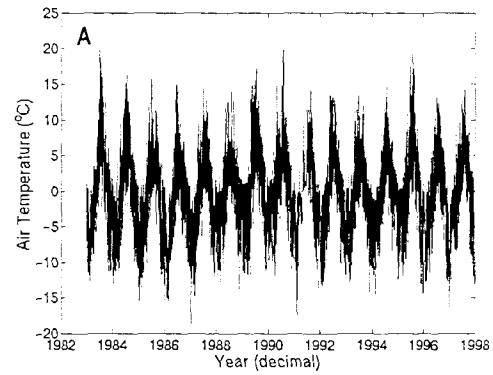

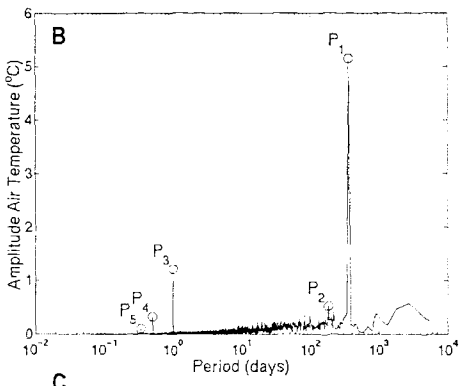

C

	P_1	P_2	P_3	P_4	P_5
T (day)	364.1	182.0	1.000	0.500	0.333
A (°C)	5.15	0.52	1.22	0.33	0.11
ϕ (rad)	2.49	-1.13	-1.59	1.96	1.41

Wind Speed Observations (Plymouth), 1983 to 1997

A – Time Series
B – Frequency Series
C – Peak Characteristics

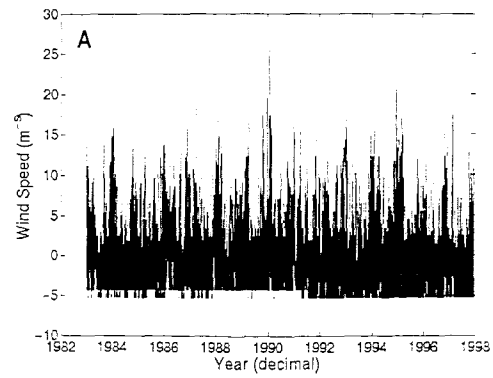

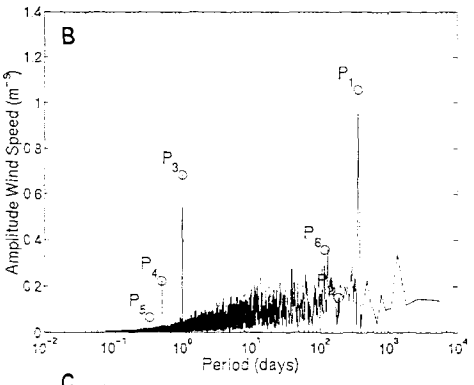

C

	P_1	P_2	P_6	P_3	P_4	P_5
T (day)	364	182	116	1.00	0.50	0.33
A (ms^{-1})	1.06	0.15	0.36	0.68	0.22	0.07
ρ (rad)	-0.4	-0.7	-2.8	-2.3	1.1	-1.9

Appendix 12B – Model Data; Time and Frequency

Model Simulations of Maximum SML Depth, 1983 to 1997

A – Time Series
B – Frequency Series
C – Peak Characteristics

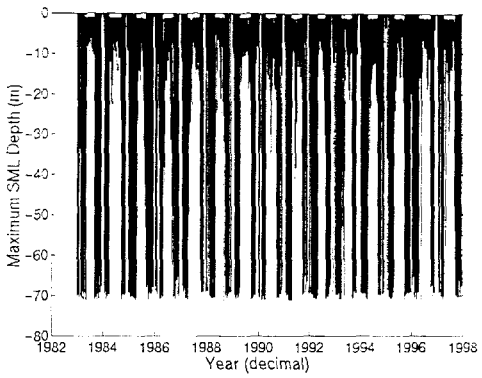

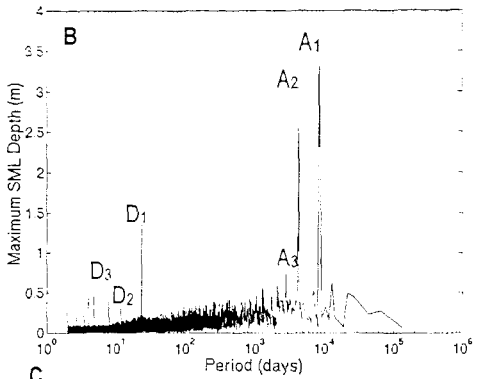

C

	A_1	A_2	A_3	D_1	D_2	D_3
T (day)	364	182	121	1.00	0.50	0.33
A (m)	3.53	3.28	0.81	1.47	0.39	0.62
φ (rad)	2.13	-0.77	2.35	-0.36	-2.63	2.11

Model Simulations of Maximum Thermocline Depth, 1983 to 1997

A – Time Series
B – Frequency Series
C – Peak Characteristics

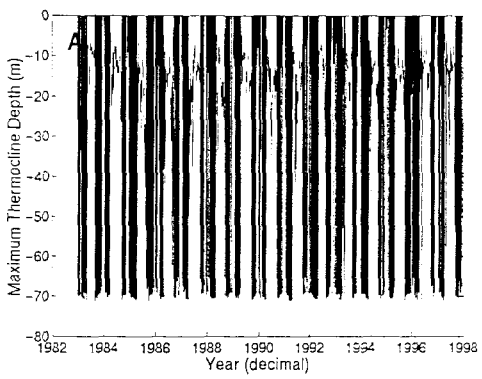

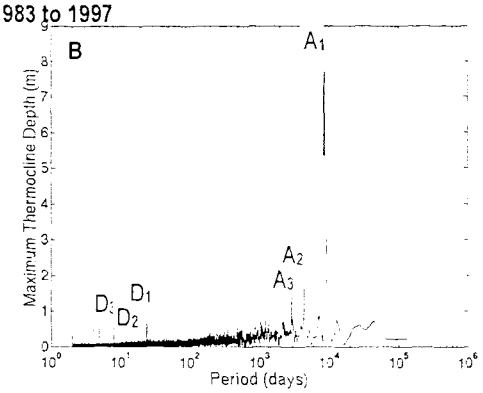

C

	A_1	A_2	A_3	D_1	D_2	D_3
T (day)	364	182	121	1.00	0.50	0.33
A (m)	8.21	2.04	1.90	1.08	0..30	0.42
φ (rad)	1.50	1.76	1.65	2.36	1.33	1.98

Model Simulations of SML Temperature, 1983 to 1997

A – Time Series
B – Frequency Series
C – Peak Characteristics

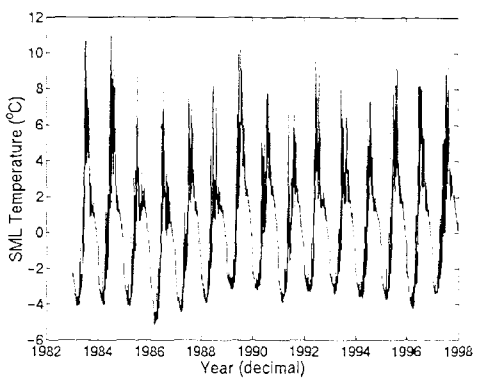

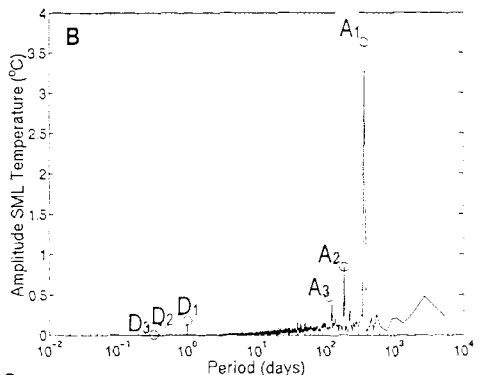

C

	A_1	A_2	A_3	D_1	D_2	D_3
T (day)	364	182	121	1.00	0.50	0.33
A (W m^{-2})	3.63	0.84	0.43	0.18	0.05	0.01
ϕ (rad)	2.09	-0.28	1.82	-3.11	-2.40	-1.23

Model Simulations of BML Temperature, 1983 to 1997

A – Time Series
B – Frequency Series
C – Peak Characteristics

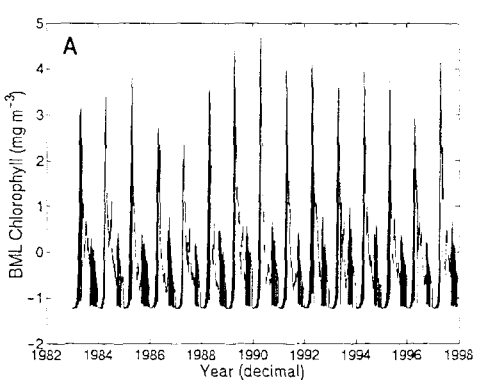

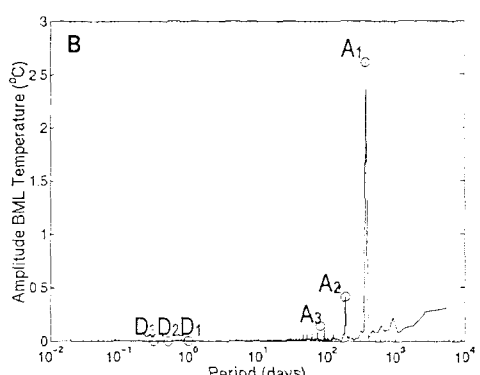

C

	A_1	A_2	A_3	D_1	D_2	D_3
T (day)	364	182	121	1.00	0.50	0.33
A (W m^{-2})	2.61	0.42	0.07	0.002	0.000	0.000
ϕ (rad)	1.50	1.76	1.65	2.36	1.33	1.98

Model Simulations of SML Nutrient, 1983 to 1997

A – Time Series
B – Frequency Series
C – Peak Characteristics

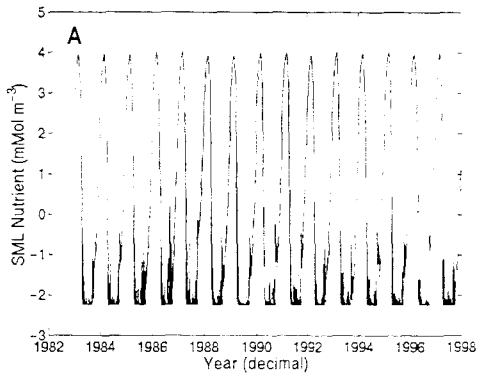

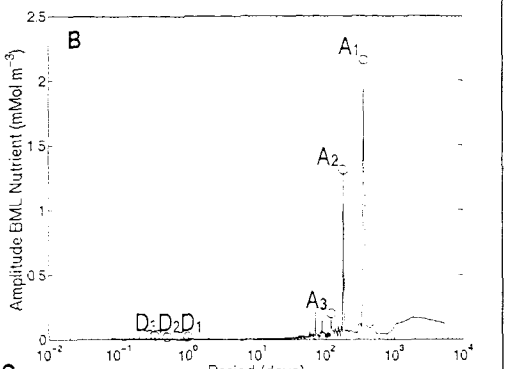

C

	A_1	A_2	A_3	D_1	D_2	D_3
T (day)	364	182	121	1.00	0.50	0.33
A mmol m^{-3}	3.00	1.12	0.45	0.040	0.006	0.002
o (rad)	0.63	1.84	2.76	-0.45	0.35	-2.63

Model Simulations of Thermocline Nutrient, 1983 to 1997

A – Time Series
B – Frequency Series
C – Peak Characteristics

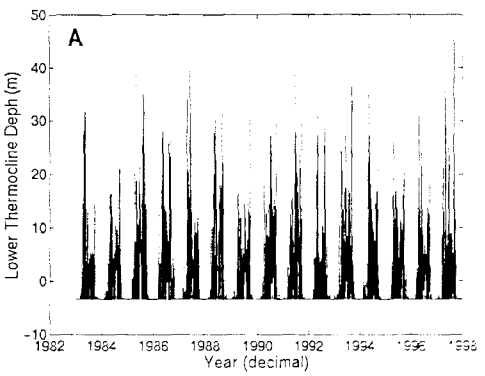

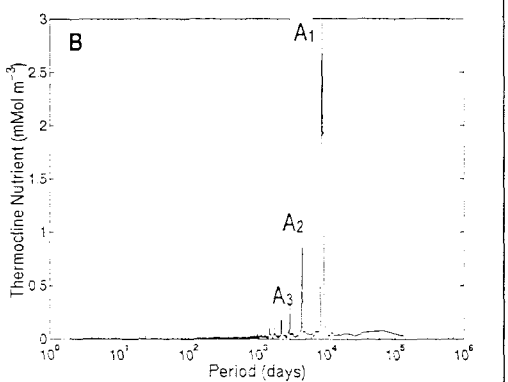

C

	A_1	A_2	A_3	D_1	D_2	D_3
T (day)	364	182	121	1.00	0.50	0.33
A mmol m^{-3}	2.98	1.11	0.48	0.008	0.001	0.000
ϕ (rad)	-0.74	1.86	1.11	1.93	0.69	3.44

Model Simulations of BML Nutrient, 1983 to 1997

A – Time Series
B – Frequency Series
C – Peak Characteristics

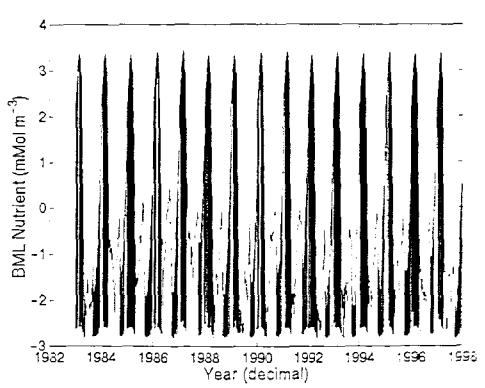

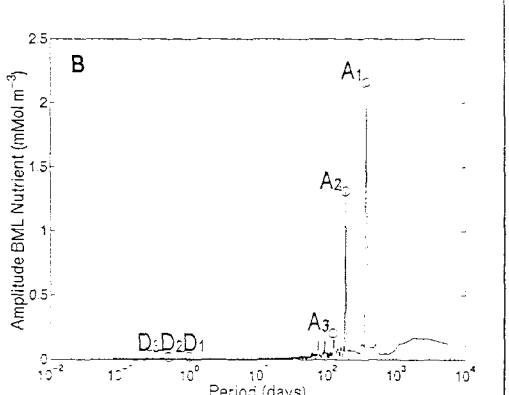

	A_1	A_2	A_3	D_1	D_2	D_3
T (day)	364	182	121	1.00	0.50	0.33
A mmol m^{-3}	2.16	1.31	0.20	0.021	0.018	0.029
o (rad)	-0.75	-1.76	2.03	0.31	0.69	3.01

Model Simulations of SML Chlorophyll, 1983 to 1997

A – Time Series
B – Frequency Series
C – Peak Characteristics

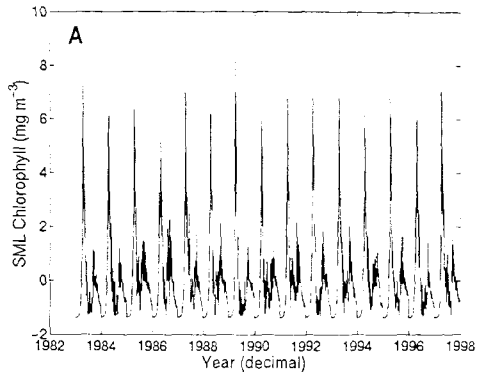

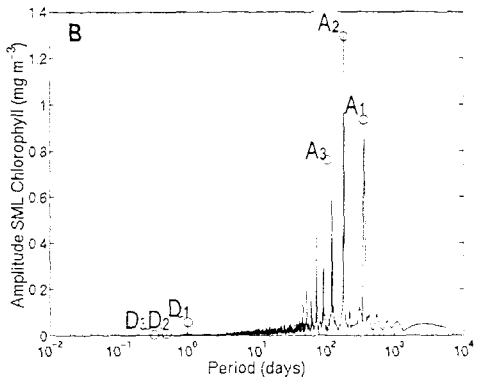

C

	A_1	A_2	A_3	D_1	D_2	D_3
T (day)	364	182	121	1.00	0.50	0.33
A (mg m^{-3})	0.93	1.29	0.75	0.057	0.007	0.002
ϕ (rad)	-2.60	2.21	0.04	2.66	-0.46	1.15

Model Simulations of Thermocline Chl, 1983 to 1997

A – Time Series
B – Frequency Series
C – Peak Characteristics

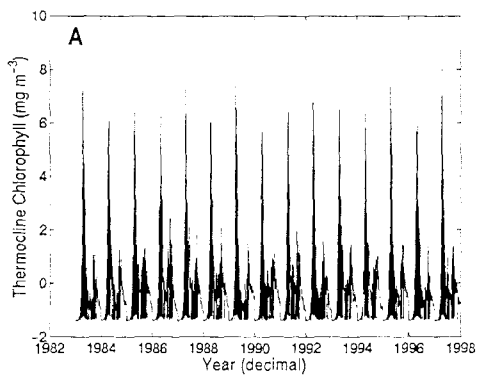

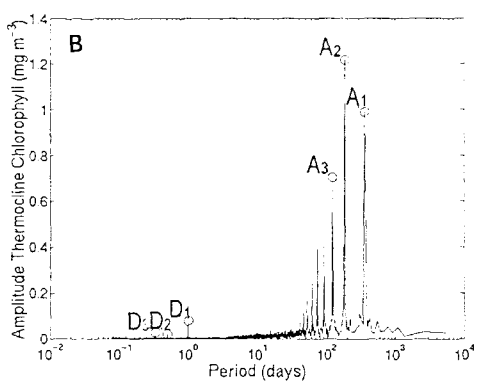

C

	A_1	A_2	A_3	D_1	D_2	D_3
T (day)	364	182	121	1.00	0.50	0.33
A (mg m^{-3})	0.99	1.22	0.70	0.080	0.021	0.028
ϕ (rad)	-2.67	2.17	0.02	2.47	-2.10	-2.73

Model Simulations of BML Chlorophyll, 1983 to 1997

A – Time Series
B – Frequency Series
C – Peak Characteristics

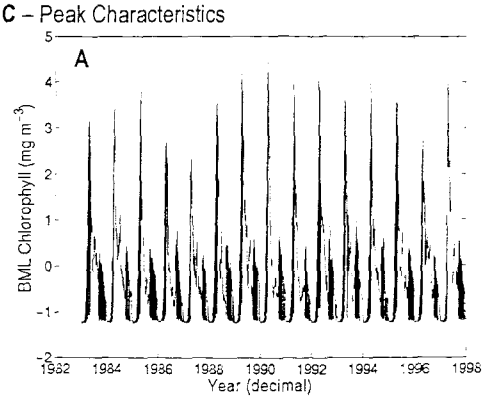

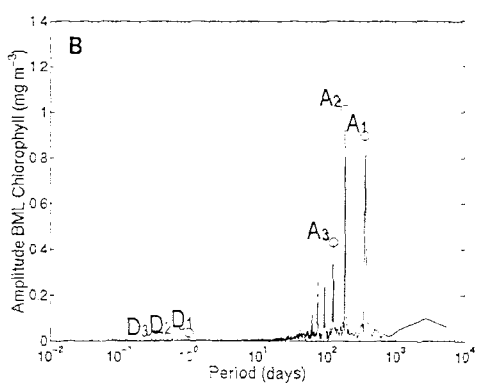

C

	A_1	A_2	A_3	D_1	D_2	D_3
T (day)	364	182	121	1.00	0.50	0.33
A (mg m^{-3})	0.90	1.01	0.53	0.033	0.011	0.013
ϕ (rad)	-2.66	1.93	0.10	2.24	-2.42	3.10

References

Agoumi A., Gosse, P., Khalanski, M., (1985): Temperature and Phytoplankton. In: Gibbs, P.E. (Ed.) *Proceedings of the 19th European Marine Biology Symposium.* Cambridge University Press, Cambridge, UK, pp. 23-38.

Aiken, J. & Bellan I., (1990): Optical oceanography: an assessment of towed measurement. In: Herring, P.J., Campbell, A.K., Whitfield, M. & Maddock, L. (Eds.) *Light and Life in the Sea.* Cambridge University Press, Cambridge, UK, pp. 39-57.

Anon (1999), Signal Processing Toolbox. *The MathWorks Inc.*

Atlas, D. & Bannister, T.T. (1980): Dependence of mean spectral extinction coefficient of phytoplankton an depth, water colour and species. *Limnol. Oceanogr,* 25, 157-159.

Austin, R.W. & Petzold T.J., (1977): Considerations in the design and evaluation of oceanographic transmissometers. In: Tyler, J.E. (Ed.) *Light in the Sea.* Dowden Hutchinson Ross, Stroudsbury, pp 104-120.

Austin, R.W. & Petzold T.J., (1981): The determination of the diffuse attenuation coefficient of sea water using the CZCS. In: Gower J.F.R. (Ed.) *Oceanography from Space.* Plenum Press, New York, USA, pp 239-256.

Baretta, J.W., Baretta-Bekker, J.G. & Ruardij, P., (1998): Data needs for ecosystem modelling. *ICES J. Mar. Sci.,* 55, 756-766.

Beckwith, T.G., Marangoni, R.D. & Lienhard, J.H., (1993): *Mechanical Measurements, Fifth Edition*, Addison-Wesley Publishing Company, Inc., 1993.

Bisagni, J.J. & Sano M.H., (1993): Satellite observations of sea surface temperature variability on southern Georges Bank. *Continental Shelf Res.*, 13, 1045-1064.

Bisagni, J.J., (1990): Differences in the annual stratification cycle over short spatial scales on southern Georges Bank. *Continental Shelf Res.*, 12, 415-435.

Blackford, J.C. & Radford, P.J., (1995): A structure and methodology for marine ecosystem modelling. *Neth. J. Sea Res.*, 33, 247-260.

Blackman, F.F., (1905): Optima and limiting factors. *Ann. Bot.* 19, 281-295.

Bowers, D.G. & Simpson, J.H., (1987): Mean position of tidal fronts in European-shelf seas. *Cont. Shelf Res.*, 7, 35-44.

Bowman, M.J. & Esais W.E., (1981): Fronts, stratification and mixing in Long Island and Block Island Sounds. *J. Geophys. Res.*, 86, 4260-4264.

Bowman, M.J., Kibblewhite, A.C. & Ash, D.E., (1981): M_2 tidal effects in Cook Strait, New Zealand. *J. Geophys. Res.*, 85, 2728-2742.

Bricaud, A., Babin, M., Morel, A. & Claustre, H., (1995): Variability in the chlorophyll-specific absorption coefficients of natural phytoplankton: Analysis and parameterisation. *J. Geophys. Res.*, 100, 13321-13332.

Carruthers, J.N., (1935): The flow of water through the Straits of Dover as guaged by continuous current meter observations at the Varne light vessel. *Fish. Invest. Minist. Agric. Fish Food G.B. Ser.II,* 14, 1-67.

Cayula, J.F. & Cornillon, P., (1992): Edge-detection algorithm for SST images. *J. Atmos. Ocean Tech.*, 9, 67-80.

Cayula, J.F. & Cornillon, P., (1995): Multiimage edge-detection algorithm for SST images. *J. Atmos. Ocean Tech.*, 12, 821-829.

Chavez, F.P., Buck, K.R., Bidigare, R.R., Karl, D., Hebel, M., Latasa, M., Campbell, L. & Newton, J., (1995): On the chlorophyll-a retention properties of glass fibre GF/F filters. *Limnol. Oceanogr.*, 40, 428-433.

Chelsea Instruments (1990): AlphaTracka 660nm (Red) Handbook, Document reference HB106 issue 3, 19 pp. Chelsea Instruments Ltd, Surrey, U.K.

Chen, C. & Beardsley, R.C., (1995): A numerical study of stratified tidal rectification over a finite-amplitude symmetric banks. *J. Phys. Oceanogr.*, 25, 2090-2110.

Clark, D.K., (1981): Phytoplankton pigment algorithms for the Nimbus-7 CZCS. *Oceanography form Space,* (Gower, J.F.R. ed.), 227-373, Plenum Press.

Cohen, E.B., Grosslein, M.D., Sissenwine, M.P., Steimle, F. & Wright, W.R., (1982): Energy budget of Georges Bank. *Canadian Special Publications of Fisheries and Aquatic Sciences*, 59, 95-107.

Colebrook, J.M. & Taylor, A.H., (1979): Year-to-year changes in sea surface temperature, North Atlantic and North Sea, 1948 to 1974. *Deep Sea Res.*, 26A, 825-850.

Colebrook, J.M. & Taylor, A.H., (1984): Significant time scales of long term variability in the plankton and the environment. *Rapp. P.-v. Reun. Cons. int. Explor. Mer.*, 183, 20-26.

Cooley, J.W. & Tukey, J.W., (1965): An algorithm for the machine calculation of complex Fourier series. *Mathematical Computation*, 19, 297-301.

Davies, A.G., De Madariaga, I., Bautista, B., Fernandez, E., Harbour, D.S., Serret, P. & Tranter, R.P.G., (1992): The ecology of a coastal *Phaeocystis* bloom in the north-western English Channel in 1990. *J. Mar. Biol. Ass. U.K.*, 72, 691-708.

Droop, M.R., (1983): Twenty-five years of algal growth kinetics, a personal view. *Botanica Marina,* 26, 99-112.

Dugdale, R.C. (1967): Nutrient limitation in the sea: dynamics, identification and significance. *Limnol. Oceanogr.*, 12, 528-531.

Dugdale, R.C., Morel, A., Bricaud, A. & Wilkerson, F.P., (1989): Modelling new production in upwelling centres: a case study of modelling new production from remotely sensed colour and temperature. *J. Geophys. Res.*, 94, 18119-18132.

Edinger, J.E., Duttweiler, D.W. & Geyer, J.C., (1968): The response of water temperatures to meteorological conditions. *Water Resources Res.*, 4, 1137-1145.

Elliott, A.J. & Li, Z., (1995): A model of the annual cycle of temperature in the north-west European shelf seas with stochastic wind forcing. *Estu. Coast. Shelf Sci.,* 40, 265-280.

Falkowski, P.G., Dubinsky, Z. & Wyman, K., (1985): Growth-irradiance relationships in phytoplankton. *Limnol. Oceanogr.,* 30, 311-321.

Fasham M.J.R. & Evans G.T., (1995): The use of optimisation techniques to model marine ecosystem dynamics at the JGOFS station at 47° N 20°W. *Phil. Trans. R. Soc. Lond.*, B 348, 203-209.

Fasham, M.J.R., Ducklow, H.W. & McKelvie, S.M., (1990): A nitrogen-based model of plankton dynamics in the ocean mixed layer. *J. Mar. Res.*, 48, 591-639.

Fasham, M.R. & Platt, T., (1983): Photosynthetic response of phytoplankton to light: A physiological response. *Proc. R. Soc. Lond. B,* 219 355-370.

Fasham, M.R., Platt, T., Irwin, B. & Jones, K., (1984): Factors affecting the spatial pattern of the deep chlorophyll maximum in the region of the Azores Front. *Prog. Oceanogr.*, 14, 129-165.

Franks P.J.S. & Walstad L.J., (1997): Phytoplankton patches at fronts: a model of formation and response to wind events. *J. Mar. Res.*, 55, 1-29.

Franks, P.J.S. & Chen, C., (1996): Plankton production in tidal fronts: a model of Georges Bank in summer. *J. Mar. Res.*, 54, 631-651.

Franks, P.J.S., (1992): Phytoplankton blooms at fronts: patterns, scales and physical forcings. *Rev. Aquat. Sci.*, 6, 121-137.

Franks, P.J.S., (1995): Coupled physical-biological models in oceanography. *Rev. Geophysics Supp.* July 1995, 1177-1187.

Franks, P.J.S., Wroblewski, J.S. & Flierl, G.R., (1986): Behaviour of a simple phytoplankton model with food-level acclimation by herbivores. *Mar. Biol.*, 91, 121-129.

Garrett, C.J.R. & Loder J.W., (1981): Dynamical aspects of shallow sea fronts. *Phil. Trans. R. Soc. Lond.*, A 302, 562-581.

Garrett, C.J.R., Keeley, J.R. & Greenberg, D.A., (1978): Tidal mixing versus thermal stratification in the Bay of Fundy and Gulf of Maine. *Atmosphere-Ocean*, 16, 403-423.

Garwood, R.W., (1977): An oceanic mixed layer model capable of simulating cyclicd states. *J. Phys. Oceanogr.*, 7, 455-468.

Gieskes, W.W. & Kraay, G.W., (1983): Unknown chlorophyll-a derivatives in the North Sea and the tropical Atlantic ocean revealed by HPLC analysis. *Limnol. Oceanogr.*, 28, 757-766.

Gordon, H.R. & Morel, A.Y., (1983): Remote assessment of ocean colour for interpretation of satellite visible imagery: review. *Lecture notes on Coastal and estuarine studies*, 4.

Gordon, H.R., Clark, D.K., Brown, J.W., Brown, O.B., Evans, H.R. & Broenkow, W.W., (1983): Phytoplankton pigment concentrations in the Middle Atlantic Bight: Comparison of ship determinations and CZCS estimates. *Appl. Opt.*, 22, 20-36.)

Harvey, H.W., (1925): Hydrography of the English Channel. *Rapp. P.-v. Reun. Cons. Int. Explor. Mer.*, 37, 59-89.

Hochman, H.T., Walsh, J.J. & Carder, K.L., (1995): Analysis of ocean colour components within stratified and well-mixed waters of the western English Channel. *J. Geophys. Res.*, 100, 10777-10787.

Holligan P.M., (1981): Biological implicatioons of fronts on the northwest European continental Shelf. *Phil. Trans. R. Soc. Lond.*, A 302, 547-562.

Holligan, P.M. & Harbour, D.S., (1977): The vertical distribution and sucession of phytoplankton in the western English Channel in 1975 and 1976. *J. Mar. Biol. Ass. UK*, 57, 1075-1093.

Holligan, P.M., Harris, R.P., Newell, N.C., Harbour, D.S., Head, R.N., Linley, E.A.S., Lucas, M.I., Tranter, P.R.G. & Weekley, C.M., (1984a): Vertical distribution and partitioning of organic carbon in mixed, frontal and stratified waters of the English Channel. *Mar. Ecol. Prog. Ser.*, 14, 111-127.

Holligan, P.M., Viollier, M., Dupouy, C. & Aiken, J., (1983): Satellite studies on the distributions of chlorophyll and dinoflagellate blooms in the Western English Channel. *Continental Shelf Res.*, 2, 81-96.

Holligan, P.M., Williams, P.J. LeB., Purdie, D. & Harris, R.P., (1984b): Photosynthesis, respiration and nitrogen supply of plankton populations in stratified, frontal and tidally mixed shelf waters. *Mar. Ecol. Prog. Ser.*, 17, 201-213.

Hooker, S.B., Esaias, W.E., Feldman, G.C., Gregg, W.W. & McClain, C.R., (1992): An overview of SeaWiFS and ocean colour. *NASA Tech. Memo. 104566,* Hooker, S.B. & Firestone, E.R. eds, 24pp. NASA GSFC, Maryland, USA.

Ikushima, (1967) Referenced in: Walsh, J.J., (1988): *On the nature of continental shelves*, Academic Press, San Diego, pp. 112-213.

IPCC, (1995): *IPCC Second Assessment Report: Climate Change.* IPCC, Geneva, Switzerland.

Ishisaka, J., (1990): Coupling of Coastal Zone Color Scanner data to physical-biological model of the southeastern U.S. continental shelf ecosystem. 3. Nutrient and phytoplankton fluxes and CZCS data assimilation. *J. Geophys. Res.*, 95, 10897-10908.

James, I.D., (1977): A model of the annual cycle of temperature in a frontal region of the Celtic Sea. *Estu. Coast. Shelf Sci.*, 5, 339-353.

Jassby, A.D. & Platt, T., (1976): Mathematical formulation of the relationship between photosynthesis and light for phytoplankton. *Limnol. Oceanogr.*, 21, 540-547.

Jenkins, G.M. & Watts, D.G. (1986). *Spectral Analysis and its applications*. Holden-Day. San Francisco.

JGOFS (Joint Global Ocean Flux Study) (1991): JGOFS core measurement protocols. *JGOFS Report No. 6*, Scientific Committee on Oceanic Research, 40 pp..

Jordan, M.B. & Joint, I., (1998): Seasonal variation in nitrate:phosphate ratio in the English Channel 1923-1987. *Estu. Coast. Shelf Sci.*, 46, 157-164.

Kiorbe, T. &Nielsen, T.G., (1990): Effects of wind stress on vertical water column structure, phytoplankton growth, and productivity of planktonic copepods. *In* "Trophic Relationships in the Marine Environment" (Barnes, M. & Gibson, R.M. eds), pp28-40. Aberdeen University Press, Aberdeen.

Kiorbe, T., (1992): Turbulence, Phytoplankton cell size and the structure of pelagic food webs. *Adv. Mar. Biol.*, 29, 1-72

Kirk, J.T.O., (1994): Light and Photosynthesis in Aquatic Ecosystems. 509pp, Cambridge University Press. Cambridge.

Kraus, E.B. & Turner J.S. (1967): A one-dimensional model of the seasonal thermocline. 2: The general theory and its consequences. *Tellus*, 19, 98-105.

Laabir, M., Poulet, S.A., Harris, R.P., Pond, D.W., Cueff, A., Head, R.N. & Ianora, A., (1998): Comparative study of the reproduction of *Calanus helgolandicus* in well-mixed and seasonally stratified coastal waters of the English Channel. *J. Plankton. Res.*, 20, 407-421.

Large W.G., McWilliams, J.C. & Doney, S.C., (1994): Oceanic vertical mixing: a review and a model with a nonlocal boundary layer parameterization. *Rev. Geophys.* 32, 363-403.

Lavin-Peregrina, M.F., (1984): The seasonal cycle and variability of stratification in the Western Irish Sea. PhD Thesis, University College of North Wales, Bangor, UK.

LeFevre, J., (1986): Aspects of the biology of frontal systems. *Adv. Mar. Biol.*, 23, 164-299.

Lenhart H.J., Radach, G., Backhaus, J.O. & Pohlmann, T., (1995): Simulations of the North Sea circulation, its variability, and its implementation as hydrodynamical forcing in ERSEM. *Neth. J. Sea Res.*, 33, 271-299

Loder, J.W. & Greenberg, D.A., (1986): Predicted positions of tidal fronts in the Gulf of Maine region. *Continental Shelf Res.*, 6, 397-414.

Loder. J.W. & Platt, T., (1985): Physical controls on phytoplankton production at tidal fronts. In: Gibbs, P.E. (Ed.) *Proceedings of the 19th European Marine Biology Symposium*. Cambridge University Press, Cambridge, UK, pp. 3-21.

Lorenzen, C.J., (1966): A method for the continuous measurement of *in-vivo* chlorophyll concentration. *Deep Sea Res.*, 13, 223-227.

Maddock, L. & Swann, C.L., (1977): A statistical analysis of some trends in sea temperature and climate in the Plymouth area in the last 70 years. *J. Mar. Biol. Ass. U.K.*, 57, 317-338

Marra, J. & Ho, C., (1993): Initiation of the spring bloom in the northeast Atlantic (47°N, 20°W): a numerical simulation. *Deep-Sea Res. II*, 40, 55-73.

Marra, J., Bidigare, R.R. & Dickey, T.D., (1990): Nutrients and mixing, chlorophyll and phytoplankton growth. *Deep Sea Res.*, 37, 127-143.

McKee, D., Cunningham, A. & Jones, K., (1999): Simultaneous measurements of fluorescence and beam attenuation: instrument characterisation and interpretation of signals from stratified coastal waters. *Estu. Coast. Shelf Sci.*, 48, 51-58.

Mellor, G.L. & Yamada, T., (1982): Development of a turbulence closure model for geophysical fluid problems. *Rev. Geophys. Space Phys.*, 20, 851-875.

Miller P, Groom S, McManus A, Selley J and Mironnet N., (1997): PANORAMA: a semi-automated AVHRR and CZCS system for observation of coastal and ocean processes. In: *RSS97: Observations and Interactions, Proceedings of the Remote Sensing Society*, The Remote Sensing Society, London, pp 539-544.

Morel, A. & Prieur, L., 1977: Analysis of variations in ocean colour. *Limnol. Oceanogr.*, 22, 709-722

Morin, P, LeCorre, P. & LeFevre, J., (1985): Assimilation and regeneration of nutrients off the west coast of Britany. *J. Mar. Biol. Ass. U.K.*, 65, 677-695.

Morin, P., Wafar, M.V.M. & LeCorre, P., (1993): Estimation of nitrate flux in a tidal front from satellite-derived temperature data. *J. Geophys. Res.*, 98, 4689-4695.

Muller, J.L. & Austin, R.W., (1995): Ocean Optics Protocols for SeaWiFS Validation, Revision 1. *NASA Tech. Memo. 104566,* 35, NASA Goddard Space Flight Center, Greenbely, Maryland, 90pp.

Newton, J.A. & Morello, T.A., (1998): Phytoplankton growth and loss rates over the course of blooms in a temperate embayement. *EOS*, 79, 141.

O'Reilly, J.E., Maritorena, S., Mitchell, B.G., Siegel, D.A., Carder, K.L., Garver, S.A. & McClain, C.R., (1998): Ocean colour chlorophyll algorithms for SeaWiFS. *J. Geophys. Res.,* (submitted).

Oreskes N, Shrader-Frechette, K. & Belitz, K., (1994): Verification, validation and confirmation of numerical models in the earth sciences. *Science,* 263, 641-646.

Osborne, B.A. & Geider, R.J., (1986): Effect of nitrate-nitrogen limitation on photosynthesis of the diatom *Phaeodactylum tricornutum* Bohlin. *Plant, Cell, Environment,* 9, 617-625.

Parker, R.A., (1986): Simulating the development of the chlorophyll maxima in the Celtic Sea. *Ecological modelling,* 33, 1-11.

Pingree, R.D. & Griffithis, K.D., (1978): Tidal fronts on the shelf seas around the British Isles. *J. Geophys. Res.,* 83, 4615-4622.

Pingree, R.D. & Griffithis, K.D., (1980): Currents driven by a steady uniform wind stress on the shelf seas around the British Isles. *Oceanologica Acta,* 3, 227-235.

Pingree, R.D. & Griffiths, K.D., (1981): S_2 tidal simulations on the North-West European Shelf. *J. Mar. Biol. Ass. U.K.,* 61, 609-616.

Pingree, R.D. & Pennycuick, L., (1975): Transfer of heat, fresh water and nutrients through the seasonal thermocline. *J. Mar. Biol. Ass. U.K.,* 55, 261-274.

Pingree, R.D., (1980): Physical Oceanography of the Celtic Sea and English Channel. *The Northwest European Shelf Seas: the Sea Bed and the Sea in Motion. II. Physical and Chemical Oceanography and Physical Resources.* (Banner, Collins & Massie, eds.), 415-465.

Pingree, R.D., Holligan, P.M. & Head, R.N., (1977b): Survival of dinoflagellate blooms in the western English Channel. *Nature,* 265, 266-269.

Pingree, R.D., Holligan, P.M. & Mardell, G.T., (1978): The effects of vertical stability on phytoplankton distributions in the summer on the northwest European Shelf. *Deep Sea Res.*, 25, 1011-1028.

Pingree, R.D., Holligan, P.M., Mardell, G.T. & Head, R.N. (1976): The influence of physical stability on spring, summer and autmn phytoplankton blooms in the Celtic Sea. *J. Mar. Biol. Ass. U.K.*, 56, 845-873.

Pingree, R.D., Maddock, L. & Butler, E.I., (1977a): The influence of biological activity and physical stability in determining the chemical distributions of inorganic phosphate, silicate and nitrate. *J. Mar. Biol. Ass. U.K.*, 57, 1065-1073.

Pingree, R.D., Mardell, G.T. Holligan, P.M., Griffiths, K.D. & Smithers, J., (1982): Celtic Sea and Armorican current structure and the vertical distributions of temperature and chlorophyll. *Continental Shelf Res.*, 1, 99-116.

Pingree, R.D., Pugh, P.R., Holligan, P.M. & Forster, G.R., (1975): Summer phytoplankton blooms and red tides along tidal fronts in the approaches to the English Channel. *Nature*, 258, 672-677.

Pinkerton M.H., & Aiken J., 1997: A moored databuoy for the calibration and validation of remote observations of ocean colour. PlyMBODy, a preliminary assessment. In Griffiths G. & Pearson D. (Eds). *RSS97 Observations and Interactions*, Remote Sensing Society, pp. 551-556.

Platt, T., Gallegos, C.L. & Harrison, W.G., (1990): Photoinhibition of photosynthesis in natural assemblages of marine phytoplankton. *J. Mar. Res.*, 38, 687-701.

Prestidge, M.C. & Taylor, A.H., (1995): A modelling investigation of the distribution of stratification and phytoplankton abundance in the Irish Sea. *J. Plankton Res.*, 17

Prezlin B.B. & Ley, A.C., (1980): Photosynthesis and chlorophyll-a fluorescence rhythms of marine phytoplankton. *Mar. Biol.*, 55, 295-307.

Price, J.F., Weller, R.A. & Pinkel, R., (1986): Diurnal cycling: observations and models of upper ocean response to diurnal heating, cooling and wind mixing. *J. Geophys. Res.*, 91, 8411-8427.

Radach, G., Berg, J. & Hagmeier, E., (1990): Long-term changes of the annual cycles of meteorological, hydrographic, nutrient and phytoplankton time series at Helgoland and at ELBE 1 in the German Bight. *Continental Shelf Res.*, 10, 305-328.

Richardson, K., Beardall, J. & Raven, J.A., (1983): Adaptation of unicellular algae to irradiance: an analysis of the strategies. *New Phytologist,* 93, 157-191.

Ridderinkhoff, H., (1992): On the effects of variability in meteorological forcing on the vertical structure of a stratified watercolumn. *Continental Shelf Res.*, 12, 25-36.

Robinson, I.S., (1985): *Satellite Oceanography.* Ellis Horwood, Chichester.

Rotunno, N., (1994): A synopsis of coastal meteorology: A review of the state of the science. In: *Environmental Science in the Coastal Zone: Issues for Further Research*, pp 14-19, National Academy Press, Washington.

Ruardij, P., Van Haren, H. & Ridderinkhof, H., (1997): The impact of thermal stratification on phytoplankton and nutrient dynamics in shelf seas: a model study. *J. Sea Res.,* 38, 311-331.

Ryther, J.H. & Dunstan, W.M., (1971): *Science,* 171, 1008-1013.

Sathyendranath, S. & Morel, A., (1983): Light emerging from the sea – interpretation and uses in remote sensing. In: *Remote Sensing Applications in Marine Science and Technology.* (Cracknell, A.P. ed.), pp 323-357, Reidel Publishing, Dortrecht.

Schanz, F., Senn, P. & Dubinsky, Z., (1997): Light absorption by phytoplankton and the vertical light attenuation: ecological and physiological significance. *Oceanogr. Mar. Biol. Ann. Rev.,* 35, 71-95.

Sharples, J. & Simpson J.H., (1996):The influence of the springs-neaps cycle on the position of shelf sea fronts. *Coast. Estu. Shelf Sci.*, 53, 71-82.

Sharples, J. & Tett, P., (1994): Modelling the effect of physical variability on the midwater chlorophyll maximum. *J. Mar. Res.*, 52, 219-238.

Sharples, J. (*in press*): The role of vertical mixing in controlling the seasonal distribution of phytoplankton at tidal mixing fronts.

Simpson, J.H. & Bowers, D.G., (1981): Models of stratification and frontal movement in shelf seas. *Deep Sea Res.*, 28A, 727-738.

Simpson, J.H. & Bowers, D.G., (1984): The role of tidal stirring in controlling the seasonal heat cycle in shelf seas. *Annales Geophysicae*, 2, 411-416.

Simpson, J.H. & Hunter, J.R., (1974): Fronts in the Irish Sea. *Nature*, 250, 404-406.

Simpson, J.H. & Sharples, J., (1994): Does the Earth's rotation influence the location of shelf sea fronts? *J. Geophys. Res.*, 99, 3315-3319.

Simpson, J.H. & Tett, P.B., (1986): Island stirring effects an phytoplankton growth. *Lecture Notes on Coastal and Estuarine Studies,* 17, 41-76.

Simpson, J.H., Crawford, W.R., Rippeth, T.P., Campbell, A.R. & Cheok, J.V.S., (1978): The vertical structure of turbulent dissipation in shelf seas. *J. Phys. Oceanogr.*, 26, 1579-1590.

Sinha, B. & Pingree, R.D., (1997): The principal lunar semidiurnal tide and its harmonics: baseline solutions for M_2 and M_4 constituents on the North West European Continental Shelf. *Continental Shelf Res.*, 17, 1321-1365.

Smith, N.R., (1993): Ocean Modelling in a Global Ocean Observing System. *Rev. Geophysics,* 31, 281-317.

Smith, R.C. & Baker, K.S., (1978): Optical classification natural waters. *Limnol. Oceanogr..,* 23, 260-267.

Southward, A.J., (1995): The importance of long time-series in understanding the variability of natural systems. *Helgolander Meeresuntersuchungen*, 49, 329-333

Stigebrandt, A., (1981): Cross-thermocline flow on continental shelves and the location of shelf fronts. In: Nihoul, J.C.J. (Ed.) *Marine Interfaces Hydrodynamics, Elsevier Oceanography Series*, 42, Amsterdam, Netherland, 51-66.

Stigebrandt, A., (1985): A model for the seasonal pycnocline in rotating systems with application to the Baltic Proper. *J. Phys. Oceanogr.,* 15, 1392-1402

Stramska, M. & Dickey, T.D., (1993): Phytoplankton bloom and the vertical thermal structure of the upper ocean. *J. Mar. Res.,* 51, 819-842.

Svedrup H.U., (1953): On conditions for the vernal blooming of phytoplankton. *J. Cons. Perm. Int. Exp. Mer*, 18, 287-295.

Taylor, A.H. & Joint, I., (1990): A steady-state analysis of the microbial loop in stratified systems. *Mar. Ecol. Prog. Ser.,* 59, 1-17.

Taylor, A.H. & Stephens, J.A., (1980): Seasonal and year-to-year variations in surface salinity at the nine North Atlantic weather stations. *Oceanolog. Acta,* 3, 421-430.

Taylor, A.H. & Stephens, J.A., (1983): Seasonal and year-to-year changes in the temperatures of the English Channel and the Southern North Sea. *Oceanolog. Acta,* 6, 63-71.

Taylor, A.H. & Stephens, J.A., (1993): Diurnal variations of convective mixing and the spring bloom of phytoplankton. *Deep-Sea Res.,* 40, 389-408.

Taylor, A.H., Harris, J.R.W. & Aiken, J., (1986): The interaction of physical and biological processes in a model of the vertical distribution of phytoplankton under stratification. In: Nihoul, J.C.J. (Ed.) *Marine Interfaces Hydrodynamics, Elsevier Oceanography Series*, 42, Amsterdam, Netherland, 313-330.

Taylor, A.H., Watson, A.J., Ainsworth, M., Robertson, E. & Turner, D.R., (1991): A modelling investigation of the role of phytoplankton in the balance of carbon at the surface of the North Atlantic. *Global Biogeochemical Cycles,* 5, 151-171.

Taylor, B.N. & Kuyatt, C.E. (1994): Guidelines for Evaluating and Expressing the Uncertainty of NIST Measurement Results. *NIST Technical Note 1297*, NIST, Washington, 24 pp..

Tett, P. & Edwards, A., (1984): Mixing and plankton: an interdisciplinary theme in oceanography. *Oceanogr. Mar. Biol. Annu. Rev.*, 22, 99-123.

Tett, P., (1981): Modelling phytoplankton production at shelf-sea fronts. *Phil. Trans. R. Soc. Lond.*, A302, 605-615.

Tett, P., Edwards, A. & Jones, K., (1986): A model for the growth of shelf sea phytoplankton in summer. *Estu. Coast. Shelf Sci.*, 23, 641-672.

Tett, P., Joint, I., Purdie, D., Baars, M., Oosterhuis, S., Daneri, G., Hannah, F., Mills, D., Plummer, A., Pomroy, D., Walne, A.W. & Witte, H.J., (1993): Biological consequences of tidal mixing gradients in the North Sea. *Phil. Trans. R. Soc. Lond.*, A340, 493-508.

Toplis, B.J., Hunter, R.J. & Simpson, J.H., (1980): Simultaneous measurements of transparency and irradiance in the coastal waters of North Wales. *Mar. Environmental Res.,* 4, 65-79.

Van Aken, H.M., (1984): A one dimensional mixed-layer model for stratified shelf seas with tide- and wind-induced mixing. *Deutsche Hydrographische Zeitschrift*, 37, 3-27.

Varela, R.A., Cruzado, A. & Gabaldon, J.E., (1995): Modelling primary production in the North Sea using the European Regional Seas Ecosystem Model. *Neth. J. Sea Res.*, 33, 337-361.

Voillier, M. & Sturm, B., (1984): CZCS data analysis in turbid coastal waters. *J. Geophys. Res.*, 89, 4977-4985.

Voss, K.J., (1992): A spectral model of the beam attenuation coefficient in the ocean and coastal areas. *Limnol. Oceanogr.*, 37, 501-509.

Walsh, J.J., (1988): *On the nature of continental shelves*, Academic Press, San Diego, pp. 112-213.

Walstad, L.J. & Robinson, A.R., (1990): Hindcasting and forecasting of the POLYMODE data set with the Harvard open ocean model. *J. Phys. Oceanogr.*, 20, 1682-1902

Walstad, L.J., Allen, J.S., Kosro, P.M. & Huyer, A., (1991): Dynamics of the coastal transition zone through data assimilation studies. *J. Geophys. Res.*, 96, 14959-14997.

Wood, E.D., Armstrong F.A.J. & Richards, F.A., (1967): Determination of nitrate in seawater by cadmium-copper reduction to nitrite. *J. Mar. Biol. Ass. U.K.* 47, 23-31.

Woods, J.D. & Barkmann, W., (1986): The response of the upper ocean to solar heating-I. The mixed layer. *Quarterly J. R. Met. Soc.*, 112, 735-756.

Woods, J.D., (1980): Diurnal and seasonal variation of convection in the wind-mixed layer of the ocean. *Quarterly J. R. Met. Soc.*, 106, 379-394.

Yentsch, C.S. & Menzel, C.M., (1963): A method for the determination of phytoplankton chlorophyll and phaeophytin by fluorescence. *Deep Sea Res.*, 10, 221-231.